

The role of N-Src kinases in neuronal differentiation

Philip Lewis

PhD

University of York

Biology

September 2014

Abstract

The ubiquitous proto-oncogene C-Src has two neuronal splice variants, N1- and N2-Src, which contain 6 and 17 amino acid inserts in their SH3 domains respectively. These inserts are thought to modify SH3 domain binding in a manner that decreases auto-inhibition and changes substrate specificity. Although high levels of neuronal Src expression are associated with neuronal differentiation, both during development and in the developmental cancer neuroblastoma, the functions, molecular mechanisms and specific substrate proteins of neuronal Srcs remain largely uncharacterised.

Employing a highly multidisciplinary approach, this project aimed to characterise the role of N-Src expression in neuronal differentiation. Neuronal Srcs were demonstrated to be highly active in neuroblastoma cell lines, and overexpression can drive significant neuritogenesis in the retinoic acid-resistant cell lines KELLY and SK-N-AS. N2-Src expression was also shown to decrease the expression of Ki67 in SK-N-AS cells, indicating that N2-Src can drive neuroblastoma cells into quiescence.

Using the *Xenopus* embryo as a model system for neuronal development, the expression pattern of xN1-Src during neurulation was characterised and a novel neuronal splice variant was identified in this species. It was demonstrated that xN1-Src is essential for healthy primary neurogenesis, and that xN1-Src knockdown caused a dramatic locomotive and patterning phenotype in *X.tropicalis*. Using stable, inducible HeLa cell lines, a phosphoproteomic screen demonstrated significant changes in the phosphotyrosine profile between C- and N2-Src over-expressing cells. Several candidate N2-Src substrates were identified, including paxillin, plakophilin and BCAR1. Bioinformatic analyses of the proteomic data revealed the enrichment of signalling pathways and protein complexes involved in membrane traffic and cell adhesion.

Through these multidisciplinary approaches, the cellular effects of N1- and N2-Src signalling during both neuronal precursor and neuroblastoma differentiation have been characterised. Furthermore, a library of potential N-Src substrates has been generated that provides a framework for future studies.

Table of contents

Title.....	1
Abstract.....	2
Table of contents	3
List of figures.....	9
List of tables.....	11
List of accompanying material.....	12
Acknowledgements.....	13
Declaration.....	14
1 Introduction.....	15
1.1 Regulation by Phosphorylation	15
1.1.1 Tyrosine phosphorylation.....	16
1.1.2 Receptor tyrosine kinases.....	17
1.1.3 Non-receptor tyrosine kinases.....	18
1.2 Src Family Kinases.....	18
1.2.1 SFK structure	19
1.2.2 The SH4 domain	19
1.2.3 The Unique Domain.....	21
1.2.4 The SH3 domain	25
1.2.5 The SH2 domain	28
1.2.6 The kinase domain.	30
1.2.7 The C-terminal Tail.....	33
1.2.8 Regulation of Src.....	33
1.3 Cellular functions of Src.....	37
1.3.1 Tissue specific expression and activity of Src	38
1.3.2 Neuronal roles of Src	39
1.4 Neuronal Src splice variants.....	42
1.4.1 Differential effects of N1-exon insertion on the SH3 domain	44
1.4.2 The effects of N1-exon insertion on auto-inhibition.....	46
1.4.3 Effects of N1-exon insertion on N1-Src localisation	46
1.4.4 Effects of N1-exon inclusion on cell morphology	47
1.4.5 Expression of N1-Src during neuronal differentiation.....	48
1.4.6 Expression of N1-Src in the mature brain.....	49
1.4.7 The regulation of N1-Src splicing.....	50

1.4.8	Neuronal Srcs in Neuroblastoma	51
1.5	Aims	55
2	Materials and Methods	57
2.1	Materials	57
2.2	Molecular biology methods	58
2.2.1	Agarose Gels	58
2.2.2	DNA separation by acrylamide gel electrophoresis	59
2.2.3	SDS-PAGE	59
2.2.4	Protein transfer to PVDF	60
2.2.5	Western Blotting	60
2.2.6	Preparation of competent <i>E.coli</i> for cloning	61
2.2.7	Bacterial transformation	61
2.2.8	Plasmid purification	62
2.2.9	Cloning	62
2.2.10	DNA sequencing	64
2.3	Cell culture methods	64
2.3.1	Culture of cell lines	64
2.3.2	Transient transfection of cells for immunocytochemistry	65
2.3.3	Transient transfection of cells for western blotting	65
2.3.4	Stable transfection of HeLa cells	66
2.3.5	Immunocytochemistry	67
2.3.6	Wound healing assay	68
2.3.7	Image quantification	68
2.3.8	Statistical analyses of neuritogenesis assays	69
2.4	Mass spectrometry methods	69
2.4.1	Phosphotyrosine immunoprecipitation from HeLa cells	69
2.4.2	Mass spectrometry	70
2.4.3	Bioinformatics	71
2.4.4	WebGestalt	71
2.4.5	DAVID	72
2.4.6	Phosphosite	72
2.4.7	GPS 2.0	72
2.4.8	ScanSite	73
2.4.9	STRING	73
2.5	Developmental biology methods	73

2.5.1	Plasmid linearisation	73
2.5.2	<i>In vitro</i> transcription of synthetic mRNA for injection into <i>Xenopus</i> species	74
2.5.3	Injection of <i>Xenopus</i> embryos.....	75
2.5.4	Collecting phenotypes.....	76
2.5.5	<i>In situ</i> hybridisation	76
2.5.6	Lacz staining	77
2.5.7	Imaging phenotypes and in situs.....	78
2.5.8	RNA isolation	78
2.5.9	cDNA synthesis.....	78
2.5.10	rtPCR.....	79
3	The role of N-Srcs in neuroblastoma differentiation.....	80
3.1	Introduction	80
3.2	Results	82
3.2.1	Neuronal Srcs are more active than C-Src in B104 cells.....	82
3.2.2	The effects of N1- and N2-Src overexpression on B104 cell morphology	84
3.2.3	Characterising human neuroblastoma cell lines.....	87
3.2.4	Confirming N-Src shRNA function	89
3.2.5	Knockdown of neuronal Srcs in LAN-5 cells.....	90
3.2.6	Over-expression of N-Srcs in the SK-N-AS cells.....	93
3.2.7	Expression of N2-Src induces neuritogenesis in KELLY cells	93
3.2.8	The effects of N-Src expression on neuroblastoma cell proliferation..	95
3.3	Discussion	97
3.3.1	Increased activity of neuronal Srcs expressed in neuroblastoma.....	98
3.3.2	Decreased abundance of N-Srcs in Western blot samples	99
3.3.3	Detection of an additional Y416 band in N2-Src transfected B104 cells	101
3.3.4	Knockdown of N-Src expression in LAN-5 cells does not decrease neuritogenesis.....	102
3.3.5	Reduced effect of N-Src expression on constitutively differentiated cell lines	103
3.3.6	Overexpression of neuronal Srcs in RA resistant neuroblastoma cell lines induces neuritogenesis.....	104
3.3.7	Overexpression of N2-Src causes a decrease in proliferation of SK-N-AS neuroblastoma cells.....	105

3.3.8	Parallels between N2-Src and Vanadate mediated neuroblastoma differentiation.....	106
3.4	Concluding remarks	107
4	Identification of N2-Src specific substrates by mass spectrometry	109
4.1	Introduction	109
4.2	Results	110
4.2.1	Establishment of the stable, inducible Src expressing HeLa cell lines 110	
4.2.2	N2-Src expression appears to be restricted to the Golgi region.....	110
4.2.3	N-Src expression induces elongation of HeLa cells	113
4.2.4	Expression of N1- and N2-Src in HeLa cells reduces cell migration	115
4.2.5	N2-Src expression does not increase the proportion of HeLa cells exiting the cell cycle.....	118
4.2.6	Preparation of HeLa cell lysates for LC/MS/MS.....	118
4.2.7	Processing LC/MS/MS results	122
4.2.8	Identification of tyrosine phosphorylation sites in immunoprecipitated proteins	125
4.2.9	Interaction mapping of enriched proteins using STRING	127
4.2.10	Identification of enriched functional clusters of proteins	129
4.2.11	In-depth analysis of N2-Src enhanced proteins: Endocytosis.....	132
4.2.12	In depth analysis of N2-Src enhanced proteins: Adherens	136
4.2.13	In depth analysis of N2-Src enhanced proteins: COPII coat proteins	137
4.2.14	Confirming Sec23A immunoprecipitation for N2-Src expressing HeLa cells	137
4.3	Discussion	138
4.3.1	Cellular effects of N2-Src are not limited to neuronal cells.....	139
4.3.2	N2-Src appears to co-activate endogenous SFKs	139
4.3.3	Appraisal of the chosen phosphoproteomic methodology.....	139
4.3.4	Interpretation of the identified tyrosine phosphopeptides.....	142
4.3.5	Specific enrichment of endocytosis related proteins in N2-Src expressing HeLa cells	144
4.3.6	Specific enrichment of adherens-related proteins in N2-Src expressing HeLa cells.....	145
4.3.7	Specific enrichment of the COPII coat in N2-Src overexpressing cells 147	
4.3.8	Other notable proteins increased in abundance in N2-Src samples ...	148
4.4	Concluding remarks	151

5	The role of Neuronal Src expression in the neuronal development of <i>Xenopus</i>	152
5.1	Introduction	152
5.2	Results	153
5.2.1	xN1-Src replicates the cytoskeletal rearrangement caused by N1-Src in fibroblasts.....	153
5.2.2	xN1-Src expression correlates with <i>Xenopus</i> primary neurogenesis .	155
5.2.3	Mammalian neuronal Src overexpression causes posteriorisation in <i>X.laevis</i>	158
5.2.4	Injection of endogenous xN1-Src into <i>Xenopus</i> embryos.....	160
5.2.5	Design of a morpholino to specifically skip xN1-Src micro-exon inclusion <i>in vivo</i>	161
5.2.6	xN1-Src knockdown causes aberrant tail formation and a severe locomotive phenotype	163
5.2.7	xN1-Src knockdown inhibits n-tubulin expression at primary neuritogenesis.....	165
5.2.8	xN1-Src knockdown does not decrease Sox3 expression during neurulation.....	169
5.2.9	Attempting to rescue xN1-Src knockdown with xN1-Src mRNA expression.....	171
5.3	Discussion	171
5.3.1	xN1-Src as a model for N1-Src in development	172
5.3.2	Increased xN1-Src expression begins at the very beginning of neurulation.....	173
5.3.3	Expression of the novel Src splice variant xN3	175
5.3.4	Isoform-specific effects of Src overexpression in <i>X.laevis</i>	175
5.3.5	Blocking neuronal splicing of C-Src causes defects in <i>Xenopus</i> locomotion	177
5.3.6	xN1-Src knockdown reduces neuronal marker expression during primary neurogenesis	179
5.4	Conclusion.....	180
6	General discussion.....	183
6.1	Summary of works	183
6.2	Differential regulation of C-, N1- and N2-Src	183
6.3	Neuronal Srcs in development	185
6.3.1	Neuronal Srcs contribute to differentiation of neuronal progenitors .	185
6.3.2	Development: Patterning effects of neuronal Src expression	186
6.3.3	Potential substrates of Neuronal Srcs during development.....	187

6.3.4	Localisation of xN1-Src during development	189
6.4	Neuroblastoma.....	189
6.4.1	The effects of neuronal Srcs on neuroblastoma proliferation and differentiation.....	189
6.4.2	FAK and Paxillin as potential N-Src substrates.....	190
6.4.3	Potential downstream effectors of FAK/N-Src	191
6.4.4	Notch as an N-Src substrate	193
6.4.5	N-Cadherin, Plakoglobin and β -catenin.....	194
6.5	The role of the COPII transport vesicle system in N2-Src function.....	195
6.6	Neuronal Srcs as a therapeutic target in neuroblastoma.....	197
6.7	Final words	198
	Appendices	200
	List of Abbreviations	259
	References	261

List of figures

Chapter 1

Figure 1-1	Src family kinase domain summary	20
Figure 1-2	Crystal structure of the C-Src SH3 domain	26
Figure 1-3	Mechanism of SFK activation	35
Figure 1-4	Genomic map of Src intron and exon sequences	43
Figure 1-5	Model for tissue specific N1-Src expression	50

Chapter 3

Figure 3-1	Western blotting of C-, N1- and N2-Src-FLAG over-expressed in B104 cells	83
Figure 3-2	Effect of N-Src expression on B104 cell morphology	85
Figure 3-3	Characterisation of human neuroblastoma cell lines	88
Figure 3-4	Characterising pSUPER shRNA construct function	90
Figure 3-5	Effect of N-Src knockdown on LAN-5 differentiation	91
Figure 3-6	Effect of N-Src over-expression on SK-N-AS differentiation	92
Figure 3-7	Effect of N-Src over-expression on KELLY differentiation	94
Figure 3-8	The effect of N-Src overexpression on KELLY and SK-N-AS proliferation	96

Chapter 4

Figure 4-1	Generation and characterisation of stable, inducible T-REx HeLa cell lines	111
Figure 4-2	Intracellular localisation of Src splice variants	112
Figure 4-3	Effects of neuronal Src overexpression on HeLa cell morphology	114
Figure 4-4	Effects of neuronal Src overexpression on HeLa cell migration	116
Figure 4-5	Effect of neuronal Src over-expression on HeLa cell proliferation	119
Figure 4-6	Phosphotyrosine immunoprecipitation from T.REx HeLa cell lines	121
Figure 4-7	Summary of LC-MS/MS approach	
Figure 4-8	STRING diagrams of proteins enriched in C-Src or N2-Src samples	124 128
Figure 4-9	In depth analysis of endocytosis associated proteins enriched in N2-Src samples	133
Figure 4-10	In depth analysis of adherens associated proteins enriched in N2-Src samples	134
Figure 4-11	In depth analysis of COPII coat proteins enriched in N2-Src samples	135
Figure 4-12	Identification of Sec23A abundance in T.REx HeLa phosphotyrosine IPs.	138

Chapter 5

Figure 5-1	Effect of xN1-Src on COS7 cell morphology	154
Figure 5-2	Temporal expression of neuronal Src isoforms during <i>Xenopus</i> neurulation	156
Figure 5-3	Effect of mammalian N-Src expression on <i>Xenopus laevis</i> development	159

Figure 5-4	Effect of xN1-Src on <i>Xenopus laevis</i> development	161
Figure 5-5	Confirmation of xN1-Src Morpholino function	162
Figure 5-6	Effects of exon-skipping xN1-Src Morpholinos on <i>Xenopus tropicalis</i> development	164
Figure 5-7	Effects of exon-skipping xN1-Src Morpholinos on n-tubulin expression during primary neurogenesis	166
Figure 5-8	Effects of exon-skipping xN1-Src Morpholinos on Sox3 expression during primary neurogenesis	168
Figure 5-9	xN1-Src Morpholino rescue	170

List of tables

Introduction

Table 1-1	Major post-translational modifications of SFKs	24
-----------	--	----

Materials and methods

Table 2-1	Western blotting antibody concentrations and blocking method	60
Table 2-2	Sequences and PCR conditions of primer pairs used during rtPCR and cloning steps	63
Table 2-3	Antibody combinations and concentrations used in immunocytochemistry	65

Chapter 3

Table 3-1	Summary of cell line characteristics for three human neuroblastoma cell lines	88
-----------	---	----

Chapter 4

Table 4-1	Numeric summary of LC-MS/MS data processing	123
Table 4-2	Summary of C- and N2-Src phosphotyrosine hits from LC-MS/MS	126
Table 4-3	Summary of functionally enriched clusters	131
Table 4-4	Summary of other notable proteins enriched in N2-Src samples	149

List of accompanying material

Figure 5-6 D Video files of the locomotive defects exhibited by *Xenopus tropicalis* embryos injected with control and xN1-Src morpholinos

Acknowledgements

I would firstly like to thank Gareth for his sage council, gentle encouragement and relentless verbal abuse which have served me well in equal parts throughout the duration of my PhD. Thanks also to the Evans lab members Keenan, Wethers and Clare who have provided a friendly and supportive lab environment over the years, and to Ryan and Sarah for introducing me to real ale. I would particularly like to thank members of the *Xenopus* labs for their immense contribution to my research. Without Harv's unyielding enthusiasm for this project and Betsy, Rich, Hannah, Simon, Di and Fiona's help and advice, some of the most exciting portions of this thesis and my experience at York in general would be missing. Thanks also to Adrian Mountford, for his role on my training and advisory panel for the last four years, and Emma for her advice during the writing process. I would also like to thank members of the Centre for Excellence in Mass Spectrometry who were eponymously excellent in both their advisory and practical contributions to this work.

My parents deserve special thanks, without them I would never have made real my ambition of pursuing a career in science. The support and pride expressed by all of my family has always propelled me through the tougher times and for that I owe them a great deal. Lastly, and most importantly, I'd like to thank Lauren. It is no understatement to say that without her, I wouldn't be who I am, where I am, or as happy as I am in life.

Declaration

The work presented in this thesis was performed by the author in the Department of Biology, University of York, in the labs of Dr Gareth Evans and Dr Harv Isaacs. This work has not previously been published, or submitted for examination at this, or any other institution for another award. All experiments were performed by the author, with the exception of liquid chromatography and mass spectrometry, which was performed by Dr David Ashford and members of Centre of Excellence in Mass Spectrometry York as described in the methods.

Introduction

1.1 Regulation by Phosphorylation

Protein kinases and phosphatases catalyse the reversible post-translational modification of protein by the addition and removal of a phosphate group from a compatible amino acid. A protein kinase catalyses the transfer of γ -phosphate from ATP (or less commonly GTP) to an appropriate amino acid substrate, and phosphatases catalyse removal of the phosphate group onto a molecule of water. It is difficult to overstate the importance of protein phosphorylation in the maintenance of eukaryotic life. Protein phosphorylation in some way regulates almost every conceivable process in eukaryotic cells. From proliferation to apoptosis, gene expression to protein degradation, memory to immunity; phosphorylation has a role in transducing the signalling from almost all of the major signalling pathways in the cell. The transient, reversible nature of phosphorylation signalling allows tight temporal control over signalling events and since phosphorylation requires that proteins be in physical contact, phosphorylation is further regulated by intracellular localisation of proteins. Commonly, cell signalling by phosphorylation occurs as part of multi-tiered pathways or signalling cascades; where phosphorylation of one protein activates multiple further phosphorylation events, proliferating the signal throughout the cell. Examples of phosphorylation cascades include the MAP kinase signalling where signalling at the cell membrane activates a cascade of phosphorylation events that leads to activation of gene expression in the nucleus (Cuadrado and Nebreda, 2010). As such, phosphorylation is one of the most prevalent, flexible post-translational modifications, it is estimated that up to 30% of the proteins in the human genome are phosphorylated (Cohen, 2000) and the Phosphosite database identified over 17,000 unique proteins with at least one such modification (Hornbeck et al., 2012).

As the application of phosphorylation is broad, so too are the effects of amino acid phosphorylation upon protein function. Phosphorylation regulates protein function in two main ways, through inducing conformational change of the protein, or by creating or disrupting a site of protein-protein interaction. As such the effect of protein phosphorylation is highly variable, depending heavily upon the structural and cellular context into which the phosphate group is added or removed. Protein phosphorylation can variably induce a protein to be activated or inactivated, degraded

or transported, indeed in many cases multiple phosphorylation sites exist with highly contradictory affects upon a single protein, one phosphorylation site which may activate the protein; another which may mark it for transportation to another subcellular localisation.

With such a diverse range of function and action, it is no surprise that a relatively large proportion of the human genome is given over to the regulation of phosphorylation. Over 518 protein tyrosine kinases have been identified in the human genome, representing in excess of 1.7% of the known human genes (Manning et al., 2002), and around 200 phosphatase proteins which catalyse the removal of phosphate groups (Sacco et al., 2012). Due to their roles in cell signalling, the importance of effective phospho-transferase function is self-evident, and mutation of kinases and phosphatases is known to cause a variety of diseases from cancers to myopathies and diabetes (Cohen, 2001).

1.1.1 Tyrosine phosphorylation

In eukaryotes there are only three amino acids which are commonly phosphorylated; serine, threonine and tyrosine. Of these three, serine and threonine represent the most abundantly detected phosphorylation events, (79% and 17% respectively) whilst phosphorylated tyrosine represents only 4% of total protein phosphorylation events (Olsen et al., 2006). Whilst tyrosine represents a relatively small proportion of phosphorylated amino acids, tyrosine kinases are crucially important to normal cell signalling, so much so that the discovery of many tyrosine kinases was preceded by their discovery in oncogenic viruses, which hijack control of cell proliferation by use of only a few of these proteins (Courtneidge et al., 1980).

Tyrosine phosphorylation was first identified by Eckhart, Hutchinson and Hunter (1979) in studies of polyoma virus. Prompted by the discovery of the tumour inducing viral kinase v-Src (as yet unidentified as a tyrosine kinase), Eckhart and colleagues looked for and identified increased phosphorylation of polyoma virus antigens in infected cells. When attempting to confirm the phosphorylation by gel separation of the separated, ³²P-labeled, amino acids of the polyoma virus antigen immunoprecipitate, Tony Hunter found that the phosphorylated antigen ran between

the phosphothreonine and phosphoserine markers, and subsequently identified the first phosphorylated tyrosine (Hunter and Eckhart, 2004, Eckhart et al., 1979).

Since this discovery, the dysregulation of tyrosine phosphorylation has been strongly associated with oncogenesis. Through both mutated viral versions of mammalian tyrosine kinases, to somatic and germ line mutations and dysregulation of endogenous tyrosine kinases, over half of the 90 tyrosine kinases identified are implicated with human malignancies (Blume-Jensen and Hunter, 2001). This association is due to their importance as signalling regulators of pathways controlling development, proliferation and cell-cell communication. Throughout normal development, tyrosine kinases are crucial in regulating the multiplication of stem cells and the differentiation of those cells to form the tissues of the body. When the tyrosine kinases involved in regulating these processes become dysregulated, control over division is often lost, or in many cases unrestricted proliferation is promoted.

There are two families of protein tyrosine kinases, Receptor Tyrosine Kinases (RTKs) and non-Receptor Tyrosine Kinases (nRTKs). Of the 518 protein kinases identified by Manning and colleagues, 90 were identified as being tyrosine kinases, 58 RTKs, and 32 nRTKs (Manning et al., 2002).

1.1.2 Receptor tyrosine kinases

RTKs are a family of cell-surface receptors which possess extracellular ligand binding domains, and a cytoplasmic tyrosine kinase domains linked by a single membrane spanning helical domain (Lemmon and Schlessinger, 2010). Activation of these RTKs is usually facilitated by ligand-mediated oligomerisation of the receptor, by signalling factors expressed by other cells. Ligand binding draws receptors together, bringing the catalytic intracellular RTK domains close enough to allow trans-activation of their kinase domains via phosphorylation of the kinase activation loop. With the kinase activity enhanced by these trans-activating events, further auto-phosphorylation occurs in other regions of the cytoplasmic domain. These further phosphorylation events often create docking sites for phosphotyrosine binding modular domains, resulting in the recruitment and activation of downstream signalling molecules (Hubbard and Till, 2000). By this method, RTKs initiate signal

transduction cascades beginning with the recognition and binding of extracellular signalling factors and resulting in recruitment of cytosolic proteins which proliferate that signal. With such central roles in cell-cell signalling, RTKs are highly conserved through evolution and mutation of RTKs is implicated in numerous disorders and diseases, most prominently, cancer. Oncogenic signalling by RTKs allows cancer cells to stimulate the ligand-free downstream signalling events usually caused by exogenous growth factors, allowing the uncontrolled proliferation causative of tumour genesis (Lemmon and Schlessinger, 2010).

1.1.3 Non-receptor tyrosine kinases

Of the 90 known protein tyrosine kinase genes, 32 code for non-receptor tyrosine kinases (Manning et al., 2002). By contrast with RTKs the majority of nRTKs are cytosolic, although many associate with membranes via N-terminal post-translational modifications such as myristoylation. Whilst there is considerable functional diversity within nRTKs they generally play roles in trans-cytoplasmic cell signalling, translating signals from receptors, to which they often associate and act as a kinase domain module of receptors without intrinsic kinase activity (Neet and Hunter, 1996).

1.2 Src Family Kinases

The largest family of nRTKs is the Src Family of kinases (SFKs) which in vertebrates comprises 9 proteins Src, Yes, Fyn, Lck, Lyn, Fgr, Hck, Blk and Yrk. The first SFK to be discovered was Src, originally identified by its oncogenic, viral counterpart v-Src as the causative agent of transformation in Rous sarcoma virus, a protein singly capable of cell transformation (Stehelin et al., 1976). Src has since proceeded to the workhorse protein for the study of tyrosine kinases, Src was the first identified proto-oncogene as well as the causative protein behind the phosphorylation event responsible for the first identification of phospho-tyrosine in cells (Brown and Cooper, 1996, Hunter and Eckhart, 2004, Eckhart et al., 1979). Studies of C-Src then prompted a search for related proteins which resulted in identification of the remainder of the Src family kinases.

SFKs can be roughly divided into two groups, those that are expressed only in a limited subset of cells; Lyn, Hck, Fgr, Blk and Lck, and those which are expressed throughout the body; Src, Yes, Fyn and Yrk. This second group of proteins (with the exception of Yrk which has yet to be identified in mammals) are expressed ubiquitously, albeit at differing concentrations in different cell types (Brown and Cooper, 1996). Members of this group have been shown to be compensatory in their function as mouse knockouts of either Src, Fyn or Yes are largely tolerated, with some cognitive and bone-formation impairment (Lowell and Soriano, 1996), however double knockouts Fyn/Yes causes severe renal degeneration and Src/Yes or Src/Fyn knockouts cause prenatal death (Stein et al., 1994).

1.2.1 SFK structure

All SFKs have a common domain structure which feeds strongly into their functions within cells. From N- to C-Terminus each SFK is structured as follows; i) N-terminal membrane associated region (SH4 domain), ii) unique domain, iii) SH3 domain, iv) SH2 domain, v) kinase domain, vi) C-terminal tail region (Fig. 1-1) (Brown and Cooper, 1996). Amino acid positions on SFK proteins will be referred to by their chicken Src numbering throughout this thesis.

1.2.2 The SH4 domain

The N-terminal region of SFKs is essential for the effective association of family members with the plasma membrane and other intracellular membranes (Resh, 1993). Membrane association has been shown to be essential for effective function of SFKs. For example 80-90% of the constitutively active v-Src is membrane localised to the membrane and non-membrane bound mutants of v-Src are incapable of transforming cells (Courtneidge et al., 1980, Cross et al., 1985).

This region, known as the SH4 domain (Resh, 1994), consists of ~15 highly conserved amino acids which are the site of both lipid modification and membrane targeting amino acid sequences of SFKs (Resh, 1993). Myristoylation of the glycine at position two of the N-terminus by N-Myristoyl-transferase occurs in all SFKs and

requires conservation of the 7 most N-terminal amino acids of the SFK (Cross et al., 1984). This irreversible post-translational modification occurs immediately after translation, and, although myristoylation is not singly sufficient to guarantee membrane localisation, without myristoylation SFKs are incapable of localising to the plasma membrane (Buss et al., 1984). Myristoylation is not a specific targeting modification, as N-terminal myristoylation occurs in many other proteins and these proteins are found in various subcellular locations including the ER, Golgi, nucleus and cytoplasm in addition to the plasma membrane (Resh, 1994).

In addition to myristoylation, with the exception of Src and Blk, SFKs are also palmitoylated at N-terminal cysteine 3 which contributes further to membrane association but requires pre-existing myristoylation (Koegl et al., 1994). Whilst post-translational addition of the myristoyl group is permanent, palmitoylation appears to be reversible (Paige et al., 1993) suggesting that palmitoylation of the SFK is dynamically regulated by the cell in order to change cellular localisation and activity. Palmitoylation appears to be important in enhancing the myristoyl-derived membrane

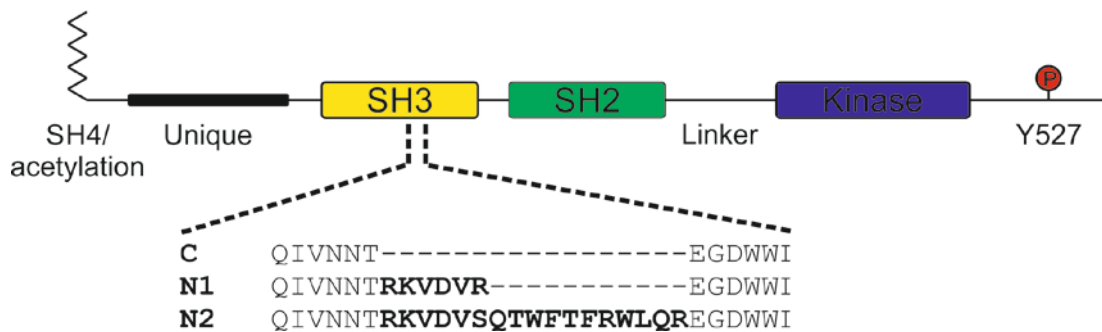


Figure. 1-1. Src family kinase domain summary.

SFKs all share a common domain structure. The length of each domain is as follows (human numbering) SH4: 1-15, Unique: 15-84, SH3: 84-145, SH2: 151-248, Kinase 270-523. The N-terminal SH4 domain is the principal site of membrane association, containing both sites of myristoylation and palmitoylation. The unique domain is an intrinsically disordered region with no tertiary structure and varies greatly between SFKs. The unique domain is the site of extensive post-translational modification and regulatory actions by interacting enzymes. SH3 domains are modular protein binding domains with specificity for left-handed type II polyproline (PPII) helices on substrates. The SH3 domain is also crucial for intramolecular inhibition of kinase activity through binding to the SH2-kinase linker sequence. The sequences of the three Src splice variants (C-, N1-, and N2-Src) are indicated below and insert into the SH3 domain. SH2 domains bind to phosphotyrosine residues, in both auto-inhibitory intramolecular (T527) and a substrate-specifying, activating capacity. The kinase domain is the catalytic site of src activity, transferring the γ -phosphate from ATP onto substrate tyrosine residues. Though each SFK contains these modular domains there are sequence and structural differences in each domain of each protein, resulting in the unique regulation and substrate specificity that affords them their functional differences.

affinity of SFKs. In experiments upon two Hck splice variants unpalmitoylated p59-Hck and palmitoylated p61-Hck only 30% of the unpalmitoylated splice variant associates with membranes, compared to the completely membrane associated p59-Hck variant which is palmitoylated. When the palmitoylation of these two variants is reversed by mutation of the N-terminal domain, 70-75% of p61-Hck is membrane associated, and no p59-Hck is identified at the membrane (Robbins et al., 1995). This suggests that the reversible palmitoylation of SFKs, alongside other localisation signals, can act to variably localise SFKs to membranes, as such exposing them to a different subset of substrates and facilitate different protein-protein interactions.

Whilst Src and Blk are not palmitoylated, their membrane affinity is enhanced in the SH4 region by inclusion of basic arginine residues at positions 14-16 (Resh, 1994, Kim et al., 1991). These residues are thought to act in a similar fashion to basic residues observed around other myristoyl regions, where local highly basic regions interact with the acidic phospholipids of membranes (Kim et al., 1991, Ben-Tal et al., 1996). Association with membranes as promoted by the SH4 domain allows for the SFKs to interact with important receptors and substrates. Without this capacity these kinases would be incapable of performing their functions within the cell, as demonstrated by the failure of unmyristoylated v-Src to transform cells (Cross et al., 1985).

1.2.3 The Unique Domain

Following the SH4 domain is the eponymous unique domain which is the main site of variance between the different family members. Unlike other well characterised domains, the divergence between the sequences of the unique domain means that no single function for all family members has been identified in this region. The unique domain is between 50 and 80 amino acids in length and is an Intrinsically Disordered Region (IDR), a region of protein sequence which lacks tertiary structure. The many IDRs across the proteome are variable in their function however mutation in IDRs of intrinsically disordered proteins has previously been shown to result in the loss of important post translational modifications and aberrant interactions with physiological partners (Uversky et al., 2008, Li et al., 2010). As such it is apparent that whilst IDRs lack a tertiary structure, they are accessible to enzymes as both substrates, and as

protein-protein interaction partners (Amata et al., 2014) Several of these interactions are summarised in Table 1-1.

In the SFK Lck residues in the unique region form disulphide bonds to the transmembrane receptors CD4 and CD8 (Shaw et al., 1989). Phosphorylation of S59 has been identified during mitosis and is shown to regulate the specificity of the SH2 domain (Joung et al., 1995, Kesavan et al., 2002). This phosphorylation also decreases the interaction between Lck and Nck, an adaptor protein involved in signal transduction by association with plasma membrane elements. Phosphorylation of Lck at S59 ablates interaction between Nck and Lck, and has been shown to modify Lck mediated activation of signalling events (Vazquez, 2007). Similarly, Fyn and Lyn may also form low affinity contacts with B and T cell antigen receptors via their unique domains which act concomitantly with high affinity SH2 binding to phosphotyrosine sites (Clark et al., 1994b).

Phosphorylation of tyrosine residues between position 25 and 34 has been identified in Lyn, Hck, Lck, Yes and Fgr (Hornbeck et al., 2012, Ariki et al., 1997, Oppermann et al., 2009). In Lyn Y32 is phosphorylated by the EGF receptor, which leads to phosphorylation of MCM7 and an increase in cellular proliferation. *In vivo* Y32 is identified in breast cancer cells with a poor prognosis (Huang et al., 2013). In Fgr, phosphorylation in this region is detected at a higher rate in leukaemia patients (Oppermann et al., 2009). Interestingly, it has been shown that Hck is capable of autophosphorylating both the activation loop of the kinase and also Y29 of the unique domain. This increases the activity of the kinase by 2 fold, contributing towards a 20-fold increase in activity when both the activation loop of the kinase domain and Y29 are phosphorylated in unison (Johnson et al., 2000).

In Fyn, phosphorylation of Y28 shows similarity with Hck Y29 phosphorylation, significantly increasing activity of the kinase when phosphorylated by the stimulated PDGF receptor. Y28F mutation shows that Fyn activation by stimulated PDGFR is significantly decreased suggesting a crucial role in the phosphorylation of this residue in activation of Fyn in response to membrane signalling (Hansen et al., 1997).

Both Fyn and Src contain the conserved PKA substrate motif RxxS in their unique domains, and in Fyn this serine residue (S21) is specifically targeted by PKA.

This has been shown to have functional implications upon Fyn association with FAK as perturbing Fyn phosphorylation by PKA appears to negatively affect Fyn activity, resulting in a decrease in migration (Yeo et al., 2011).

Src, being arguably the most well studied and characterised SFK, has an extensive amount of literature on its function, providing an interesting mechanistic insight into its roles in Src localisation and degradation. As previously mentioned, Src associates with the acidic phospholipids of membranes through a highly basic region of three arginine residues at sites 14-16 (Resh, 1994). This electrostatic interaction is disrupted by the phosphorylation of S17 in PDGF stimulated cells by PKA phosphorylation. This phosphorylation brings a positive charge close to the site of electrostatic interaction, resulting in Src detaching from the plasma membrane and localising in the cytosol (Obara et al., 2004). This phosphorylation event is required for some of the cellular effects of cAMP treatment including Rap1 activation and inhibition of cell growth.

In addition to interaction with membranes through myristoylation and the triple arginine site, Src has recently been shown to interact with membranes via its unique domain, in a partially structured region termed the Unique Lipid Binding Region (ULBR) (Pérez et al., 2009). This 15 amino acid region (positions 60-75) possesses a strong electrostatic affinity for negatively charged lipids and when mutated, causes a conditional lethal phenotype in *Xenopus* oocytes (Pérez et al., 2013). The affinity of the ULBR is disrupted by flanking phosphorylation events at T37 and S75, which, similar to S17 phosphorylation, cause electrostatic repulsion from acidic membranes. These sites are phosphorylated by CDK1 in a cell-cycle dependent manner. Phosphorylation by CDK1 of T37 and S75 also causes a decreased affinity for intramolecular binding of the SH2 domain to phosphorylated Y527, an auto-inhibitory interaction, resulting in increased activity (Shenoy et al., 1992, Stover et al., 1994). This dual effect of repulsion from cell membranes and activation of Src activity could function to increase association of active Src with cytosolic substrates which drive cell cycle progression and proliferation; similar to in v-Src transformation where 60% of v-Src is located in the cytosol (Bjorge et al., 2000, Willingham et al., 1979).

Table 1-1. Major post-translational modifications of SFKs.

Each SFK has a unique pattern of protein interactions, many of which regulate the protein via post-translational modification. Some, such as N-terminal myristoylation, Y416 phosphorylation and Y527 phosphorylation are shared between all SFKs whilst others are unique to each protein.

Domain	Group	Site	Affected SFK(s)	Effect	Reference
N-terminus	Myristoyl	G2	All	Membrane localisation	(Cross et al., 1984)
	Palmitoyl	C3	All except Src, Blk	Dynamic, reversible membrane localisation	(Paige et al., 1993, Koegl et al., 1994)
Unique domain	Phosphate	S12, S17	Src	Disrupts electrostatic association of R14-16 with plasma membrane phospholipids	(Obara et al., 2004, Resh, 1994, Yaciuk et al., 1989)
	Phosphate	S21	Src, Fyn	Phosphorylated by PKA. Decreases Fyn association with FAK	(Yeo et al., 2011)
	Phosphate	Y25-Y34	Fgr, Hck, Lck, Lyn, Yes,	Various, increased phosphorylation often associated with oncogenesis	(Hornbeck et al., 2012, Ariki et al., 1997, Oppermann et al., 2009)
	Phosphate	Y28	Fyn	Increases kinase activity, Phosphorylation stimulated by PDGFr	(Hansen et al., 1997)
	Phosphate	Y29	Hck	Increases kinase activity	(Johnson et al., 2000)
	Phosphate	Y32	Lyn	Phosphorylated by EGF receptor, leads to MCM7 phosphorylation and proliferation	(Huang et al., 2013)
	Phosphate	T34, T46, S72	Src	Cell cycle dependent CDK1 phosphorylation decreases SH2 affinity for pY527	(Shenoy et al., 1992, Stover et al., 1994, Roskoski, 2005)
	Phosphate	S59	Lck, possibly others	Regulation of binding specificity of SH2 domain	(Joung et al., 1995, Kesavan et al., 2002)
	Phosphate	S69	Src	Appears mutually exclusive with S72 phosphorylation, may attenuate CDK5 S72 degradation pathway	(Pérez et al., 2013, Oppermann et al., 2009, Amata et al., 2014)
Phosphate	S72	Src	CDK5 phosphorylation targets active Src for ubiquitin-mediated degradation	(Pan et al., 2011)	
Kinase domain	Phosphate	Y416	All	Activating phosphorylation of the kinase domain	(Kmiecik and Shalloway, 1987)
C-terminus	Phosphate	Y527	All	Inhibitory phosphorylation, bound by SH2 constraining kinase activity	(Cooper et al., 1986)

Although phosphorylation of S75 usually occurs by CDK1 in a cell-cycle dependent manner in both neurons and some cancer cell lines, S75 is also phosphorylated by CDK5 independent of cell cycle, although this is dependent upon Src activity rather than cell cycle progression (Kato and Maeda, 1999). CDK5 phosphorylation of S75 of active Src targets Src for ubiquitination and cullin-5-dependent degradation (Pan et al., 2011). In addition to its role as a kinase of S17 in Src, PKA actively suppresses dephosphorylation of Src at Ser75 by phosphatases, suggesting a support role for PKA in the degradation of active Src (Amata et al., 2013). This S75 linked degradation is likely a control mechanism to prevent a loss of cell cycle control as a result of an accumulation of activated Src, similar to that seen in v-Src. This phosphorylation event is mutually exclusive to phosphorylation of S69, as identified in an assay where the unique domain of Src with *Xenopus* cell extracts (Pérez et al., 2013). To date, the S69 phosphorylation has only been identified in humans has in cancer cell lines (Oppermann et al., 2009), suggesting that degradation of active Src by S75 phosphorylation may be being attenuated by S69 phosphorylation in these cells (Amata et al., 2014). As Src is a potent oncogene the maintenance of a large pool of active Src would be positively selected for by cancer cells, and S69 phosphorylation may mediate that effect.

In addition to the regulation of membrane binding and protein degradation in the Src unique domain, Perez and colleagues also identified an intramolecular interaction between the unique domain and the SH3 domain (Pérez et al., 2013). This interaction has to date only been identified by Nuclear Magnetic Resonance (NMR) spectroscopy, and as such the function of this interaction, if it occurs *in vivo*, is not yet known (Pérez et al., 2013). Whilst until recently the functions of the unique domain of SFKs have proven enigmatic to researchers, studies in the last ten years have provided an insight into the regulation of Src activity, binding, localisation and degradation facilitated by the unique domain.

1.2.4 The SH3 domain

The Src Homolog 3 domain is a non-catalytic, globular domain of between 55 and 75 amino acids in length. SH3 domains are a highly conserved modular domain present throughout evolution, in all eukaryotic life (Kaneko et al., 2008), as well as in

viruses and prokaryotes (Whisstock and Lesk, 1999). Originally identified in the adaptor protein Crk (Mayer et al., 1988), over 300 other SH3 domains have been identified in the human genome since (Kärkkäinen et al., 2006), making the SH3 one of the most abundant protein modules found in nature. Whilst SH3 domains are found in a large variety of different proteins with a plethora of functions - from GTPase activating proteins, to phospholipases, kinases, phosphatases, adaptor proteins and beyond - they usually function in the same way; as a protein-protein, or occasionally as a protein-lipid, interacting module.

In the case of SFK proteins, the SH3 carries out important roles in substrate recognition, regulation of kinase activity, and intracellular localisation (Gmeiner and Horita, 2001, Sriram et al., 2011). Src was the first SFK to have the structure of its SH3 domain solved (Yu et al., 1992), swiftly followed by Fyn (Noble et al., 1993) (Fig 1-2). Yu and colleagues identified that the Src SH3 domain consists of two three stranded anti-parallel β -sheets, these sheets are packed against each other at approximately right angles, with the interface between the sheets forming the hydrophobic core of the domain (Yu et al., 1992). This hydrophobic region, in the fold between the two β -sheets, forms the binding face of the SH3 domain and contains the distal, RT and n-Src loops which connect the β -sheets (Musacchio et al., 1992, Ren et al., 1993, Brannetti et al., 2000). Yu and colleagues also identified that the C-

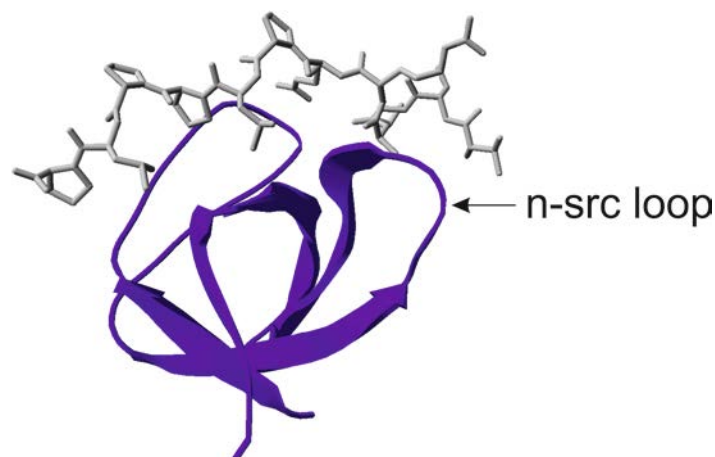


Figure. 1-2. Crystal structure of the C-Src SH3 domain.

The C-Src SH3 domain (purple) bound to the class I ligand VSL12 (grey), from the crystal structure solved by Feng and colleagues, 1995. The side-chains of the amino acids forming the binding face of the SH3 domain interact with ligands at three points, forming two hydrophobic 'recognition pockets' which bind proline, and one 'specificity pocket' which binds to arginine or lysine. The site of the n-src loop (indicated) partially forms the specificity pocket and is the site of N1- and N2-Src exon inclusion. Image of crystal structure provided by Dr Gareth Evans. PDB code 1QWF.

and N- terminal peptides of the SH3 domain were located adjacent to each other which suggests that the extensive use of the SH3 domain as a protein module throughout evolution is, at least in part, due to the ability to incorporate it into a protein with minimal disruption to the surrounding structure (Yu et al., 1992).

SH3 domains predominantly bind to short, proline-rich regions on target substrates. The high proline content of these regions typically means that they adopt a left-handed type II polyproline (PPII) helix conformation when bound (Yu et al., 1994). These proline rich regions typically match either Class I R/KxPxxP or Class II PxxPxR/K motifs (Zarrinpar et al., 2003), with both motifs binding a single recognition surface of the SH3 in opposing N- or C- terminal orientations (Yu et al., 1994, Feng et al., 1994, Lim and Richards, 1994, Lim et al., 1994). Recognition of these motif is accomplished by insertion of the ridges of the PPII helix into a complementary pair of 'recognition' pockets on the SH3 surface, defined by well-conserved aromatic residues (Zarrinpar et al., 2003). Adjacent to this core region of recognition are the RT and n-Src loops which form a third pocket, the 'specificity pocket', by making several unique interactions with the ligand residues flanking the core PxxP ligand motif (Kay et al., 2000, Shi et al., 2010).

Although adherence to the core R/KxPxxP or PxxPxR/K is important for binding specificity, these motifs allow for considerable sequence variation with little impact on the relatively weak binding affinity of this core sequence (Rickles et al., 1994). Rickles and colleagues identified the importance of flanking residues by using a biased phage display library based upon their previously established core motifs, and expanding these motifs in both N- and C- terminal directions (Rickles et al., 1995, Feng et al., 1995). In these experiments they identified that within the core binding of the SH3 domain, the two 'recognition' pockets functioned as two xP dipeptide binding pockets docking via hydrophobic interactions. The third 'specificity' pocket forms a salt bridge between the positively charged substrate arginine or lysine and tryptophan W118 (Feng et al., 1995, Rickles et al., 1995).

In addition to canonical Class I and Class II ligands, the binding face of the SH3 domains can make interactions with non-consensus ligands. Unlike canonical Class I and Class II ligands, non-consensus binding does not always require the ligand to adopt a typical PPII helical conformation, and often these ligands do not make use

of both xP-binding pockets of the SH3 domain. In addition to an unusually strong binding affinity, non-canonical binding to the SH3 is also notable for its extensive interaction with the specificity pocket. Whilst salt bridge formation between Class I and Class II ligands and the specificity pocket also dictate the orientation of binding, resulting in the canonical form of binding described above, non-canonical ligands make more elaborate sets of contacts with the residues of the specificity pocket, contributing to both the specificity and affinity observed for this region (Saksela and Permi, 2012).

This versatility of SH3 domain binding contributes in part to the diversity seen between SFKs, whilst all SFKs appear to maintain commonality in the two hydrophobic recognition pockets of their binding face, considerable diversity of both amino acid sequence and conformation is observed in the loops that make up the specification region (Noble et al., 1993).

In addition to the protein-protein interactions of the SFK SH3 domain, and the intramolecular binding of the SH3 to the SH2-kinase domain linker (discussed extensively in 3.1) the Src SH3 domain has also been implicated in lipid binding. Isolated fragments of the SH3 were shown to bind lipids both independently, and in combination with unique domain binding. This interaction occurred on the opposing face of the SH3 domain to the protein-protein interaction face of the SH3 (Pérez et al., 2013). This same study was the first to reveal that the SH3 was capable of interacting with the unique domain *in vitro*. This interaction was shown to be abolished by SH3 binding to a typical RXPxxP SH3 peptide ligand, probably due to allosteric interference as, although peptide and lipid binding occur on opposing faces of the SH3 domain, both rely upon the n-src and RT loops for binding (Pérez et al., 2013). This implies that, whilst the SH3 domain can bind to this region of the unique domain, it does not do so in the presence of a peptide substrate.

1.2.5 The SH2 domain

The Src homology 2 domain (SH2), is a modular non-catalytic phosphotyrosine binding domain of approximately 100 amino acids (Moran et al., 1990, Matsuda et al., 1990, Liu et al., 2006). SH2 domains are the largest class of

phosphotyrosine binding domain in the human proteome, found in 111 proteins (Liu et al., 2006), and have been identified immediately prior to the evolution of multicellular organisms reflecting their importance in regulation of higher order signalling pathways (Li et al., 2008).

Binding by SH2 to phosphotyrosine residues is both high affinity, and highly sequence specific, requiring a conserved amino acid sequence in the region surrounding the target phosphotyrosine. In an assay to identify sequence specificity of the SH2 domain, SFK SH2 domains were tested against a library of phosphotyrosines and demonstrated remarkable conservation of sequence specificity, all selecting the motif of pY-E-E-I (Songyang et al., 1993). More in depth study of this sequence specificity later identified that residues pY - 2 and pY + 4 residues either side of phosphotyrosine significantly impacted sequence specificity of SH2 binding (Filippakopoulos et al., 2009).

Structurally, the SFK SH2 is formed from a β -meander, formed of two distinct β -sheets flanked on either face by two α -helices. The central β sheet forms the core of the structure, dividing the SH2 into two distinct sides; one side is primarily concerned with binding phosphotyrosine, the other binds the three residues in positions pY + 1, pY + 2 and pY + 3. The crystal structures of substrate bound Src and Lck SH2 domains revealed remarkably similar substrate binding structures (Eck et al., 1993, Waksman et al., 1993). Though seven amino acids of the substrate, from pY - 2 to pY + 4, make some contact with the SH2 domain. pY - 2, pY - 1 and pY + 4 have their functional groups face away from the SH2, and as such have only a weak affinity for the SH2 domain. The main portion of the binding affinity for the SH2 domain, arises from pY to pY + 3, hence the highly specific pYEEI binding identified by Songyang and colleagues for SFKs (Songyang et al., 1993). The flat surface of the central β -sheet supports the weak ionic hydrogen bonding of glutamic acid residues at pY + 1 and pY + 2, whereas pY and pY + 3 fall into high affinity 'pockets' resulting in 'two pronged' binding of these residues (Songyang et al., 1993). The principal difference observed by Waksman and colleagues between high and low affinity SH2 domain binding was the pY + 3 isoleucine, this resulted in increased overall affinity of peptide binding by binding tightly to a number of hydrophobic residues forming a deep 'hydrophobic pocket' on the face of the SH2 opposing phosphotyrosine binding (1993). Phosphotyrosine binding by the SH2 domain occurs in a well formed pocket

of positively charged residues (Waksman et al., 1993). The central residue in this interaction is R175, which forms specific hydrogen bonding interactions between the two terminal nitrogens and the two phosphate oxygens. Since arginine is the only amino acid capable of forming this highly specific interaction, mutation of R175 results in loss of SH2 binding (Waksman et al., 1992).

Though SH2 domains appear to have originally evolved in pre-metazoans to promote processive phosphorylation of kinase substrates, where one phosphorylation event is bound by the SH2 domain, providing an anchor for further kinase phosphorylation of the same protein (Mayer et al., 1995), this role has been extensively elaborated in modern SFKs. Processive phosphorylation of the ζ chain of the T-cell receptor by Lck (Lewis et al., 1997), and hyperphosphorylation of p130CAS by v-Src are just two of many identified processive phosphorylation events in mammalian cells (Pellicena and Miller, 2001). With the complexity of multicellular signalling, SH2 domains assumed an additional regulatory role, with regulated intramolecular binding causing allosteric regulation of kinase activity (Kuriyan and Eisenberg, 2007). In SFKs, phosphorylated Y527 (or equivalent) binding by the SH2 domain results in a stable, compact and inactive conformation of the kinase, wherein the SH2/pY527 inhibits kinase domain auto-phosphorylation by fixing the lobes of the kinase domain in an 'open' conformation. This interaction between the SH2 domain and pY527 is not optimal, meaning that the SH2 domain is displaced from its auto-inhibitory interaction by the presence of a phosphotyrosine residue on a substrate protein. This has the dual effect of targeting the SFK to the substrate protein, in addition to relieving the inhibition on kinase activity, effectively targeting and activating the protein in one binding action, such as occurs with the putative Src substrate Focal Adhesion Kinase (FAK) (Thomas et al., 1998). The importance of SH2 binding for auto-regulation will be discussed extensively in **3.1**.

1.2.6 The kinase domain.

The kinase domain is the catalytic site of tyrosine phosphorylation in SFKs. The kinase domain in SFKs possesses the characteristic bi-lobed protein kinase structure shared by both tyrosine, and serine/threonine kinase domains (Boggon and Eck, 2004). The smaller of the two lobes is located N-terminally, and is composed of

five β -strands and a single α -helix. The N-terminal lobe, by contrast with the more rigid C-lobe, is much more flexible, with a conserved glycine-rich loop that allows entry of ATP into the region of catalysis. The large C-terminal lobe, is predominantly composed of α -helices with the exception of a β -sheet present at the active site cleft. Importantly this is the lobe which contains the regulatory activation loop, the site of the important phosphorylation event which is required for activation of the kinase domain (Kmieciak and Shalloway, 1987). In addition the C-terminal lobe contains the catalytic loop, important for the catalytic activity, as well as the P + 1 loop which recognises and docks with the peptide sequence around tyrosine substrates (Boggon and Eck, 2004, Hubbard et al., 1994, Knighton et al., 1991, Yamaguchi and Hendrickson, 1996).

Active kinase domains catalyse the phosphorylation of tyrosine by combined action of the two lobes, the movement between the two lobes opening and closing the catalytic site (Ozkirimli and Post, 2006). When the site of catalysis is open, the kinase can bind to ATP and substrate peptides, and closing of the domain causes the catalytic activity, transferring the γ -phosphate of ATP to the substrate tyrosine. The importance of the phosphorylation of the activation loop of the kinase domain is in the resultant stabilisation of the kinase domain within the rigid structural restrictions that phosphorylation requires (Brown and Cooper, 1996, Roskoski, 2005). This stabilising effect of activation loop phosphorylation upon the kinase domain is elegantly demonstrated by Huse and colleagues (2002) who highlight the extensive variability in protein structure between different inactive kinase domains by contrast with the highly conserved structure of those domains once activated.

After the identification of this activating phosphorylation event in 1981 (Smart et al.), debate emerged around whether this phosphorylation event was occurring intramolecularly, or as the result of interaction between two separate Src proteins. It has since been confirmed that both of these modes of action are possible. Sugimoto and colleagues confirmed that intra-molecular auto-phosphorylation occurs through assessing that the rate of auto-phosphorylation of v-Src was independent of concentration and aggregation (Sugimoto et al., 1985). Later experiments identified activation loop phosphorylation in catalytically dead kinase domain mutants, confirming that trans-phosphorylation between proteins was also possible (Cooper and MacAuley, 1988).

Although considerable kinase substrate specificity is established through the sequence specificity of both SH3 and SH2 binding, which allows the docking of kinase to substrate, the kinase domain itself also plays a major role in substrate determination (Songyang et al., 1995). This fact was demonstrated by transplanting the kinase domain from viral versions of the tyrosine kinase Src into another, ErbB (Chang et al., 1995). Both of these viral oncogenes have distinct phosphorylation profiles and cellular phenotypes when overexpressed in cells, and the chimera protein was screened for both of these characteristics. The ErbB/Src chimera protein presented a phosphorylation profile somewhere between that of Src and ErbB, however a distinctly Src-like effect upon fibroblast cells which were transformed in a manner typical of v-Src expression (Chang et al., 1995). This study demonstrated that although there was extensive conservation of structure within kinase domains, significant variance existed in the substrate proteins targeted by the kinase domains of different proteins.

An extensive study pairing a peptide library with a selection of protein tyrosine kinases identified considerable variance in substrate specificity existed between kinase domains, even between different SFKs (Songyang et al., 1995). Whilst the optimal C-Src kinase domain motif was identified as E-E-I-Y-[G/E]-E-F-F, the motif for Lck was divergent and lower in specificity, with a consensus of E-X-[I/V/L]-Y-G-V-[L/V/F/I]-F. The major outcome from the perspective of SFK structure was that the cytosolic protein tyrosine kinases, including SFKs, demonstrated a kinase substrate preference remarkably similar to their own SH2 domain substrate preference (Songyang et al., 1995). This led to the conclusion that kinase domain is creating binding sites for the SH2 domain, a correlation which enables multi-site, processive phosphorylation. Multi-site phosphorylation has wide ranging implications on protein signalling, as specific patterns of phosphorylation create unique effects upon the micro-environment of the substrate amino acids, in addition to the bulk effect of multiple phosphorylation events changing the charge of large regions of the protein (Patwardhan and Miller, 2007).

1.2.7 The C-terminal Tail

The final 15-17 amino acids at the carboxyl-terminus of SFKs are notable principally for the conserved tyrosine residue (Y527 in C-Src). This tyrosine residue is a critical of phosphorylation in SFKs as phosphorylation at this site causes auto-inhibitory intramolecular binding by the SH2 domain (Cooper et al., 1986). Regulation at this site most notably occurs via phosphorylation by the eponymous C-terminal Src Kinase (Csk) (Bergman et al., 1992) in addition to the closely related Chk (Chong et al., 2005). In spite of significant divergences in sequences of the various SFKs, the C-terminal tail is highly conserved, allowing Csk to act as a master regulator of all SFKs (Nada et al., 1993, Imamoto and Soriano, 1993).

1.2.8 Regulation of Src

Effective regulation of Src activity is crucial to its normal cellular function. Src has roles in signal transduction pathways involved in cell motility, survival and proliferation, making dysregulated Src a potent oncogene. This is no better characterised than in the viral oncogene v-Src, which is singly capable of transforming cells (Brugge and Erikson, 1977). The transforming potential of v-Src is less the result of changes to substrate specificity of Src rather than of uncontrolled activity caused by mutation or deletion of important sequences of auto-inhibition (Smart et al., 1981).

The oncogenic potential of Src necessitates the many, complex inter- and intra-molecular mechanisms employed in its regulation. Src is extensively regulated by auto-inhibition, however an overlooked manner of regulation is mediated through the unique domain. Studies in v-Src have demonstrated that mutations in v-Src which prevent N-terminal mediated membrane localisation becomes incapable of cell transformation (Cross et al., 1985). As discussed in **2.2**, Src localisation to membranes can be dynamically regulated by post-translational modification of its unique domain, which invariably regulates substrate phosphorylation (Pérez et al., 2013). Additionally unique domain phosphorylation at S75 of active Src has been identified as a marker for ubiquitin-mediated protein degradation (Pan et al., 2011). By this method the cell appears to be able to regulate the quantity of active C-Src present, and there are indications that the mutually exclusive S69 phosphorylation could further

regulate this degradation by acting as a protective phosphorylation event (Amata et al., 2013).

Intramolecular inhibition of Src is regulated by three main features of its architecture; the binding of the SH3 domain to the SH2-kinase linker; the binding of the SH2 domain to phosphorylated Y527 and the inhibiting the phosphorylation of the kinase domain activation loop. These three components work in a co-ordinated fashion to assure that Src remains in its inactive state. I will first discuss the mechanism behind each of these independently before addressing their co-ordination.

Phosphorylation of Y527 of Src by Csk, and the resultant intramolecular SH2 binding, is a fundamental component of C-Src inhibition. Experiments which have eliminated this regulation, both by Y527F mutagenesis and by Csk knockout have demonstrated that this causes constitutive activation of Src, resulting in an increase in its transforming potential and, in Csk knockout mice, embryonic lethality (Oneyama et al., 2008, Imamoto and Soriano, 1993, Nada et al., 1993). SH2/pY527 binding mediates auto-inhibition by forcing Src into a partially closed conformation, made completely closed when the SH3 domain binds to the SH2-Kinase linker. The motif around Y527 that is bound by the SH2 domain is interestingly not an ideal Src SH2 binding motif, replacing the important Y + 3 isoleucine residue, vital for the 'two pronged binding' discussed in 2.3 with a glycine. As such the SH2/pY527 binding is relatively low affinity, allowing for dynamic regulation that can be displaced by the presence of an appropriate substrate molecule. For example the integrin activity-mediated phosphorylation of the Focal Adhesion Kinase (FAK) provides an optimal SH2 binding motif for Src which results in displacement of SH2 domain from pY527 (Parsons and Parsons, 1997). This binding results in phosphatase activity on Y527 furthering the activation of Src phosphorylation.

SH2/pY527 mediated inhibition of Src works in combination with SH3 mediated auto-inhibition. The SH3 domain of Src binds to canonical Class I and Class II ligands which are proline rich and adopt PPII type - left-handed helical conformations. The SH2/kinase domain linker sequence (henceforth referred to as the 'linker' sequence), despite containing only one proline residue, adopts a PPII helical conformation, which allows weak binding by the SH3 domain to this region. This has a dual effect on cell regulation, simultaneously sequestering the binding capacity of

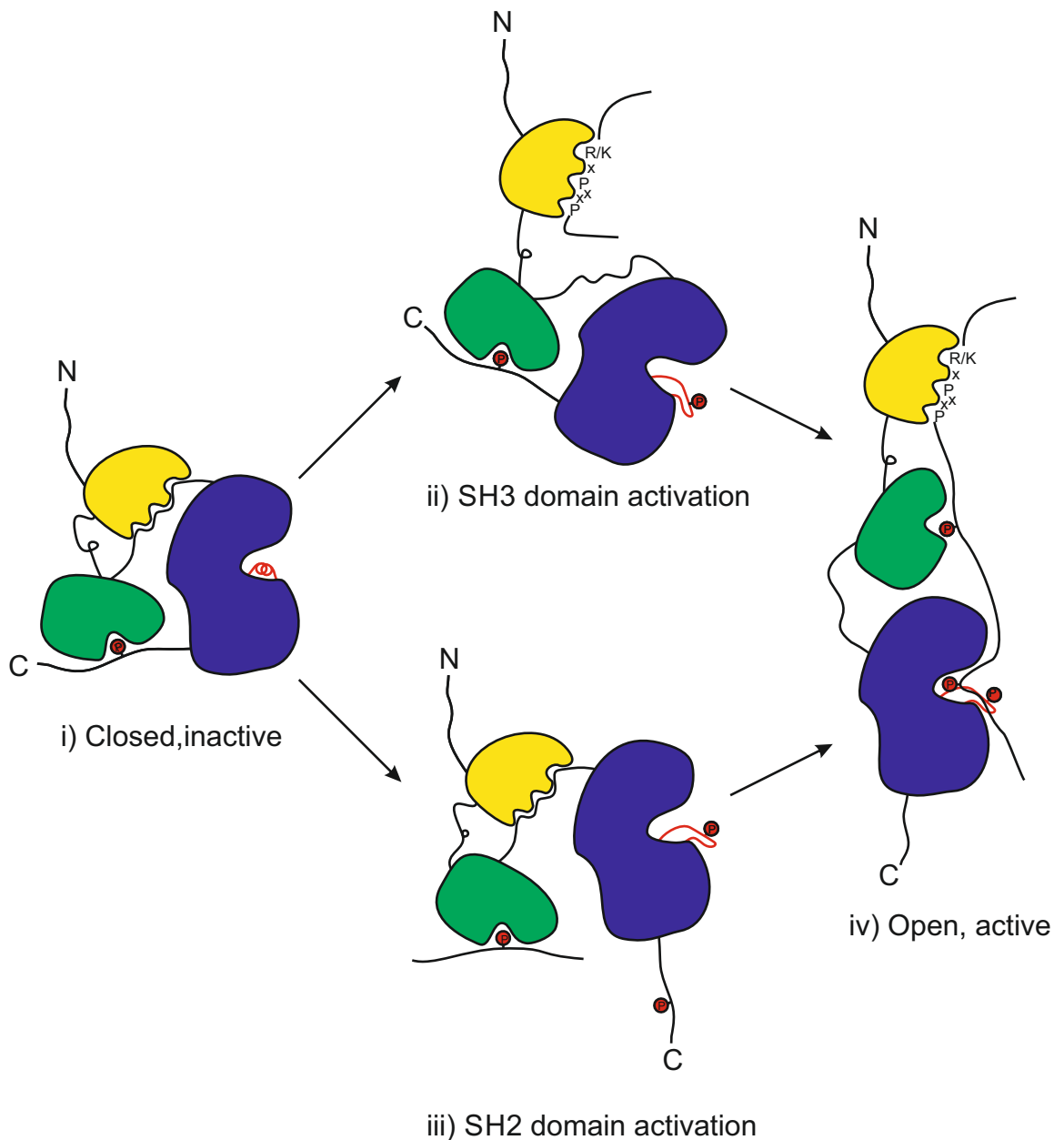


Figure 1- 3. Mechanism of SFK activation.

i) In a closed inactive conformation (i) autoinhibition of SFKs occurs via SH3 (yellow) binding to the SH2 domain-kinase domain linker sequence and SH2 binding (green) to phosphorylated tyrosine 527. These two regulatory events affect kinase domain (blue) folding, causing the kinase domain to be held in a more open, disordered state. Whilst in this conformation the activation loop of the kinase domain forms an alpha helix which prevents phosphorylation of Y416. The intramolecular interactions of the SH2 and SH3 are sub-optimal and displaced in the presence of a superior ligand. This binding of the SH2 (ii) or SH3 (iii) domains to a substrate allows partial activation of the protein and phosphorylation of the activation loop of the kinase domain. In the fully active conformation (iv) both the SH3 and SH2 domains are displaced from their internal binding events. It is still unclear whether displacement of one intramolecular interaction is sufficient to displace the other or whether a fully active conformation is the result solely of substrate binding.

the SH3 domain for weaker binding motifs, and also contributing to the SH2-SH3 mediated, kinase inhibiting, and closed Src conformation. Due to the lack of a PxxP motif in the linker, the SH3 domain is readily displaced by superior ligands, allowing situational activation of Src where appropriate. The importance of the SH3/linker interaction was demonstrated by mutagenesis of the PPII helical region of the linker, which prevented binding of the SH3 domain to the linker, causing constitutive activity of the Src and a transforming phenotype (Potts et al., 1988).

This closed Src conformation was observed and described in the first crystal structure of a whole Src molecule (Xu et al., 1997, Williams et al., 1997, Xu et al., 1999) (Fig. 1-3). Although the SH2/pY527 interaction was already identified in previous studies, the interaction between the SH3 domain and the SH2-kinase linker and its effects on auto-inhibition were entirely without precedent. In the closed conformation, intramolecular SH2/pY527 and SH3/linker binding pulls the SH2 and SH3 domains together and against the kinase domain, on the opposing surface to its catalytic site. In the “closed” conformation the SH2 and SH3 domains do not physically block substrate access to the catalytic site, instead they induce and maintain distortions of the active site indirectly through SH3/N-lobe and SH2/C-lobe interactions. Kinase inhibition was observed in the crystallographic structure to occur in three main ways. Firstly the activation loop adopts an α -helical motif which prevents binding of substrate sequences to the catalytic cleft of the kinase domain. Secondly, catalysis is prevented by displacement of the catalytically important E310 residue from the active site. Finally the SH3 and SH2 domains restrict the conformational flexibility of the N- and C-lobes of the kinase domain, preventing the domain from re-adjusting into an active conformation (Williams et al., 1997, Boggon and Eck, 2004) (Fig. 1-3). More recent studies have also identified that SH2 and SH3 mediated inhibition hides the activating Y416 residue by steric interference, preventing its phosphorylation (Huse and Kuriyan, 2002).

Through use of weak sub-optimal intramolecular binding motifs, Src is maintained in an inactive conformation in the absence of a suitable ligand. When a substrate protein is within proximity of Src, possessing either a superior SH3 or SH2 ligand, the “closed” configuration is readily reversed, freeing the kinase domain to reconfigure into an active conformation. This then allows auto-phosphorylation of the activation loop and full activation of Src kinase activity, only where appropriate

1.3 Cellular functions of Src

The list of cellular substrates of C-Src is long and diverse, and includes proteins with crucial roles in cell differentiation, proliferation, survival and motility (Roskoski, 2004). Src is heavily involved in the transduction of extracellular signals through integrin binding through its association at focal adhesions with focal adhesion kinase (FAK) (Schwartz et al., 1995). FAK is a cytoplasmic protein tyrosine kinase central to regulation of cell motility and morphogenesis in the developing nervous system. The initial step of activation of FAK occurs by phosphorylation of FAK Y397 in response to both integrin engagement and activation of G-protein-coupled receptors (Rodríguez-Fernández and Rozengurt, 1998, Hanks and Polte, 1997). This initial phosphorylation step can also be performed by constitutively active v-Src (Guan and Shalloway, 1992). Phosphorylation of Y397 of FAK provides an SH2 domain to which Src binds, activating Src activity by removal of SH2 auto-inhibition (Cobb et al., 1994). Src then phosphorylates FAK at several locations (Hanks and Polte, 1997), which massively increases FAK kinase activity (Calalb et al., 1995). This activation of FAK by Src has been shown to be necessary for FAK phosphorylation of several of its downstream effectors including the adaptor protein Paxillin (Shen and Schaller, 1999). The association of activated FAK and Src have extensive signalling roles, including activation of Jnk, Erk and Ras mediated MAPK signalling cascades (Miyamoto et al., 1995, Schlaepfer et al., 1994). Through these cascades the Src/FAK signalling pathway has extensive, important effects on gene transcription and cellular proliferation. In addition to its role in integrin signalling, Src also has roles in adherens, where it is known to interact with and phosphorylate β -catenin, which causes dissociation of β -catenin from E-cadherin (Coluccia et al., 2006). This dissociation causes an increased nuclear localisation of β -catenin resulting in increased transcriptional activity, which increases growth and motility of cells in diseases such as prostate cancer (Coluccia et al., 2006).

In addition to these roles, C-Src also influences ligand-stimulated signal transduction, such as at the EGF receptor, among others. C-Src has been shown to physically associate with EGF receptor variants in various cancer models, and both healthy and aberrant EGF receptor signalling requires C-Src for signal propagation

and cellular response (Luttrell et al., 1988, Wilson et al., 1989, Roche et al., 1995b). Src further facilitates EGFR signalling through the internalisation of EGF by Clathrin (Wilde et al., 1999). Src also has direct roles in cytoskeletal organisation through phosphorylation of Cortactin, which, when activated by C-Src, promotes polymerisation and rearrangement of the actin cytoskeleton (Wu and Parsons, 1993).

The above examples offer only a snapshot of the substrates and roles of Src within cells. The substrates, and as such activities, of Src within the cell are plethora, dependent upon - and required for cellular response to - external stimuli such as ligands (Wilde et al., 1999) or adhesion (Schaller, 2004), cell cycle progress (Roche et al., 1995a), cell division (Chackalaparampil and Shalloway, 1988) and more.

1.3.1 Tissue specific expression and activity of Src

Although Src is ubiquitously expressed in mammals, Src abundance is notably higher in some specific cell types. Src expression has been identified as between 5-200 fold increased in osteoclasts, platelets and neurons, with particularly high fluctuations during development (Brown and Cooper, 1996).

The specific role that Src plays in these systems is unclear, however the importance of Src expression in osteoclasts is made apparent by the defects of Src knockout mice. Whilst the effects of Src knockout mice are mild, there is a significant increase in osteoporosis due to decreased bone resorbing activity of osteoclasts. This suggests that whilst C-Src expression can be compensated for by other SFKs in most tissues, most notably Fyn and Yes, the specific functions of C-Src in osteoclasts are unique to C-Src (Lowell and Soriano, 1996). Recent studies have indicated that the Src has specific roles associated with mitochondria, where it phosphorylates and activates cytochrome *c* oxidase (Cox). This Src-induced activation is required to produce the high levels of ATP required for bone resorption activity of osteoclasts (Miyazaki et al., 2006).

Src is present in extremely high concentrations in platelets, representing up to 0.4% of total protein. After thrombin-induced platelet activation Src is observed to be transiently activated, and dephosphorylated at Y527. This occurs concomitantly with Src association with the signalling molecule phosphatidylinositol 3-kinase (PI3K) and

the platelet surface receptor α IIB β 3 suggesting a key role in signalling at the plasma membrane in this system (Clark et al., 1994a). Src has also been associated in platelets with Cortactin and WASp phosphorylation, regulating the important cytoskeletal rearrangements involved in platelet activation (Senis et al., 2014).

1.3.2 Neuronal roles of Src

Src family kinases have extensive roles in functions of both the developing, and mature nervous system. Speculation of a specific role for Src activity in the brain began with Cotton and Brugge's observation of 10 fold enrichment of C-Src from the developing brain when compared to other tissues (Cotton and Brugge, 1983). This increased expression also varied significantly during the course of neuronal development, which could broadly be split into biphasic expression. The first phase of increased C-Src expression occurs in the neuro-ectodermal cells in late gastrula stage, and occurs concomitantly with the specification of cells to the neuronal lineages (Maness et al., 1986). The second phase was observed in neuronal progenitor cells undergoing terminal differentiation and neurite outgrowth in the cerebellum (Fults et al., 1985). Much of this expression was later determined to be that of an 'activated form of C-Src', later demonstrated to be N1-Src, and the roles of this variant in neurons will be discussed in **4.1**.

Specific identification of C-Src substrates in the brain unveiled specific roles for Src in the regulation and plasticity of the receptors and ion channels of the synapse (Kalia et al., 2004). The importance of effective communication across synapses for neuronal function cannot be overstated, a healthy balance of signals and receptors between the pre-synaptic nerve terminal and their post-synaptic target is essential for nearly all brain functions, from cognitive processes to motor control and synaptic plasticity (Cline, 2005). In the mammalian central nervous system, synaptic transmission is predominantly chemically mediated across a synaptic cleft, with excitatory or inhibitory signals increasing or decreasing the likelihood of an action potential occurring in the target cell respectively. Both excitatory and inhibitory neurotransmitters result from chemicals, commonly released from the pre-synaptic-nerve terminal, binding to receptors on the post-synaptic target neuron. Excitatory neurotransmitters induce depolarisation of the post-synaptic cell, whereas inhibitory

transmitters typically lead to hyperpolarisation. The effective regulation and balance of both the excitatory and inhibitory neurotransmitters and their receptors is essential to the control of healthy brain function on both the cellular and tissue level (Kalia et al., 2004).

Src phosphorylation and regulation has been identified in several receptor and channel proteins of the post-synapse, the NMDA receptor (NMDA-R, (Wang and Salter, 1994)), voltage gated potassium channels (Fadool et al., 1997), calcium channels (Cataldi et al., 1996), GABA_A receptors (Moss et al., 1995) and the nicotinic acetylcholine receptor are all known to be regulated in some way by Src. Probably the best characterised of these interactions is Src regulation of NMDA-R

The NMDA-receptor was the first discovered of a family of ionotropic glutamate receptors, which transduce excitatory neurotransmission signals in the post-synaptic neurons throughout the CNS by functioning as ligand-gated ion channels. Glutamate is the primary neurotransmitter for mediating excitatory synaptic transmission in the CNS, and is released from pre-synaptic vesicles into the synaptic cleft via calcium-dependent exocytosis. The glutamate-dependent influx of calcium through these receptors plays important roles in both development and the synaptic plasticity that underlies learning and memory (Dingledine et al., 1999).

The NMDA-R is a multi-protein complex, with a variety of functional subtypes dependent upon its subunit composition. NMDA-R subunits NR1, NR2, and often NR3 comprise the core and form the central ion channel, associated with a variety of scaffolding, adaptor and signalling proteins which together constitute the whole NMDA-R complex (Husi et al., 2000). When the extracellular portion of the NMDA-R is bound by both glutamate, and a co-activating glycine molecule, the NMDA-R channel is opened, allowing the influx of Na⁺, K⁺, and Ca²⁺ into the cell. Regulation of NMDA-Rs occurs in a variety of manners, both by extracellular modulation of the binding site and channel pore, and by intracellular kinase activity.

Early electrophysiological studies in neurons indicated that inhibition of phosphorylation by SFK inhibition or exogenous phosphatase introduction decreased NMDA-R currents, whilst inhibiting endogenous phosphatase activity or introducing exogenous Src enhances NMDA-R currents (Wang and Salter, 1994, Wang et al., 1996). Various studies have since confirmed this Src modulation of the NMDA-R, in

a variety of systems including HEK cells (Köhr and Seeburg, 1996), *Xenopus* oocytes (Chen and Leonard, 1996), cultured neurons (Yu et al., 1997) and hippocampal slices (Lu et al., 1998). This positive modulation of NMDA-R activity by Src was also shown to be required for induction of Long Term Potentiation (LTP) in Schaffer collateral CA1 synapses of the hippocampus, suggesting a role in learning and memory (Pelkey et al., 2002).

The mechanism behind this action is in the specific phosphorylation of the NR2A and NR2B subunits of the core NMDA-R complex by Src and Fyn. Y1472 was later confirmed as the main site of SFK phosphorylation of NR2B (Cheung and Gurd, 2001). Mutation of this residue caused significant impairment of fear learning (which the author suggests is due to decreased LTP in the amygdala) which correlated with a failure of the sub-unit to correctly localise (Nakazawa et al., 2006). Yang and Leonard (2001) identified three phosphotyrosine sites in the cytoplasmic C-terminal tail of NR2A which may be the Src substrate residues which mediate Src modulation of the complex. By contrast with NR2B regulation, Src phosphorylation of NR2A was shown to have a very different method of NMDA-R modulation. Studies of an NMDA-R comprised of recombinant NR2A and NR2B indicated that phosphorylation by Src potentiates NR2A activity by weakening the effect of zinc inhibition of the NMDA-R (Xiong et al., 1999, Zheng et al., 1998).

In addition to its roles in potentiating post-synaptic receptors and channels, Src is also enriched in pre-synaptic vesicles (Linstedt et al., 1992). As observed by Foster-Barber and Bishop (1998), Src is up-regulated in a variety of secretory cells (neurons, endocrine cell, platelets and osteoclasts) as well as in a variety of subcellular localisations involved in membrane traffic (endosomes, synaptic vesicles and secretory granules), which prompted investigation into Src interaction with membrane trafficking proteins critical to neuronal function. Immuno-precipitation and immunofluorescence of Src in neurons showed that Src binds to and co-localises with both synapsin and dynamin, suggesting a role for Src in regulating synaptic vesicle life-cycle in addition to more general roles in membrane trafficking (Foster-Barber and Bishop, 1998). Src has also been implicated in the LTP associated strengthening of synapses by multi-site phosphorylation of synaptophysin (Evans and Cousin, 2005).

1.4 Neuronal Src splice variants

N1-Src was first identified in studies of C-Src expression in the central nervous system (CNS). Cultures of rat neurons and astrocytes were shown to express a Src variant with decreased mobility on acrylamide gels that was specifically expressed in neurons but not astrocytes, and had 5-7 fold higher kinase activity; as measured by comparing phosphorylation of enolase by neuron isolated, and fibroblast isolated Src (Brugge et al., 1985). The decreased mobility of N1-Src was later identified to be the result of inclusion of a 6 amino acid micro-exon into the SH3 domain, between exons 3 and 4 of C-Src (Martinez et al., 1987). Inclusion of a neuronally expressed micro-exon between Src exons 3 and 4 is strongly conserved in neurons throughout vertebrate evolution (Martinez et al., 1987, Levy et al., 1987, Raulf et al., 1989). Identical 6 amino acid neuronal Src inserts are observed in humans, rodents (Martinez et al., 1987) and chicks (Levy et al., 1987), whereas fish and amphibians express 6 and 5 amino acid N1-Src exons respectively with 50% sequence homology to mammalian N1-Src (Pyper and Bolen, 1989). By contrast C-Src expression is identified in multicellular organisms as early as sea sponges (*Perifora*) (Ottillie et al., 1992). The sequence conservation, restricted expression and evolutionary emergence in the vertebrate nervous system (although no neuronal exons of C-Src are observed in hydra (Raulf et al., 1989)) suggests an evolutionary link to the elaborations of the nervous system in Chordates.

Further investigations into neuronal splicing of Src identified a second alternative Src exon, N2-Src, which inserts into the Src mRNA immediately after the N1-Src exon, adding an additional 33 nucleotides (or 11 amino acids) to the SH3 domain. Since N1-Src acts as the splice-acceptor for N2-Src it is always included in N2-Src mRNA, making N2-Src a total of 17 amino acids longer than C-Src. N2-Src inclusion also alters the final nucleotide of the N1-Src exon from coding for an arginine to a serine (Pyper and Bolen, 1990) (Fig. 1-4). Inclusion of the N2-Src exon is highly conserved between human and mouse brain tissues, however is absent in chicks (Pyper and Bolen, 1990). Interestingly inclusion of the N2-Src micro-exon has never been identified in the absence of the N1-Src exon. This apparent dependency of N2-Src on N1-Src expression occurs in spite of the fact that N2-Src inclusion into C-Src would not introduce a frame-shift mutation, suggesting that the N1 micro-exon contributes essential residues to the N2-Src SH3 domain (Black, 1992).

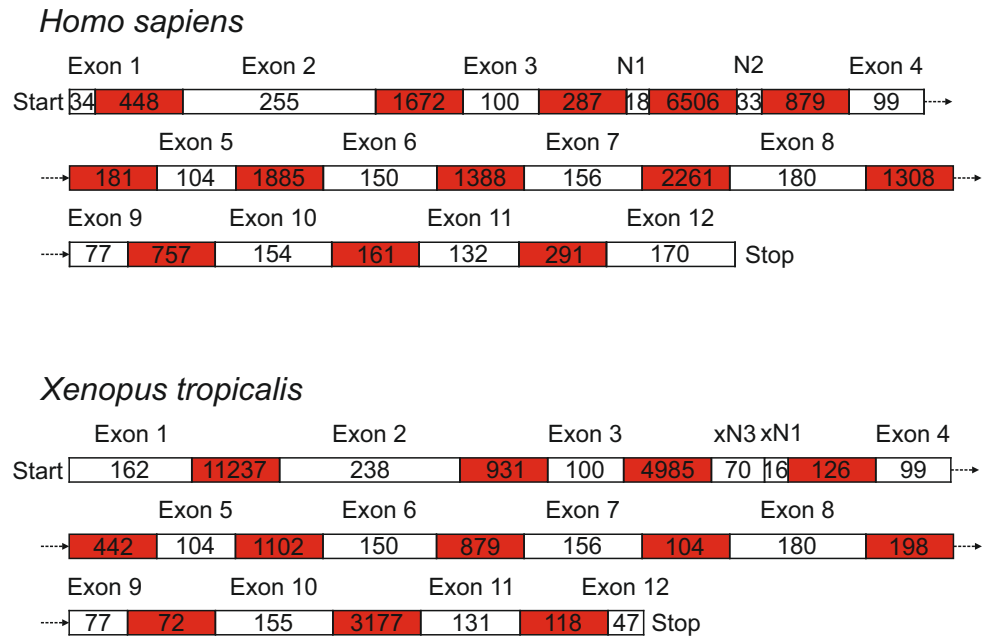


Figure 1-4. Genomic map of Src intron and exon sequences in both *Homo sapiens* and *Xenopus tropicalis*.

The number of base pairs each intron and exon sequence contains is indicated in the white and red boxes respectively. Exon length is reflected proportionally in the size of the box, however for the purposes of conciseness, the size of the introns is constant. The principal difference between the sequences of these genes is in the different lengths of exons 1 and 12; whilst *Homo sapiens* have a relatively short exon 1 sequence and a longer exon 12 sequence, *Xenopus tropicalis* are converse in this, however the total length of both C-Src sequences is similar at 1662 and 1685 base pairs total, respectively. Interestingly, the organisation of the N1-Src exon in the genomic space between exons 3 and 4 also differs, with N1-Src appearing far earlier in humans, than xN1-Src in *Xenopus species*.

1.4.1 Differential effects of N1-exon insertion on the SH3 domain

Both the N1- and N2-Src micro-exons are inserted between exons 3 and 4 of C-Src, introducing 6 and 17 amino acid sequences into the SH3 domain of Src respectively. Inclusion of the neuronal micro-exons occurs in the middle of the n-Src loop of the SH3 domain, directly infringing upon the third 'specificity pocket' of the binding face of the SH3 domain (Dergai et al., 2010). This inevitably causes a change in the substrate specificity of the SH3 domain. Whilst little work has been done to identify N2-Src specific substrates, or the effect of N2-Src inclusion on the SH3 domain structure or function, N1-Src has been studied with some success.

The first instance of altered N1-Src SH3 domain binding is in an assay by Weng and colleagues (1993) which identified via GST pull-down that inclusion of the 6 amino acids of the N1-exon dramatically reduced the affinity of the Src SH3 domain for C-Src SH3 domain substrates. Whilst an overall decrease in N1-SH3 binding was detected in 3T3 cells when compared to C-Src SH3, more sensitive kinase assays also identified substrates specifically phosphorylated by N1-Src and not C-Src. This shows that the N1-Src SH3 domain, rather than simply reducing SH3 binding efficiency, changes the substrate specificity, preferentially binding a different subset of substrates than C-Src (Weng et al., 1993).

The first protein specifically identified to bind N1-Src with less affinity than C-Src was SH3-Binding Protein 1 (SH3BP1) (Ren et al., 1993). SH3BP1 is a GTP activating protein and modulator of Rac activity, initially identified for its binding to the SH3 domains of various non-receptor tyrosine kinases such as Abl. SH3BP1 binding to the C-Src, Abl, and Grb2 SH3 domains was detected at high affinity, however very limited N1-Src, Nck and Crk SH3 domain binding to SH3BP1 was identified (Ren et al., 1993), which suggested to the authors that inclusion of this short sequence changed the SH3 binding motif of N1-Src significantly. As previously mentioned, C-Src interacts in neurons with both dynamin and synapsin, an interaction which is abolished by inclusion of the N1-Src exon (Foster-Barber and Bishop, 1998). Similarly, N1-Src exon inclusion abolished SH3 binding to the C-Src SH3 substrates FAK, its neuronal isoform FAK⁺ (Messina et al., 2003) as well as Alzheimer's associated protein Tau (Reynolds et al., 2008), and signal transduction associated RNA binding protein Sam68 (Finan et al., 1996). As a result of the decrease in

substrate binding for these functionally significant C-Src substrates, it is clear that N1-Src is not performing the same cellular functions in neuronal cells as C-Src. In addition to this decreased binding for putative C-Src substrates, several substrates have been identified to which N1-Src binds to exclusively, or with a higher affinity than C-Src.

Santoro and colleagues (1997) using the yeast two-hybrid system with the N1-Src SH3 domain as bait, identified only one peptide, a novel voltage gated potassium channel of a family of previously undiscovered proteins, termed BCNG-1, later renamed Hyperpolarization-activated and Cyclic Nucleotide-gated channel 1 (HCN1). HCN1 showed a strong interaction with the N1-Src SH3 domain, however failed to bind C-Src Fyn and Abl SH3 domains. Later studies of the family to which HCN1 belongs (as reviewed by Wahl-Schott & Biel (2009)) have extensively expanded our knowledge of its structure and function.

The HCN family, unlike the vast majority of voltage gated potassium channels, is activated by hyperpolarisation rather than depolarisation. HCN1 expression has been identified in both the brain and, interestingly, the heart muscle. In neuronal cells HCN1 has been implicated in the integration of excitatory synaptic input from dendrites, constraint of long term potentiation and with various roles in how the cell responds electrochemically to synaptic input (Wahl-Schott and Biel, 2009). These cellular roles translate in the brain to effects upon motor learning and control of the working memory. N1-Src may contribute to these roles by regulating HCN1 through phosphorylation of its intracellular domain, as phosphorylation of this domain is known to regulate HCN membrane permeability (Zong et al., 2005, Arinsburg et al., 2006). Unfortunately, as yet, the observation of interaction between HCN1 and N1-Src is yet to be repeated, however an interaction between C-Src and HCN2 has been identified (Zong et al., 2005). Whilst the HCN family proteins function in a largely similar fashion, the expression patterns and protein-protein interactions of each member of the family differ significantly, allowing for the possibility that C- and N1-Src are regulating different members of the same protein family independently of each other.

A second yeast two-hybrid assay identified Delphilin as a possible substrate of N1-Src. Delphilin is a Glutamate Receptor Ionotropic Delta 2 (GRID2) associated

protein with many protein-protein interacting motifs, including PxxP, suggesting that it is a scaffold protein linking GRID2 with multiple signalling networks including the actin cytoskeleton (Miyagi et al., 2002). More recently, N1-Src binding to the C-terminus of the NR2A subunit of the NMDA-R has also been identified (Groves et al., 2012) suggesting that, whilst N1-Src may not bind synapsin and dynamin, N1-Src certainly has a role at the pre-synaptic nerve terminal.

1.4.2 The effects of N1-exon insertion on auto-inhibition

It has widely been shown that the role of the SH3 domain in auto-inhibition, as covered in **3.1**, is affected by inclusion of the N1-Src micro-exon. Even before the identification of an alternative splice variant, increased abundance and activity of Src in was observed in neurons which varied across developmental stage (Cotton and Brugge, 1983). N1-Src was first identified as a structurally modified form of C-Src observed to be 6-12 fold more active than C-Src in the same cells. (Brugge et al., 1985). This constitutively increased activity is likely due to a decrease in the auto-inhibitory interaction between the SH3 to the n-terminal lobe of the kinase domain. It has previously been demonstrated in C-Src that mutation of the 'n-src loop' of the SH3 domain, into which the N1-Src micro-exon is inserted, decreases this auto-inhibitory interaction, increasing the activation state of the protein (Brábek et al., 2002). This increased activity not entirely uncontrolled as differential activation of N1-Src has been observed, and activity is still modulated by the SH2 domain (Mukherjee et al., 2003). Although modification of the n-src loop decreases intramolecular binding, inserting short amino acid sequences into the n-src loop does not appear to disrupt overall protein folding, as demonstrated by a 10-glycine insert by Grantcharova and colleagues (2000).

1.4.3 Effects of N1-exon insertion on N1-Src localisation

As described in **3.1** the SH3 domain also appears to play important roles in intracellular localisation, and the intracellular localisation of N1-Src appears to be affected by N1-exon inclusion. From very early in the study of N1-Src, the splice variant was identified both in structures of the cell soma in addition to the plasma

membrane. Maness and colleagues (1988) identified an increase in the ‘active form’ of C-Src in the growth cones at the leading edge of neurite extension in differentiating rat neurons, which was later confirmed as being N1-Src (Maness and Matten, 1990). N1-Src was further localised by electron microscopy to endoplasmic reticulum and associated polysomes in the cell soma, in addition to localisation at synapses (Atsumi et al., 1993). N1-Src was identified in the post-synaptic density (the protein-rich region at the post-synaptic membrane associated with neurotransmitter release and signalling), in addition to both the pre-synaptic vesicles and the pre-synaptic membrane (Atsumi et al., 1993). Interestingly, unlike C-Src, N1-Src has been identified associated with lipid rafts, a localisation usually restricted to SFKs with two lipid modifications in the SH4 domain (Mukherjee et al., 2003). In the adult brain, N1-Src has been identified localised to the cell soma, as well as dendritic processes, axons and in nerve terminals (Sugrue et al., 1990).

This differential intracellular localisation may be in part due to the effects of the N1-Src exon on the structure of the SH3 domain, however it may also be due to differential post-translational modification of N1- and C-Src. Mukherjee (2003) noted that the differential N1-Src intracellular localisation was not due to its modified SH3 domain. The subcellular localisation of N1-Src could, therefore, be due to changes in the post-translational modification of the unique domain, as observed by differential N-terminal phosphorylation of a serine residue in N1-Src (Brugge et al., 1987).

1.4.4 Effects of N1-exon inclusion on cell morphology

The differential Src localisation, specification and activity as a result of N1-exon inclusion inevitably has consequences on neuronal function. Overexpression of Src constructs in differentiating Purkinje neurons showed that whilst wild-type N1-Src and constitutively active C-Src had minimal effects on the morphology of these cells, constitutively active N1-Src caused significant aberrations in microtubule organisation resulting in deformed neurites (Kotani et al., 2007). Similarly, when testing the effects of C- and N1-Src upon axonogenesis in differentiating *Xenopus* neurons, Worley and colleagues (1997) noted differential effects of both wild-type and constitutively active C- and N1-Src. Whilst wild type C-Src had limited effects on axonogenesis, there was an observable enhancement in axonogenesis in N1-Src

overexpressing cells. Constitutively active C- and N1- mutants both impaired axonogenesis, however whilst constitutively active C-Src, however the N1-Src effect was minimal by comparison to C-Src (Worley et al., 1997). Interestingly when the C- and N1-Src constructs were expressed in *Xenopus* A6 epithelial cells, N1-Src induced significant elongation in the cells, with cells producing a neurite-like process, quite contrary to the rounded phenotype of C-Src transfected cells (Worley et al., 1997). These phenotypes taken as a whole suggest that N1-Src is promoting neuronal cytoskeletal rearrangement, even in the absence of a neuronal background of protein expression.

1.4.5 Expression of N1-Src during neuronal differentiation

In mice, N1-Src is the dominant form of C-Src in the developing brain, both in terms of protein concentration and activity (Wiestler and Walter, 1988). Before embryonic day 9 (E9) in mice, when neuroblasts are proliferating and migrating rapidly, N1-Src activity is negligible and C-Src is the dominant Src isoform. As major brain structures are formed during E12 and beyond, N1-Src activity increases rapidly, exceeding C-Src by orders of magnitude, peaking at E18 (Wiestler and Walter, 1988). This period of rapidly increasing N1-Src activity occurs while, in addition to continuing proliferation and migration of neuroblasts, an increasing proportion of neuroblasts are beginning to exit the cell cycle and differentiate. This observation of increased N1-Src expression in neuronal precursor cells undergoing differentiation is supported by *in vitro* experiments with cultured neurons of the rat striatum. These cells show little detectable N1-Src activity until serum starvation for three days, which induces neuronal differentiation and N1-Src activity seven fold higher than C-Src (Cartwright et al., 1987). Similarly, embryonic carcinoma cells treated with retinoic acid to induce neuronal differentiation express increased levels of N1-Src (Lynch et al., 1986), and there an increase in both N1-Src and N2-Src expression during differentiation of the neuroblastoma cell line LAN-5 (Matsunaga et al., 1993a).

Expression of N1-Src during early neuronal development has also been characterised in the frog species *Xenopus laevis*. *X.laevis* N-Src (xN1-Src) expression is temporally regulated, as it is not detectable in the maternal mRNA pool, or at the end of gastrulation (developmental stage 11), however is detectable mid-neurulation

(stage 15) and is localised to the site of neurulation at stage 16 (Collett and Steele, 1992). This temporal and physical localisation to the site of neurulation suggests that inclusion of the xN1-Src micro-exon is concurrent with neuronal specification of the cells of the dorsal ectoderm that become the neural plate. Studies using ectoderm explants have shown that xN1-Src expression is dependent upon the presence of the mesoderm underlying the neural ectoderm. In the absence of neural inductive signals from the mesoderm, xN1-Src isn't expressed and the cells do not express neuronal markers (Collett and Steele, 1993). This signalling mechanism was further confirmed by induction of xN1-Src by mimicking mesoderm induction signals using the PKC activator 12-O-tetradecanoylphorbol-13-O-acetate (TPA). This induction was shown to be rapid, occurring without the need for new protein synthesis (Collett and Steele, 1993). The increased expression of xN1-Src during neurulation and primary neurogenesis suggest that in this model N1-Src is being expressed at times of both neuronal specification, and neuronal differentiation.

1.4.6 Expression of N1-Src in the mature brain

N1-Src expression in the mature rat brain has been well characterised by both antibody and *in situ* hybridisation (Sugrue et al., 1990, Ross et al., 1988) with both studies reporting widespread expression of N1-Src throughout the brain. Specific regions of increased abundance of N1-Src in the brain include in the hippocampus, mesencephalon, and Purkinje neurons of the cerebellum, in addition to the Pons, medulla and forebrain. Across the brain, Sugrue and colleagues (1990) reported that expression of N1-Src was increased in discrete subpopulations of neurons with no common classification. Ross and colleagues (1988), noted that whilst in the hindbrain C- and N1-Srcs were broadly comparable, in the forebrain N1-Src expression was much higher, which they suggest links N1-Src to both higher brain development. In general both studies agreed that the regions of enriched N1-Src activity were regions commonly linked with increased neuronal plasticity (Sugrue et al., 1990, Ross et al., 1988).

1.4.7 The regulation of N1-Src splicing

The regulation of splicing of N1-Src through development suggests that N-Src splicing is regulated temporally during neuronal development, likely in response to developmental signalling. The lab of Douglas Black is unparalleled in the work that it has done to establish the molecular mechanism behind neuron-specific inclusion of the N1-Src exon (Summarised in Fig. 1-4). The neuroblastoma cell line LAN-5 includes the N1-exon in over 90% of Src mRNA and has been used extensively by Black and colleagues to identify the proteins necessary for exon inclusion, when compared to the cancer cell line HeLa which expresses no N1-Src (Black, 1991). By utilizing an N1-Src mini-gene, constructed of C-Src cDNA with genomic DNA present between exons 3 and 4, it was established by deletion mapping of the introns

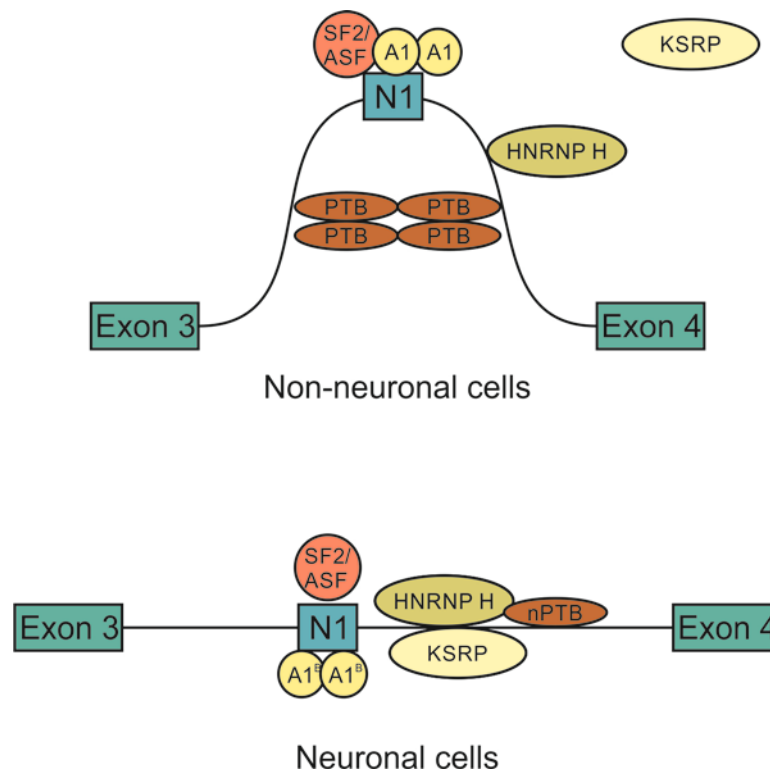


Figure. 1-5. Model for tissue specific N1-Src expression based on Rooke, 2013.

In non-neuronal cells, PTB binds to CU repeats both up- and down-stream of the N1-exon, repressing exon inclusion. In neuronal cells PTB binding is removed, allowing splicing elements to include N1-Src in the processed mRNA. hnRNPA1 (A1) molecules that bind to N1 may be replaced with hnRNPA1B molecules in neuronal cells to contribute to the enhancement of N1-Src inclusion. KSRP has been shown to localise with Src mRNA in neuronal cells, however not non-neuronal cells, although its role in neuronal splicing is uncertain. Some components of this system, such as hnRNP H and F are known to interact with the splicing machinery, although their role in the process is unknown.

up- and downstream from the N1-exon that the region of RNA responsible for N1-Src inclusion was in the immediate vicinity of N1-Src (Black, 1991).

A sequence of RNA 38-142 base pairs downstream of the N1-exon was identified that was necessary for LAN-5 inclusion of the N1-exon and if duplicated, increased N1-exon inclusion (Black, 1992). Binding proteins for both this region, and a negative regulatory element upstream of the N1-exon were identified as PTB, hnRNP F, hnRNP H and KSRP (Min et al., 1995, Modafferi and Black, 1997). Although all of these proteins are present in tissues throughout the body, KSRP was identified as a possible candidate for neuron-specific modulation (Hall et al., 2004). The intracellular localisation of KSRP and N1-Src expression were shown vary dependent upon the differentiation state of a mouse neuroblastoma cell line NIE-115. In undifferentiated neuroblastoma cells KSRP was not co-localised to the site of Src RNA and inhibitory N1-exon splicing modulator PTB and C-Src was the only detected Src isoform. Upon treatment with 2% DMSO, shown to differentiate these neuroblastoma cells into neuronal cells, KSRP co-localises with Src RNA and the inhibitory PTB protein resulting in N1-Src exon inclusion (Hall et al., 2004).

1.4.8 Neuronal Srcs in Neuroblastoma

The link between the expression of N-Srcs and the differentiation of neuroblastoma is well established. Early work in neuronal Srcs established that expression of N1-Src and the differentiation of neuroblastoma cell lines identified high 'C-Src' activity and an 'amino terminal modification' in neuroblastoma cell lines which were highly differentiated (Mellström et al., 1987). Neuroblastoma is a childhood cancer of the sympathetic nervous system, arising from cells of neural crest lineage, occurring most commonly in young children under 4 years of age. In the USA neuroblastoma accounts for 6-10% of all childhood cancers, occurring in approximately 1 in 10,000 live births (Gurney et al., 1995). The neuroblastoma screening program in Japan ran from 1985 to 2004. At its peak the program screened over a million six month old infants a year for elevated levels of homovanillic acid and vanilmandelic acid, metabolites commonly produced by neuroblastoma (Tsubono and Hisamichi, 2004). Although the program was successful in identifying

neuroblastoma cases, it had little impact on the mortality of the disease nationally, as did similar programs that were run briefly in Canada and Germany (Schilling et al., 2002, Woods et al., 2002). The conclusions made after these programs was that, due to the self-resolving nature of the majority of cases of neuroblastoma in patients under 1 year old, as such patients were over-diagnosed by the screening program when they didn't stand to benefit from the earlier diagnosis and treatment.

This is principally because of the remarkable correlation between the age of neuroblastoma diagnosis, and the prognosis of the disease. Whilst in total approximately 70% of neuroblastoma cases have a successful 5 year outcome, over the age of 18 months this number drops to as low as 50% (Howlader et al., 2011). The progression of neuroblastoma is categorised into 4 main stages depending upon the disease severity and spread. Stage 1 denotes the initial development of the cancer, where the tumour is fully visible and operable. Stage 2 begins when either the whole tumour is no longer excisable by surgery, or the cancer has spread to nearby lymph nodes. Stage 3 represents more severe metastasis; to nearby organs, and lymph nodes and stage four represents an aggressive, widespread cancer, present in distant lymph nodes and organs. Stage 4 is split into two subtypes; stage 4, an extremely high risk cancer, with only a 30% survival rate and 4S. Whilst both Stage 4 subtypes widely metastasise, stage 4S tumours are more operable and the disseminated cancer has a significant chance of spontaneously differentiating into a harmless neuronal phenotype. This stage is exclusively observed in infants under the age of 18 months, once again emphasising the key role played by age on the chance of harmless cancer differentiation. Standard treatment for neuroblastoma of any stage in children over 18 months usually involves surgery to remove large masses, followed by intensive rounds of chemotherapy and radiotherapy.

N2-Src expression has been observed to correlated inversely with N-Myc gene amplification (Matsunaga et al., 1994a), although not in samples with increased N-MYC expression from a single copy of the gene, usually found in low risk tumours discovered by mass screening (Matsunaga et al., 2000). Myc is a basic helix turn helix zipper DNA binding transcription factor, targeting the enhancer box of genes and forming complexes that can both up- (with Max) and down- (through Miz-1) regulate transcription (Peukert et al., 1997). In addition to its standard functions as a

transcription factor, Myc can also interact with histone acetyltransferases, which decrease histone affinity for DNA, loosening up the winding of DNA to allow greater transcription (Knoepfler et al., 2006, Cotterman et al., 2008). The main factor causing Myc to be a major proto-oncogene and prognostic determinant is the genes with which it interacts, with many mitotic, cell cycle and survival genes under Myc control. As such Myc over-expression is a feature in many cancers. The effects of Myc over expression are wide-ranging, involving up-regulation of cyclins, ribosomal RNA and proteins, and down regulation of Bcl-2 and p21, resulting in increased cell growth and division and decreased apoptosis and differentiation. A recent study on the role of Myc in neuroblastoma differentiation looked at LAN-5, a readily differentiating neuroblastoma cell line with high Myc expression, and SK-N-AS, a cell line highly resistant to differentiation with only a single copy of Myc (Guglielmi et al., 2014). This study identified Myc as permissive for neuronal differentiation of these cell lines, as knockdown in LAN-5 prevented- and overexpression in SK-N-AS increased- drug induced differentiation.

The absence of acceptable levels of progress in the treatment of neuroblastoma necessitates the identification of new, novel targets to promote neuroblastoma differentiation, quiescence or senescence *in vivo*. Between 1979 and 2005 the 10 years survival rate of patients with stage 4 neuroblastoma increased from 6.7% to 26%, an increase largely attributed to the intensification of chemotherapy which has occurred since 1985, rather than from the development of any targeted neuroblastoma therapies (Haupt et al., 2010). Due to the age of neuroblastoma patients, intensive chemotherapy is not an ideal treatment option, with many patients with a positive outcome still suffering from complications such as hearing loss, hypothyroidism, ovarian failure, and musculoskeletal and pulmonary abnormalities (Laverdière et al., 2005). As such, the identification of druggable targets for neuroblastoma therapy which are highly tumour-specific is of vital importance.

Several studies and clinical trials have focussed on targeting generic signalling pathways that are thought to contribute in neuroblastoma proliferation through dysregulation, such as PI3K (Spitzenberg et al., 2010, Fulda, 2009), mTOR (Seegerström et al., 2011) and the IGF-I receptor (Coulter et al., 2008). Whilst rapamycin has been ruled out as a treatment due to associated increased Survivin

expression (Samkari et al., 2012), and targeting IGF-IR performed poorly in clinical trials (King et al., 2014), several promising PI3K inhibitors are undergoing preliminary clinical trials (Lim et al., 2014).

Therapies targeted specifically at genes with expression restricted to neuroblastoma cells include targeting the human norepinephrine transporter hNet, expressed in 90% of neuroblastoma tumours (Carlin et al., 2003). Radiation therapy can be targeted specifically to neuroblastoma cells by ¹³¹I-metaiodobenzylguanidine (MIBG), which is taken up by the hNet transporter, causing a build-up of radiation specifically within these cells, and represents a promising therapy (Matthay et al., 2012). Similarly the expression of the GD2 ganglioside on the surface of >98% of neuroblastoma cells has for many years been an enticing target for antibody mediated therapies. Utilising anti-GD2 antibodies coupled with IL-2 to target immune attack upon neuroblastoma cells has demonstrated some success with an increase in overall survival of 10% demonstrated compared to standard therapy (Yu et al., 2010).

An interesting tyrosine kinase target in neuroblastoma is anaplastic lymphoma kinase (ALK). ALK expression is typically only found in the developing nervous system (Iwahara et al., 1997) however the alteration of ALK in cancer as the result of chromosomal translocation and gene fusion has been identified in anaplastic large cell lymphoma (Morris et al., 1994), non-small lung cell cancers (Soda et al., 2007) and inflammatory myofibroblastic tumours (Palmer et al., 2009). ALK is expressed in around 50% of neuroblastoma tumours and correlates strongly with Myc-N expression in advanced tumours with a poor prognosis (Wang et al., 2013). Studies indicate that ALK is a good candidate for neuroblastoma therapy, with the inhibitor Crisotinib showing promise in clinical trials, although it is shown to bind poorly to some known ALK mutations which may lead to development of resistance during therapy (Bresler et al., 2011).

Whilst there are a considerable number of candidate genes for neuroblastoma therapy, the 'silver bullet' of neuroblastoma treatment remains the identification of a way to induce in neuroblastoma cells the spontaneous differentiation that is characteristic of the cancer. Induction of neuroblastoma cell differentiation by RA is already a well-regarded treatment aimed at inducing differentiation in cells remaining after intensive rounds of chemotherapy, radiotherapy and surgery. Treatment with a

high, intermittent dose of 13-*cis*-retinoic acid has been shown to increase event free survival of patients and is now a recommended therapy (Cernaianu et al., 2008). Treatment with vanadium-based tyrosine phosphatase inhibitors (which increase phosphotyrosine levels by acting as a competitive inhibitor for phosphotyrosine) has been shown *in vitro* to increase the effectiveness of retinoic acid in inducing neuronal differentiation by activating both AKT and ERK signalling (Clark et al., 2013).

Interestingly, both the age and the prognosis of neuroblastoma patients, correlates with the presence or absence of N1- and N2-Src, and their relative expression levels when compared with C-Src. N2-Src in particular has been associated with a less metastatic disease, with expression of N2-Src being significantly associated with a longer event free survival in patients (Matsunaga et al., 2000). This link between N2-Src expression and a positive prognosis was confirmed in a study by Terui and colleagues (2005), who correlated N2-Src with both a positive outcome, as well as with the expression of another favourable marker ShcB, which they speculated could be a substrate protein. There is also strong evidence that N2-Src may be favourably expressed in neuroblastomas discovered by mass screening, rather than by symptom (Matsunaga et al., 2000). These neuroblastomas are largely benign, with between 70 -90% being of favourable, stage I, II or the spontaneously regressing 4S and tend not to be Myc amplified (Bessho, 1998). Matsunaga and colleagues (1993b) showed that, in LAN-5 and SK-N-SH neuroblastoma cell lines, a pattern of neuronal Src expression is matched by an ability to differentiate under cAMP/Retinoic Acid. In SK-N-SH, C-Src is the dominant isoform, and N2-Src is entirely absent, whilst in LAN-5 cells N1-Src is more highly expressed than C-Src, and N2-Src is expressed at detectable levels (Matsunaga et al., 1993a). This suggests that a large number of N2-Src expressing neuroblastoma tumours are resolved without any treatment, or even symptoms.

1.5 Aims

Very little is known about the roles of N1- and N2-Src during neuronal differentiation, both during healthy development and in the differentiation of the developmental cancer neuroblastoma. The aim of this project is to characterise the

roles and effects of N1- and N2-Src during neuronal differentiation and to identify candidate genes and pathways through which they may function. This will then provide better insight into the mechanisms regulating neuronal differentiation both during development and neuroblastoma, and potentially identify potential candidates for targeted therapies to induce neuroblastoma differentiation both in vivo and in vitro.

Materials and Methods

2.1 Materials

Oligonucleotide primers were ordered from Eurogentec (Seraing, Belgium) and Sigma (St. Louis, MO). Morpholinos were ordered from Gene Tools (Philomath, OR) after receiving advice from Gene Tools staff on their design. Usage of Thermo Scientific NanoDrop was provided by the Technology Facility in the Department of Biology, University of York. The gels as part of the mass spectrometry were run using the XCell SureLock Mini-Cell gel system, Novex NuPAGE 10% Bis-Tris pre-cast gels and Novex NuPAGE MES SDS Running Buffer provided by the Centre for Excellence in Mass Spectrometry in the University of York Technology Facility. Sybr Safe was purchased from Life Technologies (Paisley, UK). Laemmli loading buffer was purchased from Sigma (St. Louis, MO). Protein molecular weight ladders were purchased from Bio-Rad (Hercules, CA). The original XL-10 Gold stock was purchased from Stratagene (Santa Clara, CA) and competent cells made from the stock in-house. Restriction enzymes XhoI, BglIII, KpnI and XbaI were purchased from NEB (Ipswich, MA). Ligase and ligation buffer were purchased from Promega (Fitchburg, WI). Taq polymerase was used for all non-cloning PCR steps and was a kind gift from Dr Daniel Ungar, University of York. Pfu polymerase was used for all cloning PCR steps and was purchased from Thermo Scientific (Waltham, MA).

The Src pFLAG plasmids were made in-house by Dr Gareth Evans by replacing GFP in pEGFP-N1 with the FLAG epitope tag sequence and the pmCec plasmid was a gift from Dr Rory Duncan (Herriot Watt University) (Rizzo et al., 2004). The T.REX HeLa cell line in addition to the pOG44 and pcDNA5/FRT/TO plasmids were gifts from Dr Paul Prior, University of York. pCS2+ plasmid was a gift as part of a collaboration with the lab of Harv Isaacs. The human neuroblastoma cell lines LAN-5, KELLY, and SK-N-AS were kind gifts from Dr Andrew Stoker, University College London. PVDF membrane (Immobilon-P) in addition to the Immobilon chemiluminescent HRP substrate was purchased from Millipore (Billerica, MA). α -PY20 antibody was purchased from BD Bioscience (San Diego, CA), α -FLAG (M2) was purchased from Sigma (St. Louis, MO), α -pY488, α -pY527 and α -Sec23a antibodies were purchased from Cell Signalling Technology (Boston, MA), α -actin B antibody was purchased from Abcam (Cambridge, UK). Agarose conjugated

α -4G10 antibody was purchased from Merck Millipore (Billerica, MA). α -GFP antibody was a gift from Dr Paul Prior, University of York. α -TGN46 antibody was a gift from Dr Danny Ungar, University of York. α -Ki67 antibody was a gift from Dr Paul Genever, University of York. Secondary HRP conjugated α -mouse and α -rabbit antibodies was purchased from Sigma (St. Louis, MO), Molecular Probes' secondary ALEXAfluor-conjugated antibodies were purchased from Invitrogen (Paisley, UK). DMEM containing pyruvate, high glucose and glutamine; Hepes buffered DMEM without bicarbonate; RPMI with sodium bicarbonate, without L-glutamine; FBS (South American); Hygromycin B; were purchased from Invitrogen (Paisley, UK).

The following were all materials purchased jointly by the Isaacs and Pownall labs and used as part of the collaboration with the Isaacs lab. Restriction enzymes Asp718 and SureCut buffers were purchased from Promega (Fitchburg, WI) and Roche (Sussex, UK). Megascript SP6 Transcription Kit was purchased from Ambion (Paisley, UK). RQ1 RNase free DNase, L-Cysteine and L-Cysteine hydrochloride, Formaldehyde solution, acetic anhydride, Heparin, Denharts, CHAPS, and the First Strand Synthesis buffer kit were purchased from Sigma (St. Louis, MO). Proteinase K, Anti-DIG Fab fragments coupled to alkaline phosphatase, BMB, and BM purple were purchased from Roche (Sussex, UK). Lamb Serum used to make the heat treated lamb serum used in *in situs* was purchased from Fisher Scientific (Paisley, UK). Total yeast RNA used in the *in situs* was purchased from ICN Biochemicals (Aurora, OH). All unlisted chemicals were purchased from either Sigma or Melford (Ipswich, UK).

2.2 Molecular biology methods

2.2.1 Agarose Gels

DNA separation for the purposes of cloning was carried out by agarose gel electrophoresis. 60-100 ml 1x TAE buffer (40 mM Tris, 20 mM acetic acid, and 1 mM EDTA) containing 0.7-3% (w/v) agarose was mixed into suspension and the mixture heated using a microwave until the agarose was fully dissolved (~2 min, full power), then cooled to below ~60 °C before addition of SYBR Safe at a dilution of 1:20,000 (v/v). Once the gel had set the gel tray was submerged in 1x TAE buffer and the DNA, diluted in 5x Orange G buffer (15% glycerol, 0.2% Orange G dye, in dH₂O)

loaded onto the gel. DNA was then separated by electrophoresis and visualised by Safelight, before U.V transillumination for acquisition of image.

2.2.2 DNA separation by acrylamide gel electrophoresis

Small DNA fragments, amplified by rtPCR from cDNA samples, were separated by TBE poly-acrylamide gel electrophoresis, using the Bio-Rad Mini-PROTEAN Tetra gel electrophoresis kit (Bio-Rad). Each 15% poly-acrylamide gel (per 7.5ml gel: 3.75 ml of 30% acrylamide, 2.95 ml of distilled water, 0.75 ml of 10x TBE (890 mM Tris, 890 mM boric acid, 20mM EDTA), 60 µl of 10% (w/v) ammonium persulfate, 3.75 µl of Tetramethylethylenediamine (TEMED)) was mixed in the order listed below and was cast in Bio-Rad Mini-PROTEAN gel plates using 10 or 15 well combs. DNA samples were diluted in 5x SYBR Safe loading dye and loaded into wells. The gels were run in 1x TBE for between 60 and 90 min at 200 mV. Gels were removed from the plates and stained immersed in 1x TBE (89 mM Tris, 89 mM boric acid 2 mM EDTA) containing a 1:50,000 (v/v) dilution of SYBR Safe, kept gently agitated for at least an hour then visualised by Safelight and transilluminated by U.V for acquisition of image.

2.2.3 SDS-PAGE

Protein separation was achieved by SDS-polyacrylamide gel electrophoresis (SDS-PAGE) using the Bio-Rad mini-PROTEAN Tetra gel electrophoresis kit (Bio-Rad). Gels were composed of a resolving gel (375 mM Tris pH 8.8, 0.1% SDS, 0.05% APS, 0.01% TEMED, 7.5% to 15% acrylamide) in addition to a stacking gel (125 mM Tris pH 6.8, 0.1% SDS, 4% acrylamide, 0.05% APS, 0.01% TEMED).

Samples were either lysed directly into 2x Laemmli loading buffer or diluted in 2x Laemmli loading buffer, then boiled at 95°C for 10 min prior to loading. The gel was run in 1x SDS running buffer (25 mM Tris, 192 mM glycine, 0.1% SDS). Gels were electrophoresed at 120 V until the dye front passed the stacking gel boundary (typically 20-30 min) and then increased to 160 V until the pre-stained

protein molecular weight marker (Bio-Rad) indicated that sufficient resolution of the target protein size had been achieved.

2.2.4 Protein transfer to PVDF

SDS-PAGE gels were transferred to PVDF membranes for western blotting using the Bio-Rad Mini Trans-Blot system. Transfer was carried out as per the manufacturer's instructions, using transfer buffer A (Transfer buffer: 25 mM Tris pH 8.3, 192 mM glycine, 20% methanol) for 1 h at 66 V or overnight at 20 V.

		Primary antibody		Secondary antibody	
Ab	Block	Conc.	Ab	Conc.	
Actin B	3% Marvel in PBS	1:90,000	α -rabbit HRP	1:5000	
FLAG (M2)	3% Marvel in PBS	1:1000	α -mouse HRP	1:5000	
PY20	3% BSA in PBS	1:1000	α -mouse HRP	1:5000	
pY416	3% BSA in PBS	1:1000	α -rabbit HRP	1:5000	
pY527	3% BSA in PBS	1:1000	α -rabbit HRP	1:5000	
Sec23a	3% Marvel in PBS	1:1000	α -rabbit HRP	1:5000	

Table 2.1 Western blotting antibody concentrations and blocking method.

Conditions used in blocking PVDF membranes in addition to primary and secondary antibody combinations and concentrations

2.2.5 Western Blotting

All incubations during Western blotting were agitated on a gel shaker. Following transfer, membranes were washed in water and PBS before blocking for an hour at room temperature or overnight at 4 °C in PBS supplemented with either 3% Marvel milk powder or 3% BSA (see Table 2-1). After blocking, membranes were probed with primary antibodies (Table 2-1) for 2 h at room temperature or overnight at 4 °C. Following the primary antibody step, membranes were washed for 3 x 5 min in PBS Tween (PBS + 0.5% Tween). Secondary antibodies were either anti-rabbit or anti-mouse antibodies conjugated to HRP and were used in combination with the relevant primary antibody (Table 2-1). The membrane was incubated with secondary antibody for 1 h at room temperature then washed three times with PBS Tween. Reagents A and B of the Immobilon chemiluminescent HRP substrate were mixed 1:1 immediately prior to application to the PVDF membrane and incubated for 1-3 min

before visualising bands in a dark room using Ultracruz Autoradiography film (Santa Cruz).

2.2.6 Preparation of competent *E.coli* for cloning

XL-10 Gold ultracompetent *E.coli* cells (Stratagene) were used for all cloning and DNA purification steps. XL-10 cells were kept at -80°C and used to generate stocks of competent cells. Competent cells were generated by putting a scraping of the original stock into 5 ml of sterile LB medium (per litre: 10 g tryptone, 10 g NaCl, 5 g yeast extract) without antibiotic, incubated shaking at 200 rpm at 37 °C overnight. The overnight culture was then diluted into 200 ml of fresh LB medium supplemented with 4 ml of sterile 1 M MgSO₄ and incubated for several hours to an OD₆₀₀ of ~0.5. From this point the culture was kept at 4 °C until the end of the protocol. The culture was centrifuged at 4°C at 4500 G for 5 min to pellet the cells. The supernatant was discarded and the pellet gently resuspended in 50 ml of ice-cold TFB1 (30 mM potassium acetate, 10 mM calcium chloride, 50 mM manganese chloride, 0.1 M rubidium chloride, 15% glycerol). The cells were incubated on ice for 5 min, then pelleted for 5 min again at 4 °C & 4500 G, before discarding the supernatant and gently resuspending the pellet in 5 ml of ice-cold TFB2 (10 mM MOPS, 75 mM calcium chloride, 10 mM rubidium chloride, 15% glycerol). This solution was incubated on ice for 45 min, mixing occasionally by inversion. The cells were then gently mixed then divided into 100 µl aliquots in sterile Eppendorfs and snap frozen in a dry ice/isopropanol bath. The competent cells were then stored at -80 °C until needed.

2.2.7 Bacterial transformation

Plasmids were transformed into competent XL-10 Gold cells (described above) for relevant cloning steps and DNA production from plasmid stocks where glycerol stocks were not available. All of the following steps were performed using aseptic technique. 1-5 µl of DNA added on ice to 50 µl of a stock of competent XL-10 cells and mixed by stirring, then incubated on ice for 15-30 min. The cells were then heat-shocked at 42 °C for exactly 45 s and incubated for 2 min on ice. Following this, 200 µl of 37 °C LB medium was added and the tubes mixed at 37 °C and 200 rpm

for between 30-60 min. Agar plates (per litre: 10 g tryptone, 10g NaCl, 5 g yeast extract, 20g agar) containing the appropriate antibiotic were pre-warmed to 37 °C and up to 100 µl of the transformation was spread over the agar plate which was incubated for 16-18 h at 37 °C.

2.2.8 Plasmid purification

Plasmid DNA was purified from XL-10 Gold cells either from single colonies selected from the agar plates of bacterial transformations or from scrapings of glycerol stocks stored at -80°C. For cloning, only small quantities of DNA were required so 5-10 ml of inoculated LB medium was processed via the Machery-Nagal Quick-Spin mini-prep kit as per the manufacturer's (Machery-Nagal) instructions. For larger quantities of DNA, or DNA required at a higher concentration or purity, 200 ml of LB medium was inoculated with a 10 ml starter culture, and processed via a Midi-Prep kit (Qaigen) as per the manufacturer's instruction. Quantification of DNA concentration was performed using a NanoDrop spectrophotometer (Thermo-scientific) in the Technology Facility in York University.

2.2.9 Cloning

The primers used for all cloning procedures can be found in Table 2-2. The full length Src C-, N1- or N2-Src open reading frames with c-terminal FLAG tag (pFLAG constructs) was sub-cloned to generate the pCS2+ constructs used to create RNA to inject in *Xenopus* cells, and the pDNA5/FRT/T0 plasmids used to generate stable, inducible HeLa cell lines. The FLAG-tagged genes were amplified by PCR from pFLAG using the blunt-ended PCR enzyme *Pfu* DNA polymerase (Thermo Scientific). The PCR product was then cloned into the pJet 1.2sub-cloning plasmid using the clonJET kit (Thermo Scientific) as per the manufacturer's instructions. The pJet 1.2sub-cloning plasmid and vector plasmids were digested with *XhoI* (NEB) for 1 h in NEB buffer 3 by standard lab protocol (1% BSA, 1x NEB 3, 2 µl restriction enzyme, to 60 µl with dH₂O) and purified by gel extraction from agarose gel using the Qaigen gel extraction kit. The purified vector and insert DNA fragments were ligated,

and then the correct orientation of the gene was confirmed by *Taq* PCR using one internal and one external primer.

The xN1-Src gene was acquired from the IMAGE clone library (IMAGE number: 5572523) and amplified from the source plasmid by *Pfu* DNA polymerase PCR and ligated into pJet 1.2 using the clonJET kit (Thermo Scientific) as per the manufacturer's instructions. xN1-Src was then digested from pJet 1.2 into the empty pFLAG vector by double digest with *Bgl*III and *Kpn*I. The FLAG tagged xN1-Src construct was then excised from pFLAG by *Xba*I digest and ligated in to pCS2+.

The ligation of insert DNA into plasmid vectors was accomplished at a 3:1 molar ratio of insert to vector. The mass of vector was constant at 100 ng and the quantity of insert varied dependent upon the size of the fragment. 1 µl of T4 DNA ligase (1-3 units/µl), 1 µl of 10x ligase buffer (both Promega) and 100 ng of vector was made up to 10 µl with insert DNA and dH₂O. This mix was incubated either at room temperature for 20 min, or at 4 °C overnight before transformation into competent bacteria.

	Primer Pair	Forward primer Sequence	Reverse Primer Sequence	Anneal temp	Extension time
Cloning	Cloning Srcs from pFLAG	CTC-GAG-ACC-ATG-GGC-AGC-AAC-AAG-AGC-AAG-CCC	CTC-GAG-TTA-CTT-GTC-GTC-ATC-GTC-TTT-GTA	51 °C	2 min
	Cloning xN1-Src from IMAGE	AGA-TCT-CTC-TAG-AAC-CAT-GGG-TGC-CAC-TAA-AAG-CAA-GCC-A	GGT-ACC-GTA-GAT-CCA-AGG-TGT-TCC-CCA-GGC-TGG-TAC-TG	57 °C	2 min
rtPCR	Pan-Src	ATC-TCG-CAC-CGA-GAC-AGA-CT	ACT-GAG-TGC-GAG-ACG-TGA-TG	60 °C	45 sec
	xN1-Src	ACT-GTG-ACC-TGA-CGC-CTT-TT	CTT-CCC-TCA-TGT-CAG-GTC-TC	58 °C	50 sec
	L8 control	GGG-CTG-TCG-ACT-TCG-CTG-AA	ATA-CGA-CCA-CCA-CCA-GCA-AC	57 °C	45 sec

Table 2-2 Sequences and PCR conditions of primer pairs used during rtPCR and cloning steps.

PCR reactions were performed using either *Taq* (rtPCR and screening cloning colonies) or *Pfu* polymerase, as described in 2.2.9. Primers were used at a concentration of 100 nM for each primer pair and the product separated by either agarose or acrylamide gel electrophoresis as described in 2.2.1 and 2.2.2.

To sequence the Src splice variants identified by rtPCR of *Xenopus tropicalis* cDNA, the cDNA samples were amplified using *Pfu* polymerase separated on a 3% agarose gel. Individual splice variants were then excised, purified and ligated into pJet 1.2 by the clonJET system (Thermo Scientific) and sequenced.

All of the above plasmids were sequenced upon completion by York Technology facility as described in **2.2.10**.

2.2.10 DNA sequencing

DNA sequencing was carried out by the Technology Facility at the University of York. A 3.2 µl pre-mix consisting of 100 ng of plasmid DNA and 3.2 mM of primer was submitted to the Technology Facility and the sequence obtained was analysed using Sequence Scanner 1.0 (Applied Biosystems). Plasmid sequences were then confirmed by alignment of *in silico* plasmids to the sequencing results.

2.3 Cell culture methods

2.3.1 Culture of cell lines

Cell lines were maintained in culture in 25 cm² or 75 cm² flasks at 37°C in a humidified atmosphere of 5% CO₂. COS7, SK-N-AS, HeLa and B104 cells were maintained in DMEM (containing pyruvate, high glucose and glutamine (Gibco)) with 10% FCS, 100 units/ml penicillin and 0.1 mg/ml streptomycin. LAN-5 and KELLY cells were maintained in RPMI-1640 medium (with sodium bicarbonate, without L-glutamine (Gibco)) with 10% FCS, 100 units/ml penicillin and 0.1 mg/ml streptomycin. Cells were passaged 2-3 times per week upon reaching confluency. Passage consisted of removing culture media, washing cells with sterile PBS, and detaching cells from the cell culture flask with 0.5-1 ml of warmed trypsin/EDTA in PBS. Upon detachment, trypsin action was halted by the addition of 5-10 ml of culture medium. Cells were centrifuged in 15 ml Falcon tubes for 5 min at 120 G. The supernatant was discarded and the cell pellet resuspended in 1 ml of culture medium. The cells were split at ratios between 1:2 and 1:10 dependent upon their proliferation

rate. If the cells were required for plating, the cell density was determined using a haemocytometer and plated at the appropriate density.

2.3.2 Transient transfection of cells for immunocytochemistry

Ten thousand HeLa, B104 or COS7 cells, or 30,000 LAN-5, SK-N-AS or KELLY cells were plated onto 13 mm² coverslips, with 500 µl of medium per well of a 24 well plate. Coverslips were sterilised in an oven at 180 °C for at least 30 min prior to use. Cells were transfected one day after plating using Ecotransfect (Oz Biosciences) according to the manufacturer's instructions. Briefly, transfections were carried out using a total of 1 µg of plasmid DNA (0.5 µg of each plasmid if performing a double transfection) and 2 µl of Ecotransfect, each diluted in 50 µl of DMEM or RPMI as appropriate. The two solutions were mixed and incubated for 20 min at room temperature before pipetting drop-wise onto the culture media in each well. The 24 well plate was gently agitated before being returned to the incubator. After 6 h the transfection media was replaced with 500 µl of fresh media. The fresh media added contained any relevant drug treatment which included 5 µM 13-*cis*-Retinoic Acid, 1 mM dibuteryl cAMP, or 0.5 µl of 1 µg/ml doxycycline.

Antibody	Primary antibody	Secondary antibody	
	Conc.	Antibody	Concentration
FLAG (M2)	1:1000	α-mouse ALEXA 594	1:500
GFP	1:1000	α-rabbit ALEXA 488	1:500
Ki67	1:200	α-rabbit ALEXA 488	1:500
TGN46	1:1000	α-rabbit ALEXA 488	1:500

Table 2-3 Antibody combinations and concentrations used in immunocytochemistry. Antibody combinations and concentrations used in immunocytochemistry. All samples were blocked in BSA and permeabilised in triton prior to antibody labelling, as described in 2.3.2

2.3.3 Transient transfection of cells for western blotting

One hundred thousand B104 cells were plated per well of a 6 well plate and transfected with Ecotransfect. Two days following the transfection, the cells were washed twice with PBS and then treated for 10 min with either 100 µM pervanadate solution (100 µM orthovanadate, 0.2 mM hydrogen peroxide in PBS) or PBS. After

incubation, the solution was removed and the cells lysed in 120 μ l of Laemmli SDS sample buffer.

2.3.4 Stable transfection of HeLa cells

HeLa cells were stably transfected with Src isoforms using the Invitrogen T-REx/Flp-in systems. Flp-in, T-REx HeLa cells stably express the tetracycline repressor element, in addition to having a genomic, stably transfected pFRT/*lacZeo* plasmid. One hundred thousand HeLa cells were plated in 2 ml of culture medium per well of a 6 well plate and transfected using Ecotransfect (Oz Bioscience). 3 μ g of DNA comprising 0.3 μ g of the relevant pcDNA5/FRT/TO plasmid and 2.7 μ g of pOG44 were mixed in 100 μ l of DMEM, and the solution mixed with 100 μ l of DMEM containing 6 μ l of Ecotransfect. One day after transfection the culture medium on the cells was changed. Two days after transfection the culture medium was removed from the cells and the cells washed with PBS and treated with 500 μ l of Trypsin/EDTA for 3-5 min in the incubator to detach the cells from the 6 well plate. The HeLa cells were diluted in 8 ml of culture medium at varying concentrations (5% - 50%), and plated onto 10 cm cell culture dishes and returned to the incubator. The following day the cell culture medium was either supplemented, or replaced with medium containing 500 μ g/ml of Hygromycin B (Invitrogen). The cells were kept in Hygromycin B containing medium for several weeks until colonies between ~5-8 mm in diameter were visible by eye on the plates, with medium changed three times a week.

Individual colonies were selected using cloning rings (1-2 cm rings cut from the end of a blue pipette tip), and a glass petri dish with its base coated with silica gel; both of which were autoclaved and dried before use. The 10 cm plate of HeLa cells was gently washed twice with 8 ml PBS, and the PBS removed. Each cloning ring was then pressed onto the silica gel to coat the base of the cloning ring with a chemically inert sealant before placing the cloning rings over colonies that were sufficiently spatially separated from neighbouring colonies. One hundred ml of Trypsin/EDTA was added to each well created by cloning rings and the dish was left for 3-5 min at room temperature to allow the trypsin to detach the cells of each

colonies. The trypsin cells were then further detached by repeated pipetting of the cell/trypsin suspension onto any remaining cells, before the suspension was moved in to a 24 well plate containing 1 ml of 500 µg/ml Hygromycin B containing culture medium. The cells were allowed to grow to confluence in a 24 well plate, with media changed 3 times a week, before being passaged in 200 µl of trypsin into a 25 cm² cell culture flask.

The stably transfected cell lines were then tested for the proportion of doxycycline induced FLAG expressing cells by immunocytochemistry, and for doxycycline induced expression of a Src splice variant by Western blotting. Successful clones were proliferated and stored frozen in aliquots to create stocks of cells.

2.3.5 Immunocytochemistry

Cells were stained by immunocytochemistry after being transfected or drug treated as outlined in **2.3.2**. Cells undergoing immunocytochemistry were plated on to 13 mm glass coverslips in the wells of a 24 well plate. Culture medium was removed from the cells and the cells gently washed three times with 1 ml PBS, before being fixed for 20 min at room temperature in PFA (4% paraformaldehyde and 4% sucrose in PBS, pH to 7.4). The cells were then gently washed three times in 1 ml PBS before permeabilisation for 30 min in PBS + 1% BSA + 0.1% Triton X-100. The permeabilisation buffer was removed and replaced with one or two primary antibodies (all antibodies raised in either mouse or rabbit, Table 2-3) in PBS + 1% BSA for 2 h at room temperature. After incubation with the primary antibody(s) the cells were gently washed three times in 1 ml PBS before application of the secondary antibody, diluted 1:500 in PBS + 1% BSA. Secondary antibodies were either Alexa Fluor 488-conjugated goat anti-rabbit IgG or Alexa Fluor 594-conjugated goat anti-mouse IgG, or both if mouse and rabbit primary antibodies were used in combination. The cells were incubated in secondary antibody in the dark at room temperature for 1 h. The cells were then washed gently three times in PBS and washed once in dH₂O. Coverslips were then removed from wells and air-dried on tissue before mounting on slides using Mowial mountant (10% Mowial, 25% glycerol in 0.1 M Tris pH 8.5) containing 1 µg/ml DAPI.

Images were acquired using a 40x objective on a Nikon TE 200 epifluorescence inverted microscope using a RoleraXR CCD (QImaging) camera controlled by SimplePCI Software (Hamamatsu).

2.3.6 Wound healing assay

Fifty thousand HeLa cells were plated per well of a 24 well plate. Eight h after plating, the cells were treated with 1 µg/ml doxycycline. The following day the culture media from these wells was replaced with HEPES buffered DMEM (10% FBS, 100 u/ml penicillin, 0.1 mg/ml streptomycin) containing 1 µg/ml doxycycline. After 2 h in HEPES buffered DMEM the cells were wounded using a 200 µl pipette tip and the medium changed to remove cell debris. The plate was then sealed by Parafilm and transferred to the microscope stage maintained at 37 °C and humidified. Regions of interest on each well were identified in the SimplePCI software and these sites were then imaged every ten min over a two day time period using an automated XY2 Prior stage with auto-focussing.

2.3.7 Image quantification

All computation image analysis was performed using ImageJ (NIH). The NeuronJ (Popko et al., 2009) plugin was used to measure neurite lengths of both LAN-5 and B104 cells. Neurites were traced using the 'add tracings' tool and measured from the closest point to the cell soma, where the neurite was below 2 µm in diameter, to the end of the neurite. The traced neurites were measured by NeuronJ and compiled and calibrated from pixels to microns in Microsoft Excel, using a scale set by a calibration image.

To measure the area migrated in a wound healing assay, a multi-image TIF was compiled in SimplePCI software. The migration front of the cells was outlined on the first image of the time-course using the polygon tool, then again on the final image of the time-course and the area covered between these outlines was measured by ImageJ. The data for these time-courses was collated and analysed in Microsoft Excel.

To quantify the circularity of HeLa cells, cells were outlined using the polygon tool, with CFP as a guide to the outline of the cells. The outline was measured for perimeter and area and the data compiled in Microsoft Excel. The roundness was calculated on a scale of 0 to 1 by the formula $4*\pi*(Area/Perimeter^2)$ (Schneider et al., 2012).

2.3.8 Statistical analyses of neuritogenesis assays

Statistical analyses on neuritogenesis assays were performed where at least three biological replicates of the data were available. The mean values for each replicate were calculated and compared for statistical significance by ANOVA, using a Bonferroni correction unless otherwise stated

2.4 Mass spectrometry methods

2.4.1 Phosphotyrosine immunoprecipitation from HeLa cells

HeLa cell lysates were subjected to anti-phosphotyrosine immunoprecipitation to provide immunoenriched eluate for mass spectrometry. For each condition of the experiment two confluent 75 cm² flasks were passaged into six 75 cm² flasks. The day following the passage, the relevant cells were treated with 1 µg/ml doxycycline and the cells incubated for two days. After two days the flasks were (in batches of three) washed three times in PBS and treated for 10 min at 37 °C with 100 mM pervanadate (100 µM pervanadate solution, 0.2mM hydrogen peroxide in PBS), or PBS. This was removed and 1 ml of RIPA buffer was added to each flask on ice and the cells scraped from the bottom of the flask using a cell scraper. The flask was then tipped 45° upright and the lysed cells incubated in the bottom corner of the flask, on ice for 10 min. After this incubation the cells were moved to a 1.5 ml Eppendorf and spun for 10 min at 4°C and 16,000 G to separate the RIPA insoluble fraction, the supernatant was then pooled in a chilled 15 ml centrifuge tube kept in ice.

The protein concentration of the pooled lysates was established by Bradford assay and the concentration of all samples adjusted to match that of the sample with the lowest concentration. Samples of each lysate were taken and equal quantities of

the lysate were used for the immunoprecipitation. 50-100 μ l of agarose bead conjugated 4G10 antibody (Merck Millipore) was added to each sample and the tubes were incubated mixing end-over-end overnight at 4 $^{\circ}$ C.

The following day the agarose beads was separated from the supernatant by centrifugation for 5 min at 4 $^{\circ}$ C and 720 G, the supernatant was removed and retained. 0.4 μ m Spin-x filter tubes (Corning) were washed twice with fresh 100 mM Tris pH 7.4. The beads were resuspended in 100 mM Tris buffer pH 7.4 and transferred to 0.4 μ m Spin-x filter tubes and washed five times in 400 μ l 100 mM Tris pH 7.4 by centrifugation at 4 $^{\circ}$ C at 16,000 G for 20 s. Following these washing steps the IP was eluted by addition of 50-100 μ l Laemmli sample to the beads in the filter tubes and the tubes rolled at RT for 20 min. Following this, the eluate was collected by 10 min of centrifugation at 16,000 G and stored at -20 $^{\circ}$ C.

2.4.2 Mass spectrometry

40 μ l of Eluate from the 4G10 IPs was loaded on a pre-cast NuPAGE 10% Bis-Tris Gel (Novex) separated by a well with 10 ml loading dye to prevent contamination. The samples were run for six minutes at 200 V using the xCell SureLock Mini-Cell system in 1x Nupage MES SDS Running Buffer (Novex). The gel was then removed from the cast and incubated in SafeBlue Protein stain (NBS Biologicals), rocking gently for 1 h, and then de-stained in molecular grade water overnight. The region of the gel stained by the SafeBlue Protein stain was excised from the gel and dissected into \sim 1mm pieces and transferred to LoBind Eppendorf tubes (Sigma).

The gel was then treated twice with 25 mM ammonium bicarbonate in 50% acetonitrile. The gel was then washed in acetonitrile for 5 min before the supernatant was removed and the gel dried by speedvac for 20 min. The gel pieces were then treated in 10 mM dithioerythritol (DTE) in 100 mM ammonium bicarbonate at 56 $^{\circ}$ C for 1 h. After returning to room temperature the gel pieces were then treated with iodoacetamide (50 mM in 100 mM ammonium bicarbonate) in the dark for 30 min. The gel pieces were then washed with 100 mM ammonium bicarbonate for 15 min, then in 25 mM ammonium bicarbonate in 50% acetonitrile for 15 min, then in acetonitrile solution for 5 min. After this incubation the supernatant was removed and

the gel pieces dried again in the SpeedVac for 20 min. The proteins in the gel pieces were then digested by 25 µg/ml trypsin in 25 mM ammonium bicarbonate at 37 °C overnight.

The supernatant containing the digested peptides was removed and retained and additional peptides were recovered by treating the gel pieces with 50% acetonitrile three times for 15 min and the supernatants retained. The combined supernatants were then dried in the SpeedVac and reconstituted in 20 ml of 0.1% trifluoroacetic acid. The peptides were then run on the MaXis 3G high resolution Q-ToF mass spectrometer by Dr David Ashford of the University of York Technology Facility, Centre of Excellence in MS (COEMS).

2.4.3 Bioinformatics

Lists of peptides identified by the MaXis 3G system were processed through Mascot and lists of proteins clustered by the protein family were retrieved from the database with associated Uniprot identifying codes and values. The data were collated and processed in Microsoft Excel as described in **4.2.7** and Fig. 4-7 to give the lists of protein accessions put into various bioinformatics programs. Since the majority of these programs do not recognise Uniprot IDs, the lists of Uniprot ids were converted by the Uniprot batch retrieval function (<http://www.uniprot.org/uploadlists/> (Consortium, 2014)) and lists of official gene symbol used for the bioinformatics inputs.

2.4.4 WebGestalt

The processed protein lists assembled in Microsoft Excel were inputted into WEB-based GENE SeT AnaLysis Toolkit (WebGestalt) in the category `hsapiens__gene_symbol` (<http://bioinfo.vanderbilt.edu/webgestalt/> (Zhang et al., 2005)). Enrichment analysis was performed upon the list against the reference set `hsapiens__genome` using the statistical method Hypergeometric, and the Benjamini & Hochberg multiple test adjustment (Hochberg and Benjamini, 1990) to a significance

of 0.05%. Enrichment analysis of the KEGG pathways and WikiPathways was performed by WebGestalt and the data saved and compiled in Microsoft Excel.

2.4.5 DAVID

Functional annotation of the processed protein lists assembled in Microsoft Excel were inputted into DAVID (<http://david.abcc.ncifcrf.gov/>) (Huang et al., 2009b). The list of gene names using the OFFICIAL_GENE_SYMBOL identifier were inputted as text. The chart output for the Gene_Ontology categories GOTERM_BP_FAT, GOTERM_CC_FAT and GOTERM_MF_FAT were adjusted for multiple tests by the Benjamini & Hochberg method (Hochberg and Benjamini, 1990). Outputs were copied into and collated in Microsoft Excel.

2.4.6 Phosphosite

Proteins of interest were searched in the PhosphoSite database by their official gene symbol (Hornbeck et al., 2012). A list of the phosphorylated tyrosine residues was assembled in Microsoft Excel, along with annotations about whether the site was identified by high throughput phosphoproteomics techniques or specifically identified in the literature.

2.4.7 GPS 2.0

GPS 2.0 (GPS (Xue et al., 2008)) requires input of amino acid sequences that were in FASTA format. The amino acid sequence for proteins of interest was obtained by searching the Uniprot database for by the Uniprot ID, then inputted into GPS. GPS analysis was carried out using the high stringency criteria, which only shows sites that were below a false positive discovery rate of 4%. GPS was then used to analyse the amino acid sequence for motifs that matched a consensus sequence for phosphorylation by Src. The list of positions of the tyrosine residues along with the assigned score were then transferred and collated in Microsoft Excel.

2.4.8 ScanSite

The same amino acid sequences inputted into GPS were also used with ScanSite. ScanSite (Obenauer et al., 2003) was used to identify tyrosine residues in the sequence that matched the consensus motif for Src kinase domain phosphorylation. Due to the much lower number of output proteins from ScanSite compared with GPS, the lowest stringency was used, which identifies sequences in the top 5% of possible binding motifs. The resulting list of tyrosine residues, along with their position and statistical significance were then collated in Microsoft Excel.

2.4.9 STRING

Interaction maps of the processed protein lists were generated using STRING (Franceschini et al., 2013). The list of official gene symbols was entered into STRING's web interface as a list of multiple human protein names. The default parameters were used to generate the protein interaction network and the interaction map exported as a tab-delimited table. The table was then imported into Cytoscape (Smoot et al., 2011) where it was modified by grouping nodes of interest to highlight specific clusters enriched in the bioinformatics tools.

2.5 Developmental biology methods

2.5.1 Plasmid linearisation

The Src isoforms C-, N1-, xN1- and N2-Src were all cloned into the *Xenopus* expression vector pCS2+ and sequenced to confirm orientation and sequence fidelity. The C- N1- and N2-Src plasmids were linearised by restriction digest by Asp718 (5 µg of DNA, 5 µl of SuRE/Cut buffer B, 2 µl of ASP718, to 50 µl with dH₂O), xN1-Src was digested by NotI as above using SuRE/Cut buffer H. After digest the linearised plasmid DNA was checked on a gel, then purified by a phenol-chloroform extraction as follows.

The 50 µl digest was supplemented with 100 µl dH₂O and 140 µl of phenol-chloroform. The reaction was vortexed thoroughly for 30 s and centrifuged for 5 min

at 4 °C and 16,000 G. The aqueous phase was removed and kept, and 10 µl 3 M sodium acetate was added in addition to 250 µl 100% ethanol. The sample was then vortexed briefly to mix and stored on dry ice for 30 min before a 15 minute centrifugation at 4 °C and 16,000 G. The supernatant was removed, being careful to avoid disturbing the DNA pellet, and the pellet washed in 1 ml 70% ethanol. The sample was briefly centrifuged to return the pellet to the base of the Eppendorf tube before the supernatant was removed and the pellet dried in a vacuum chamber for 10 min. The linearised DNA pellet was then resuspended in 10 µl of molecular grade water and the concentration quantified by NanoDrop.

2.5.2 *In vitro* transcription of synthetic mRNA for injection into *Xenopus* species

Synthetic mRNA was generated from the pCS2+ plasmid using the Megascript SP6 Transcription Kit (Life Technologies). The transcription reaction was mixed as follows (4.5 µl RNase-free water, 2 µl 50 mM ATP, 2 µl 50 mM CTP, 2 µl 50 mM UTP, 2 µl 5 mM GTP, 2.5 µl 40 mM mGTP cap, 2 µl 10x transcription buffer, 1 µl 1 µg/µl linearised template DNA, 2 µl SP6 enzyme) and incubated for 4 h at 37 °C. At this point 2 µl of the reaction was run on a 2% acrylamide gel, stained with approximately 0.1-0.5 µg/µl ethidium bromide, to confirm that transcription had been successful. One microliter of RQ DNase I was then added to the mixture and incubated at 37 °C for 15 min. One hundred and fifteen microliters dH₂O and 15 µl ammonium acetate were then added to stop the reaction.

The RNA was then purified as follows, all centrifugation steps were performed at 4 °C and 16,000 G. 150 µl of phenol-chloroform was added and vortexed thoroughly for 1 minute before 5 min of centrifugation. The aqueous phase was removed and retained, then supplemented with 150 µl of chloroform, this mix was vortexed for 1 minute then centrifuged for 5 min. The aqueous phase was again retained and supplemented with 150 µl of isopropanol, this mix was vortexed and centrifuged, then incubated for 30 min at -20 °C. The mix was then centrifuged for 15 min to pellet the RNA, after which the supernatant was carefully removed. Following this the pellet was washed in 1 ml of ice cold 70% ethanol, then briefly vortexed to

remove the pellet from the bottom of the Eppendorf tube. The mix was again centrifuged and the supernatant removed and pellet dried by vacuum pump. The pellet was thoroughly resuspended in 20 μ l of dH₂O by pipetting up and down, and the concentration of the RNA determined by NanoDrop.

2.5.3 Injection of *Xenopus* embryos

Handling of animals and *in vitro* fertilisation of *Xenopus* embryos was performed by members of the Isaacs and Pownall labs, and injection was only performed where excess embryos were available when other lab members were performing similar experiments. Fertilised *tropicalis* embryos were cultured at 21 °C in MRS/9 (11 mM NaCl, 0.2 mM KCl, 0.22 mM CaCl₂, 0.11 mM MgCl₂ and 0.5 mM HEPES) in 55 mm petri dishes coated in 1% agarose/dH₂O. Approximately 40 min after fertilisation was completed, embryos were de-jellied in cysteine (MRS/9 + 3% L-cysteine, pH 7.8). Fertilised *tropicalis* embryos were cultured at 18 °C in NAM/10 (NAM/10 (NAM: 110 mM NaCl₂, 2mM KCl, 1 mM Ca(NO₃)₂, 0.1 mM EDTA), 5 mM HEPES, 25 pg/ml gentamycin) in 55 mm petri dishes coated in 1% agarose/dH₂O. ~1 h after fertilisation was completed embryos were de-jellied in cysteine (NAM/10 + 3% L-cysteine hydrochlorate monohydrate, pH 7.8).

Xenopus embryos were microinjected with the appropriate concentration of mRNA and/or morpholino using either a pneumatic micro-injector (Harvard apparatus/Narishige) or Drummond injector (Drummond Scientific Company) and glass needles. Fresh aliquots of the mRNA or morpholino were mixed and diluted on the morning of injection with molecular grade water. Morpholinos thawed from storage at -80 °C were heated to 65 °C for 10 min to bring the morpholino into solution.

Embryos were injected in NAM/3 (NAM/3, 5 mM HEPES, 25 pg/ml gentamycin) or MRS/9 medium supplemented with 5% Ficol. Varying volumes of solution were injected into both *laevis* and *tropicalis* embryos, however, not exceeding a volume of 10 nl per blastomere at the two cell stage or 5 nl per blastomere at the four cell stage. Bilateral and unilateral injections for phenotypes were performed at both two and four cell stages. Dorsal injections were performed at the four cell stage only. Embryos were changed from NAM/3 and MRS/9 prior to the onset of gastrulation,

typically 3-4 h after injection, and into NAM/10 and MRS/20 (5 mM NaCl, 90 mM KCl, 0.1 mM CaCl₂, 0.1 mM Mg Cl₂, 5 mM HEPES, 100 µg/ml gentamycin).

2.5.4 Collecting phenotypes

At approximately NF stage 40, embryos were analysed for a locomotive phenotype. Stage 40 embryos were imaged individually, both still and moving in response to gentle physical contact from forceps, on a dissection microscope using a JVC TK-C1381 colour video camera (JVC) with ArcSoft ShowBiz video software. Following imaging of the embryos, they were fixed and stored in 3.7% formaldehyde.

2.5.5 *In situ* hybridisation

Embryos were cultured until NF stage 13 when the vitelline membranes were removed. Embryos were then cultured to stage 14 and fixed in MEMFA (100 mM MOPS pH 7.4, 2 mM EGTA, 1 mM MgSO₄, 3.7% formaldehyde solution) for 1 h and then dehydrated and stored in 100% methanol at -20 °C.

Embryos were rehydrated through a series of methanol/PBSAT (PBS, 0.1% Tween) washes (100%, 75% and 50% methanol). Embryos were then permeabilised with a 14 min proteinase K digest (6 µg/ml proteinase K in PBSAT) at room temperature. Embryos were subsequently washed twice for 10 min in 0.1 M triethanolamine pH 7.8, with acidic anhydride added for 5 min (to a ratio of 0.25%) following the second wash. The embryos were then washed in PBSAT and refixed for 20 min in 10% formalin (3.7% formaldehyde, PBSAT). Following this the embryos were washed five times in PBSAT before being equilibrated in a 1:4 ratio of hybridisation buffer:PBSAT and then transferred into hybridisation buffer (50% formamide, 5x SSC, 100 µg/ml Heparin, 1x Denharts solution, 0.1% CHAPS, 10 mM EDTA, 0.1% Tween, pH 7) for 10 min at 60 °C. Embryos were then blocked in hybridisation buffer + 1 mg/ml yeast RNA for 2 h, gently agitated at 60 °C. The buffer was then replaced with hybridisation buffer + 1mg/ml yeast RNA + DIG labelled RNA probe overnight.

The probe was removed and retained the following day and excess probe removed by two washes in hybridisation buffer, three 2x SSC + 0.1% Tween-20 washes all at 60 °C. N-tubulin hybridisation necessitated an additional RNase digestion step, embryos were incubated for 30 min in 2x SSC supplemented with 20 µg/ml of RNase A at 37 °C, then washed in 2x SSC for 10 min at room temperature. This was followed by three washes with 0.2x SSC + 0.1% Tween-20 at 37 °C. Embryos were then washed twice in maleic acid buffer (MAB: 100 mM maleic acid, 150 mM NaCl, 0.1% Tween-20, pH 7.8) and then blocked in MAB + 2% BMB+ 20% heat treated lamb serum for 2 h at room temperature. The embryos were then incubated overnight in the MAB blocking solution + the anti-DIG antibody.

The following morning, embryos were washed five times in MAB at 60 °C then three 1 h MAB washes at room temperature. Embryos were washed in AP buffer (100mM Tris base, 50mM MgCl₂, 100mM NaCl, 0.1% Tween-20, pH 9.5) then the samples were developed using a 1:3 solution of BM purple in AP buffer for between 3 and 72 h. The reaction was stopped when suitable staining contrast was achieved by two washes in PBSAT and incubation and storage in formalin at room temperature.

2.5.6 Lacz staining

Embryos co-injected with lacz, in order to determine the site of injection were stained for lacz following embryo fixation for 1 h in MEMFA, prior to dehydration in 100% methanol. Embryos were washed three times in PBSAT and then treated in warmed X-Gal staining solution (20 mM K₃Fe(CN)₆, 20 mM K₄Fe(CN)₆, 2 mM MgCl₂, 0.01% deoxycholate, 0.02% NP-40) supplemented with 1.5 mg/ml X-Gal (from a 80 mg/ml X-Gal stock in DMSO) for between 2 min to an hour. The reaction was halted by two washes in PBSAT and a brief 10 minute re-fixation of the embryos in MEMFA before dehydration in 100% methanol.

2.5.7 Imaging phenotypes and in situs

Both *in situs* and fixed phenotypes were imaged using a LeicaMZ FLIII microscope (Leica), a SPOT 14.2 Colour Mosaic camera and SPOT Advanced software (Diagnostic Instruments Inc.).

2.5.8 RNA isolation

Embryos taken for rtPCR experiments were incubated until the stage indicated then flash frozen on dry ice in 1.5 ml Eppendorfs. These embryos were homogenised on ice in 1 ml of tri-reagent and then centrifuged for 10 min (for this protocol all centrifugation steps were at 16,000 G and 4 °C). The aqueous layer was then removed and retained and left to stand for 5 min on ice before addition of 200 µl of chloroform. The mixture was then vortexed thoroughly for 1 minute and then stood at room temperature for five min before 15 min of centrifugation. The aqueous phase was then removed and retained and mixed with 500 µl isopropanol before being precipitated at -20 °C for 30 min. Following this incubation the sample was then centrifuged for 15 min and the isopropanol removed, avoiding contact with the RNA pellet. The pellet was then washed briefly in 70% ethanol then the pellet dried by vacuum pump. The pellet was then resuspended in 100 µl dH₂O, then 120 µl of 7.5 M LiCl/50 µM EDTA added and mixed by pipetting. The sample was then incubated overnight at -80°C.

The following day the sample was centrifuged for 20 min and the pellet washed in 1ml of ice cold 70% ethanol. The pellet was then dried by vacuum pump before resuspension in 50 µl dH₂O. The concentration of the RNA was established by NanoDrop and stored at -80 °C.

2.5.9 cDNA synthesis

cDNA synthesis was achieved through use of the First Strand Synthesis kit (Invitrogen). The reaction (1 µl Oligo dT primer, 100 ng RNA, 1 µl mM dNTPs, to 14 µl with dH₂O) was mixed by pipetting then incubated for 5 min at 65 °C (all temperature incubations in this protocol were performed in a PCR machine). Following this incubation the mix was kept briefly on ice before addition of 4 µl 5x

1st strand buffer + 2 µl 0.1 M DTT + 1 µl dH₂O. The mix was then incubated for 2 min at 42 °C before addition of 1 µl SuperscriptII and further incubation at 42 °C for 1 h. The superscript was inactivated by a 15 minute incubation at 80 °C. The cDNA was then diluted 1:1 in dH₂O and stored at -20 °C.

2.5.10 rtPCR

rtPCR of *X.tropicalis* cDNA was achieved using thermo Scientific 2x PCR Master Mix following the manufacturer's instructions. The primer pairs used and their annealing temperatures and extension times were listed in Table 2-2. The PCR mix for rtPCR consists of; 12.5 µl of 2x PCR Master Mix, 1 µl 10 µM forward primer, 1 µl 10 µM reverse primer, 1 µl cDNA, up to 25 µl with dH₂O. The PCR reaction occurred as follows: 3 min 95 °C, then 35 cycles of 30 s at 95 °C, 30 s at the annealing temperature, then a 72 °C as required by the product length, concluded by a 72 °C final extension for 15 min.

The role of N-Srcs in neuroblastoma differentiation

3.1 Introduction

Neuroblastoma is a developmental cancer of the sympathetic nervous system, arising from the sympathoadrenal lineage of the neural crest (Davidoff, 2012). It is also the most common extra-cranial solid tumour in children. In the USA, neuroblastoma accounts for up to 10% of cancer cases and 15% of cancer-related mortalities in children (Gurney et al., 1995). Neuroblastoma incidence is highest in children under five, with 30% of incidences of neuroblastoma in the USA being reported in children under 1 year of age (Ishola and Chung, 2007). The age at which neuroblastoma is diagnosed correlates significantly with the survival rates of the disease. The overall survival rate is 88% in infants (<18 months), 49% in children (18 months to 12 years), but only 10% in adolescents over 12 years of age (Cheung et al., 2012). Neuroblastoma is a highly heterogeneous cancer, whilst low grade tumours in patients diagnosed at under 12 months often demonstrate spontaneous regression and differentiation, up to 30% of high risk cancers are un-treatable with current therapies (Brodeur, 2003).

Onset of neuroblastoma is most commonly sporadic, with only 1-2% of cases linked to familial gene mutations such as in the ALK or PHOX2B genes (Mossé et al., 2008). Neuroblastoma is one of very few cancers that demonstrate spontaneous regression in cases with a positive prognosis. This regression is characterised by a differentiation of neuroblastoma cells into post-mitotic, neuronal cells and is indicative of the developmental nature of the cancer (Evans et al., 1976). The onset of neuroblastoma can be characterised as arising from neuronal stem cells that have missed, or are resistant to their differentiation cues, resulting in constitutive cell proliferation without differentiation. Tumour progression varies from spontaneous regression without therapeutic intervention, to an aggressive, malignant phenotype that is poorly responsive to treatment (Riley et al., 2004). The prognosis of neuroblastoma patients has been associated with the expression of N1- and N2-Src. Matsunaga and colleagues demonstrated that the expression of N1- and N2-Src was higher in lower stages of the disease, associated with a more positive prognosis. In a screen of 40 localised tumours and 20 metastatic tumours, it was observed that N2-Src expression exceeding 15% of total Src expression correlated significantly with a

longer event free survival in patients (Matsunaga et al., 1998). The relative expression of N2-Src mRNA compared to total Src mRNA proved to be a more valuable prognostic tool than the total N2-Src mRNA expression (Matsunaga et al., 1993a). This correlation was later confirmed independently (Terui et al., 2005). The model neuroblastoma cell line LAN-5 is used extensively to research both N1-Src expression (Min et al., 1995, Black, 1992), and more broadly as a model for neuronal differentiation (Borriello et al., 2000) and neuronal diseases such as Alzheimer's disease (Businaro et al., 2006). Matsunaga and colleagues demonstrated that during RA/cAMP induced differentiation LAN-5 cells, which express N1- and N2-Src in control conditions, levels of N1- and N2-Src mRNA increased whilst C-Src levels decreased.

Treatment for neuroblastoma varies with the risk stratification of the disease and ranges from observation only, to standard cancer treatment methods such as surgery, chemotherapy and radiotherapy. In addition to these methods, treatment for high risk neuroblastoma also aims to differentiate the cancer using drugs such as RA to induce neuronal maturation of neuroblastoma cells remaining after other treatments, in order to prevent relapse (Matthay et al., 1999). Due to the age of neuroblastoma patients, the treatments associated with neuroblastoma therapy have significant long term complications including hearing loss, hypothyroidism, ovarian failure, and musculoskeletal and pulmonary abnormalities (Laverdière et al., 2005). As such, the identification of a 'silver bullet' in neuroblastoma treatment that will induce differentiation or apoptosis in the tumour cells without damaging normal childhood development is of critical importance.

For this reason, characterising novel signalling pathways that contribute to neuroblastoma differentiation is of the utmost importance, as these pathways may provide novel drug targets for future neuroblastoma therapies. The link between neuronal Src expression and a positive prognosis in neuroblastoma, in addition to its temporal and spatial expression patterns during development, suggests that N1- and N2-Src may have an important role in neuronal differentiation. Although N1- and N2-Src may not be themselves druggable, identification of the upstream regulators of their expression and their downstream effectors could provide novel targets for neuroblastoma differentiation therapies.

The aims of this chapter are to identify whether neuronal Src expression contributes to the differentiation in neuroblastoma *in vitro*, in addition to characterising the role that these splice variants may have in that process.

3.2 Results

3.2.1 Neuronal Srcs are more active than C-Src in B104 cells

Neuronal Srcs have previously been shown to possess increased kinase activity compared to C-Src. In order to determine whether overexpression of the FLAG tagged Src constructs I used throughout my experiments demonstrate this variance in activity in neuroblastoma cells, the rat neuroblastoma cell line B104 was transfected with the C-, N1-, or N2-Src-FLAG constructs or a vector control. Typically, fusion of molecular tags such as FLAG or GFP to Src either interferes with myristoylation at the N-terminus or folding and auto-regulation at the C-terminus. Sandilands and colleagues demonstrated successful fusion of GFP to Src by use of C-terminal a glycine/serine-rich flexible linker peptide, which has been utilized in our FLAG constructs (Sandilands et al., 2004). Cells were incubated for two days post-transfection and then incubated in the presence or absence of 100 μ M NaVa₄³⁻ solution (used in this experiment to increase overall Src activity in the cells) in PBS for 10 min at 37° prior to lysis in SDS sample buffer. The lysates were then separated on a 10% SDS poly-acrylamide gel and probed by Western blotting.

Western blotting detected similar levels of the FLAG epitope tag attached to C- and N1-Src whilst detecting lower levels of N2-Src, especially so in pervanadate treated samples (Fig. 3-1). This decreased detection could be due to a lower transfection efficiency, decreased proliferation of N2-Src expressing cells, or a post translational modification of N2-Src preventing detection of the N2-Src FLAG signal (Fig. 3-1).

Phosphorylation of the activation loop of the kinase domain at Y416 is a well-established indicator of Src kinase activity (Kmiecik and Shalloway, 1987) and N1- and N2-Src showed significantly increased phosphorylation compared with C-Src at this site (Fig 1). Interestingly, two bands were identified in the N2-Src lanes of the

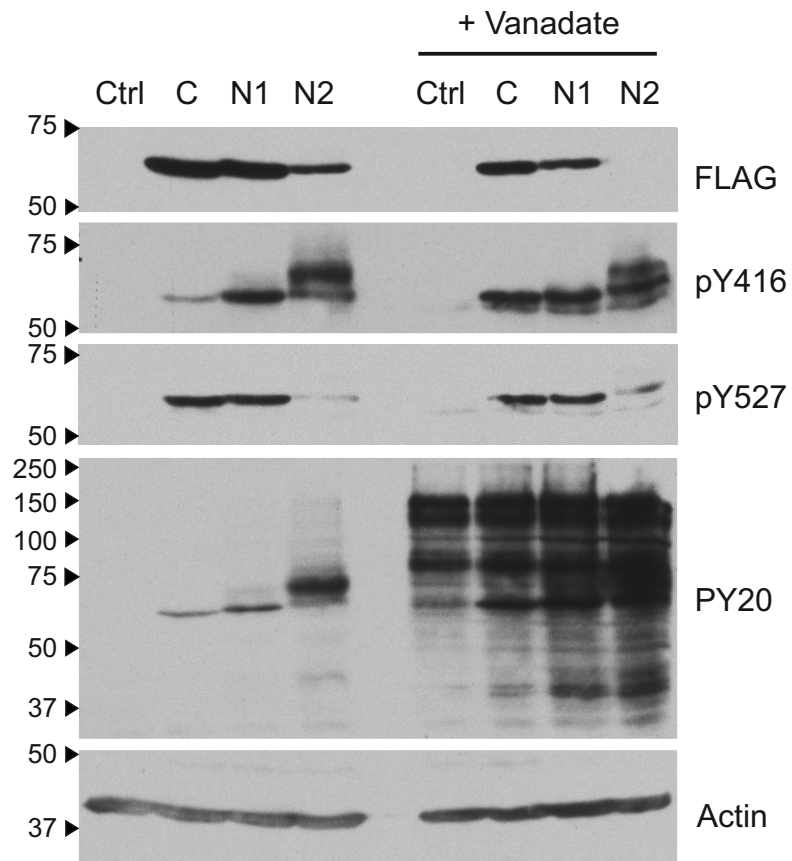


Fig. 3-1. Western blotting of C-, N1- and N2-Src-FLAG over-expressed in B104 cells with and without pervanadate treatment.

Cells were transfected for two days and transiently treated with either PBS/pervanadate or PBS alone at 37 degrees for 10 minutes before lysis. Lysates were run on 12.5% poly-acrylamide gel and transferred to PVDF membrane and Western blotted as described in 2.2.3. Actin is shown as a loading control. Total phosphotyrosine is identified by PY20 staining, Src construct abundance is identified by FLAG staining. This blot is representative of three replicates performed of this experiment.

blot, indicating possible post-translational modification of N2-Src in B104 cells, or alternatively that N-Src is causing an increase in either transcription or phosphorylation of another Src Family Kinase of higher molecular weight (Fig. 3-1). Y416 SFK phosphorylation was detected in all vanadate samples (Fig. 3-1). This is likely to be un-tagged endogenous Src, however due to the conservation of Y416 in SFKs, the antibody could be cross-reacting with a similar SFK.

Phosphorylation of SFKs at Y527 activates auto-inhibitory intramolecular binding by the SH2 domain, and is an often-used indicator of negative regulation of SFKs (Zheng et al., 2000). C-Src and N1-Src were similarly phosphorylated at this site in B104 cells, however N2-Src exhibited much less pY527 staining, indicating increased activity of the enzyme under basal conditions. This relative decrease was also observed in the pervanadate treated samples (Fig. 3-1) suggesting decreased N-terminal inhibition of N2-Src activity when compared to C- and N1-Src.

In order to identify whether increased activity of N1- and N2-Src translated to increased phosphorylation of substrates, the samples were probed with a monoclonal phosphotyrosine antibody, clone PY20. General phosphotyrosine staining identified the same pY416 phosphorylation events discussed above, in addition to weaker phosphotyrosine signals at a variety of molecular masses in N2-Src transfected cells, suggesting N2-Src increases global phosphotyrosine levels under basal conditions to a greater extent than C- or N1-Src. In all vanadate treated samples, global phosphotyrosine levels were significantly increased compared to corresponding untreated samples. Global phosphotyrosine levels of vanadate treated samples increased in the following order; control < C-Src < N1-Src < N2-Src (Fig. 3-1).

3.2.2 The effects of N1- and N2-Src overexpression on B104 cell morphology

Matsunaga and colleagues (1993a) demonstrated that increased N-Src expression tends to correlate with more favourable neuroblastoma prognosis and increased differentiation of neuroblastoma cell lines. To test whether N-Srcs are capable of driving the differentiation, we sought to identify any morphological effects of increased N1- and N2-Src activity that may indicate differentiation in the neuroblastoma cell line B104. Cells were co-transfected with FLAG tagged Src

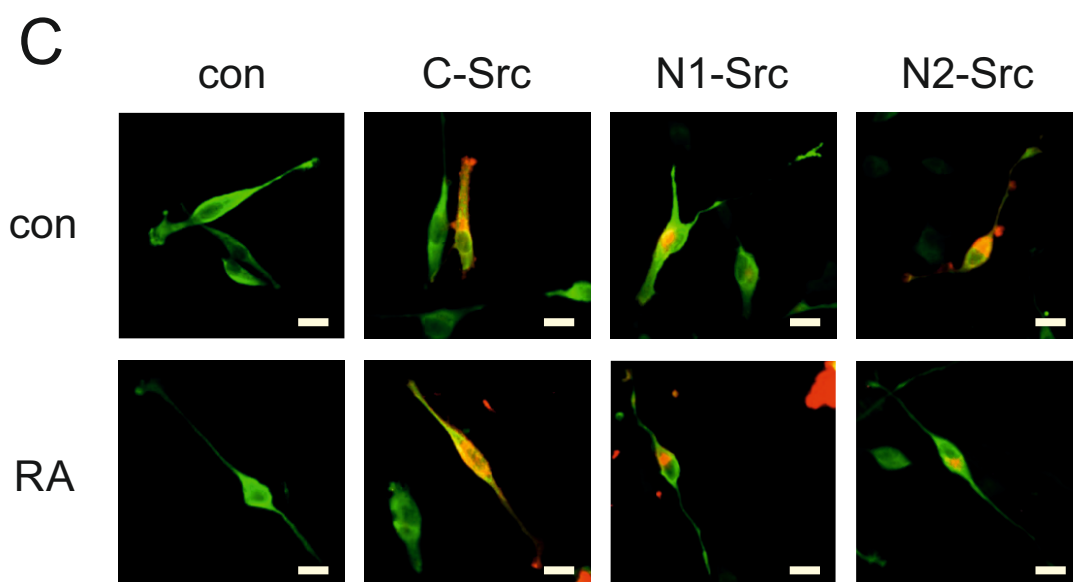
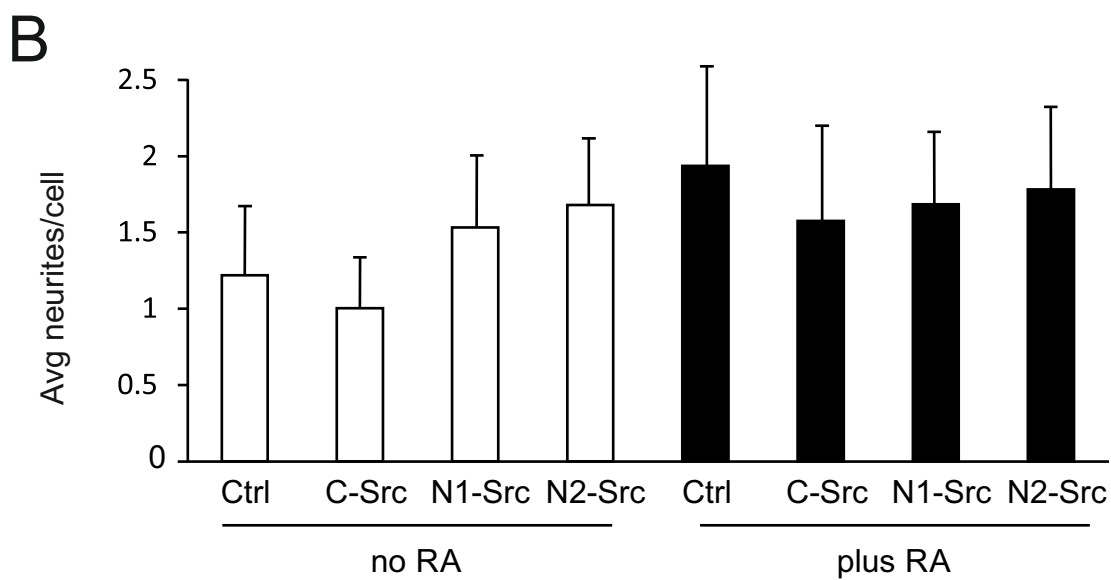
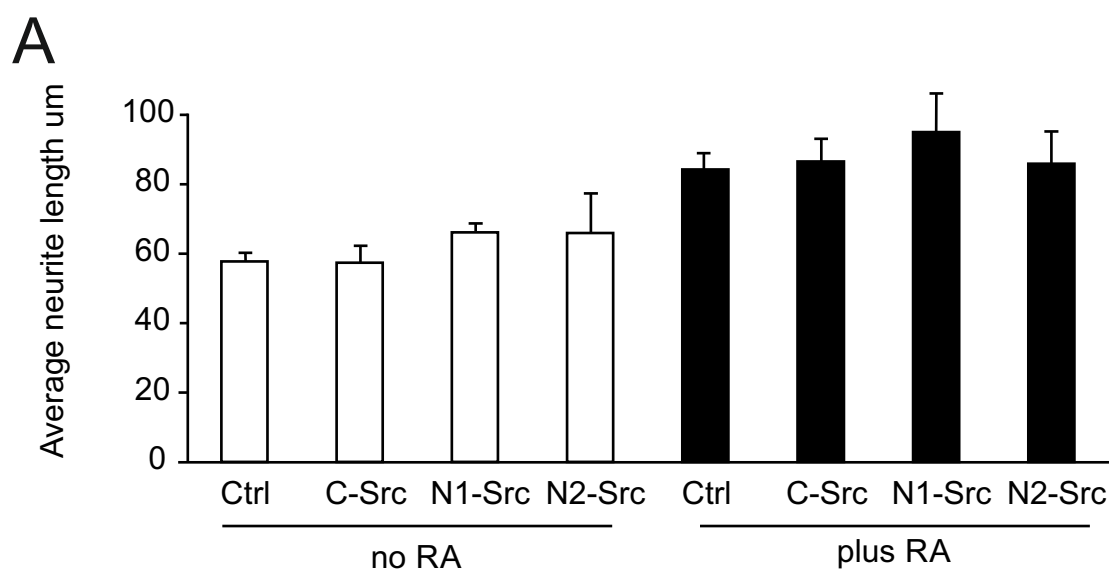


Figure. 3-2 (page 85). Effect of N-Src expression on B104 cell morphology.

Cells were co-transfected for four days with FLAG tagged Src constructs and a soluble CFP gene, in the presence or absence of 5 μ M retinoic acid. Cells were fixed after 4 days, and stained with mouse α -FLAG and rabbit α -GFP antibodies primary antibodies then ALEXA 416 α -rabbit and ALEXA 594 α -mouse secondary antibodies. The cells were then imaged and analysed. The experiment was repeated three times. Neurite lengths (A) and numbers (B) were measured and counted using NeuronJ. Error bars show Standard Error of the Mean, calculated from the mean values of each replicate. The change in cell morphology as a result of plasmid expression was found to be non-significant by ANOVA. C) Shows a representative image for each condition. CFP is shown in green and FLAG staining is shown in red. Scale bar 20 μ m.

constructs (or a vector control) and soluble CFP and then maintained in culture for 4 days prior to fixing and immunostaining. The cells were then imaged using CFP fluorescence to define the cell edge, and the number and length of neurites in each cell were quantified. Neurites were defined as extensions from the cell of greater than one diameter of the cell body in length and below 2 μ m in diameter (Tojima et al., 2003). This experiment was performed in the presence or absence of 5 μ M retinoic acid (RA). RA is a potent differentiating agent of neuroblastoma both *in vitro* and *in vivo* (Sidell, 1982, Matthay et al., 1999) and was used in this instance to detect whether any changes in neurite length and number by N1- and N2-Src overexpression were additive to RA induced differentiation.

In addition to neurite length and number analyses, inspection of the cells revealed a differential subcellular localisation between C-, N1-, and N2-Src. Whilst C-Src tends to be expressed throughout the cell in a punctate manner, with a slight increase in perinuclear abundance; N1- and N2-Src demonstrate a particularly restricted subcellular localisation to one portion of the perinuclear region. This localisation is also observed in other cell lines such as COS7 cells (Fig. 5-1), and HeLa cells (Fig. 4-1), and was later identified to co-localise with the trans-golgi network (Fig. 4-2).

Analysis of the average length of the B104 neurites revealed an increase in the length of neurites in cells transfected with N2-Src (Fig 2A, B). This increase does not appear to be additive to the effects of retinoic acid treatment upon B104 cells (Fig. 3-2A, B). Similarly N1- and N2-Src caused a small increase in the average number of neurites per cell compared to controls. This difference between control and N-Src samples was, again, reduced in RA treated samples. By contrast, C-Src caused a

decrease in the average number of neurites per cell, both in the presence and absence of RA (Fig. 3-2A, B). Stringent statistical analyses of the mean values of each of the three replicates of this experiment failed to identify a statistically significant effect in the data, however, the trends described above occurred consistently in each replicate. It is likely that an alternative quantification method would be needed to observe statistical significance in the small effects of N1- and N2-Src on B104 differentiation.

3.2.3 Characterising human neuroblastoma cell lines

To better clarify the effects of neuronal Src expression on neuroblastoma differentiation, I selected three human neuroblastoma cell lines and assessed their capacity for differentiation whilst manipulating the expression levels of neuronal Srcs.

The three human neuroblastoma cell lines chosen for assaying the effects of neuronal Srcs on neuroblastoma differentiation were LAN-5, SK-N-AS and KELLY. LAN-5 cells readily differentiate and express differentiation markers under RA stimulation (Fig. 3-3, Table 3-1 (Guglielmi et al., 2014)) and are induced towards neuronal differentiation by cAMP treatment (Fig. 3-3). They also are known to express both N1- and N2-Src (Matsunaga et al., 1993a), which makes them an ideal candidate to assess the effects of neuronal Src knockdown upon their capacity for differentiation. In contrast, the SK-N-AS cell line shows very little neuronal differentiation under control conditions, and is resistant to both RA and cAMP induced differentiation (Fig. 3-3). Furthermore, while LAN-5 cells express multiple copies of the potent oncogene Myc-N, SK-N-AS cells express only a single copy (Guglielmi et al., 2014). Although it is not known whether N1- and N2-Src are expressed in SK-N-AS cells, their lack of a neuronal phenotype, and resistance to differentiation, suggests that they are unlikely to express these splice variants due to their association with differentiated neurons. Finally, KELLY cells represent a mid-point in terms of their capacity for differentiation. Although KELLY cells are RA resistant, they show a higher basal level of neuronal differentiation than SK-N-AS cells and can be induced to further differentiate by stimulation of cAMP signalling (Fig. 3-3). Detailed information about the tumour from which KELLY cells are derived is not available,

	LAN-5	SK-N-AS	KELLY
N-Src expression	N1- and N2-Src detected	Unknown	Unknown
Patient	5 month old male	8 year old female st.4	Unknown
Cell line origin	Bone marrow metastasis	Bone marrow metastasis	Unknown
Myc amplification	Amplified	Single copy	Amplified
Retinoic acid	Neuronal differentiation	Resistant	Resistant
cAMP	Neuronal differentiation	Resistant	Partial resistance

Table 3-1. Summary of LAN-5, SK-N-AS and KELLY cell line information.

Information on each of the three human neuroblastoma cell lines used in chapter 3. Information for these cell lines was acquired from the literature (Matsunaga et al, 1993, Thiele, 1998, Guglielmi, 2014) and from the ATCC website (www.lgcstandards-atcc.org/)

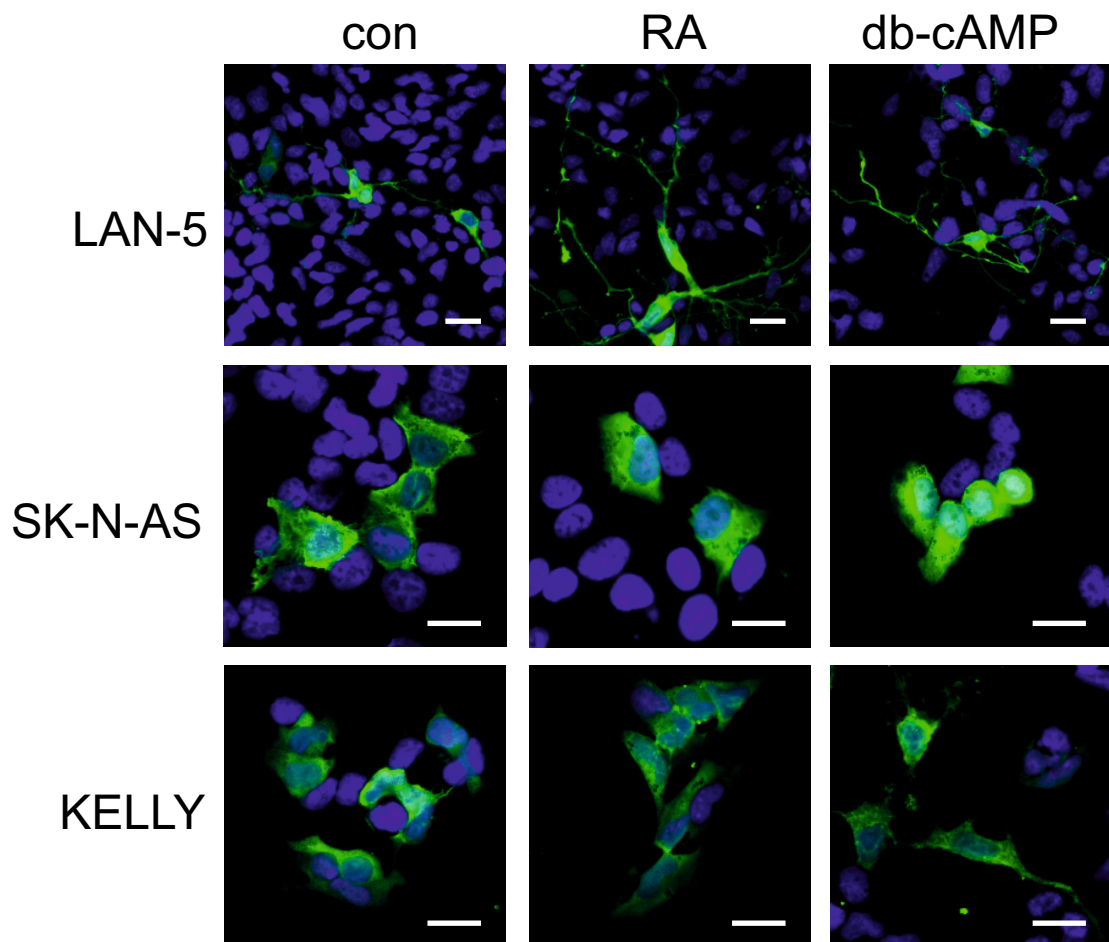


Fig. 3-3. Characterisation of human neuroblastoma cell lines

Representative images showing of the effects of differentiating agents on human neuroblastoma cell lines. Cells were transfected with soluble CFP for four days and treated with 5 μ M Retinoic Acid or 1mM dibutyryl cyclic AMP. Cells were mounted using mowial mountant containing 1 μ g/ml DAPI. GFP is shown in green, DAPI in blue. Scale bar is 20 μ m.

but they have been demonstrated to have Myc-N amplification (Chanthery et al., 2012).

By introducing neuronal Srcs into SK-N-AS and KELLY cell lines and depleting N-Src expression in LAN-5s, I aimed to understand the effects of N-Src expression on neuroblastoma differentiation.

3.2.4 Confirming N-Src shRNA function

To identify the specific effects of N1- and N2-Src knockdown during neuronal differentiation, shRNAs were designed that specifically targeted the N-Src microexons (Table 2-2). Unfortunately shRNA designed to target only C-Src, avoiding N1- and N2-Src knockdown by spanning the exon 3/4 boundary were not effective (data not shown), hence only neuronal Src knockdown was assayed. pSUPER plasmids (Brummelkamp et al., 2002) were prepared that expressed the N1- or N2-Src shRNA sequences and soluble GFP from HI and CMV promoters respectively, and used alongside the empty pSUPER-GFP as a control.

To test the function and specificity of the shRNA plasmids, combinations of the shRNA plasmids were co-transfected into the monkey fibroblast cell line COS7 with C-, N1- and N2-Src-FLAG constructs. These cells were chosen due to their high transfection efficiency and the absence of endogenous N-Src expression. The cells were then cultured for 2 days before lysis in SDS sample buffer. Detection of the FLAG epitope by Western blotting indicated that depletion only occurred when the Src construct was co-expressed with its corresponding shRNA. This demonstrated that the shRNAs were both functional and splice-variant specific (Fig. 3-4).

Whilst the FLAG tagged Src-FLAG constructs originate from rat cDNA, the sequence conservation between rat and human Src isoforms was such that there are no base pair substitutions within the regions targeted by the shRNAs (data not shown). Specificity of the shRNAs was achieved by targeting the sequences within the specific N-Src exon sequence. This suggests that the N1- and N2-Src pSUPER shRNAs would be effective at knocking down expression of endogenous human mRNAs.

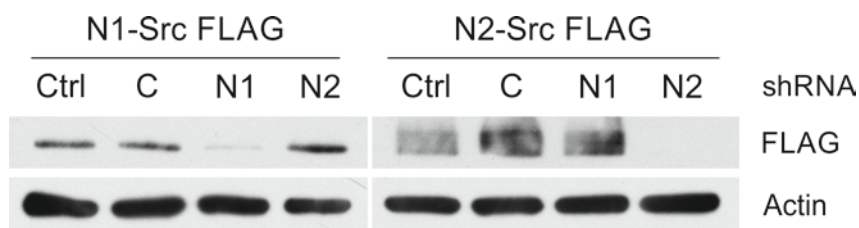


Figure. 3-4. Characterising pSUPER shRNA construct function.

COS7 cells were co-transfected with pFLAG Src constructs and pSUPER shRNA constructs for 2 days, then lysed in Laemmli SDS sample buffer and run on 12.5% SDS PAGE then transferred to PVDF for Western blotting as described in 2.2.3. Actin is shown as a loading control and expression of Src constructs is indicated by FLAG staining.

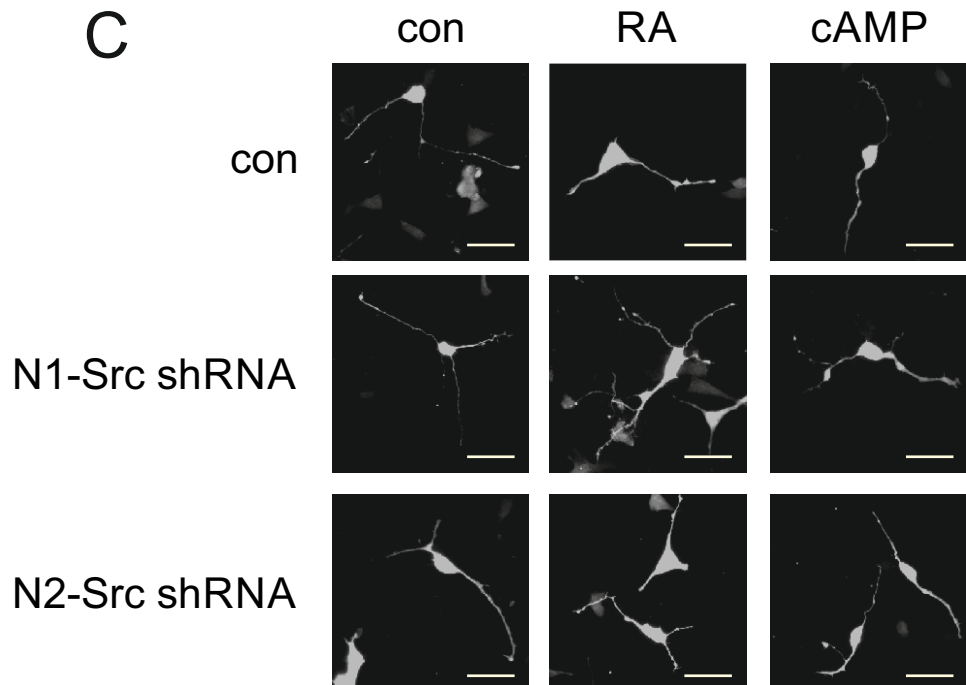
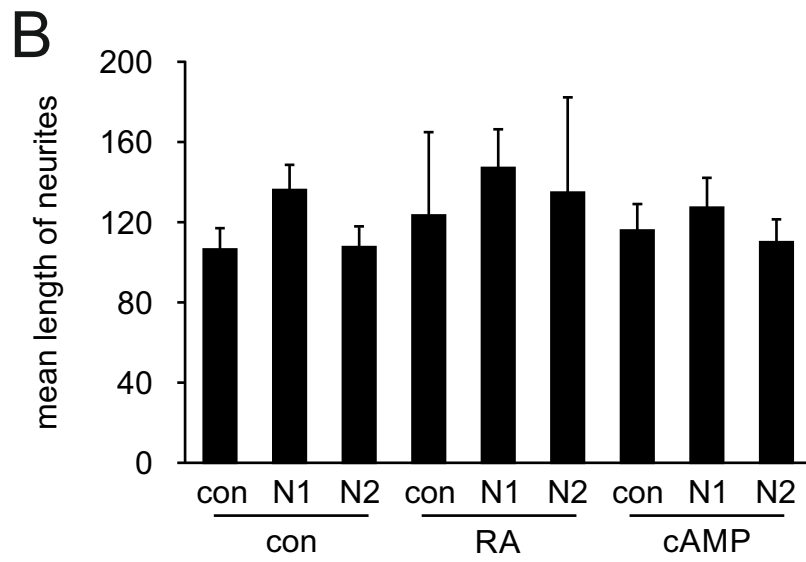
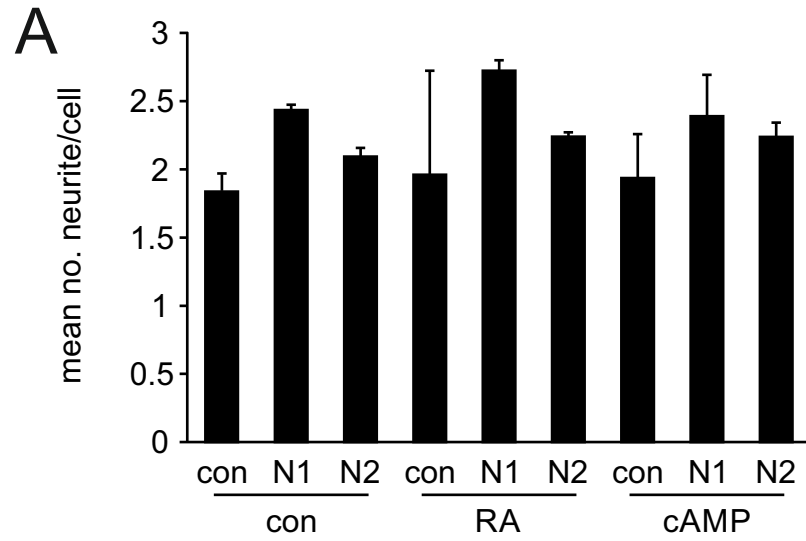
3.2.5 Knockdown of neuronal Srcs in LAN-5 cells

N1- and N2-Src pSUPER shRNA plasmids or the pSUPER-GFP vector control were transfected into LAN-5 cells in either control, RA or cAMP containing media. After four days the cells were fixed and immunostained to enhance the GFP signal. Fluorescent cells were then imaged and the neurite lengths and numbers quantified using NeuronJ (Meijering et al., 2004). No significant decrease in differentiation was observed when N1- and N2-Src was knocked down (Fig. 3-5). Surprisingly, cells transfected with the N1-Src shRNA demonstrated an increase in the number of neurites being produced, in both control and drug samples (Fig. 3-5). Additionally, the mean lengths of neurites increased marginally in the N1-Src knockdown condition (Fig. 3-5). The pSUPER N2-Src shRNA plasmid had no significant effects upon the length or number of neurites (Fig. 3-5).

The failure of these cells to exhibit the expected morphological effect as a result of N1- and N2-Src knockdown suggests that neuronal Srcs may have more complex roles in neuronal differentiation than was originally hypothesised.

Figure. 3-5 (page 91). Effect of N-Src knockdown on LAN-5 differentiation.

LAN-5 cells transfected for 4 days with shRNA plasmids in the presence or absence of 5 μ M RA. After four days cells were fixed and stained with rabbit α -GFP primary and ALEXA 488 α -rabbit secondary antibodies. Neurite number (A) and length (B) were quantified using NeuronJ. This experiment was performed twice, as such statistical analyses were not performed. Error bars show Standard Error of the Mean. C) Representative images from each condition. Scale bar shows 20 μ m.



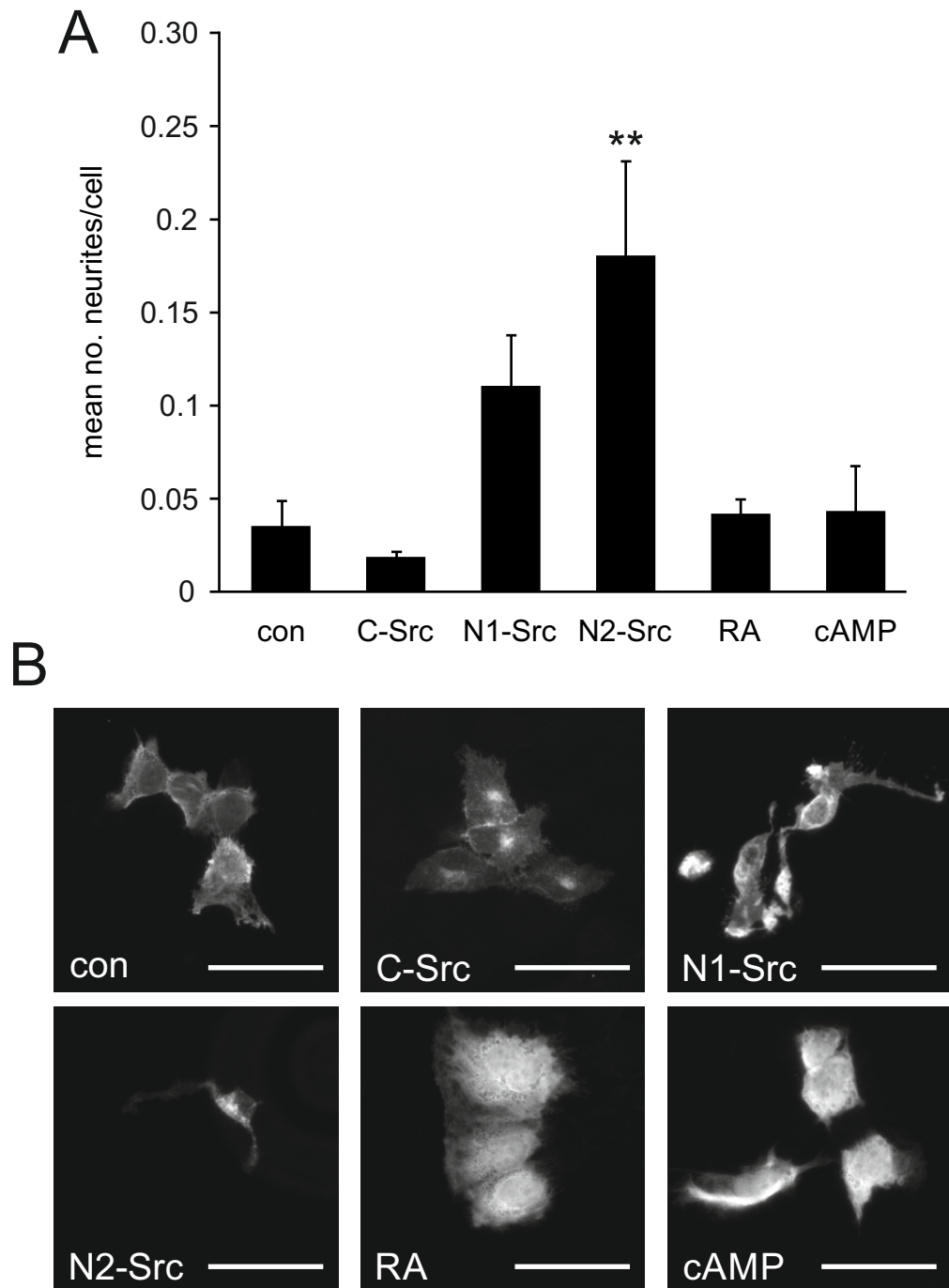


Fig. 3-6. Effect of N-Src over-expression on SK-N-AS differentiation.

Over-expression of FLAG tagged C-, N1- and N2-Src in SK-N-AS cells. Cells were co-transfected for 4 days with C-, N1- or N2-Src pFLAG constructs and the soluble CFP plasmid pmCer. The cells co-stained with mouse α -FLAG and rabbit α -GFP primary, and ALEXA 594 α -mouse and ALEXA 488 α -rabbit secondary antibodies. Cells were then imaged and (A) the number of neurites per cell counted for each condition and the SEM calculated from the means of four replicates of the experiment. Statistical significance was assessed by ANOVA of the mean data of each replicate ** = $p > 0.005$. B) Representative images showing CFP staining in control, RA and cAMP conditions, and FLAG staining in C- N1- and N2-Src conditions. Scale bar is 40 μ m.

3.2.6 Over-expression of N-Srcs in the SK-N-AS cells

To test whether enhancing N-Src expression could contribute to neuronal differentiation in high risk neuroblastoma cells, SK-N-AS cells were either co-transfected with C-, N1-, N2-Src or a vector control, and soluble CFP and incubated in the presence or absence of 5 μ m RA or 1 mM cAMP. Cells were incubated for 4 days to allow neuritogenesis to occur and then fixed and immunostained. Thirty fields of view were imaged at 40x magnification across four replicates and were quantified for neurite outgrowth (Fig. 3-6). Neurites were defined as extensions from the cell soma exceeding the diameter of the cell body and less than 5 μ m in thickness.

In the control, C-Src, and cAMP conditions, the ratio of neurites to cells was below 0.05 (Fig. 3-6) and fewer than 5% of cells extended neurites (data not shown). Cells overexpressing N1-Src showed a small increase in this ratio to 0.1 neurites per cell and 0.18 neurites were observed per cell in N2-Src. Whilst 0.18 neurites per cell seems relatively small, the resistance of SK-N-AS to neuritogenesis in all other conditions means that the N2-Src induced neuritogenesis is statistically significant (Fig. 3-6). In addition to the neuronal phenotype and neurite quantitation, it was observed that cells expressing N1- or N2-Src were very rarely observed in clusters or groups. This correlation was observed in all three replicates, and contrasted sharply with the clusters of three or four cells observed in C-Src overexpressing cells (data not shown). This suggests that, in addition to inducing cytoskeletal remodelling, N-Src overexpression in neuroblastoma cells may decrease proliferation, or cause more cell death than C-Src and the differentiating agents RA and cAMP. This fits with a model of N1- and N2-Src as promoters of both differentiation and cell cycle exit in neuroblastoma and neuronal precursors.

3.2.7 Expression of N2-Src induces neuritogenesis in KELLY cells

As previously stated, KELLY cells represent an intermediate between LAN-5 and SK-N-AS cells in both their basal differentiation and their capacity for RA/cAMP-induced neuronal differentiation. To identify whether enhanced neuronal Src expression can also drive differentiation in this system, I transfected and analysed the KELLY cell line under the same conditions previously stated for SK-N-AS cells.

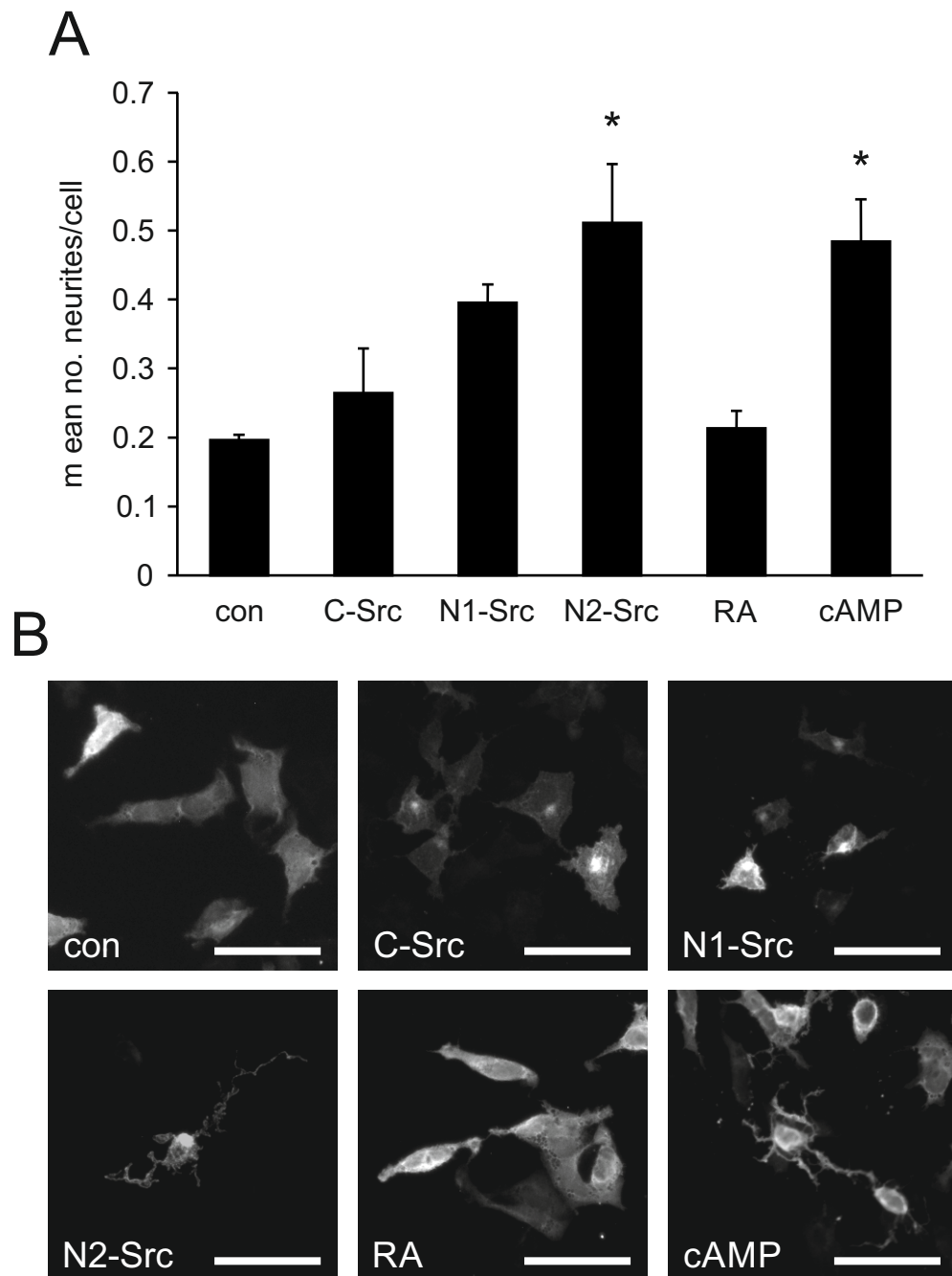


Fig. 3-7. Effect of N-Src over-expression on KELLY differentiation.

Over-expression of FLAG tagged C-, N1- and N2-Src in KELLY cells. Cells were co-transfected for 4 days with C-, N1- or N2-Src pFLAG constructs and the soluble CFP plasmid pmCer. The cells co-stained with mouse α -FLAG and rabbit α -GFP primary, and ALEXA 594 α -mouse and ALEXA 488 α -rabbit secondary antibodies. Cells were then imaged and (A) the number of neurites per cell counted for each condition and the SEM calculated from the means of three replicates of the experiment. Statistical significance was assessed by ANOVA of the mean data of each replicate * = $p < 0.05$. B) Representative images showing CFP staining in control, RA and cAMP conditions, and FLAG staining in C- N1- and N2-Src conditions. Scale bar is 40 μ m.

These data confirmed the observation that treatment of KELLY cells with RA does not increase neurite outgrowth above that observed in controls (con 0.19 neurites/cell \pm 0.007, RA 0.21 neurites/cell), however neuronal differentiation was increased significantly with the addition of 1 mM cAMP (0.5 neurites/cell) (Fig. 3-7). Although a negligible increase in neurite number was observed in C-Src treated cells (0.26 neurites/cell), the most significant effect on the cells was caused by N1 and N2-Src (Fig. 3-7). N1-Src transfection significantly increased the formation of neurites to 0.4 neurites/cell (Fig. 3-7). Following the pattern observed in other experiments, N2-Src overexpression caused a statistically significant increase in neurite outgrowth, with 0.5 neurites present per cell (Fig. 3-7).

Whilst a significant effect upon the number of neurites per cell was observed in KELLY cells expressing N2-Src, only 29% of N1-Src expressing cells bore neurites, which is not significantly greater than 18% for the controls. A significantly higher proportion of N2-Src cells (41%) and cAMP cells (38%) expressed neurites than controls. This is because a higher proportion of cells in N1- and N2-Src expressing cells bear more than one neurite. The increased neuronal phenotype suggests that in cells that are induced towards neuronal differentiation by N1- and N2-Src, a more significant neuronal differentiation is occurring. This is evident by the morphology observed in the individual cells (Fig. 3-7).

3.2.8 The effects of N-Src expression on neuroblastoma cell proliferation

In order to address the apparent decrease in the abundance of N2-Src transfected SK-N-AS cells when compared to C- and N1-Src, I sought to determine whether the N2-Src transfected cells were dividing. SK-N-AS and KELLY cells were transfected with the FLAG-tagged Src isoforms, or a vector control, and incubated for three days in the presence or absence of 5 μ M RA or 1 mM cAMP before fixing and immunostaining. Alongside antibody staining of the FLAG epitope tag, the cells were probed with the proliferation marker Ki67, a widely used marker for cell proliferation expressed throughout all proliferative stages of the cell cycle (Gerdes et al., 1983).

Thirty fields of view were imaged for each FLAG construct resulting in over 100 cells showing FLAG staining assessed for Ki67 antibody staining within the

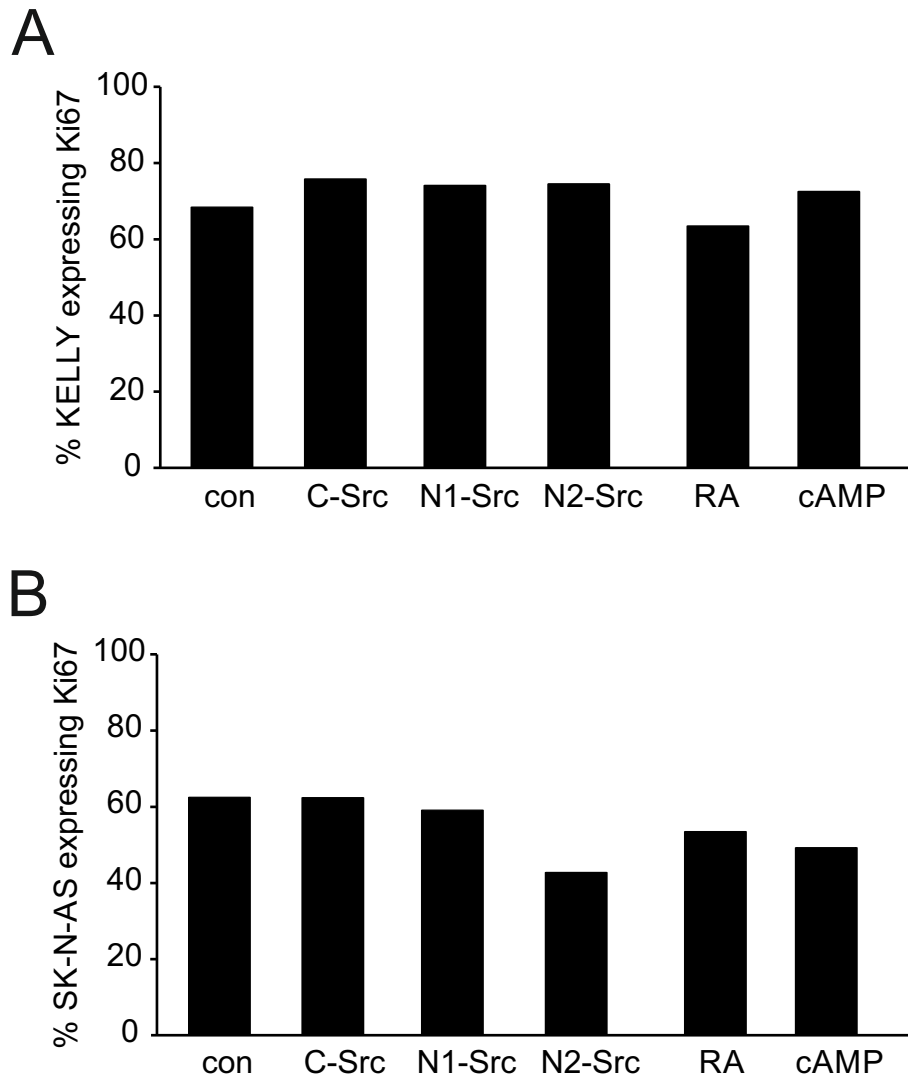


Fig. 3-8. The effect of N-Src overexpression on KELLY and SK-N-AS proliferation.

KELLY (A) and SK-N-AS (B) cells were transfected with control, C- N1- and N2-Src pFLAG plasmids or treated with RA or cAMP for three days. Cells were co-stained with mouse α -FLAG and rabbit α - Ki67 primary and ALEXA 594 α -mouse and ALEXA 488 α -rabbit secondary antibodies and mounted in mowial containing 1 μ g/ml DAPI. Each experiment was only performed once, as such statistical significance was not tested. Cells were imaged at 20x magnification over ten fields of view and the percentage of cells expressing nuclear Ki67 calculated. A) KELLY con n=510, C-Src n=161, N1-Src n=85, N2-Src n=90, RA n=509, cAMP n=655. B) SK-N-AS con n=575, C-Src n=168, N1-Src n=103, N2-Src n=140, RA n=625, cAMP n=551.

nucleus. In the vector control, RA and cAMP conditions, the top left quadrant of 10 fields of view were analysed, resulting in over 400 cells per condition.

These data showed that in SK-N-AS cells there was no noteworthy difference in nuclear Ki67 detection and, as such, cell proliferation between control, C-Src and N1-Src cells (63%, 63%, and 59% of cells respectively). As hypothesised by the decrease in abundance of N2-Src expressing cells in previous experiments, 20% fewer N2-Src expressing cells were proliferative when compared to control and C-Src expressing cells. This exceeds the decreased cell proliferation caused by both RA (54%) and cAMP (49%). These data suggest that N2-Src, in addition to inducing neuritogenesis, also removes a portion of cells from the cell cycle, suggesting that N2-Src induced neuroblastoma differentiation is terminal.

Interestingly, whilst SK-N-AS cells showed a profound decrease in cell proliferation in N2-Src treated cells, KELLY cells showed no difference in Ki67 staining between splice variants (C-Src 76%, N1- and N2-Src 74%). These data suggest that, whilst KELLY cells show a higher level of neuritogenesis when transfected with N2-Src, this is not indicative of terminal differentiation of these cells, as indicated by exit from the proliferative cell cycle in SK-N-AS cells.

3.3 Discussion

Taken together, the experiments in this chapter have demonstrated that the neuronal isoforms of C-Srcs are constitutively more active than C-Src when expressed in a neuroblastoma cell line, and that overexpression of these N-Srcs in differentiation resistant cell lines increases neuronal differentiation. The data also suggest that a more complex relationship between N-Src expression and neuronal phenotype exists, as whilst N2-Src can induce differentiation in KELLY and SK-N-AS cells, knockdown of expression in the human neuroblastoma cell line LAN-5 failed to elicit a reduction in differentiation. Finally, analysis of Ki67 expression in SK-N-AS cells indicates that N2-Src overexpression in this neuroblastoma cell line is decreasing proliferation.

3.3.1 Increased activity of neuronal Srcs expressed in neuroblastoma

Western blotting of Src transfected B104 lysates indicated that both N1- and N2-Src have a significantly higher basal activity than C-Src in neuroblastoma cells (Fig. 3-1). In addition to the increased detection of tyrosine phosphoproteins in these samples, N1- and N2-Src are both observed to have higher phosphorylation of the Y416 kinase domain activation loop. In all cases N2-Src is shown to be the most active, with the greatest global tyrosine phosphorylation and the highest pY416 signal, in addition to a much lower detection of the inhibitory 527 staining (Fig. 3-1). This observed increased activity is highly reproducible, and is also evident when the Src splice variants are overexpressed in HeLa cells and developing *Xenopus* embryos (Fig. 4-12; Fig. 5-3).

The mechanism of constitutive neuronal Src activation could be attributed to a decrease of the inhibiting intramolecular interaction between the SH3 domain and the SH2-kinase linker sequence. This interaction is highly important for locking the kinase domain in an open, unstructured and inactive conformation, in which the activation loop forms an alpha helix, preventing the activating phosphorylation of Y416 (Huse and Kuriyan, 2002). Mutation of the n-src loop of the C-Src SH3 domain, into which the neuronal exons insert, is known to decrease the SH3-SH2/kinase linker binding, increasing the activation state of the protein (Brábek et al., 2002). N1-Src exon inclusion into the n-src loop has been shown to change the affinity of N1-Src binding to C-Src substrates (Weng et al., 1993), as such disruption of the SH3/SH2-kinase linker interaction could be expected. The increased Y416 phosphorylation of N2-Src by comparison to N1-Src is likely due to inclusion of the larger N2-Src micro-exon in the SH3 domain further disrupting intramolecular auto-inhibition, contributing to constitutive activity.

Whilst phosphorylation of Src at Y416 activates the catalytic activity, Src is only between 0.2% and 20% active if both Y416 and Y527 are phosphorylated (Boerner et al., 1996). SH2 domain binding of phosphorylated Y527 is a key regulatory mechanism in Src, as it forces the molecule into a partially closed conformation (Xu et al., 1997). Under basal conditions, as part of the negative regulation of C-Src by CSK, 90-95% of C-Src is phosphorylated at Y527 (Zheng et al., 2000). In addition to the increased phosphorylation of Y416, blotting of B104

lysates (Fig. 3-1), as well as past data in the fibroblast cell line COS7 (Keenan et al., manuscript in preparation), indicates that Y527 dephosphorylation occurs concomitantly with increased Y416 phosphorylation in neuronal Src isoforms. The combination of Y416 phosphorylation and Y527 dephosphorylation suggests that neuronal Src isoforms are highly active in both neuronal and non-neuronal cell lines.

The mechanism of Y527 dephosphorylation is difficult to infer. Typically Y527 is dephosphorylated when the SH2 domain of Src binds to a higher affinity site on a substrate protein, leaving the Y527 exposed to phosphatase activity (Parsons and Parsons, 1997). There is evidence that C-Src SH3 domain mutations can prevent Y527 phosphorylation by Csk (Superti-Furga et al., 1993), suggesting that N2-Src exon inclusion could prevent binding and phosphorylation by Csk. Alternatively, the partially open conformation of N2-Src caused by a lack of SH3 binding to the SH2-kinase linker may be inducing partial dissociation of Y527 from the SH2 domain. This could make pY527 accessible to one of the cytoplasmic (PTP1B, Shp1, Shp2) and transmembrane (CD45, PTP α , PTP ϵ , and PTP λ) proteins which dephosphorylate Y527 (Roskoski, 2005).

3.3.2 Decreased abundance of N-Srcs in Western blot samples

Compared with C-Src expression, detection of the N2-Src-FLAG epitope was consistently lower in both control and pervanadate conditions (Fig. 3-1). It is unlikely that it is due to decreased transfection efficiency, as all three splice variants were cloned into the same plasmid construct, vary little in length, and equal quantities of each plasmid were used in the transfection reactions. Additionally, this phenomenon is highly reproducible as this experiment was performed in triplicate with the same result. This effect does not seem limited to B104 neuroblastoma cells, as N2-Src-FLAG detection is also lower in heterologous systems such as COS7 cells (data not shown), HeLa cells (Fig. 4-1) and when mammalian N2-Src was expressed in *Xenopus laevis* (Fig. 5-3).

The decreased detection of N2-Src-FLAG could be due to three possibilities. First there is the possibility that expression of N2-Src decreases proliferation of transfected cells. When mammalian cell lines are transfected with a plasmid, it is

segregated between the daughter cells during mitosis. If N2-Src was decreasing proliferation of the B104 cells, then cells transfected with C-Src would undergo several more divisions than N2-Src, amplifying the C-Src-FLAG epitope signal relative to N2-Src. These data are backed up by the observation that in both SK-N-AS and KELLY cells, fewer N2-Src expressing cells appear in clusters (indicative of post-transfection mitosis) than other plasmids. Additionally, the number of cells observed over 90 fields of view was much lower for N2-Src than C-Src (SK-N-AS; N2-Src N=192, C-Src n=324, KELLY; N2-Src n=365, con n=485), suggesting again that little mitosis is occurring after transfection. This observation was confirmed in SK-N-AS cells in which 20% fewer cells express nuclear Ki67, a well-established marker of cell proliferation (Fig 8).

Secondly, the decreased FLAG signal could be due to a C-terminal modification in N2-Src that decreases the detection of N2-Src in comparison to C- and N1-Src. Decreased phosphorylation of C-terminal Y527 could be due to this same post translational modification, or possibly cleavage of the C-terminus of N2-Src. Removal of Y527 would considerably decrease the ability for the cell to negatively regulate N2-Src and consequently we would likely see the observed increase in Y416 phosphorylation (Fig. 3-1). We would also, however, see a decrease in the size of N2-Src by over 20 amino acids residues, which isn't reflected in the location of the pY416 signal of N2-Src.

Finally, this decrease in abundance could be the result of differential regulation of the splice variants resulting in increased degradation of N1- and N2-Src. CDK5 is known to phosphorylate active Src at Serine 75, targeting it for ubiquitination and cullin-5-dependent degradation (Pan et al., 2011, Kato and Maeda, 1999). It can be speculated that the increased activity of N2-Src is targeting it for CDK5 phosphorylation and ubiquitin-mediated degradation by the cullin-linked protein NEDD8 (Pan et al., 2004), resulting in the decreased identification of N2-Src by Western Blotting. This hypothesis is supported by the discovery that Src expressed endogenously in neuroblastoma and glioblastoma cells indicated that in the highly active form of Src expressed in neuroblastoma cell lines was serine phosphorylated at its N-terminus (Brugge et al., 1985). This could be tested using an antibody raised towards neuronal isoforms of Src. Unfortunately, due to the date of this study, neither

the specific splice variant of Src nor the site of serine phosphorylation were specifically identified.

The hypothesis that the neuronal Srcs are being degraded in a ubiquitin mediated fashion does not match observations made by immunocytochemistry. When overexpressed in neuroblastoma cells or fibroblast cell lines, there is no noticeable difference in C-, N1- or N2-Src abundance within the cells (Fig. 3-2, 6, 7 & 9; Fig. 4-1). There is however a consistent decrease in the observation of transfected cells in clusters indicative of post-transfection mitosis, suggesting that N1- and N2-Src transfected cells are dividing at a slower rate.

With these observations in mind, it seems most likely that the decreased N2-Src FLAG signal is due to a reduction in proliferation of N2-Src expressing cells. This would adequately explain why, despite acute treatment with vanadate, a phosphatase inhibitor that activates Csk and inhibits phosphatase activity, N2-Src has less detectible Y527 phosphorylation when treated with pervanadate. Additionally, decreased proliferation also supports the hypothesis that N2-Src stimulates neuronal differentiation of neuroblastoma.

3.3.3 Detection of an additional Y416 band in N2-Src transfected B104 cells

In addition to observations of consistent N2-Src Y416 phosphorylation above that of C-Src, probing for Y416 phosphorylation in B104 cells identified an additional band of interest at approximately 70 kDa exclusively in N2-Src transfected cells (Fig. 3-1). This band was observed in all three replicates of the experiment. This suggests that N2-Src is either differentially modified in these cells, causing decreased mobility of the protein by SDS PAGE, or is alternatively activating pY416 phosphorylation in another SFK which has cross-reactivity with the Y416 antibody. Differential modification of N2-Src in neuroblastoma cells could feasibly cause the observed gel shift, a similar shift is seen when Lck is double serine phosphorylated at its N-terminus (Winkler et al., 1993), and palmitoylation of N-Srcs would cause a decrease in electrophoretic mobility (Mukherjee et al., 2003). This hypothesis is discounted by the presence of only a single FLAG signal on the same gel as the pY416 doublet,

which suggests that N2-Src is phosphorylating the kinase domain of an endogenous protein (Fig. 3-1).

Due to the specificity of the antibody, it is most likely that cross-reactivity is occurring with the kinase domain of a different Src family kinase. Although all SFKs are around 60 kDa in size, only Fyn and Yes are expressed in neuronal tissues. As the phosphorylation event appears in neuroblastoma but not HeLa cells (as demonstrated in Fig. 4-12) or COS7 fibroblast cells (Keenan et al. unpublished), it is likely that the phosphorylation is of a protein restricted in its expression to neurons. The neuronal isoform of Fyn, (FynB) is approximately 62 kDa in size and expressed exclusively in neurons, making it an ideal candidate for a neuron-specific trans-phosphorylated SFK (Brignatz et al., 2009).

3.3.4 Knockdown of N-Src expression in LAN-5 cells does not decrease neuritogenesis

Due to the correlation observed by Matsunaga and colleagues between the expression of neuronal Srcs and the capacity for differentiation in neuroblastoma cells (Matsunaga et al., 1993a), it was hypothesised that the expression levels of neuronal Srcs in neuroblastoma cells could impact upon the differentiation of neuroblastoma. As neuroblastoma cells are of a neuronal origin, differentiation of neuroblastoma causes the development of neuronal morphological characteristics such as a small, round cell soma and an increased length and number of neurites. For the purposes of these experiments the length and number of neurites were the best parameters to quantify due to the difficulties in measuring cell body size in irregularly shaped cells.

To test whether neuronal Srcs were positively contributing to neuronal differentiation in neuroblastoma, it was necessary to observe whether decreased N-Src expression abrogates the capacity for neuroblastoma cells to differentiate. For this purpose I used LAN-5 cells, shown by Matsunaga and colleagues to express N1- and N2-Src endogenously and widely used experimentally for their neuronal morphology (Matsunaga et al., 1993a, Guglielmi et al., 2014, Coluccia et al., 2006). It was hypothesised that knockdown of neuronal Srcs in these cells, under control conditions and under drug-induced differentiation, would inhibit neuronal differentiation. During

my experiments, however, the LAN-5 cells did not demonstrate the expected differentiation in response to RA treatment. This has serious implications on the efficacy on the results, as the RA responsiveness of LAN-5 cells is widely reported, and typical of the cell line. The lack of any noteworthy increase in differentiation in response to RA, therefore implies that the results of N1- and N2-Src knockdown may not be reflective of the roles of N1- and N2-Src during neuritogenesis in this system. The cause of this RA unresponsiveness may be due to the high confluency of the cells inducing a high basal level of neuritogenesis, eclipsing the effects of RA treatment, or indeed the effects of N1- and N2-Src knockdown.

Additionally, we cannot directly confirm N1- or N2-Src knockdown in LAN-5 cells due to a transfection efficiency level below that which is detectable either by Western blotting or rtPCR. The control experiment demonstrating effective knockdown was performed in COS7 cells using exogenous N1- and N2-Src FLAG plasmids. In order to adequately test the function of these shRNAs, it would be necessary to utilise a viral method of shRNA plasmid delivery into LAN-5 cells.

3.3.5 Reduced effect of N-Src expression on constitutively differentiated cell lines

An additional insight into why knockdown of N-Srcs is not significantly inhibiting neuronal differentiation is that LAN-5 cells show a constitutively differentiated phenotype. In both the B104 and LAN-5 neuroblastoma cell lines manipulation of N-Src expression levels by over-expression and shRNA respectively do not yield statistically significant changes in the neurite length and number. B104 and LAN-5 cells are sensitive to both RA and cAMP induced differentiation, as well as possessing a highly neuronal phenotype in control conditions (Fig. 3-2B & 3B). These cell lines both possess a constitutively differentiated phenotype, with an average cell possessing ~1.2 and ~1.8 neurites in B104 and LAN-5 cells respectively (Fig. 3-2B & 5A). It could be that this constitutive differentiation is masking the effects of neuronal Src overexpression or knockdown on neuronal morphology. If neuronal Srcs are primarily acting during the initiation of neuronal differentiation, rather than driving and maintaining further neuritogenesis in differentiated cells, then we would not

expect to see manipulation of N-Src expression have a significant effect upon the quantity, or length of neurites in either B104 or LAN-5 cells.

3.3.6 Overexpression of neuronal Srcs in RA resistant neuroblastoma cell lines induces neuritogenesis

In all three neuroblastoma cell lines tested (B104, KELLY and SK-N-AS), overexpression of either N1- or N2-Src elicits a degree of increased neuritogenesis, when compared to controls and C-Src overexpression. The degree of this increase varies between cell lines. In B104 cells, over three replicates, the average number of neurites per cell increases marginally from 1.2 in control samples to 1.5 and 1.7 in N1- and N2-Src respectively. In SK-N-AS, analysis across four replicates indicates a statistically significant, 6 fold increase in the number of neurites per cell, from 0.03 in controls to 0.18 in N2-Src. Similarly, in KELLY cell lines neuritogenesis rose significantly, from 0.19 in controls to 0.4 and 0.5 neurites per cell in N1- and N2-Src overexpressing samples.

There are several functional implications of the significant responsiveness of KELLY and SK-N-AS cells to N-Src induced neuritogenesis. The small but not significant increase in neuritogenesis observed in B104 neuroblastoma cell lines in response to N-Src overexpression suggests there may be no specific molecular target which is differentially expressed in these cell lines, only that the capacity for differentiation was more optimal in the other cells. Whilst B104 cells show a constitutively differentiated phenotype the level of basal neuritogenesis observed in SK-N-AS and KELLY cells may be indicative of cell lines in which increases in differentiation are more readily detectible.

With regards to the specific molecular causes of the particularly high sensitivity of KELLY cells to N-Src induced neuritogenesis, it is notable that both SK-N-AS cells and B104 cells possess only a single copy of the proto-oncogene N-Myc, whereas KELLY cells are N-Myc amplified. Although N-Myc expression is commonly associated in patients with a decreased prognosis and a more aggressive metastatic tumour, there is evidence to support the claim that N-Myc amplification may well be necessary for differentiation of some cell lines in vitro. Guglielmi and

colleagues demonstrated how the capacity for retinoic acid induced differentiation in the N-Myc amplified LAN-5 cell line was diminished by N-Myc depletion, whilst SK-N-AS cells were induced towards differentiation only when N-Myc was overexpressed (Guglielmi et al., 2014). Interestingly, Matsunaga and colleagues (Matsunaga et al., 1994b) noted high N2-Src and Myc expression in neuroblastoma tumours in the youngest patients, with the best prognoses. These cases are almost exclusively detected by the Japanese neuroblastoma screening program and as such, tumours commonly self-resolve before symptoms are displayed. It is tempting to suggest from this correlation that perhaps Myc-N expression is pushing these neuroblastoma cells to a more neuronal progenitor-like phenotype, providing substrates similar to those targeted by neuronal Srcs during development.

3.3.7 Overexpression of N2-Src causes a decrease in proliferation of SK-N-AS neuroblastoma cells

Consistently, transfection of with Src isoforms has indicated that neuroblastoma cells may have been proliferating slower when transfected with N2-Src by comparison with C- and N1-Src. By Western blotting of transfected B104 cells, a lower N2-Src FLAG signal was observed compared to C- and N1-Src. When staining transfected B104, KELLY and SK-N-AS cells by immunocytochemistry, whilst the abundance of FLAG signal appeared to be the same between splice variants, the number of N2-Src cells transfected, and particularly clusters of cells indicating post-transfection proliferation were much lower than with C- and N1-Src.

To test this, SK-N-AS and KELLY cells were transfected with Src splice variants, or treated with cAMP or RA. Ki67 staining showed that 20% fewer SK-N-AS cells were proliferative when transfected with N2-Src compared with control, C-, and N1-Src conditions, however, in KELLY cells there wasn't a noteworthy effect on proliferation between the splice variants. The remarkable contrast between the effect of N2-Src on KELLY cells, where cells differentiate more without entering quiescence and SK-N-AS cells, where cells demonstrate less cytoskeletal rearrangement yet do enter quiescence, demonstrates the profound heterogeneity of neuroblastoma cell lines.

3.3.8 Parallels between N2-Src and Vanadate mediated neuroblastoma differentiation

N2-Src expression in cells consistently shows an increase in global tyrosine phosphorylation within the cell, both in neuroblastoma cells and in HeLa cells (Fig. 3-1; Fig. 4-6). This increase has been demonstrated both in basal conditions, and when cells are treated with pervanadate phosphatase inhibitors (Fig. 3-1; Fig. 4-6). The inhibition of protein tyrosine phosphatases by vanadium-based inhibitors has shown to have important roles in restricting proliferation of neuronal cells (Faure et al., 1995). In neuroblastoma cells PTP inhibition has been shown to augment the effects of retinoic acid on neuroblastoma differentiation (Clark et al., 2013). This effect was partly dependent upon the activation of Erk and Akt, both downstream effectors of Src/FAK signalling at focal adhesions (Webb et al., 2004, Wang and Basson, 2011).

PTP inhibition has long been known to increase activation of C-Src (Brown and Gordon, 1984) as well as FAK (Defilippi et al., 1995). The increases in FAK phosphorylation and activity as a result of pervanadate treatment is linked to Src activity, as mutation of Y396 or Y576/577 phosphorylation sites that are docked by the Src SH2 domain as part of Src activation and targeting to FAK, reduce FAK phosphorylation (Maa and Leu, 1998). As such, both vanadate-mediated and N2-Src mediated differentiation of neuroblastoma could be acting upon the same signalling pathways. As vanadate treatment up-regulates Src and FAK signalling in cells, and Src/FAK signalling contributes to the same MAPK pathways identified in vanadate treated neuroblastoma cells, constitutively active N2-Src could be activating FAK phosphorylation, leading to this same downstream signalling in the Erk/Akt/Ras MAPK signalling pathways.

In addition to the possibility of FAK mediated N-Src induced neuroblastoma differentiation, the vanadate model of neuroblastoma differentiation provides additional insights into N-Src function. As observed in N2-Src overexpression in B104 cells, N2-Src over-expression massively increases global tyrosine phosphorylation in neuroblastoma cells (Fig. 3-1). This increase in global phosphotyrosine is likely due to the constitutive activity of N2-Src, in comparison to C-Src. Although it is difficult to identify the specific phosphoproteins that mediate

the N2-Src induced differentiation, it is clear that an increase in Src activity in both N2-Src mediated and vanadate mediated differentiation are likely to function through at least some of the same signalling cascades. To test these hypotheses, FAK mutants could be co-transfected into the model N2-Src neuritogenesis assay in COS7 cells (Fig. 5-1) to see whether FAK mutation inhibits N2-Src mediated neuritogenesis.

3.4 Concluding remarks

Neuroblastoma are widely considered to be neuronal progenitor cells which have missed, or are resistant to their differentiation cues. The prognosis of the cancer is therefore tightly linked to the capacity for the cells to ‘remember’ their cell fate and differentiate into non-proliferative neurons. Neuronal Srcs are known to be expressed during periods of high neuronal differentiation during development (Wiestler and Walter, 1988), during neuroblastoma differentiation of LAN-5 cells (Matsunaga et al., 1993a). Data in heterologous cell lines (Fig. 5-1) indicates that overexpression of N-Srcs can induce a neuronal morphology, even in cells without a background of neuronal expression. Additionally the increased expression of neuronal Srcs has been shown to relate to a positive prognosis in neuroblastoma cases (Matsunaga et al., 1998, Terui et al., 2005).

One of the main drawbacks whilst experimenting on human neuroblastoma cell lines was a very low transfection efficiency. Despite numerous attempts to optimise the transfection protocol, neuroblastoma cell lines could not be transfected at a rate which would allow Western blotting or rtPCR. To this end I sought to create doxycycline inducible C-, N1- and N2-Src expressing neuroblastoma cell lines. Though excellent progress was made and functional inducible plasmids as well as a stable tetracycline regulatory element expressing neuroblastoma cell lines were created, time constraints did not allow the completion of this work. When completed, these cell lines will be ideal for assessing the effects of N-Src overexpression on neuroblastoma cells in the variety of methods demonstrated using the inducible HeLa cell lines described in Chapter 4.

My data consistently indicate that overexpression of neuronal Srcs in neuroblastoma cells increases the proportion of cells that are differentiating. In the

cell lines B104, KELLY and SK-N-AS, increased neurite outgrowth was observed to varying degrees in N1-Src and N2-Src transfected cells by comparison with controls and C-Src transfected cells. The next step in understanding N2-Src induced neuronal differentiation is to identify the N2-Src specific substrates that are causing the dramatic changes to tyrosine phosphorylation which are resulting in the observed neurogenesis and quiescence of neuroblastoma cells. SK-N-AS and KELLY cells in particular showed a significant increase neurite outgrowth when N1- and N2-Src transfected. The data suggest that the degree to which N1- and N2-Src drive neuronal differentiation varies greatly between cell lines, which is indicative of the heterogeneity of neuroblastoma. Identifying the specific substrates and pathways through which N1- and N2-Src elicit their cellular effects is the next crucial step in understanding their roles in neuroblastoma differentiation.

Identification of N2-Src specific substrates by mass spectrometry

4.1 Introduction

Due to the location of the neuronal exon in the Src kinase SH3 domain, it was predicted that the cellular changes induced by expression of neuronal isoforms of Src are due to a combination of increased kinase activity, as a result of decreased auto-inhibition, and a change in SH3 substrate specificity (Dergai et al., 2010, Weng et al., 1993). Advances in proteomics have made the identification of the phosphorylation status of the proteome of a biological system (phosphoproteome) increasingly efficient. Identification of differential phosphorylation in a sample is more challenging as the number of peptides produced by proteolytic digestion of a cell lysate can number in the tens of thousands allowing only the most abundant peptides to be identified by LC-MS/MS (Collins et al., 2007). Techniques such as SILAC and iTRAQ and label-free quantification methods are highly successful at quantifying peptides, however the number of proteins that are phosphorylated at any one time may be relatively low in the cell. It is therefore unlikely that a significant number of these would be identified by regular proteomics approaches. Considering that phosphotyrosine represents only 4% of total phosphorylation events, the probability of identifying a significant proportion of the proteins regulated by tyrosine phosphorylation is very low (Olsen et al., 2006).

For this reason, identification of differential tyrosine phosphorylation by mass spectrometry requires an initial enrichment step to increase the proportion of phosphotyrosine proteins or peptides in the sample prior to mass spectrometry. Phosphopeptide enrichment commonly involves immobilised metal or immunoaffinity chromatography, or immunoprecipitation of the sample proteins and/or digested peptides (Hammond et al., 2010, Kehasse et al., 2013, Zhang et al., 2012, Breitkopf et al., 2012, Cunningham et al., 2010).

Mass spectrometry, performed on phosphotyrosine enriched samples from C- and N2-Src, was used to identify substrates that could help indicate pathways that are differentially regulated by C-Src and its neuronal splice variant N2-Src using mass spectrometry.

4.2 Results

4.2.1 Establishment of the stable, inducible Src expressing HeLa cell lines

In order to perform large scale enrichment of tyrosine phosphorylated substrates and their binding partners, I established three HeLa cell lines that stably, inducibly, expressed C-, N1- and N2-Src-FLAG. To accomplish this I used the Invitrogen pCDNA5/FRT/T0 stable transfection system in Tetracycline-Regulated Expression (T-REx) HeLa cells, which stably express the tetracycline repressor (Invitrogen, (Hillen and Berens, 1994)). These cells also have a stably integrated pFRT/*laczeo* site (Invitrogen), which allows for the easy incorporation of the plasmid into the pre-existing FRT site in the genome of the cells. pCDNA5/FRT/T0 expresses the gene of interest from a hybrid human cytomegalovirus (CMV)/TetO2 promoter that contains dual tetracycline repressor sequences to ensure gene expression only occurs in the presence of tetracycline or its analogue.

I sub-cloned the Src-FLAG constructs used in experiments throughout this project into pCDNA5/FRT/T0, retaining the FLAG epitope tag. T.REx HeLa cells were stably transfected with the plasmid and successful plasmid incorporation was selected for by hygromycin resistance. Single colonies of HeLa cells were selected after 3-4 weeks and screened individually for doxycycline-dependent gene expression. The tetracycline analogue doxycycline was used due to its increased stability in culture compared to tetracycline.

Figure 4-1A shows the efficiency of the tetracycline repressor in the absence of doxycycline as well as the effective induction of C-, N2- and N2-Src expression following 48 h of doxycycline treatment. Expression in these cell lines was also confirmed by immunofluorescence, with detection of the FLAG tag consistently evident in a vast majority of cells (Fig. 4-1B).

4.2.2 N2-Src expression appears to be restricted to the Golgi region

Whilst C-Src was detected throughout the whole cell relatively evenly, with a small increase in localization in the perinuclear region, N2-Src expression was very restricted to a similar perinuclear region, with decreased, often punctate cytosolic

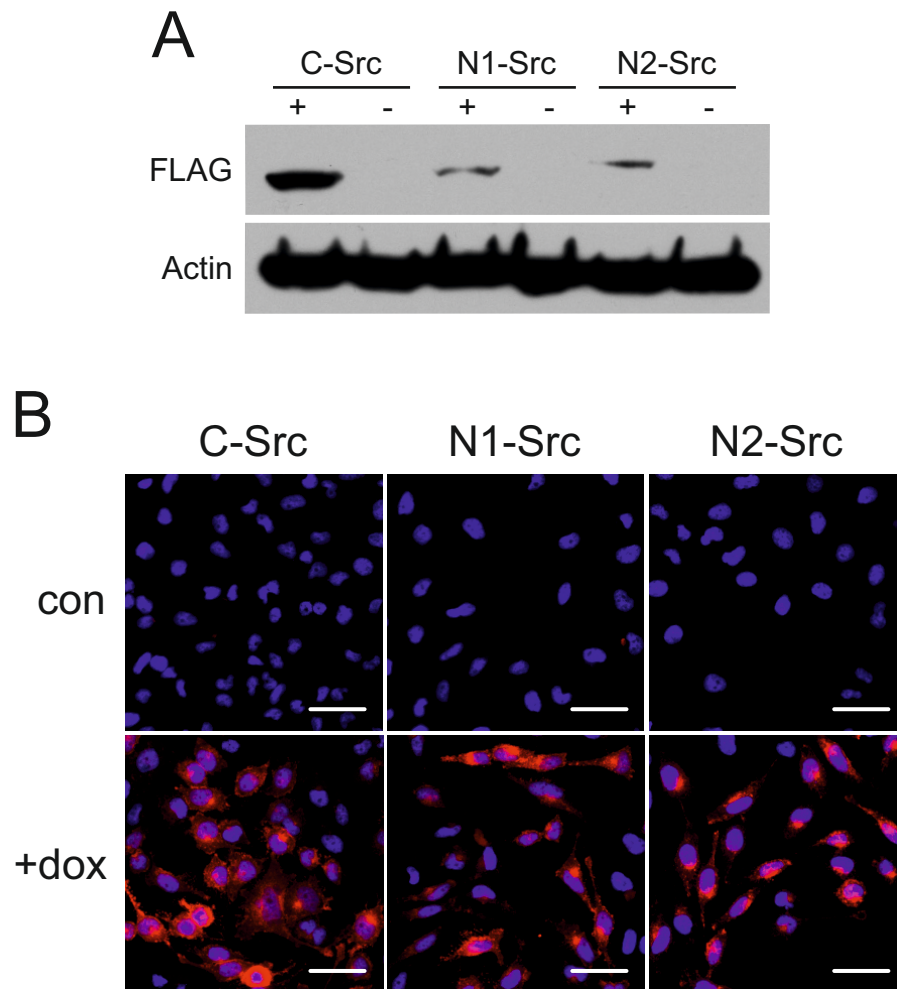


Fig. 4-1. Generation and characterisation of stable, inducible T-REx HeLa cell lines.

A) One hundred thousand C-, N1-, and N2-Src HeLa cells treated for two days with 1 $\mu\text{g/ml}$ doxycycline in a six well plate. Cells were lysed with Laemmli SDS sample buffer, boiled at 95 $^{\circ}\text{C}$ for 10 minutes then run on a 12.5% acrylamide SDS PAGE gel. After the proteins were transferred to PVDF membrane, the sample was probed with mouse α -FLAG and rabbit α -actin primary antibodies.

B) Ten thousand HeLa cells were plated onto 13 mm^2 coverslips and treated with 1 $\mu\text{g/ml}$ doxycycline for two days. Cells were then fixed in PFA, permeabilised and stained with mouse α -FLAG primary antibody. Slides were mounted in Mowial containing 1 mg/ml DAPI. FLAG staining in red, DAPI staining in blue, Scale bar 50 μm .

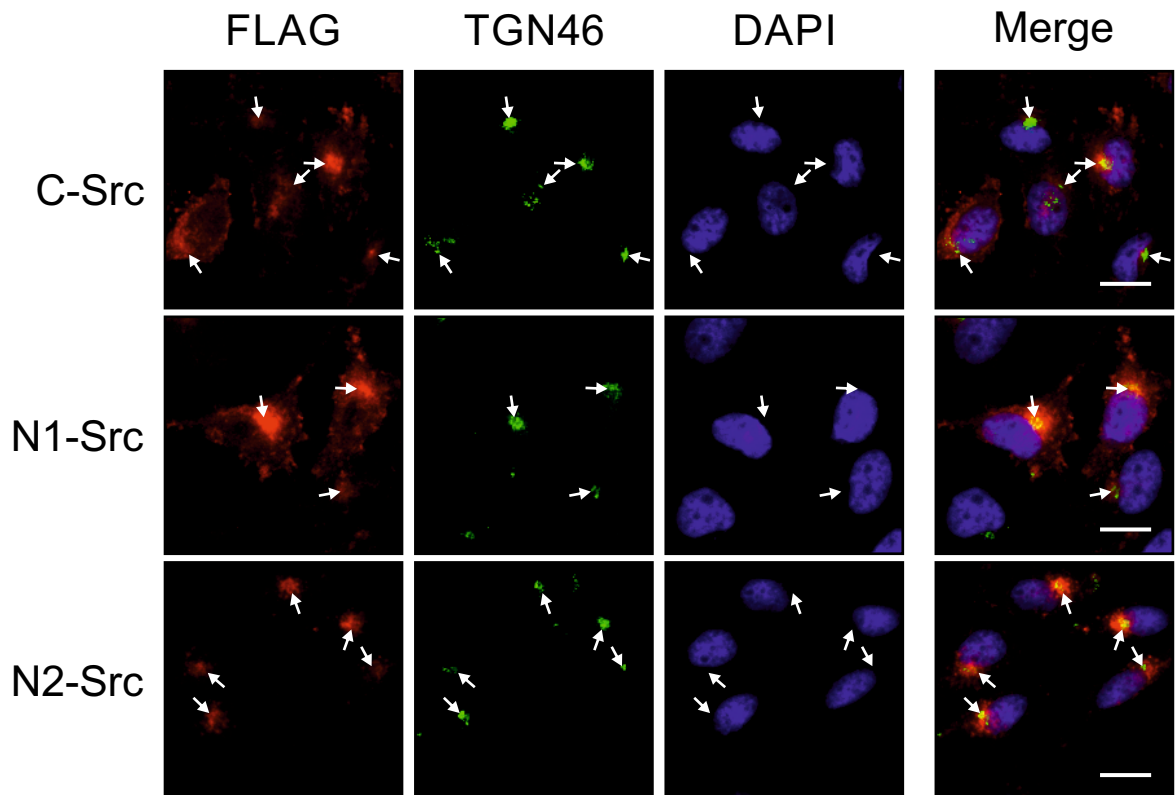


Fig. 4-2. Intracellular localisation of Src splice variants.

Ten thousand HeLa cells were plated onto 13 mm² coverslips and treated with 1 µg/ml doxycycline for two days. Cells were then fixed in PFA, permeabilised and stained with mouse α-FLAG and rabbit α-TGN46 primary antibody. Slides were mounted in Mowial containing 1 µg/ml DAPI. FLAG staining in red, TGN46 staining in green, DAPI staining in blue. Arrows show the location of the trans-golgi network, as indicated by TGN46 staining. Scale bar 20 µm.

expression. For this reason we looked for co-localisation between the Srcs and a Golgi marker, TGN46, found in the trans-Golgi network (TGN).

The maximal staining in both C-Src and N2-Src was indeed consistently located with TGN46 (Fig. 4-2). C-Src expressing HeLa cells showed extensive cytoplasmic FLAG staining, in addition to plasma membrane staining and an increase in immunoreactivity around the region of TGN46 staining. N2-Src detection consistently peaked in the region surrounding the TGN, with limited, punctate staining throughout the rest of the cells and some, limited localisation to the plasma-membrane (Fig. 4-2). N1-Src appeared to be expressed throughout the cytosol, similar to C-Src, however with less plasma membrane staining observed (Fig. 4-2). The differential cellular localisation of the three splice variants could have implications for their function and the substrates they encounter when activated.

4.2.3 N-Src expression induces elongation of HeLa cells

In previous experiments I demonstrated that expression of neuronal Src isoforms induced the extension of neurite-like processes from the cell soma in neuroblastoma cell lines. Cytoskeletal rearrangements were not observed to this extent in the Src HeLa cells, although induction of N1- or N2-Src expression consistently led to an elongation of the cells compared to C-Src. To quantify the change in morphology, I transfected the cells with soluble CFP, with or without 48 h of doxycycline treatment. In addition to the Src cell lines I used the parental T.REX HeLa cell line as a control for the effects of doxycycline expression upon the cells. For each cell line, CFP expression was used to delineate the cell boundaries and the cell perimeter and the cell area was quantified using ImageJ (Schneider et al., 2012). Using the formula $4\pi(\text{area}/\text{perimeter}^2)$, (Schneider et al., 2012) the roundness of the cell was calculated on a scale of 0-1, 1 where 1 is a perfect circle and 0 is a line with no internal area. The cell soma was outlined, ignoring all extensions from the body below 2 μm in thickness to prevent the dramatic effect that tracing filopodia would have upon the calculated roundness of the cell.

Under control conditions, each cell line was broadly similar in roundness (Fig. 4-3A), but there was a differential effect of inducing Src expression upon cell

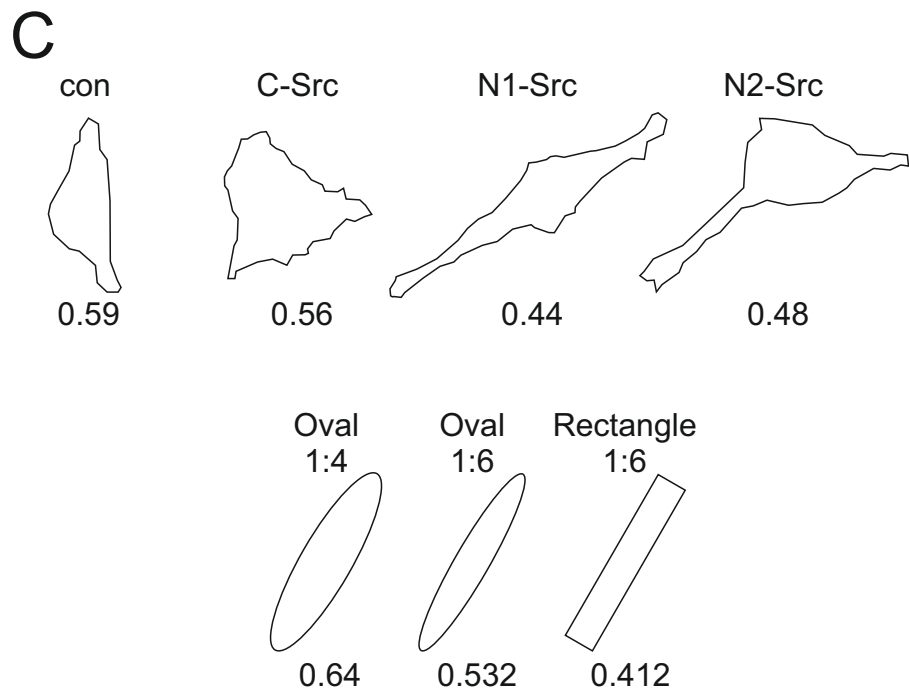
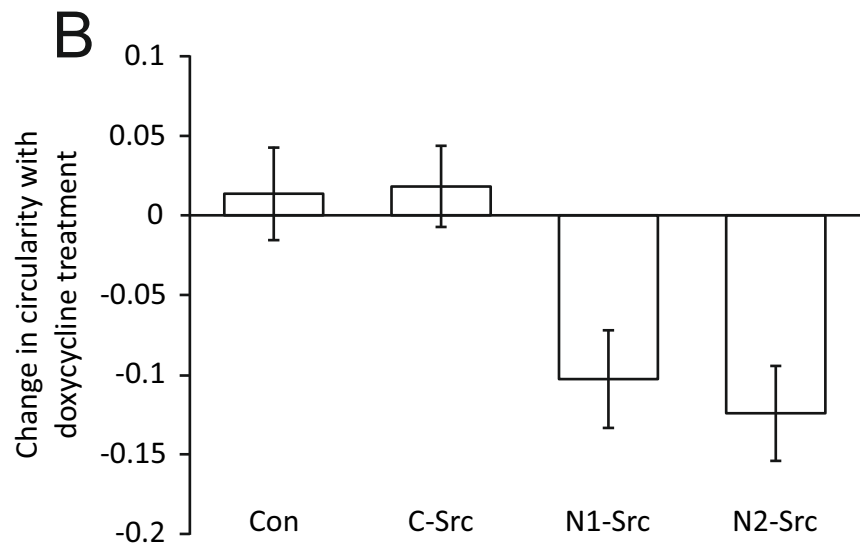
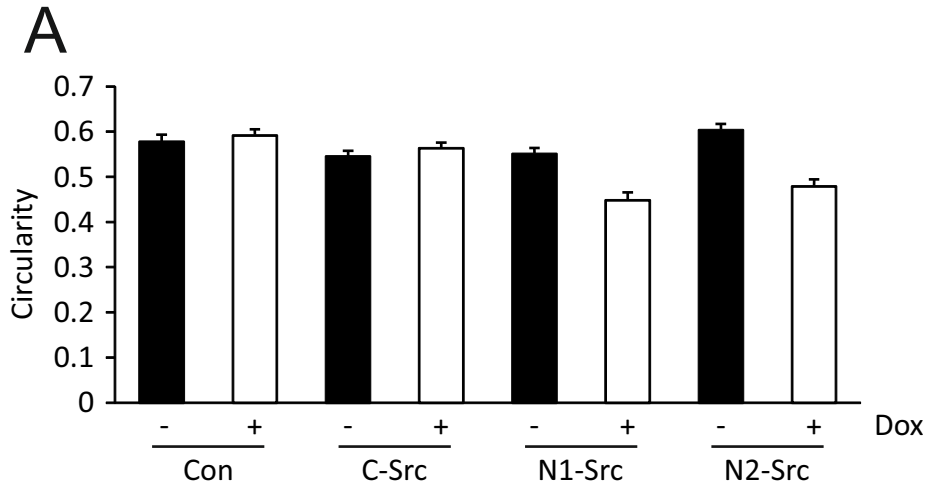


Figure. 4-3 (page 114). Effects of neuronal Src overexpression on HeLa cell morphology.

A) Ten thousand HeLa cells were plated onto 13 μm^2 coverslips and transfected with the soluble CFP vector pmCer and treated with 1 $\mu\text{g}/\text{ml}$ doxycycline for two days. Cells were fixed in PFA, permeabilised and stained with mouse α -FLAG and rabbit α -GFP primary antibody. Cell perimeter and area were measured in ImageJ and the circularity calculated using the formula $4*\pi*(\text{Area}/\text{Perimeter}^2)$. At least 98 cells were imaged per condition across two coverslips. This experiment was performed once, as such statistical analyses were not performed on these data. Error bars show standard error. B) Fold change in circularity of HeLa cell lines treated with doxycycline compared to controls. Error bars show sum of the standard error values for control and doxycycline conditions. C) Example outlines of doxycycline treated HeLa cells taken from ImageJ with the calculated circularity shown underneath. Regular shapes and circularity values are provided for perspective.

roundness. N1- and N2-Src HeLa cell lines showed a decrease in roundness of 0.1 and 0.12 respectively, a decrease approximately equivalent to that between an oval with a 1:4 ratio and an oval with a 1:6 ratio (Fig 3.C). The same change in roundness was not evident in C-Src and control cell lines where roundness was increased by only 0.01 and 0.02 respectively (Fig. 4-3B).

This quantification suggests that whilst the same scale of neuron-like morphology that we see in neuroblastoma cell lines isn't occurring in HeLa cells, N-Src expression is still having an effect on the morphology of these cells.

4.2.4 Expression of N1- and N2-Src in HeLa cells reduces cell migration

As established previously, neuronal Srcs can decrease proliferation in neuroblastoma cell lines (Fig. 3-8). To identify changes in both proliferation and migration in the stable HeLa cell lines, a wound healing assay was performed. Thirty thousand HeLa cells were seeded in each well of a 24 well plate and treated with doxycycline containing medium (1 $\mu\text{g}/\text{ml}$) the following day. After overnight incubation in doxycycline to allow gene expression to occur, the cells were wounded with a 200 μl pipette tip and imaged every 10 min for 20 h at 37°C.

To calculate the rate of cell migration, the area into which the cells migrated was calculated by establishing the location of the original wound, and tracing the area occupied by the cells after 20 h. In control cells, the area migrated into by the cells

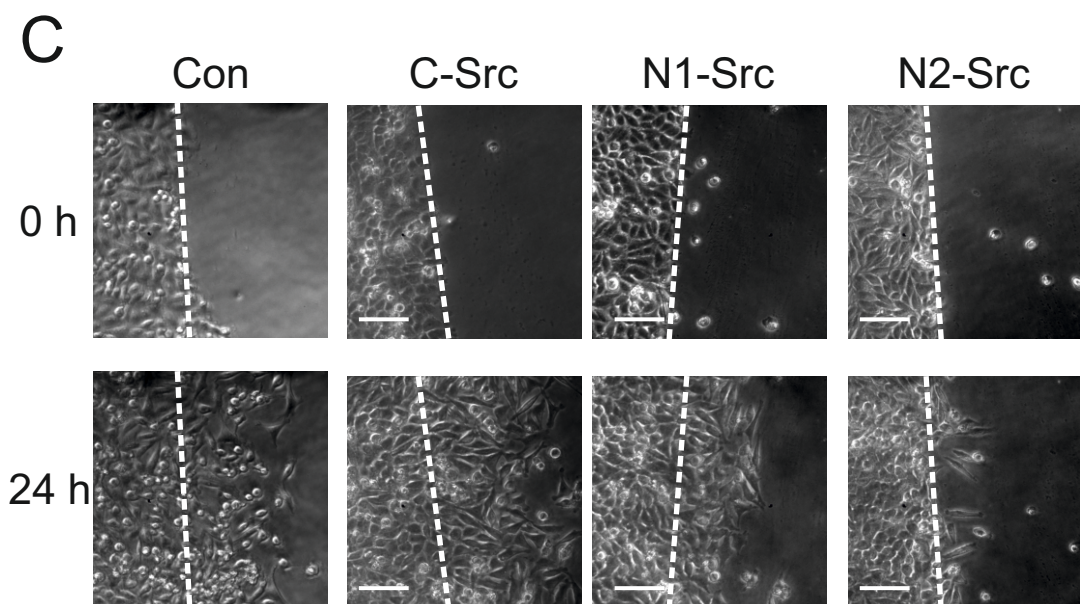
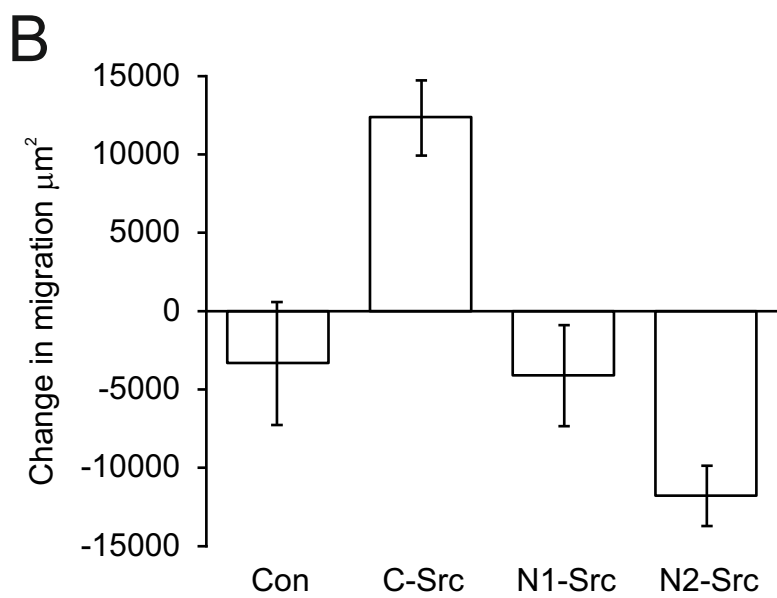
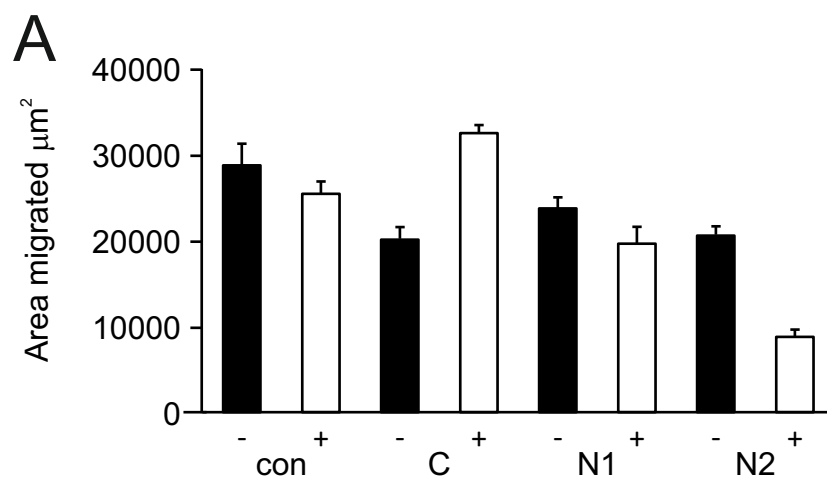


Figure. 4-4 (page 116). Effect of neuronal Src overexpression on HeLa cell migration.

Fifty thousand HeLa cells were plated per well of a 24 well plate. The cells were treated with 1 $\mu\text{g}/\text{ml}$ doxycycline overnight then wounded using a 200 μl pipette tip the following day. Regions of interest on each well were identified and then imaged every ten min over a two day time period using an automated XYZ Prior stage with auto-focussing. This experiment was performed once, as such no statistical analyses were performed. A) The change in the area covered by the cells by the cells during the time course, measured in ImageJ. Error bars show standard error. B) Fold change in migration of HeLa cell lines treated with doxycycline compared to controls. Error bars show sum of the standard error values for control and doxycycline conditions. C) Example images of doxycycline treated HeLa cells showing cells at time zero and after one day. Scale bar = 100 μm .

decreased by just 3 mm^2 with and without doxycycline treatment whilst C-Src cells occupied 12 mm^2 more under doxycycline induction than in control conditions (Fig. 4-4A, B). By contrast, N1- and N2-Src cells occupied 4 mm^2 and 11 mm^2 less area after 20 h when treated with doxycycline compared with controls (Fig. 4-4A, B, C).

Careful examination of the time lapse images revealed that C-Src HeLa cells appeared to proliferate much more rapidly, with a constant turnover of rounded cells undergoing mitosis, compared with N2-Src HeLa cells. There was a notable decrease in the number of cells observed undergoing mitosis between C- and N2-Src. Whilst C-Src HeLa cells consistently rounded and divided successfully, a decrease was observed in N2-Src HeLa cells, with rounding of the cells in an apparent attempt at mitosis often resulting in failed division or cell death. This, alongside the evidently lower cell numbers evident by the much lower area covered by cells after 20 h, suggests that N2-Src is inhibiting proliferation of HeLa cells. A more detailed analysis of individual cell behaviour during the time-lapse would reveal whether, on average fewer mitotic events are occurring in the cells. Additionally, performing the scratch test again, in the presence of blockers of mitotic activity, would demonstrate the degree to which proliferation is contributing to the increased migration in C-Src HeLa cells.

Wound healing occurred much more rapidly in C-Src HeLa cells than N2-Src HeLa cells, and the method of migration was visibly different between the time lapse movies. All cell lines were at confluency prior to wounding creating a very visible 'front' to the mass migration in C-Src expressing cells, contrasting with N2-Src cells where a large proportion of the area covered by migration resulted from a smaller number of pioneer cells (Fig. 4-4C). Compared to C- and N2-Src, N1-Src HeLa cells behaved

in an intermediate manner, with a less significant decrease in area occupied than N2-Src.

4.2.5 N2-Src expression does not increase the proportion of HeLa cells exiting the cell cycle

Ki67 immunostaining was used to test whether the apparent decrease in proliferation observed above in N-Src expressing cells is representative of an increased proportion of cells exiting the cell cycle. HeLa cells were incubated for 48 h in doxycycline containing or control media before being fixed and stained for FLAG and Ki67 expression and mounted in DAPI-containing coverslip mountant.

10 fields of view were imaged at 20x magnification for each condition to identify how many of the cells were expressing the Ki67 proliferation marker and in all cases Ki67 staining was observed in 100% of nuclei (Fig. 4-5). This demonstrates that, whilst the N2-Src expressing HeLa cells show an apparent reduction in proliferation rate, this is not indicative of an exit from the cell cycle as would be associated with quiescence or differentiation. It is, however, still plausible that N2-Src is decreasing the rate of proliferation through inhibiting the mechanisms of mitosis, such as the cytoskeletal rearrangements associated with cytokinesis, without affecting the proliferative potential of the cells as demonstrated by Ki67 expression. To confirm that N2-Src is decreasing the proliferation rate of these cells a quantitative analysis of cell proliferation rate, such as an MTS or MTT assay would need to be completed.

4.2.6 Preparation of HeLa cell lysates for LC/MS/MS

I next sought to identify proteins that are phosphorylated differentially by Src as a result of N-Src exon inclusion. N2-Src produced the most significant effects on HeLa cell morphology and migration and was hence chosen for a phosphoproteomic comparison with C-Src. Due to the inherent difficulty in identifying phosphotyrosine by standard phosphoproteomics (Olsen et al., 2006) immunoenrichment of tyrosine phosphoproteins was performed, prior to LC/MS/MS.

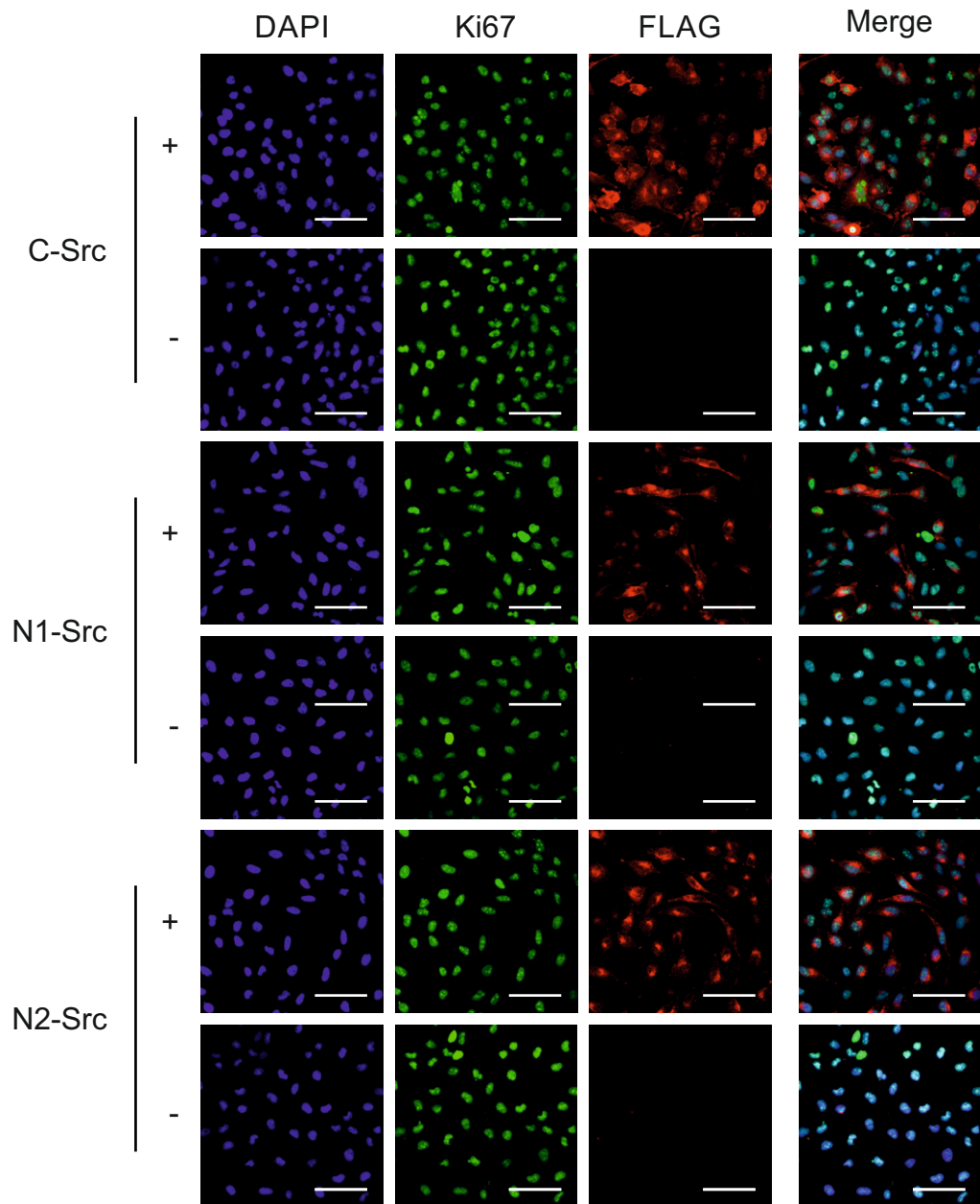


Fig. 4-5. Effect of neuronal Src over-expression on HeLa cell proliferation.

Ten thousand HeLa cells were plated onto 13 mm² coverslips and treated with 1 µg/ml doxycycline for two days. The cells were fixed in PFA, permeabilised and then stained with mouse α-FLAG and rabbit α-Ki67 primary antibodies. The coverslips were mounted in Mowial containing 1 µg/ml DAPI. This experiment was performed once. DAPI is shown in blue, Ki67 is shown in green, FLAG is shown in red. Scale bar = 50 µm.

Phosphotyrosine immunoprecipitations (IPs) were performed on lysate from control, C- and N2-Src HeLa cells that were incubated with or without doxycycline and/or acutely treated with pervanadate. Pervanadate was used as it activates Src Family Kinases, including C-Src, and as such it was hypothesised that pervanadate treatment would amplify the detection of substrates in both samples, irrespective of the basal activity of each variant (Boulven et al., 2002). Of these conditions, two conditions were performed in duplicate; C- and N2-Src cells induced doxycycline and treated with pervanadate. These two conditions were the focus of the experiment, rather than using just the N2-Src HeLa cell line with and without doxycycline because it was predicted that N2-Src shares a substantial number of substrates with C-Src. HeLa cells expressing activated C-Src provided the best control sample from which specific N2-Src specific substrate proteins could be identified.

In the first replicate of this experiment, 6 x 75 cm² flasks (containing approximately 8-10 x 10⁶ cells each) were lysed and adjusted to 1.3 mg/ml of protein. Tyrosine phosphoproteins in the lysates were enriched by incubation with 100 µl of agarose-conjugated 4G10 resin overnight, and eluted in 100 µl of sample buffer. In the second replicate, informed by the results of the first experiment, 5 x 75 cm² flasks were lysed and adjusted to 2.6 mg/ml of protein, and immunoprecipitated with 50 µl of 4G10 resin, eluted in 50 µl of sample buffer.

Equal volumes of input and supernatant, run on a Western blot with 2 µl of IP elution, showed that the IP significantly depleted tyrosine phosphoproteins from the supernatant (Fig. 4-6A, B). Blotting indicated that C- and N2-Src were expressed exclusively in doxycycline treated samples of the correct cell lines, and no FLAG signal was detected in the control cell line. Due to the risk of cross-contamination between HeLa cell lines, input from doxycycline treated samples was run together and blotted for FLAG expression, which confirmed that the C- and N2-Src cell lines had not cross-contaminated due to the visible shift in molecular weight caused by N2-exon inclusion (data not shown). Despite the activation of C-Src with pervanadate, it was interesting to note that N2-Src samples showed an increased global phosphotyrosine level in comparison to corresponding C-Src samples (Fig. 4-6A, B). FLAG staining in the IP lanes suggested that N2-Src was immuno-enriched at a much higher efficiency than C-Src in both replicates, both in the presence and absence of pervanadate. Although there was no FLAG signal in the second replicate of

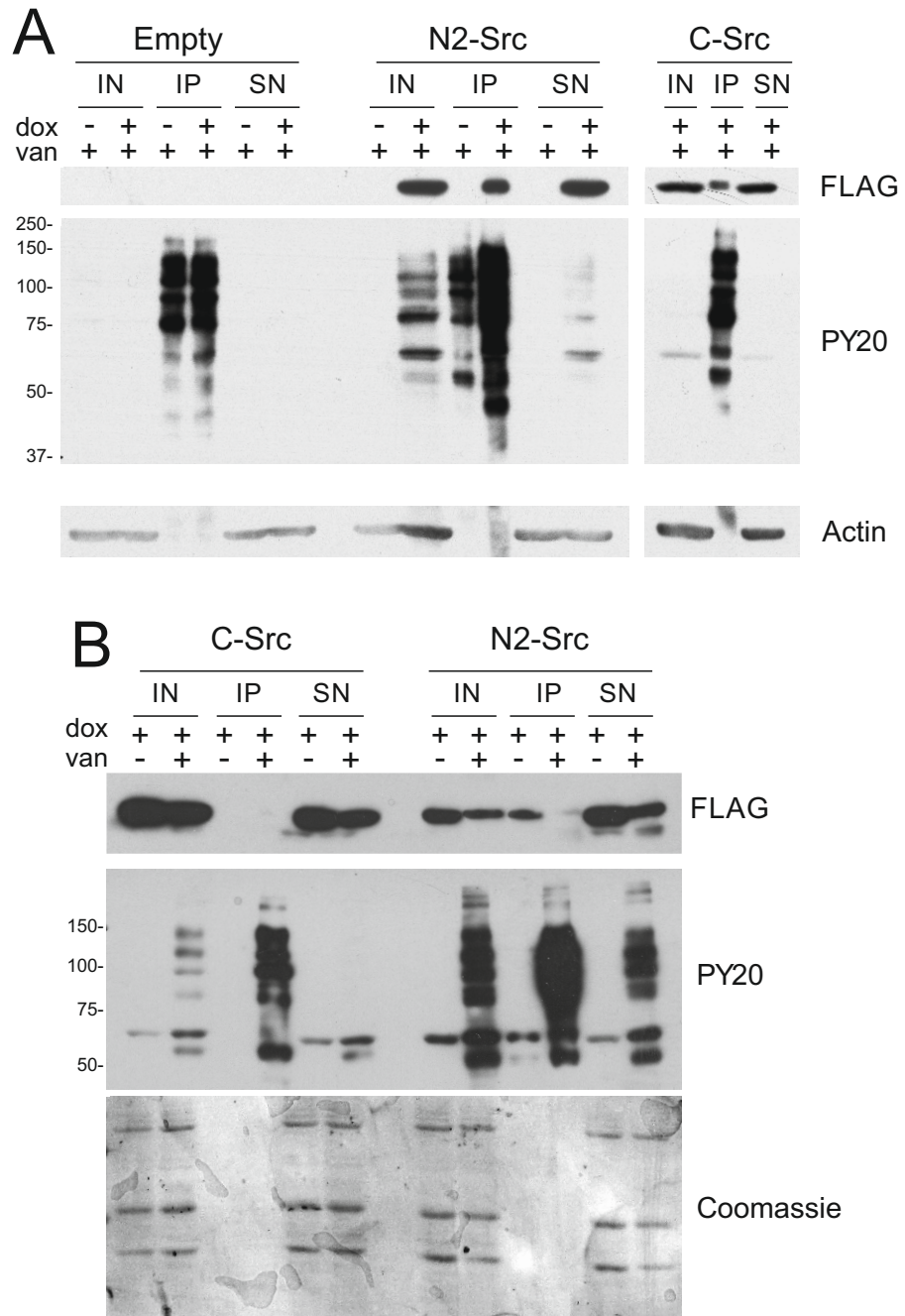


Fig. 4-6. Phosphotyrosine immunoprecipitation from T.REx HeLa cell lines.

Western blot showing the input, elution, and supernatant from phosphotyrosine immunoprecipitations from the lysate of six 75 cm² flasks of HeLa cells. Equal volumes of input and supernatant run on a Western blot with 2 μ l of IP elution. The blots were probed with mouse α -FLAG, rabbit α -Actin and (A) mouse α -phosphotyrosine primary antibodies. Loading controls for this experiment were actin (A) and Coomassie staining (B). After confirming via Western blotting that the IP had enriched for phosphotyrosine, the eluate from this experiment was then processed for LC/MS/MS.

pervanadate treated N2-Src, this could be due to high immunoreactivity causing the HRP substrate to be depleted in this area before detection takes place. In both C-Src and N2-Src samples, a protein of around 67 kDa was detected by the PY20 antibody, likely to be C- and N2-Src themselves, probably phosphorylated on pY416 (Fig. 4-6). Y416 appeared more phosphorylated at this site in N2-Src, which was similarly identified in neuroblastoma data (Fig. 3-1) and was confirmed in a later blot of these HeLa samples (Fig. 4-12).

4.2.7 Processing LC/MS/MS results

The 4G10 IP elution for each sample was run a short way on to an SDS gel before an in-gel tryptic digest of the sample. The resulting peptides were then applied to the Bruker MAXIS LC-MS/MS system by staff at York Technology Facility. The resulting LC-MS/MS data was processed in and retrieved from the Matrix Science Mascot server, grouped by peptide family and processed as shown in Figure 4-7.

The focus of the data analysis was upon the duplicate data for C- and N2-Src HeLa cell lines induced with doxycycline and acutely treated with pervanadate. The raw data for these two conditions was pooled and filtered with a very high stringency; any protein that did not have at least two separate, significant peptide sequences identified in both replicates was discarded from further analysis. Of the 972 and 930 proteins identified in the raw data for C- and N2-Src samples, only 249 and 242 of these proteins matched this stringent filtering process (Table. 4-1). Although the detection of significant sequences by the MAXIS LC-MS/MS system confirms the presence of the peptide, in order to allow semi-quantitative analysis of protein abundance placing the minimum number of significant sequences at two allows us to be sure that any change in abundance is the result of more than just the chance hits at the limits of detection. In addition, having two significant sequences in both samples confirmed that the enrichment of that protein was consistent between biological replicates.

The relative abundance of each protein in the sample was quantified using the exponentially modified Protein Abundance Index (emPAI) score (Ishihama et al., 2005). Unlike Mascot's Protein Score that is based solely upon the number and size

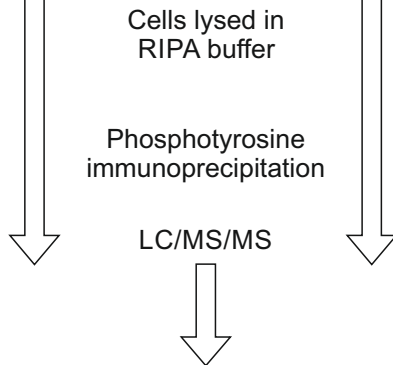
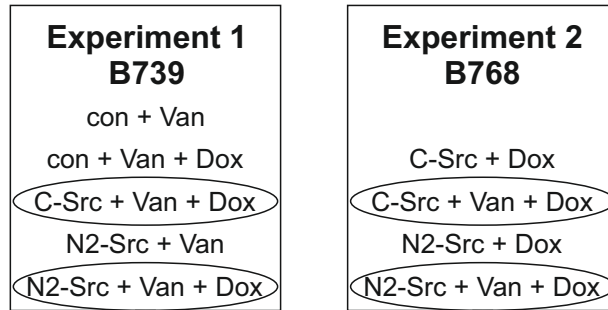
of peptide hits, emPAI normalises the peptides observed for each protein against the total number of observable peptides within that protein (Ishihama et al., 2005). This normalisation of the peptide hits means that the emPAI better reflects the protein concentration of the IP, avoiding bias caused by large or small proteins that are digested into a many or few detectible peptides.

Whilst emPAI is effective at normalising for protein size, it does not normalise between samples. Due to the sensitivity of MS, small changes in sample concentration, load volume or the quality of individual LC/MS/MS runs can contribute to relatively large sensitivity changes between samples. To normalise between samples the %emPAI (the emPAI score for each protein as a proportion of the sum of all emPAI scores within the sample (Ishihama et al., 2005)) was calculated. This allowed for comparison between runs, as increased sensitivity would increase both the diversity of proteins detected, but also the number of peptides detected for each protein, which would allow the %emPAI for high abundance proteins to remain relatively constant even with increased sample size.

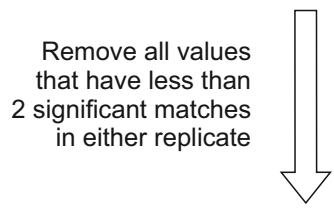
	B739		B768	
	C	N2	C	N2
Matched peptides	2713	2675	2309	2154
Unique peptides	2087	2166	1771	1521
Proteins represented	737	714	558	529
	Averaged data			
	C		N2	
Matched peptides	2511		2414.5	
Unique peptides	2087		1843.5	
Proteins represented	972		930	
Proteins unique to sample	403		360	
	Refined results (duplicate & >2 sig seq)			
Proteins represented	249		242	
Proteins unique to sample	15		8	
Proteins with over 1log(2) increased abundance	52		62	

Table 4-1. Numeric summary of LC-MS/MS data processing.

Summary of the process of the filtering the data retrieved from Mascot from the C- and N2-Source duplicate samples. Proteins were filtered out where two significant sequences didn't occur in both replicates of a condition to provide the necessary stringency for quantitation (personal communication, Adam Dowle, University of York).



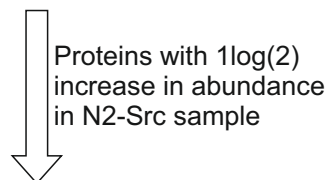
Mascott results grouped by protein family
 %emPAI calculated for each sample
 Values between biological replicates averaged



%emPAI compared between C- and N2-Src samples, protein lists made where:
 -Proteins with higher %emPAI in either sample
 -Proteins with over $1\log(2)$ relative increase in %emPAI



Enriched Gene Ontology groups, WikiPathways and KEGG pathways identified and %emPAI compared



Phosphosite, GPS and ScanSite identifications of potential Kinase domain substrate motifs.

Figure. 4-7 (page 124). Summary of LC-MS/MS approach.

HeLa cells were treated and lysed as described in 2.4.1 and the lysate probed with agarose conjugated anti-phosphotyrosine 4G10 resin. The cells were then processed for mass spectrometry as described in 2.4.2. The work of this thesis focuses almost exclusively on the averaged data from the C-Src + Van + Dox and N2-Src + Van + Dox conditions. The data for these conditions was processed to give the %emPAI, then the data averaged and any peptide without two significant sequence matches in both replicates of one condition removed. The lists of proteins generated were then processed as described in 2.4.

The %emPAI for the averaged C- and N2-Src HeLa cell lines that were treated with doxycycline and vanadate were used as the measure of abundance throughout the remainder of the analysis. The relative abundance of the filtered, processed lists of proteins identified in C- and N2-Src samples was calculated by the $\log(2)$ ratio between %emPAI values of the two conditions. From this ratio, two sets of lists that reflected difference in abundance between the two samples were created; one list that split the proteins into those with a relative increase in %emPAI of any size between the two samples, and a second list with only proteins showing a $>1\log(2)$ change in expression level, indicating that the protein was twice as abundant in one condition compared to the other. Various bioinformatic analyses were then performed on these lists to identify functional clusters of proteins that might indicate specific increases in the phosphorylation of substrates by N2-Src.

4.2.8 Identification of tyrosine phosphorylation sites in immunoprecipitated proteins

There were very few phosphotyrosine containing peptides detected for either C- or N2-Src conditions, only 18 and 22 hits respectively (Table 4-2). C- and N2-Src cell lines were identified as having pY416 phosphorylation, indicating that the kinases were active, as would be expected with transient pervanadate treatment. Whilst the majority of tyrosine phosphorylated proteins in N2-Src were also present in C-Src, Plakophilin and Paxillin-4 were exclusively identified in N2-Src. Due to the low abundance of tyrosine phosphoproteins, it isn't possible to say that these phosphopeptides are higher in abundance in the N2-Src IP sample compared to C-Src, however, both of these proteins are also enriched in N2-Src samples (Appendix 1). Phosphorylation of Plakophilin at Y465 has been identified in the Phosphosite mass spectrometry screening for phosphorylated proteins, however there is no published

Phosphotyrosine hits

Gene name	Description	C	N2
BCAR1	Breast cancer anti-oestrogen resistance protein 1	Y249 Y410	Y128 Y249 Y387 Y410 (3)
EGFR	Epidermal growth factor receptor	Y1092 Y1197	Y1197
CTTN	Src substrate Cortactin	Y421 Y446	Y421 (2) Y446
CTNND1	Catenin delta-1	Y217 or 221 (2) Y944	Y217 or Y221 Y257 (2) Y280 (3) Y904
LSR	Lipolysis-stimulated lipoprotein receptor	Y382 (2)	
PARD3	Partitioning defective 3 homolog	Y1080	Y1080
PKP4	Plakophilin-4		Y465
PXN	Paxillin		Y88
SRC	Proto-oncogene tyrosine-protein kinase Src	Y419	Y419
TUBB	Tubulin beta chain	Y106	
TUBB2B	Tubulin beta-2B chain	Y44	
TUBB4B	Tubulin beta-4B chain	Y106	

Table 4-2. Summary of C- and N2-Src phosphotyrosine hits from LC-MS/MS.

Pooled list of phosphotyrosine hits from both replicates of C- and N2-Src samples. Phosphotyrosine sites were inferred from the position of the tyrosine site on the peptide. Y217 and Y221 of CTNND1 occur on the same peptide, as such it is unknown which residue was phosphorylated. Tyrosine positions are the human numbering. Multiple hits of the same site are indicated in brackets.

literature relating to this specific phosphorylation event or its function (Hornbeck et al., 2012). Src phosphorylation of Paxillin is well documented, and Y88 is a known Src phosphorylation site (Schaller and Schaefer, 2001), however the only Y88-containing peptide in the C-Src samples was dephosphorylated.

Other notable phosphotyrosine hits include delta-catenin, for which several more tyrosine phosphorylation events were identified for N2-Src compared to C-Src, however all of these sites are known C-Src substrates (Mariner et al., 2001). Similarly BCAR1 had several more phosphotyrosine hits in N2-Src than C-Src, such as at Y387, a known C-Src phosphorylation site (Goldberg et al., 2003). Phosphorylated BCAR1 Y128 is a particularly interesting hit in N2-Src as it was identified as dephosphorylated

in C-Src samples, despite being a known C-Src phosphorylation site (Zhang et al., 2013).

4.2.9 Interaction mapping of enriched proteins using STRING

In addition to the identification of individual tyrosine phosphorylation sites on immunoprecipitated proteins, the mass spectrometry data could be mined for functional clusters of interacting proteins. Simply because phosphorylation of a protein was not detected, it did not mean the protein was of no functional importance. Since the proteins in this experiment were obtained through an IP of a native lysate in non-denaturing conditions, it is highly likely that interacting proteins and protein complexes were pulled down together. In order to identify these clusters of proteins, the lists of proteins with enhanced abundance in either C-Src or N2-Src were inputted into STRING (Franceschini et al., 2013). STRING is an online tool used to identify both physical and functional interactions between proteins, informed by the integration of interaction data from a wide variety of sources, from literature to high throughput and predicted interactions.

In addition to the STRING interaction network, these protein lists were also processed through the online Database for Annotation, Visualization and Integrated Discovery (DAVID). DAVID was used to identify enriched Gene Ontology (GO) terms, terms that are used to categorise the molecular function, cellular component association and biological processes that individual proteins are involved in (Huang et al., 2009b). DAVID compares the list of proteins provided against the human genome in order to identify whether terms associated with those proteins are significantly enriched (Huang et al., 2009b). The output from DAVID was used to inform the identification of functional clusters of proteins in the STRING network, and the grouping of nodes in the STRING network was modified in Cytoscape to more accurately reflect these functional classifications (Smoot et al., 2011).

The C-Src STRING network and GO terms indicated an enrichment in cytoskeletal, mRNA processing and translation related proteins (Fig. 4-8A). Whilst there were many other enriched categories, none possessed sufficient physical interactions to cluster on STRING. These three main clusters of proteins were also

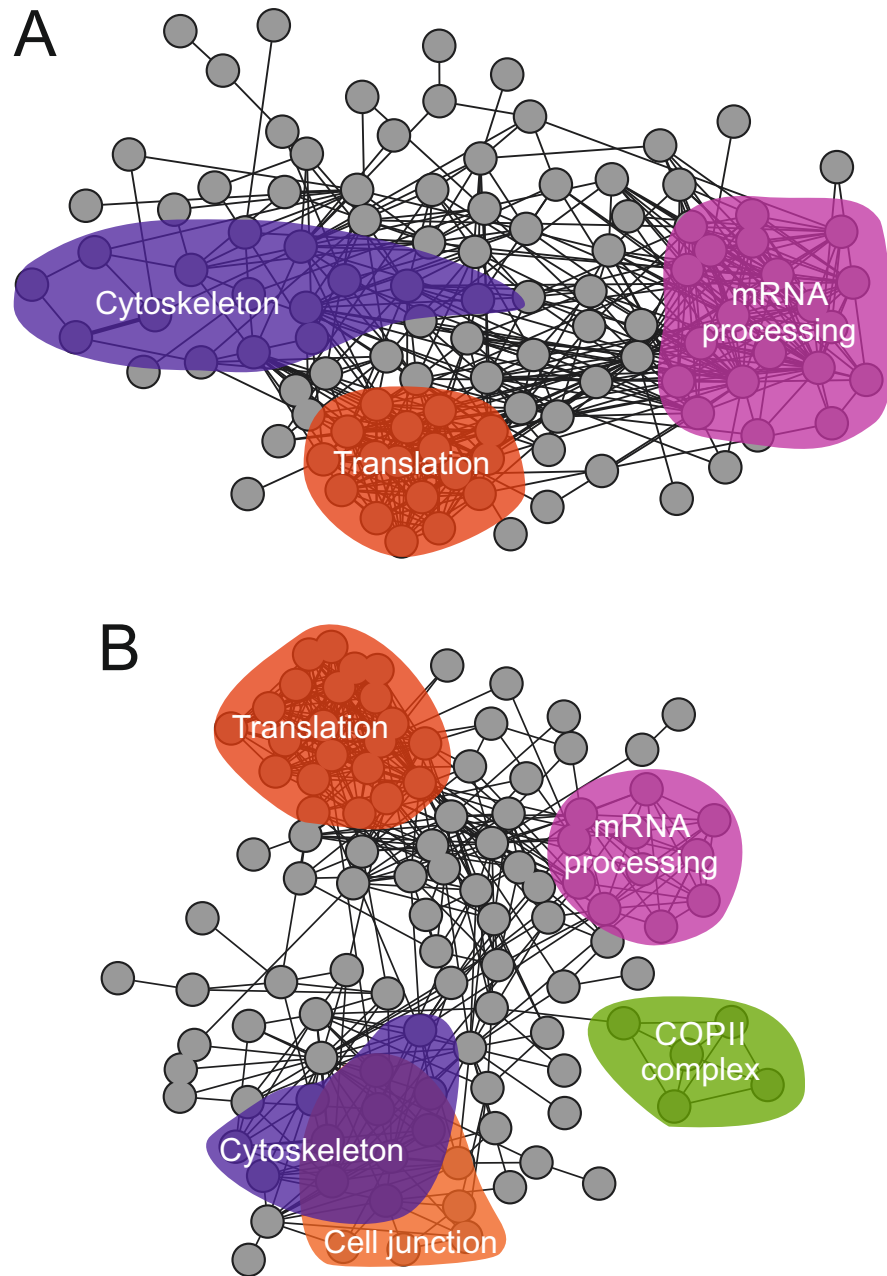


Fig. 4-8. STRING diagrams of proteins enriched in C-Src (A) or N2-Src (B) samples treated with plus vanadate and doxycycline
 Data is clustered by STRING based upon predicted and recorded interactions between proteins. Groups of proteins which have an observable functional relationship in addition to interaction clustering are highlighted. Identification of functional clusters was assisted by DAVID analysis of enriched GO terms in the samples. The STRING network was manually adjusted in Cytoscape to highlight functional and interaction clusters.

identified in the N2-Src STRING network, however, it is worth noting that the components of each of these clusters was different to those identified in the C-Src samples. Whilst these clusters are present in both samples, enrichment of different proteins in these functional categories suggests a change in their interactions or regulation due to C- and N2-Src expression.

In addition to the shared cytoskeletal, mRNA processing and translation categories, N2-Src also showed profound clustering of two additional categories of protein, namely cell adhesion molecules and components of the COPII complex (Fig. 4-8). Notably the presence of variants 2, 3, and 4 of Plakophilin alongside Junction Plakoglobin, β -catenin and Desmoplakin strongly suggests that junctional complexes were immunoprecipitated (Fig. 4-8B). Finally, the enrichment of five proteins of the COPII ER/Golgi transport system formed a cluster of interacting proteins (Fig. 4-8B). Additionally all five of these proteins were increased above a $1\log(2)$ ratio compared to C-Src and no proteins of the COPII transport system were observed in an increased abundance in the C-Src samples.

4.2.10 Identification of enriched functional clusters of proteins

Whilst identification of clusters of interacting proteins that showed any level of enrichment between C- and N2-Src samples provided an adequate method with which to coarsely identify functional groups of interacting proteins, in order to more finely identify the specific complexes that were significantly increased in abundance in the phosphotyrosine immuno-enriched samples, a higher threshold was utilised. Proteins that showed a $1\log(2)$ increase in abundance in the averaged samples for either C- or N2-Src HeLas treated with doxycycline and vanadate were analysed using DAVID and the WEB-based GENE SeT AnaLysis Toolkit (WEBGESTALT). Whilst DAVID provided excellent identification of enriched GO terms from the protein list, WEBGESTALT was also utilized as it provided analysis of both KEGG and WikiPathways (Zhang et al., 2005, Kelder et al., 2012, Kanehisa and Goto, 2000).

The $>1\log(2)$ protein lists were used to query both DAVID and WEBGESTALT and their output is summarised in Table 4-3 (after removing redundancies and categories of two or fewer proteins). These refined lists contained

far fewer proteins only 52 proteins were two fold higher in abundance in C- than N2-Src and 62 proteins more abundant in N2- than C-Src. Of the enriched groups that these proteins belonged to, those that were significant ($<0.05\%$ FDR, Web Gestalt; $<0.05\%$ Benjamini, DAVID) are listed in Table 4-3.

The majority of enriched categories identified by DAVID's GO term enrichment are, similar to the STRING analysis, involved in translation or mRNA binding with largely similar categories being identified between C- and N2-Src samples (Table 4-3), however the enrichment of the proteins of the COPII complex was identified as statistically significant by DAVID. Aside from the translation and mRNA processing pathways enriched in both samples, the significantly enhanced KEGG pathways and WikiPathways (Table. 4-3) appear to be much more divergent between C-Src and N2-Src expressing cell lines than the clustering identified by GO terms. The C-Src sample resulted in lists of proteins in both KEGG pathways and WikiPathways that were largely associated with proliferation, cell cycle and DNA replication. This is what we would expect in a cancer cell line that is overexpressing the proto-oncogene C-Src, particularly when C-Src is activated by transient vanadate treatment of the cells. This provides support for the methodology of using comparative abundance between C-Src and N2-Src samples to help identify N2-Src specific substrates.

KEGG pathways significantly enhanced in the N2-Src sample included the category 'Protein processing in the ER', a category that exclusively contains proteins of the COPII coat. The list of significantly enriched KEGG pathways also included a group of endocytosis associated proteins. Although these did not cluster on the STRING network there is a significant enrichment of proteins involved in endocytosis, such as Alix, Clathrin heavy chain and HRS. Several disease associated KEGG pathways are enhanced, although from a biological perspective the disease clusters are less informative, as often pathogenic or genetic factors are more likely to be at work in these processes than phosphorylation.

The most significant WikiPathways identified for C-Src were largely representative of its role as an oncogene in cancer cell lines, promoting cell cycle progression and proliferation (Table. 4-). In the N2-Src list, the COPII coat proteins were again identified, in this instance as a part of the SREBP signalling pathway.

C-Src

N2-Src

DAVID GO	Term	Count	FDR	Term	Count	FDR
Biological Process	GO:0006412~translation	11	1.88E-04	GO:0006412~translation	13	1.17E-05
	GO:0030529~ribonucleoprotein complex	15	5.84E-07	GO:0030529~ribonucleoprotein complex	18	7.61E-09
	GO:0043228~non-membrane-bounded organelle	28	8.89E-07	GO:0005829~cytosol	24	2.83E-07
Cellular component	GO:0031981~nuclear lumen	17	0.008093	GO:0030127~COPII vesicle coat	4	0.004055
	GO:0003723~RNA binding	16	7.44E-06	GO:0003723~RNA binding	22	3.18E-11
Molecular function	GO:0005198~structural molecule activity	12	0.007359	GO:0003735~structural constituent of ribosome	9	2.27E-04

WEBGESTALT	Enriched pathways	Count	adjP	Enriched pathways	Count	adjP
	Ribosome	6	2.83E-08	Ribosome	10	1.07E-15
	mRNA surveillance pathway	4	0.000033	Protein processing in ER	5	1.42E-05
	Parkinson's disease	4	0.0001	Arrhythmogenic right ventricular cardiomyopathy	4	1.42E-05
	Calcium signaling pathway	4	0.0003	Metabolic pathways	4	0.0779
	Huntington's disease	4	0.0003	Huntington's disease	3	0.0063
	Gap junction	3	8.00E-04	Endocytosis	3	0.0064
	Cell cycle	3	0.0012	Spliceosome	2	0.0202
KEGG pathways	Spliceosome	3	0.0012	RNA transport	2	0.0238
	RNA transport	3	0.0019			
	Cytoplasmic Ribosomal Proteins	6	1.70E-08	Cytoplasmic Ribosomal Proteins	10	7.94E-16
	G1 to S cell cycle control	3	0.0009	SREBP signalling	4	3.98E-05
	Cell cycle	3	0.0011	Arrhythmogenic right ventricular cardiomyopathy	4	7.54E-05
	Electron Transport Chain	3	0.0011	mRNA processing	3	2.20E-03
	TCR Signaling Pathway	3	0.0011	Neural Crest Differentiation	3	2.20E-03
				Lymphocyte TarBase	5	0.0022
WikiPathways				Muscle TarBase	4	0.005

Table 4-3. Summary of functionally enriched clusters.

Proteins that were 1log(2) enriched in either C- or N2-Src when compared against each other were inputted into DAVID and WebGestalt to probe the GO, KEGG and WikiPathways database. Statistically significant ($p < 0.05$) categories are listed. 'Duplicate' categories have been removed as well as categories with only two proteins. Categories identified as clusters in the STRING mapping are colour coded to match Fig. 4-8.

Interestingly the “Neural Crest Differentiation” pathway was identified, containing β -catenin, Notch2 and N-Cadherin. These genes are particularly interesting as they are essential components in neural crest differentiation, which relates strongly to known associations of N2-Src in the neural crest derived cancer neuroblastoma.

The protein clusters identified by these pathways and enriched GO terms informed a more in-depth analysis of proteins that were enhanced in N2-Src cells. As a result of these groups, three main categories were analysed in detail, endocytosis, adherens and COPII complex proteins.

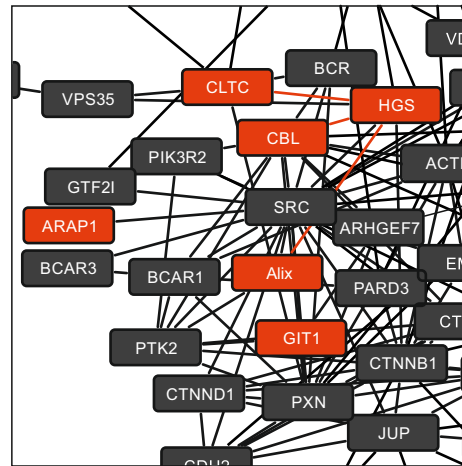
4.2.11 In-depth analysis of N2-Src enhanced proteins: Endocytosis

Six proteins involved in endocytosis were selected for further analysis, based upon their appearance in enriched GO terms, KEGG pathways and WikiPathways, in addition to applied biological knowledge of the proteins.

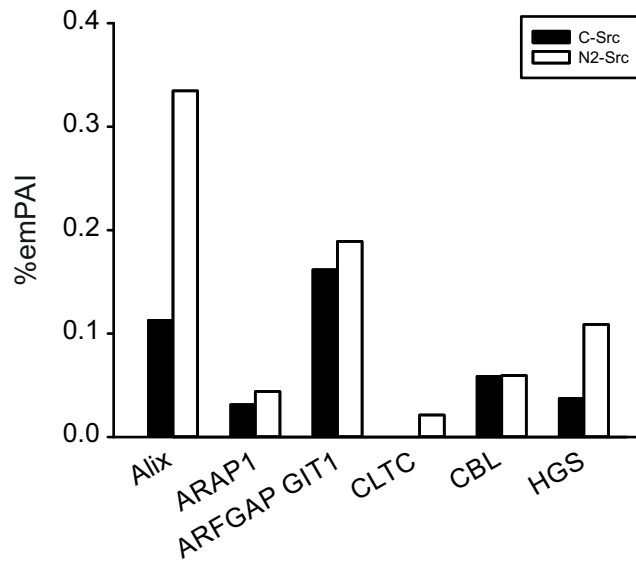
Whilst all six proteins are involved in endocytosis, only four are identified as having interactions by STRING (Fig. 4-9A) and only three have $\log(2)$ ratios above 1 when compared to C-Src abundance (Fig. 4-9B), Clathrin-heavy chain, Alix, HRS. Possible phosphorylation site for these three $>1\log(2)$ ratio proteins were identified using the Phosphosite database of phosphotyrosines identified by mass spectrometry (Hornbeck et al., 2012), in addition to Src kinase domain substrate motif analysis of amino acid sequence using both GPS (Xue et al., 2008) and ScanSite (Obenauer et al., 2003), in addition to literature searches for known phosphorylation events. This method of analysis was repeated for all proteins that were analysed in depth in order to identify both known and predicted Src substrate sites.

All three of the endocytosis proteins that are highly increased in abundance in N2-Src samples are known C-Src substrates, however many more tyrosine phosphorylation sites were identified by Phosphosite, in addition to predicted Src kinase domain motifs identified by GPS and ScanSite.

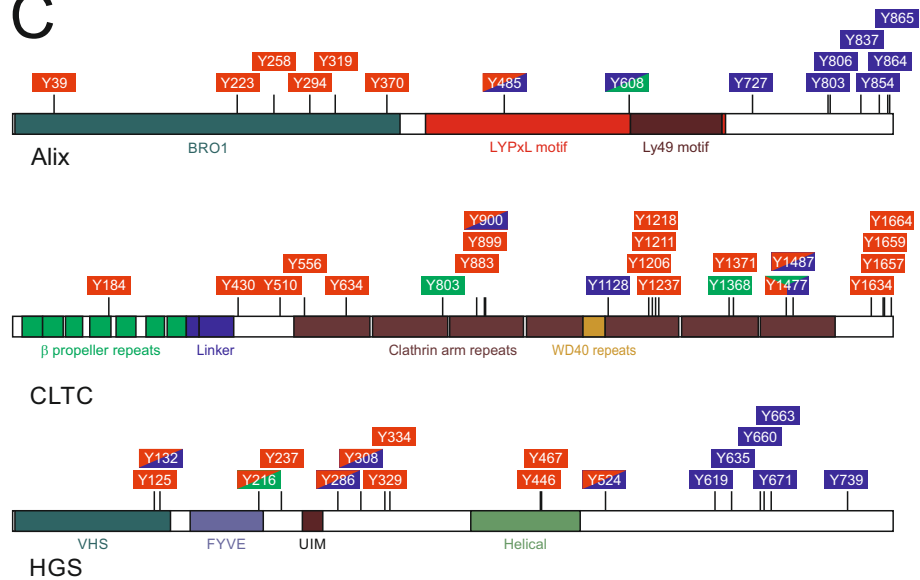
A



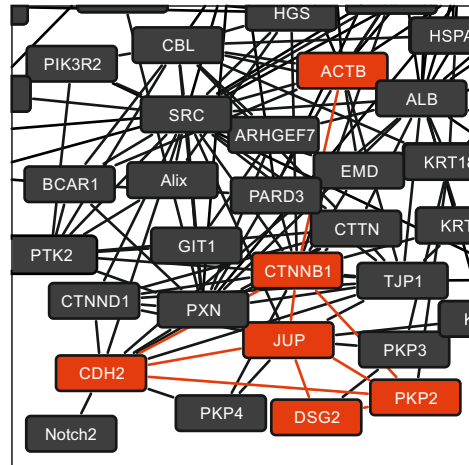
B



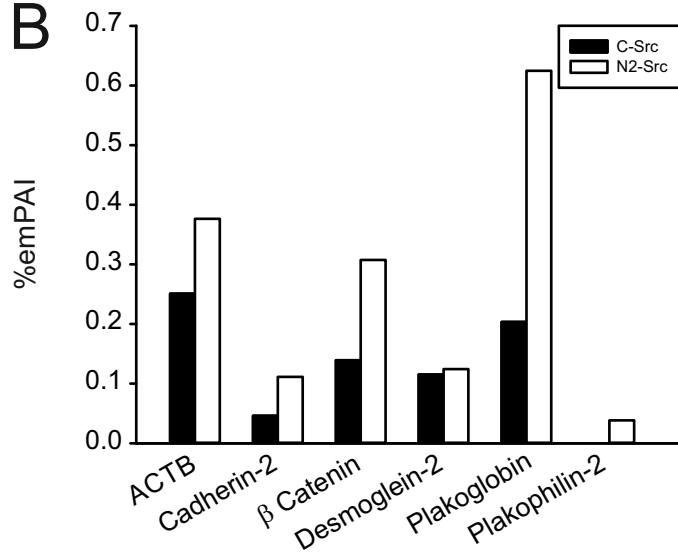
C



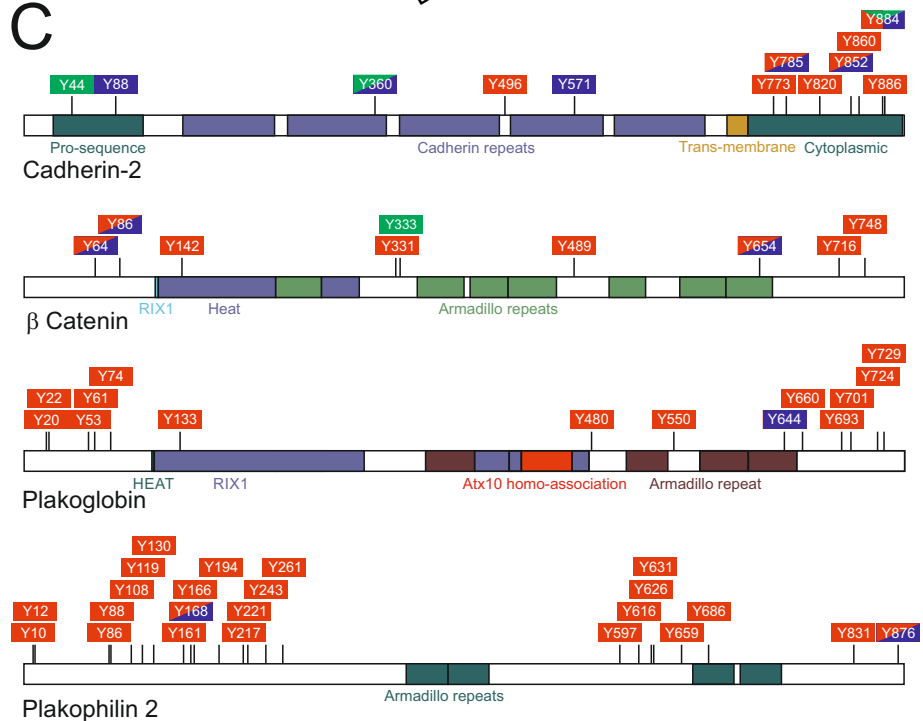
A



B



C



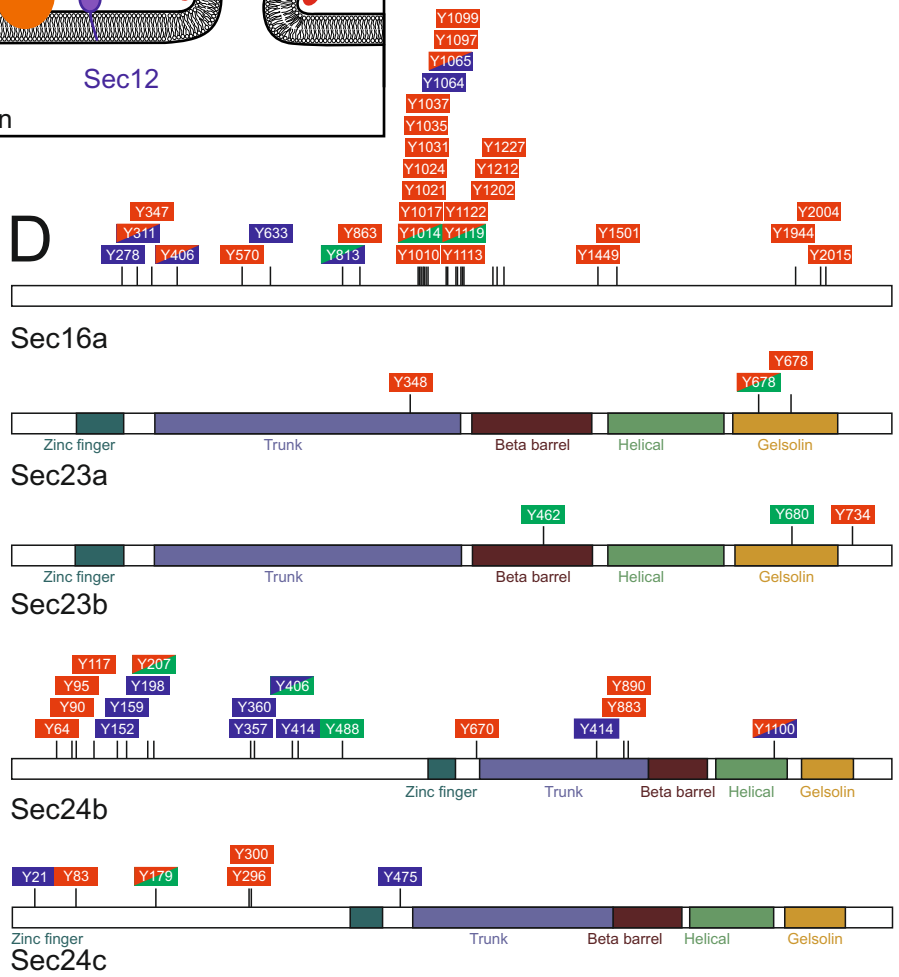
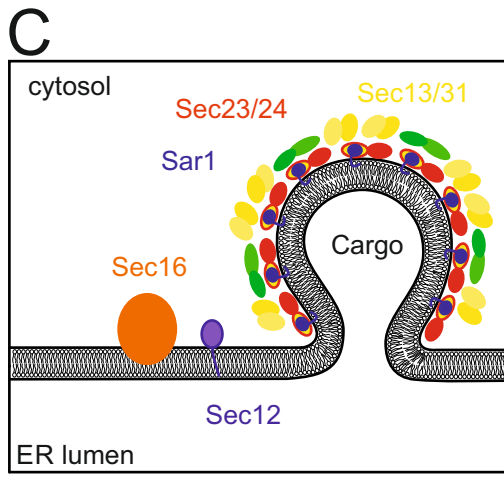
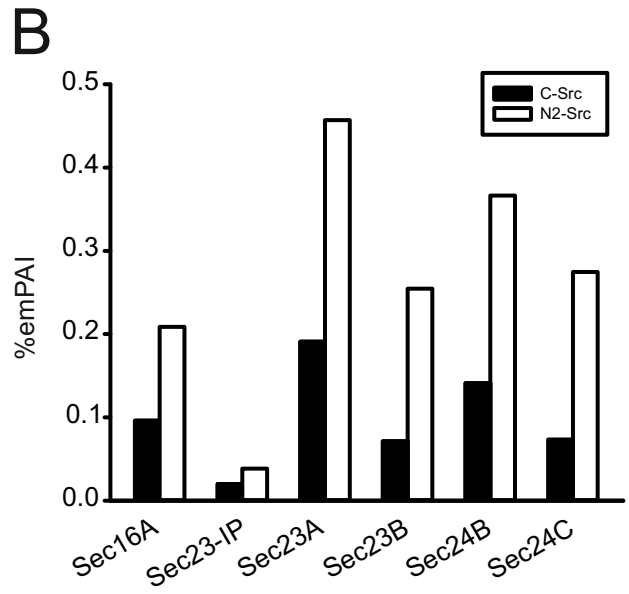
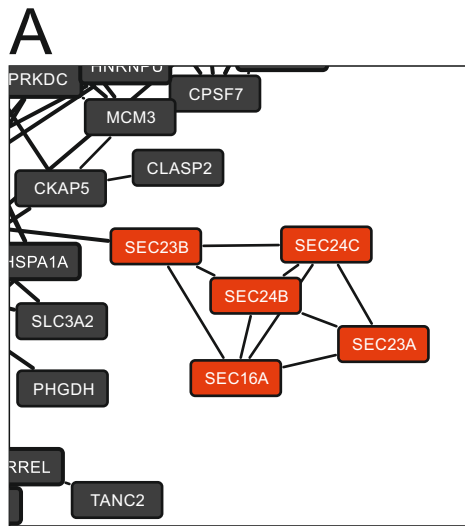


Figure. 4-9 (page 133). In depth analysis of endocytosis associated proteins enriched in N2-Src samples.

Figure. 4-10 (page 134). In depth analysis of adherens associated proteins enriched in N2-Src samples.

The following figure description applies to both figures 4-9 and 4-10. A) STRING maps highlighting interactions between the chosen endocytosis (4-9) or adherens (4-10) proteins in red B) Bar graph showing the average %emPAI values for C- and N2-Src samples. Samples with an increased abundance in N2-Src of over $1\log(2)$ were further analysed for known and potential phosphorylation sites. C) Domain summary, identified and predicted phosphorylation sites of proteins with over a $1\log(2)$ increase in abundance in N2-Src HeLa samples. Phosphosite hits shown in red, Src phosphorylation sites predicted by ScanSite shown in blue, Src phosphorylation sites predicted by GPS shown in green.

Figure. 4-11 (page 135). In depth analysis of COPII proteins enriched N2-samples.

A) STRING map showing the interaction between the COPII proteins, highlighted in red. B) Bar graph showing the average %emPAI values for C- and N2-Src samples. Samples with an increased abundance in N2-Src of over $1\log(2)$ were taken through for further analysis of phosphorylation sites. C) Diagram based upon Gillon et al, 2012, showing the function of COPII coat in assembling transport vesicles from the ER to the Golgi. Sar1 and Sec16 activate, recruit and scaffold the COPII inner coat (constructed of Sec23/24) to the ER before recruiting vesicle cargo. Outer coat proteins (Se13/31) then bind to the inner coat and polymerise to coat the vesicle, forcing the membrane to curve out into a vesicle structure which is then transported to the Golgi. D) Domain summary and identified and predicted phosphorylation sites of proteins with over a $1\log(2)$ increase in abundance in N2-Src HeLa samples. Phosphosite hits shown in red, Src phosphorylation sites predicted by ScanSite shown in blue, Src phosphorylation sites predicted by GPS shown in green.

4.2.12 In depth analysis of N2-Src enhanced proteins: Adherens

Of the proteins associated with cell-cell junctions, the six selected for more in depth analysis included Junction Plakoglobin (JUP), β -catenin, Plakophilin-2, N-Cadherin, Desmoplakin-2, Paxillin and β Actin. These proteins were selected for more in depth analysis based upon their appearance in the enriched functional pathways and GO terms as well as applied knowledge of their functions. Notably both Paxillin and a variant of Plakophilin-2 (Plakophilin-4) have specifically identified phosphopeptides in N2-Src samples which are not detected in C-Src samples (4.2.8). As is apparent from the abridged STRING diagram (Fig. 4-10A) there is a strong interconnectivity between these proteins, with β -catenin and JUP at the centre. Of these six proteins only four have a %emPAI in N2-Src more than double that observed in N2-Src (Fig. 4-10B) and these were then analysed for confirmed or predicted Src phosphorylation sites (Fig. 4-10C).

Phosphosite identified several phosphotyrosine residues on each protein, some of which were confirmed in the literature and several predicted Src kinase domain motifs were identified by GPS and ScanSite (10C). Literature searches based upon the Phosphosite database also revealed that JUP, N-Cadherin, Plakophilin-2 and β -catenin are all known Src substrates at some of these sites.

4.2.13 In depth analysis of N2-Src enhanced proteins: COPII coat proteins

Throughout analysis of the N2-Src expressing HeLa mass spec data, the cluster of Sec proteins (Sec 16A, Sec 23A, Sec 23B, Sec S4B and 24C, Fig. 4-11A) have consistently been identified as significantly enriched, and all five possess %emPAI scores in N2-Src HeLa cells over double that observed in C-Src expressing cells (Fig. 4-11B). These proteins were identified as a segregated cluster, with the only functional connection to another protein being via HSPA5, a heat shock protein family member that is also localised to the ER and has a possible role in regulating protein transport (Figure 4-11A). These Sec proteins have no known C-Src phosphorylation sites. Sec 23A and B have very few known or predicted tyrosine phosphorylation sites, suggesting that they are unlikely to be the protein specifically bound in the 4G10 IP. Several sites of tyrosine phosphorylation by Src are predicted by ScanSite and Phosphosite on Sec 16a and many phosphotyrosines have been identified in the Phosphosite database. Despite the identification of many sites by mass spectrometry on the Phosphosite database, there are no clues in the literature about any possible role for tyrosine phosphorylation in regulation of Sec 16a function.

4.2.14 Confirming Sec23A immunoprecipitation for N2-Src expressing HeLa cells

To confirm the increased abundance of the COPII complex proteins in the N2-Src expressing HeLa IP, input and IP from vanadate treated C- and N2-Src HeLa cells with and without doxycycline treatment was probed with a Sec23A antibody (Fig. 4-12). Much higher Sec23A abundance was detected in the IP elution of N2-Src suggesting that the 4G10 antibody is binding to a phosphotyrosine on Sec23A, or a protein that it is bound to, which is only phosphorylated in the presence of N2-Src.

Additionally, whilst previous blots of these samples have confirmed the presence of N2-Src by the detection of the attached FLAG epitope tag (Fig. 4-6), this blot was probed with an antibody specific for Y416 Src phosphorylation. There are two main bands of Y416 expression, likely to be that of endogenous C-Src or another SFK, and the FLAG epitope tagged C- and N2-Src splice variants that are likely to migrate slower than their endogenous counterparts due to their increased size. Interestingly, whilst both C-Src and N2-Src are tyrosine phosphorylated at Y416, N2-Src appears to significantly trans-activate the ~60kda endogenous SFK.

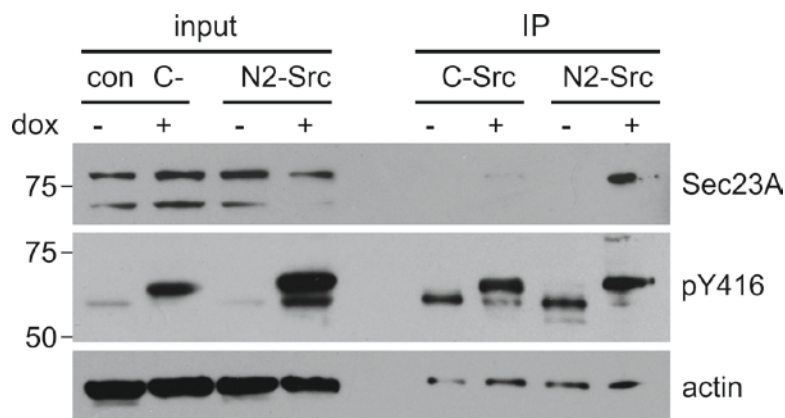


Figure. 4-12. Identification of Sec23A abundance in T.REx HeLa phosphotyrosine IPs.

Spare input and IP from the first replicate of the phosphotyrosine immunoprecipitation experiment were run on a gel to compare the expression of Sec23A. Samples were run on a 12.5% acrylamide gel by SDS PAGE before transfer onto a PVDF membrane, before probing with mouse α -Sec23A, rabbit α -pY416 and rabbit α -actin antibodies.

4.3 Discussion

The above data indicate that the differential cellular effects of neuronal Src expression, when compared to C-Src expression, are not limited to cells of a neuronal origin. This was demonstrated through analysis of the shape and migration of N-Src expressing HeLa cell lines. Mass spectrometry analysis on phosphotyrosine immunoprecipitation samples from these cells indicates that C- and N2-Src have significantly different effects upon tyrosine signalling within the cell, enriching different functional clusters of proteins. Specific phosphorylation events were identified in N2-Src expressing cells that were absent in C-Src expressing cells, and significantly enriched functional clusters of proteins included those of the ER/Golgi transport vesicle coat COPII, in addition to several adherens and endocytosis-related proteins.

4.3.1 Cellular effects of N2-Src are not limited to neuronal cells

Whilst undertaking this study in a cell line with a neuronal background of gene expression would have been ideal, N2-Src expression in non-neuronal cell lines has consistently demonstrated a differential effect on non-neuronal cells when compared to C-Src. Induced N1- and N2-Src HeLa cells were demonstrated to have differential effects on cell morphology (Fig. 4-2) and migration (Fig. 4-4), as well as a more restricted intracellular localisation than C-Src (Fig. 4-3). All of these factors support the idea that, even without a neuronal background of protein expression, the inducible HeLa cell line system will be efficient in identification of differential C- and N2-Src substrate phosphorylation.

4.3.2 N2-Src appears to co-activate endogenous SFKs

An additional band of pY416 staining is observed at around 60 kDa in western blots of N2-Src expressing HeLa cells sample (Fig. 4-12). Due to the specificity of the pY416 antibody, this band is likely to indicate trans-phosphorylation of pY416 in an endogenous SFK. Interestingly a similar effect was seen in N2-Src overexpression in the neuroblastoma cell line B104 (Fig. 3-1), however in this instance the transphosphorylated SFK was 5 kDa heavier than N2-Src. The SFK in HeLa cells is more likely to be endogenous Src as this is likely to have increased mobility compared to the larger FLAG tagged construct that the cells stably express. As Src was the only Src Family kinase observed in the mass spectrometry data for these cells, it is highly likely that the pY416 signal at this locus is endogenous Src (Appendix 1). Interestingly N2-Src seems to be trans-activating C-Src at a higher rate in these cells to C-Src, suggesting that the SH3 domain of N2-Src does not inhibit the trans-activating properties of C-Src.

4.3.3 Appraisal of the chosen phosphoproteomic methodology

This study identified several functional clusters of proteins that were enriched by phosphotyrosine immunoprecipitation of N2-Src cells, which provide extensive

scope for future work on the signalling pathways through which N2-Src may operate. It also identified three phosphopeptides that warrant further investigation (BCAR1 Y128, Plakophilin-2 Y465 and Paxillin Y88), two of which were identified as dephosphorylated in C-Src samples and one of which was an as-yet uncharacterised tyrosine phosphorylation event. In that respect this method has proven a success, however an increase in the overall number of phosphopeptides would be highly desirable if this experiment were repeated.

Through immunoprecipitation with immobilised phosphotyrosine antibody 4G10 it was expected that a large proportion of peptides identified would be tyrosine phosphorylated, unfortunately this was not the case. Due to the low abundance of phosphotyrosine in cells (tyrosine represents only around 4% of total phosphorylation events (Olsen et al., 2006)), this method of immunoenrichment of phosphotyrosine prior to mass spectrometry has been used extensively in the literature (Hammond et al., 2010, Kehasse et al., 2013, Zhang et al., 2012, Breitkopf et al., 2012, Cunningham et al., 2010).

A similar method published by Hammond and Clague coupled tyrosine immunoenrichment with Stable Isotope Labelling by Amino acids in Cell culture (SILAC) to identify common and discrete phosphotyrosine associated networks induced by EGF or HGF (Hammond et al., 2010). The identification of phosphotyrosine peptides was still modest (55 peptide hits from three runs), although the use of SILAC allowed for a direct, quantitative comparison between samples. Whilst SILAC would be desirable due to its superior quantitative power between samples, the %emPAI normalisation provided adequate ability to compare between samples for the purposes of this study. The fidelity of %emPAI quantification was confirmed by Western blotting for Sec23A which identified a similar change in Sec23A abundance between C- and N2-Src samples with and without doxycycline (Fig. 4-12).

To specifically identify differential C- and N2-Src phosphorylation events by mass spectrometry, an approach based upon work by Breitkopf and colleagues (2012) may prove more fruitful. These researchers used two methods to identify BCR-ABL targets; firstly using a BCR-ABL co-IP to identify proteins directly bound by BCR-ABL, and then identifying differential tyrosine phosphorylation in the cell by performing a tryptic digest on cell lysate, before a phosphotyrosine IP (Breitkopf et

al., 2012). Similarly, Cunningham and colleagues identified over 430 phosphotyrosine containing peptides through a two-step enrichment, first a 4G10 IP and then a titanium dioxide enrichment of phosphate following tryptic digest (Cunningham et al., 2010). Performing the phosphotyrosine enrichment on digested peptides rather than on native lysate is a particularly useful method for identifying specific phosphopeptides. This method reduces enrichment specifically for phosphopeptides and has been employed by other phosphotyrosine studies, identifying 80 (Zhang et al., 2012) to 300 (Kehasse et al., 2013) phosphotyrosine peptides.

The identification of functional clusters of proteins with known interactions is particularly important in this dataset. Performing the phosphotyrosine immunoprecipitation on cell lysate, rather than on the peptides following a tryptic digest means that it is very likely that complexes of interacting proteins are being co-enriched. Identification of differentially enriched clusters will therefore provide a great deal of insight into which signalling pathways and regulatory complexes are being tyrosine phosphorylated as a result of C- or N2-Src expression. Although performing these experiments in triplicate would have been desirable, due to the nature, and inherent cost, of this proteomic method the benefit of a further replicate of the data outweighed the cost. To address the issue of lacking triplicate data, the stringency of each stage of the analysis was incredibly high, counting only proteins which have at least two different significant peptide sequences detected in both replicates of the data, then only studying in depth those proteins that demonstrated an increase in over two fold in their %emPAI scores. As a result, despite the lack of a triplicate of data, we can be highly confident that the observed enrichment as detected by LC/MS/MS is reflected in the samples.

Over 900 unique proteins were identified in both C- and N2-Src samples and the stringent filtering of these proteins by the number of significant sequences has allowed for meaningful quantification of their relative abundance in these samples (Table 4-1). By utilizing both WebGestalt and DAVID to query the Gene Ontology, KEGG and WIKI Pathways databases I was able to identify functional clustering of proteins in each sample Table 4-3. In addition to aiding in the identification of functional clusters of proteins for further analysis and better comprehension of the dataset, these online tools also provided statistical analyses of the likelihood that these proteins would occur in a population at random. This analysis, compared the total

number of members of this group in the genome against the number of observed members in my dataset. This method of analysis is widely used and is well-regarded in its ability to identify biological relevance from large datasets (Huang et al., 2009a). The principal failing of these methods is in their inability to scale their analyses according to score, so a protein with a modest enrichment in N2-Src samples by comparison to C-Src samples would be treated identically. For this reason, filtering the protein list to only those demonstrating a two-fold increase in %emPAI score was essential in assuring that proteins with non-significant differences were not considered when regarding the biological significance of the datasets (Table 4-3).

Hence, in the absence of large numbers of tyrosine phosphopeptides, identification of functional clusters of proteins enriched by phosphotyrosine immunoprecipitation from C- and N2-Src HeLa samples is invaluable in informing future studies on the specific pathways of N2-Src action within cells during neuronal differentiation.

4.3.4 Interpretation of the identified tyrosine phosphopeptides

Of the list of tyrosine phosphopeptides identified, three phosphoproteins are of particular relevance in the identification of specific N2-Src substrates, BCAR1, Paxillin and Plakophilin-4. Whilst the majority of the phosphopeptides are well-characterised as C-Src substrates, these three hits were either specifically identified as dephosphorylated in C-Src, or, in the case of Plakophilin-4, are as-yet uncharacterised. BCAR1 phosphorylation at Y128 is increased in FGFR1 overexpressing cells (Hinsby et al., 2003) and is associated with induced carcinogenesis as well as cell growth, adhesion and motility and was identified dephosphorylated in C-Src samples.

Although Plakophilin-4 phosphorylation at Y465 has been identified by previous high-throughput phosphoproteomics studies there is currently no literature referencing this site (Jørgensen et al., 2009, Hornbeck et al., 2012). Interestingly, aside from the high-throughput tyrosine phosphoproteomic curation datasets, the only study to identify Y465 phosphorylation of Plakophilin was in a study on Ephrin receptors (Jørgensen et al., 2009). In this study Plakophilin-4 Y465 phosphorylation was identified in cells expressing both Ephrin receptors B1 and B2, receptors involved

in developmental regulation of axon guidance (Egea and Klein, 2007, Jørgensen et al., 2009). Since Plakophilin-4 has roles in cell-adhesion and cell-cell signalling, regulation of this protein by N2-Src phosphorylation, or a downstream protein, could be a part of the responses to N2-Src overexpression observed in this study. N2-Src phosphorylation would be relatively easy to confirm using antibody pull-down of Plakophilin-4 in C- and N2-Src expressing HeLa cells, followed by probing for phosphotyrosine by Western blotting.

BCAR1 phosphorylation at Y128 was observed in N2-Src expressing cells, however only the dephosphorylated peptide was identified in C-Src. Y128 phosphorylation is relatively well studied. Phosphorylation at Y128 is increased in FGFR1 overexpressing cells (Hinsby et al., 2003) and is associated with induced carcinogenesis as well as cell growth, adhesion and motility and was identified dephosphorylated in C-Src samples. Y128 is a known C-Src substrate and C-Src phosphorylation of this substrate is known to be up-regulated in colon cancer (Zhang et al., 2013). Phosphorylation of Paxillin at Y88 was also only identified in N2-Src expressing cells, with the corresponding dephosphorylated peptide identified in C-Src expressing HeLa cells. Although the cellular effect of Y88 phosphorylation has not been fully elucidated, Paxillin Y88 is also a C-Src substrate and phosphorylation is a feature of colon cancer. Mutation of Y88 to F88 in colon cancer models decreases anchorage independent growth and prevents the growth of Xenografts on nude mice (Zhao et al., 2010).

The identification of these three phosphoproteins warrants follow-up investigation to determine whether these proteins are specifically phosphorylated by N2-Src at a greater rate than C-Src, and whether this phosphorylation event could be linked to the actions of N2-Src within cells. Plakophilin-4 is of particular interest in this case as, with no known C-Src phosphorylation event at this site and only neuronal studies identifying it, it could represent an N2-Src exclusive substrate.

Although both Paxillin and Plakophilin-4 make excellent candidates for follow-up study of specific N2-Src phosphorylation, neither are enriched at over $1\log(2)$, and only one phosphotyrosine residue was identified for each protein. For this reason, it was decided that time and resources would best be spent upon studying the enrichment of proteins of the COPII coat. Although no specific COPII

phosphotyrosine residue was identified, the consistent, significant enrichment of this whole complex, in addition to co-localisation between N2-Src and the Golgi made these a better candidate for follow-up study.

4.3.5 Specific enrichment of endocytosis related proteins in N2-Src expressing HeLa cells

Several endocytosis associated proteins were specifically increased in abundance in N2-Src expressing samples. This enrichment suggests that differential tyrosine regulation of interacting components of the endocytosis pathway may be occurring in N2-Src expressing cells. Of these enriched proteins, Clathrin-heavy chain, HRS and Alix were all more than two-fold enriched in N2-Src cells, when compared to C-Src cells.

HRS is known to interact with Clathrin, Alix and CBL (Fig. 4-9A (Stern et al., 2007)) suggesting that these proteins may have been immunoprecipitated as part of a complex. HRS is important for endosomal sorting and recycling, and interacts with CBL and Alix, in this role. HRS interacts with and recruits Clathrin during the formation of Clathrin-coated regions of membranes, contributing to endocytosis. Alix also has roles in endosomal vesicle formation and also in the ESCRT pathway. Endosomal regulation is important in a wide variety of neuronal functions, from polarity to neurite extension and differentiation as well as the characteristic role in synaptic transmission in mature neurons (Schmidt and Haucke, 2007).

Each of these three proteins could be a target of N2-Src as they are all known to interact with C-Src. Regulation of HRS is known to occur via Src phosphorylation, (Wilde et al., 1999). Clathrin, is phosphorylated by Src at Y1477 in response to EGF stimulation on one of the Clathrin arm repeat domains that regulates Clathrin assembly and recruitment (Wilde et al., 1999). Src has also been shown to bind Alix C-terminally via its SH3 domain, and at Y319, via its SH2 domain, resulting in C-terminal phosphorylation of Alix (Fig. 4-9C (Schmidt et al., 2005)). Although specific C-terminal substrate residues were not identified in the literature, Y727 is identified in the specified tyrosine rich region and has been identified by GPS motif identification software as having a suitable C-Src kinase domain substrate motif (Fig. 4-9C).

These factors suggest that N2-Src overexpression is leading to tyrosine phosphorylation-mediated regulation of one or more endocytosis-related proteins. It is interesting that in addition to endocytosis-related proteins, COPII proteins, commonly associated with exocytosis, are also enriched in N2-Src samples. It is tempting to suggest that these data point towards a complex role for N2-Src in regulation of membrane dynamics. Further study is required to delineate which of these proteins is phosphorylated and whether this phosphorylation event is biologically significant.

4.3.6 Specific enrichment of adherens-related proteins in N2-Src expressing HeLa cells

Src is known to have extensive roles in adhesion mediated cell-cell signalling, both at the site of focal adhesions through its interaction with FAK, as well as at integrins and adherens junctions (Hanks and Polte, 1997, Giancotti and Ruoslahti, 1999, Mariner et al., 2001). Several adherens-related proteins were specifically enriched in N2-Src expressing HeLa cells of which Junction Plakoglobin (JUP), β -catenin, Plakophilin-2, N-Cadherin were all enriched by over two fold as determined by %emPAI. As these proteins are all known to physically interact, it is likely that they may have been precipitated as part of a complex, suggesting that N2-Src may be phosphorylating one or more of these proteins.

JUP is a catenin-family protein with roles in the structure and dynamics of submembranous plaques similar to that of β -catenin, supporting cell-cell junctions by forming a link between adherens junctions and the cytoskeleton. Whilst JUP and β -catenin are highly similar and can act interchangeably to some degree, JUP has roles in associating desmosomes with the intermediate filament cytoskeleton that β -catenin lacks (Miravet et al., 2003) and JUP cannot compensate for β -catenin in its roles in Wnt signalling. β -catenin is known for its roles in nuclear signalling, however its co-enrichment with so many other adherens-related proteins suggest that it is being enriched in complex with these, rather than in its functions in the nucleus.

Several Plakophilin proteins were identified as enriched in N2-Src samples, including Plakophilin-4 for which a tyrosine phosphopeptides hit was identified.

Plakophilin-2 associates to desmosomes, linking Cadherins to the intermediate filaments of the cytoskeleton; however it has also been identified in the cell nucleus (Chen et al., 2002). Plakophilin-2 interacts with both β -catenin and JUP (Fig. 4-11A) and can up-regulate β -catenin signalling (Chen et al., 2002). Interestingly

CDH2 (N-Cadherin) is a calcium dependent cell-cell adhesion protein that also has roles in adhesion at central nervous system synapses. N-Cadherin, whilst not restricted to neurons in expression, has several crucial roles in neuronal development (Gärtner et al., 2012). N-Cadherin is particularly important in specifying polarity in developing neurons, ectopic expression of N-Cadherin is singly sufficient to bias the appearance of the first neurite and subsequent re-organisation of organelles to accommodate this polarity (Gärtner et al., 2012). N-Cadherin has several tyrosine phosphorylation events identified in the literature (Y820, Y852, Y860, Y884, Y886 (Qi et al., 2006), Fig. 4-10C).

The abundance and co-enrichment of all of these proteins together strongly suggests that adherens junctions are being regulated by N2-Src expression in these cells. This is unsurprising given the phenotypes observed for N2-Src expressing cells and the roles of these proteins described above. All of these proteins are potential candidates for N2-Src phosphorylation as all are known substrates of C-Src. Y644 phosphorylation of JUP by C-Src decreases JUP interaction with E-cadherin and α cadherin, whilst increasing interaction with Desmoplakin (Miravet et al., 2003). Src has been implicated in oncogenic phosphorylation and activation of β -catenin in human colorectal cancer and in response to EGFR activation at Y333 (Coluccia et al., 2006, Yang et al., 2011). Known N-Cadherin Src phosphorylation events include Y860 phosphorylation that results in decreased binding between N-cadherin and β -catenin and expression of dominant negative Src inhibits dissociation of β -catenin from N-Cadherin and associated signalling and nuclear transcription (Qi et al., 2006).

Whilst a large number of known sites of Plakophilin-2 phosphorylation are identified in the Phosphosite high-throughput mass spectrometry dataset and many C-Src sites are predicted by both GPS and ScanSite, there is no literature confirming any individual C-Src phosphotyrosine sites. This is particularly interesting as no C-Src hit was identified for Plakophilin-2.

The extensive interactions between these four proteins, coupled with the known and predicted Src phosphorylation sites on these proteins indicates that N2-Src may have increased affinity for one or more of these proteins, resulting in increased phosphorylation when N2-Src is overexpressed. Due to the roles of adherens in a remarkable array of cell functions, from mechanical roles in motility to signalling roles in growth, survival and proliferation, the increased detection of these proteins in N2-Src expressing cells is particularly interesting and worth following up in future studies. Specific phosphorylation of each of these proteins could be confirmed by immunoprecipitation from C- and N2-Src expressing HeLa cells followed by Western blotting for phosphotyrosine. Point mutation of Plakophilin at the site of phosphorylation would provide some insight into the possible function of this phosphorylation event, alongside C- and N2-Src expression to determine whether this effect is splice-specific.

4.3.7 Specific enrichment of the COPII coat in N2-Src overexpressing cells

COPII vesicles are transport vesicles that carry cargo from the ER to the Golgi apparatus. The COPII coat is made up of five proteins, the small GTPase Sar1, which initiates vesicle formation when activated by Sec12, and then recruits the COPII inner coat, composed of a Sec23/24 complex (Fig. 4-11B, (Gillon et al., 2012)). The Sec23/24 complex has a slightly concave structure and formation of the Sec23/24 causes the bending of the membrane. This vesicle is then further stabilised by an outer coat formed from a Sec13/31 complex (Fig. 4-11B). The internal Sec23/24 complex is also responsible for recruiting cargo into the forming vesicle (Gillon et al., 2012).

Unlike Sec23 and 24 isoforms, Sec16A doesn't form a part of the COPII coat, however is required for the trafficking of the COPII coat from the ER to the Golgi, by acting as a scaffold on the ER membrane that defines the ER exit site (Fig. 4-11B, based upon (Gillon et al., 2012)). Although there are many predicted Src phosphorylation sites and sites identified in the Phosphosite mass spectrometry database, there is no specific literature relating to Sec16A tyrosine phosphorylation relating to function (Fig. 4-11D).

Whilst none of the enriched COPII proteins above have any literature featuring the role of tyrosine phosphorylation in their regulation it is clear that one or more of these proteins are being specifically enriched by 4G10 IP in N2-Src expressing cells, resulting in the isolation of the whole complex. This enrichment, uniquely for this study, was confirmed by Western blotting of C- and N2-Src samples with and without doxycycline treatment which corroborated the relative protein abundance in the IP demonstrated by the comparative %emPAI values. Whilst it is impossible to identify which of these proteins is being specifically phosphorylated as a result of N2-Src overexpression using the data from this experiment, there are many tyrosine phosphorylation sites identified in the Phosphosite mass spectrometry database, several of which are identified by ScanSite or GPS to possess Src kinase domain substrate motifs. This strongly suggests that perhaps an as-yet uncharacterised Src phosphorylation event is occurring on one of these proteins. This up-regulation could affect Sec16 by regulating accumulation of COPII associated proteins in the ER, or by altering the affinity of Sec23/24 for specific COPII cargo.

4.3.8 Other notable proteins increased in abundance in N2-Src samples

Whilst the above proteins occur in large, well characterised functional clusters, suggesting that they may have been immunoprecipitated as a complex, there are other proteins that are significantly increased in abundance as a result of N2-Src expression which warrant further discussion (Table. 4-4).

Although many translation and splice-associated proteins were identified as being highly enriched in the N2-Src (and C-Src) samples, hnRNP H3 is particularly noteworthy as it is associated with inclusion of the N1-Src micro-exon in neuronal Cells (Chou et al., 1999, Caputi and Zahler, 2001). HNNRNP H3 has a N2-Src %emPAI score over two fold that of its C-Src score (0.38 & 0.15 respectively) suggesting that tyrosine phosphorylation of this protein or a protein that it associated is being up-regulated in N2-Src expressing cells (Table 4-4). This presents interesting possibilities for auto-regulation of N2-Src expression.

Protein	Interactions	Cellular localisation	C-Src %emPA	N2-Src %emPA	log(2) change in abundance	C-Src pY sites
CARM1	β catenin	Nucleus; Cytoplasm	0.05845	0.14825	1.343	Y172
CLASP2	CKAP5	Golgi apparatus; Microtubule; Cytoplasm; Plasma membrane;	0.01419	0.03222	1.183	Y300; Y617; Y917
CKAP5	CLASP2	Microtubule; Centrosome; Cytoplasm; g-tubulin complex	0.005	0.02196	2.134	
DDX5	HNRNPH3; SRP14	Nucleolus; Ribonucleoprotein complex; Nucleus	0	0.32944	n/a	Y514; Y535
HNRNPH3	DDX5,	Cytoplasm; Nucleus; Ribonucleoprotein complex	0.15323	0.38348	1.323	
NOTCH2		Golgi membrane; ER membrane; Plasma membrane; Nucleus	0.01866	0.04176	1.162	Y2470
SRP14	DDX5,	Cytoplasm; Signal recognition particle; ER targeting; Nucleus	0.14755	0.39425	1.418	Y27
TIA1		Cytoplasmic granule; Nucleus; Stress granule	0.12769	0.42553	1.737	Y149
TCP1	CKAP4	Golgi apparatus; chaperonin-containing T-complex; centrosome; microtubule	0.05391	0.13849	-1.361	
VPS29	VPS35; SEC22b; CLTC	Cytoplasm; Endosome	0.06494	0.30813	2.246	
VPS35	VPS29; HGS; CLTC	Lysosome; Retromer complex; Cytoplasm; Endosome	0.09235	0.19492	1.078	Y791

Table 4-4. Summary of other notable proteins enriched in N2-Src samples.

Samples listed above did not adequately functionally cluster with the proteins in the other groups, however their abundance, presence or cellular function was judged to warrant further investigation. The information summarised for each cell line is derived largely from Phosphosite.

Other proteins were also identified that are involved in vesicle formation and maintenance. Two components of the retromer complex, VPS29 and VPS35 were identified at 2.3 and 1 log(2) increased abundance in N2-Src cells compared to C-Src (Table 4-4). These proteins are key components of the retromer complex that retrieves lysosomal enzyme receptors from endosomes in the trans-Golgi network (Pfeffer, 2001). This localisation around the trans-Golgi network links in with previous data that shows an increased abundance of N2-Src around the TGN marker TGN46 (Fig. 4-2). Proteins of the retromer complex facilitate retrograde trafficking in order to recycle cargo proteins and trans-membrane receptors. As part of this role this complex associates with several other proteins identified in the phosphotyrosine pull-down including Clathrin, HRS and Sec24b (Pfeffer, 2001). Since no phosphotyrosine sites have been identified in the literature in the case of either protein it is possible they have been pulled down as the result of an interaction with another tyrosine phosphoprotein (Table 4-3).

Whilst the adherens proteins listed above commonly associate with β -catenin at the adherens junctions, CARM1 is known to interact with and positively modulate β -catenin in its role as a gene transcriptional regulator as part of the Wnt signalling pathway (Ou et al., 2011). CARM1 in N2-Src cells has almost three times the %emPAI score than in C-Src (0.15 and 0.06 respectively) and has a phosphorylation site (Y172) that is identified in the Phosphosite mass spectrometry database and also identified as a Src kinase domain motif by GPS (Table 4-4).

Cytoskeletal proteins CLASP2 and CKAP5 are interacting proteins that regulate the dynamics of microtubule dynamics. Both had relatively low %emPAI scores in N2-Src samples (CLASP 0.022 and CKAP2 0.322), however this is still a four and two fold increase in abundance when compared to C-Src samples (Table. 4-4). What is particularly noteworthy is that, besides TCP1, the only known or predicted interactions of these proteins are between each other. This interaction, as well as their abundance and the presence of predicted Src phosphorylation motifs that have been confirmed as phosphotyrosines in the Phosphosite MS database, suggests that one of these proteins is specifically phosphorylated as a result of N2-Src overexpression and that these proteins may have been pulled down together by the phosphotyrosine IP.

4.4 Concluding remarks

The data clearly indicate that, when overexpressed in HeLa cells, C- and N2-Src elicit significantly different effects upon the phosphotyrosine mediated regulation of the cells. Whilst the data demonstrates this difference in tyrosine phosphorylation, the specific substrates differentially phosphorylated by C- and N2-Src cannot be confirmed by this study. Only three phosphotyrosine peptides (Paxillin, BCAR1, Plakophilin-4) presented specific candidate tyrosine residues that could be followed up specifically in future studies.

What this study does provide is a map of which functional groups of proteins contain elements that are specifically phosphorylated, providing an insight into systems that are differentially modulated by C- and N2-Src. In addition, potential C- and N2-Src target residues on highly enriched proteins can be identified by use of the Phosphosite phosphoproteomics library, and Src kinase motif identification by GPS and ScanSite. Of particular interest in this study is the cluster of proteins consisting of members of the COPII coat. With no known C-Src associating protein and few notable interactions with other enriched proteins, it is tempting to suggest that one of these proteins is specifically tyrosine phosphorylated by N2-Src, or as a result of differential N2-Src signalling in the cell.

The role of Neuronal Src expression in the neuronal development of *Xenopus*

5.1 Introduction

Expression of the N1 isoform of Src has been identified in the EST libraries of both frog species *X.laevis* and *X.tropicalis* (Fig. 5-1A). *X.laevis* is allotetraploid and so possesses two pseudoalleles of the C-Src gene. These two genes have acquired polymorphisms over time, resulting in slightly different N1-Src micro-exons, both of which are 5 amino acids in length and share three common amino acids with mammalian N1-Src. *X.tropicalis* is, however, a diploid, possessing a single copy of the xN1-Src insert, which is identical to *X.laevis* variant b.

Xenopus species provide an excellent model for early neuronal development, undergoing signalling and patterning processes conserved in all vertebrates. In vertebrates, neuronal cells are derived from ectodermal tissues induced towards a neural fate by signalling from the underlying mesoderm in the late gastrula. In the absence of BMP signalling, the ectoderm of developing *Xenopus* embryos develops into neuronal tissues. BMP signalling is almost ubiquitous in the ectoderm, and is only inhibited by the expression of Chordin, Noggin and Follistatin from the dorsal lip of the blastopore. The presence of these neuralising factors, in addition to FGF signalling, inhibits BMP signalling, specifying the neural ectoderm towards a neuronal fate (Delaune et al., 2005).

In amphibians, a small portion of these progenitor cells differentiate into neurons during the course of neurulation in a process known as primary neurogenesis and can be identified by expression of neuron-specific class II β -tubulin (N-tubulin) (Hartenstein, 1989, Moody et al., 1996). The expression of N-tubulin and Sox3 appears to be mutually exclusive during neurulation, reflecting their separate roles in differentiating and proliferating neuronal progenitors respectively (Bourguignon et al., 1998). This primary neuronal differentiation is the result of complex signalling involving a variety of pathways; mis-regulation of Notch, Wnt, RA, and sonic hedgehog signalling pathways can all result in disruption of primary neurogenesis (Nieber et al., 2013, Heeg-Truesdell and LaBonne, 2006, Chitnis et al., 1995).

X.laevis N-Src (xN1-Src) expression can be detected by mid-neurula stages (stage 15 (all *Xenopus* developmental stages listed refer to Neuwkoop Faber (NF) stages)) and becomes spatially localised to the neural plate by late neurula (stage 16) (Collett and Steele, 1992). The temporal and spatial localisation of xN1-Src to the prospective nervous system suggests that inclusion of the xN1-Src micro exon is concurrent with neuronal specification of the cells of the dorsal ectoderm that become the neural plate. Studies using ectoderm explants have shown that xN1-Src expression is dependent upon the presence of the mesoderm underlying the neural ectoderm. In the absence of neural inductive signals from the mesoderm, xN1-Src isn't expressed and the cells do not express neuronal markers (Collett and Steele, 1993). Further to this, xN1-Src expression can be induced in a rapid, protein synthesis-independent manner by mimicking mesoderm induction signals using the PKC activator 12-O-tetradecanoylphorbol-13-O-acetate (TPA) (Collett and Steele, 1993).

In order to further elucidate the roles of neuronal Srcs during normal developmental processes, I have used both the tetraploid *Xenopus laevis* and diploid *Xenopus tropicalis* to analyse the endogenous roles of xN1-Src and the effects of mammalian N-Src overexpression.

5.2 Results

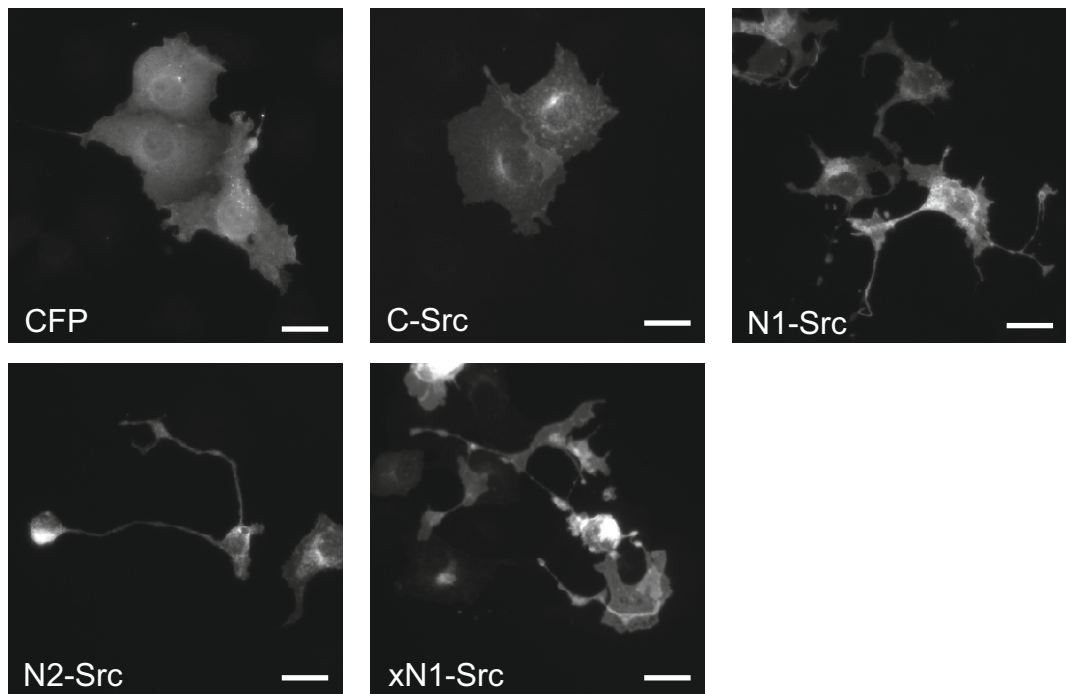
5.2.1 xN1-Src replicates the cytoskeletal rearrangement caused by N1-Src in fibroblasts

To confirm that xN1-Src has a similar biological activity to mammalian N1-Src, the neuritogenesis assay established in Chapter 3 was conducted in COS7 fibroblast cells. Cells were co-transfected with soluble CFP (to aid the visualisation of cell morphology) and a FLAG tagged Src construct or vector control. In addition to the previously described FLAG-tagged mammalian C-, N1-, and N2-Src constructs, *X.laevis* N1-Src variant b cDNA (Fig. 5-1A, IMAGE clone: 5572523 (Lennon et al., 1996)) was cloned into the same pFLAG plasmid and transfected alongside the mammalian variants. *X.laevis* xN1-Src variant b was used because it is identical to *X.tropicalis* xN1-Src. At least 30 fields of view were imaged at 40X (Fig. 5-1B) and analysed for each of three replicates and the cells were quantified by counting the

A

	Exon 3	N1 exon	Exon 4
N1-Src Human	V N N T GTC AAC AAC ACA	R K V D V R AGG AAG GTG GAT GTC AGG	E G D W GAG GGA GAC TGG
xN1-Src <i>laevis a</i>	V N N T GTC AAT AAC ACG	R - P D I R AGA - CCT GAC ATA AGG	E G D W GAA GGC GAC TGG
xN1-Src <i>laevis b</i>	V N N T GTC AAT AAC ACG	R - P D M R AGA - CCT GAC ATG AGG	E G D W GAA GGC GAC TGG
xN1-Src <i>tropicalis</i>	V N N T GTC AAT AAC ACG	R - P D M R AGA - CCT GAC ATG AGG	E G D W GAA GGC GAC TGG

B



C

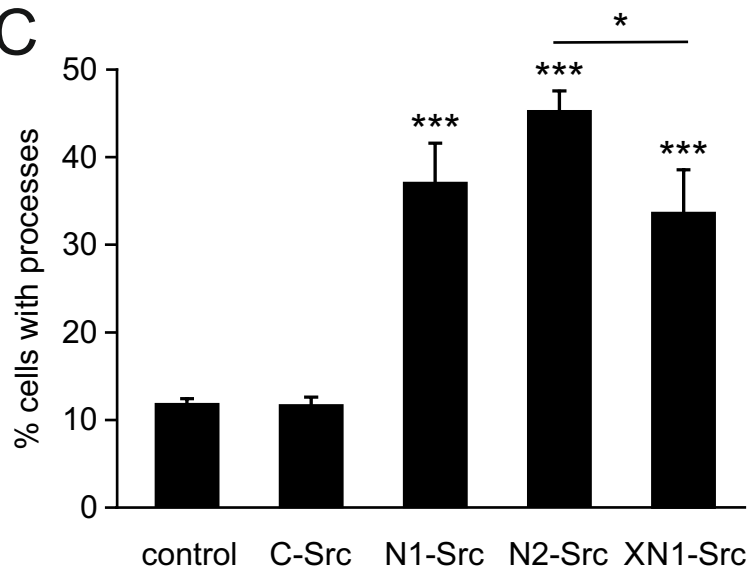


Figure. 5-1 (page 154). Effect of xN1-Src on COS7 cell morphology.

A) Nucleotide and amino acid alignment of the N1-exon in human and *Xenopus* species. B) Example cells from overexpressed of Src isoforms in the mammalian vector pFLAG in the monkey kidney fibroblast cell line COS7. 10 μm scale bar. Cells were co-transfected for four days with pFLAG Src constructs as well as pmCer - a CFP expression vector. Cells were then stained for the FLAG epitope as well as for CFP, using an anti-GFP antibody to increase the brightness of the CFP signal. The staining showed is for the FLAG epitope attached to the Src constructs with the exception of the CFP control in which CFP staining is showed. C) Quantification of process outgrowth in COS7 cells. n=3. Process outgrowth is defined by an extension longer than one diameter of the cell body less than 2 μm in diameter. Significance measured by Kruskal-Wallis two tailed analysis of variants. * =<0.05 ***=<0.001.

number of cells bearing one or more processes. Processes were defined as having a length exceeding one diameter of the cell body and a width of less than 2 μm . The number of process-producing cells was expressed as a proportion of the total cells.

In both control cells and those transfected with C-Src, the number of cells producing processes was $12 \pm 1\%$ (Fig 1C). By comparison, N1-Src showed $37 \pm 5\%$ process outgrowth and N2-Src induced outgrowth in $45 \pm 2\%$ of cells (Fig 1C). Transfection with xN1-Src had a comparable effect upon cells to mammalian N1-Src both in terms of process number ($34 \pm 5\%$) and in the overall morphological phenotypes exhibited by the cells (Fig 1B, C). This highly significant effect of xN1-Src on the morphology of a heterologous cell line, in line with that demonstrated by mammalian N1-Src, demonstrates a highly similar biological activity, confirming the *Xenopus* model as an appropriate model system with which to study the function of N1-Src in development.

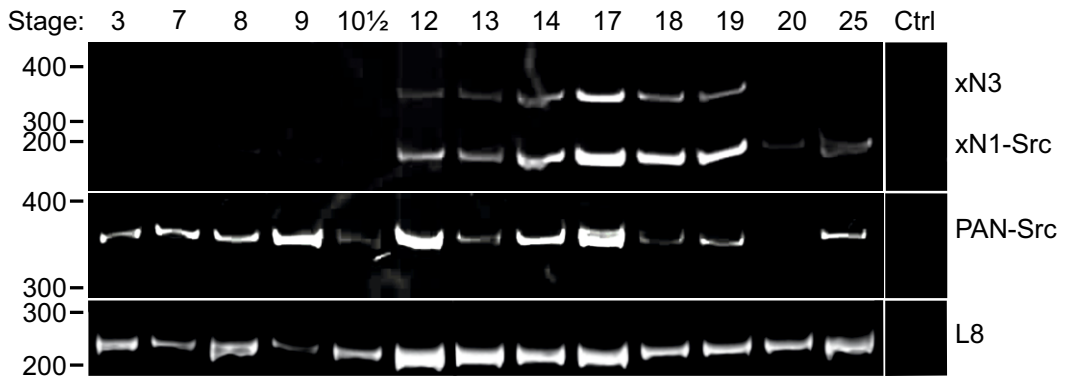
5.2.2 xN1-Src expression correlates with *Xenopus* primary neurogenesis

Previous data from stage 15 neural plate explants (mid-neurulation) showed that xN1-Src mRNA expression was restricted to the neural plate during primary neurogenesis (Collett and Steele, 1992). Based on this expression pattern, these researchers hypothesised that xN1-Src is likely to have a role in neurite outgrowth, however because the induction of neuronal marker expression begins between stages 10 and 12, they felt it unlikely that has a role in primary neurogenesis. In order to more accurately determine the initiation point of xN1-Src expression I performed a

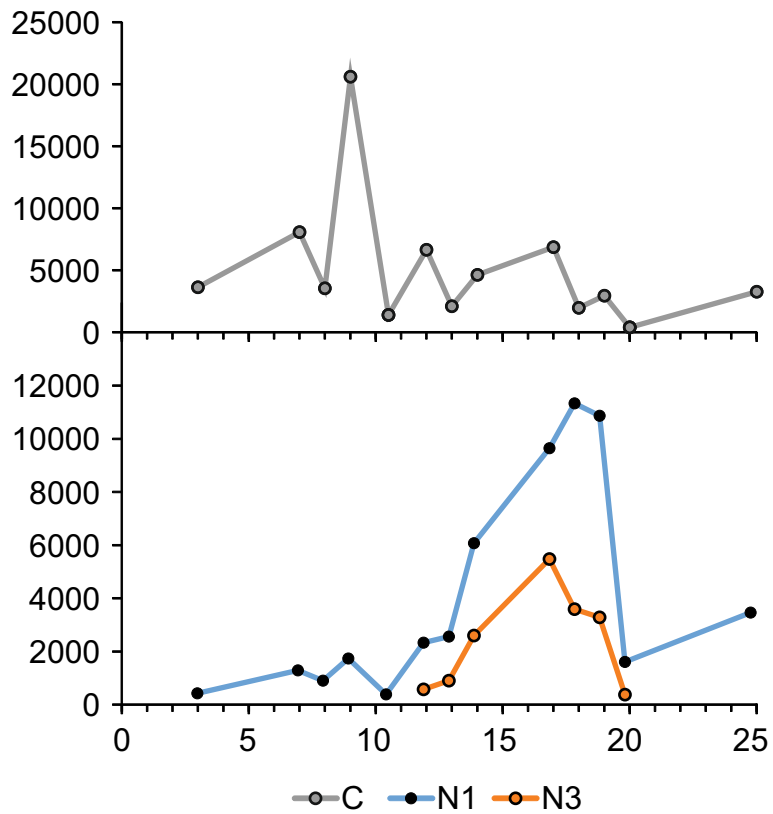
A



B



C



D

	Exon 3	xN1 exon	Exon 4 →
xN1-Src	V N N T GTC AAT AAC ACG	R P D M R AGA CCT GAC ATG AGG	E G D W GAA GGC GAC TGG
	Exon 3	xN3 exon	
xN3-Src	V N N T GTC AAT AAC ACT	F M L S V L R C G V T S H V L F P S H A V P STOP TTC ATG TTG TCT GTT TTG CGC TGT GGT GTG ACC TCT CAC GTT CTC TTT CCC TCA CAT GCT GTG CCA TAG	

Figure. 5-2 (page 156). Temporal expression of neuronal Src isoforms during *Xenopus* neurulation.

A) Design of the primers used for *Xenopus tropicalis* rtPCR. The forwards primer in red was used in both Pan-Src and xN1-Src specific PCR reactions. The xN1-Src specific primer in green overlapped the xN1-Src exon, excluding the possibility of C-Src amplification. The reverse Pan-Src in blue binds in exon 4 amplifying, in combination with the red forwards primer, C-Src sequence and any exons inserted between exons 3 and 4. B) rtPCR time-course of *X.tropicalis* Src expression. Xn3- and XN1-Src isoforms were identified by the xN1-Src specific reverse primer. PAN-Src signal used the Pan-Src reverse primers. L8 primers are used as a control. All primers, annealing temperatures and extension times are listed in materials and methods. The time-course was taken from untreated *X.laevis* embryos and the PCR products ran on a 15% TBE polyacrylamide gel. C) Quantification of (B). Band intensity was measured using ImageJ and normalised against L8 control in Microsoft Excel. Datapoints are plotted in arbitrary units on the y axis, and developmental stage on the x axis. D) Nucleotide and amino acid sequence of xN3-Src aligned to xN1-Src.

similar rtPCR time-course of xN1-Src expression during embryonic development. For this experiment I used the diploid frog species *Xenopus tropicalis* to avoid introducing the unnecessary complexity of tetraploid gene regulation in *X.laevis* (Fig 1A). *X.tropicalis* embryos were flash frozen at time-points from stage 3 during cleavage, through to stage 25 at the end of neurulation. RNA isolated from the embryos was then prepared for rtPCR and probed with three sets of primers.

Primers for the 60S ribosomal protein L8 were used as a loading control, as its expression level is known to be relatively consistent throughout early *Xenopus* development (Sindelka et al., 2006)(Fig. 5-2B, C). Pan-Src primers that amplify across the junction between exons 3 and 4, at which neuronal splicing occurs, were used to detect the expression levels of C- and xN1-Src simultaneously (Fig. 5-2A). These primers showed that Src mRNA is present in the maternal RNA pool and increases at stage 12, the onset of neurulation, stage 12 (Fig. 5-2C). The majority of the signal from the Pan-Src primers is that of C-Src, with only weak xN1- and xN3-Src signals visible. This is likely due to the restricted expression of neuronal isoforms, by comparison with the ubiquitous expression of C-Src in all cells during development. To identify neuronal splice variant levels over time without the large C-Src background, xN1-Src-specific primers were designed.

The reverse xN1-Src primer spans the xN1-Src micro-exon at its 3' end and the 5' end of exon 4 of C-Src, thus preventing amplification of C-Src isoforms (Fig. 5-2A). xN1-Src was barely detected in the maternal RNA (stage <7), but increased significantly during late gastrula and neurula stages (stages 12.5 – 20). xN1-Src expression begins increasing at stage 12, peaking at stage 17 and decreasing to lower expression levels post-neurulation (stage 25) (Fig. 5-2B, C).

Surprisingly, the xN1-Src-specific primers also amplified an additional product of approximately 340 base pairs, with expression levels concomitant with that of xN1-Src (Fig. 5-2B, C). Cloning and sequencing this additional band confirmed that it was an additional splice variant of Src, inserting 70 bases between exon 3 of C-Src and the xN1-Src micro-exon. This novel splice variant, which we termed xN3-Src, begins immediately 5' to the xN1-Src sequence, however inclusion of the xN3-Src exon introduces a stop codon, followed by a frame-shift immediately prior to the xN1-micro-exon (Fig. 5-2D). The stop codon occurs in the n-src loop of the SH3 domain, rendering the SH3 domain incomplete as critical residues for SH3 folding occur after this point. Therefore, xN3-Src splice variant does not encode a functional SH3 domain and would lack both SH2 and kinase domains (Fig. 5-2D).

5.2.3 Mammalian neuronal Src overexpression causes posteriorisation in *X.laevis*

Having confirmed that the expression of xN1-Src correlates with the timing of primary neurogenesis and neurulation, I sought to causally link these phenomena by perturbing N-Src expression levels in *Xenopus* species. First, mammalian FLAG-tagged Src constructs were overexpressed in *X.laevis*. Varying doses of the mRNA were injected dorsally at the 4 cell stage, targeting the cells that later form the neural tissues of the embryo. Embryos were then incubated until larval stage 42, allowing formation of major structures and body patterning and ensuring developmental defects are highly pronounced.

Whilst C-Src over-expression exhibited no significant effects upon the patterning of the embryo, even at the highest doses of 500 pg (n=19), both neuronal splice variants exhibited strong dose-dependent phenotypes (Fig. 5-3A). N1-Src

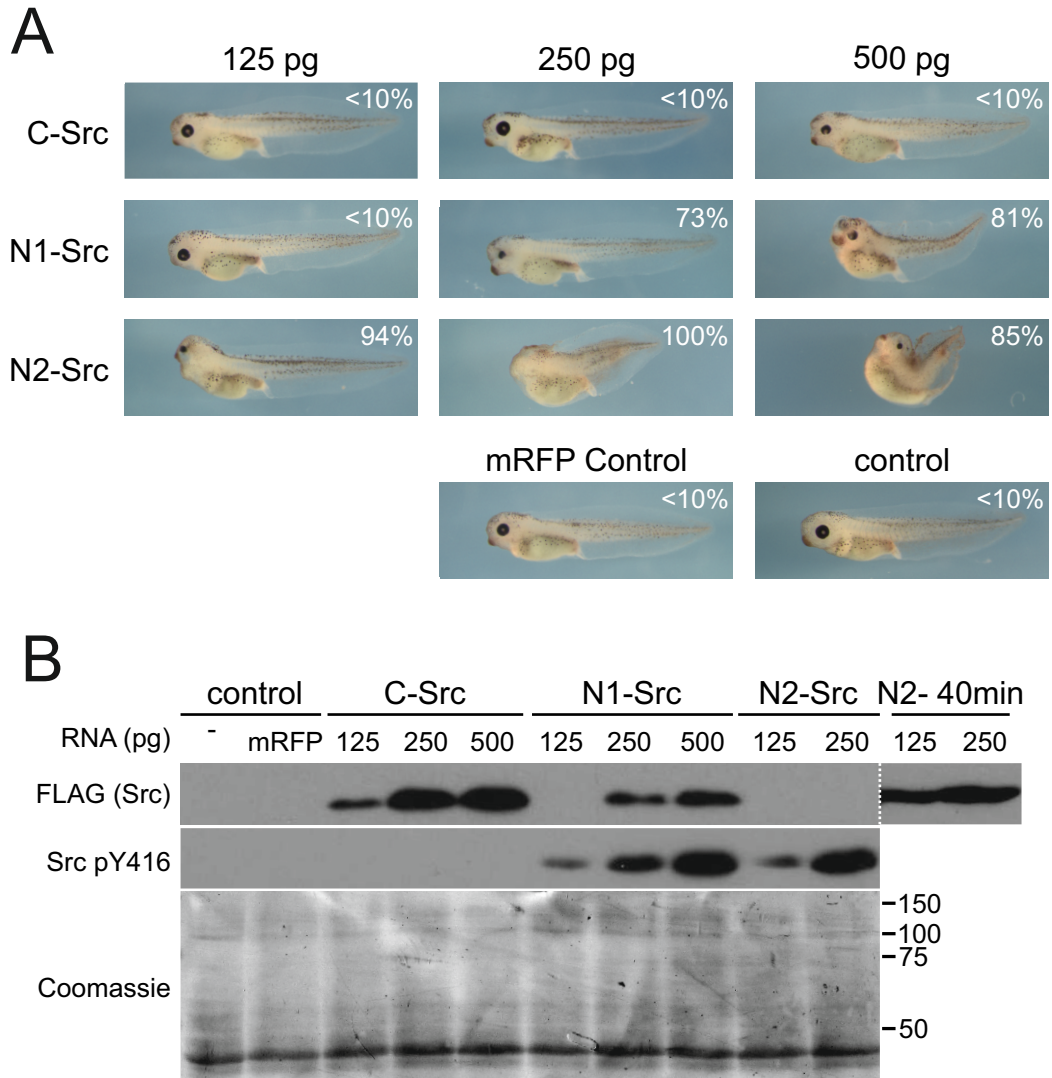


Fig. 5-3. Effect of mammalian N-Src expression on *Xenopus laevis* development.

A) Overexpression of mammalian Src variants in *Xenopus laevis*. Embryos were injected at 2 and 4 cell stage and allowed to develop to approximately stage 40. The percentages in white indicate the proportion of embryos showing anterior defects. C-Src: 125 pg n=12, 250 pg n=14, 500 pg n=19; N1-Src: 125 pg n=125, 250 pg n=19, 500 pg n=17; N2-Src: 125 pg n=17, 250 pg n=19, 500 pg n=22; mRFP control n=19; uninjected controls n=11. B) Western blot of the above phenotypes, samples flash frozen at stage 17. Membrane probed for detection of the FLAG epitope attached to Src splice variants and of Y416 phosphorylation. Coomassie staining is shown as a loading control. FLAG was blotted at an exposure of 1 minute is shown, in addition to an extended 40 minute exposure of the film to demonstrate the presence of N2-Src FLAG signal.

mRNA injection caused crano-facial defects in 75% of n=19 embryos injected with a 250 pg dosage. 500 pg of N1-Src mRNA increased the penetrance of this phenotype with 84% of n=17 embryos exhibiting crano-facial defects and often failing to form anterior structures (Fig. 5-3A). In N2-Src injected embryos, even at the lowest dosage of 125 pg, significant loss of anterior structures was observed in 94% of n=17 embryos (Fig. 5-3A). These embryos showed a significant reduction in anterior structure formation, with the majority of embryos developing only one central eye, and a misplaced or absent cement gland. The posteriorisation became even more pronounced in the 250 pg N2-Src injections with dramatic posteriorisation causing a failure to form any head structures (n=19, Fig. 5-3A). The aberrant signalling induced by 500 pg of N2-Src caused resulted in cells lacking dorsal structures, as the injected embryos failed to properly gastrulate. This phenotype was repeated in an independent experiment injecting the 125 pg dose (data not shown). The posteriorising effects of N-Srcs demonstrate a significant divergence in the intracellular functions of C- and N-Srcs, suggesting that N-Srcs act upon different developmental signalling processes compared to C-Src.

To confirm that the embryos injected with Src mRNA were expressing Src protein, 5 embryos from each condition were flash frozen in dry ice at stage 13. These embryos were then lysed in SDS sample buffer and the lysates probed by Western blotting. Increasing doses of mRNA correlated with increased FLAG immunoreactivity, however the detection of the N-Src FLAG signals was significantly lower than that of C-Src (Fig. 5-3B). N1-Src FLAG signals were lower than C-Src but readily observable, whereas detection of N2-Src FLAG immunoreactivity required much longer radiographic film exposure. In line with previous observations in mammalian cell lines, pY416 immunoreactivity was highest in N1- and N2-Src (Fig. 5-3B).

5.2.4 Injection of endogenous xN1-Src into *Xenopus* embryos

The effect of expressing xN1-Src mRNA was also assessed. The same xN1-Src-FLAG construct used in the aforementioned COS7 cell line was cloned into the pCS2+ plasmid, retaining the fused C-terminal FLAG tag, and mRNA was transcribed

in vitro. Injections of several different doses of xN1-Src mRNA did not yield a significant phenotype. Dorsal injections at the 4 cell stage of up to 500 pg were tolerated by the embryo, without the development of a perceivable phenotype (Fig. 5-4). This could be due to the ability of the embryo to better tolerate high levels of this endogenous isoform, particularly when localised to the neural plate.

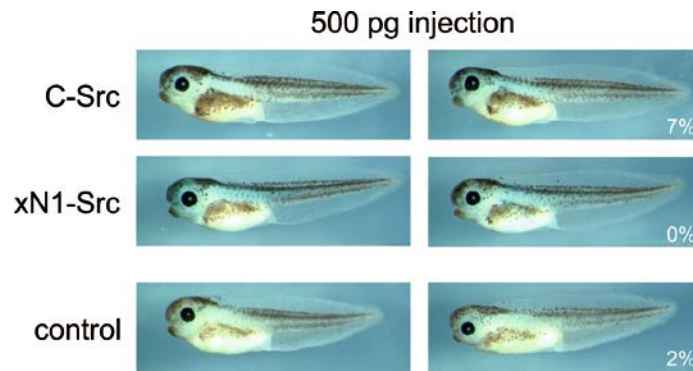


Figure. 5-4. Effect of xN1-Src on *Xenopus laevis* development.

Fixed stage 42 phenotypes of *X.laevis* embryos injected with *Xenopus laevis* N1-Src variant B, or C-Src at 2 and 4 cell stages. Two embryos shown per condition, the proportion of embryos showing malformation is indicated in white. This effect is seen in at least two other experiments under similar conditions.

5.2.5 Design of a morpholino to specifically skip xN1-Src micro-exon inclusion *in vivo*

In order to knock down expression of endogenous xN1-Src, morpholino technology was employed. C-Src is known to have wide-ranging roles within the cells, essential in many signal transduction cascades and developmental processes, as such any method to knock down xN1-Src has to avoid affecting C-Src expression.

Morpholinos bind RNA through complementary nucleic acid bases that are bound to morpholine rings instead of the deoxyribose/ribose ring of RNA. Each Morpholino subunit is also bound to the next by a phosphorodiamidate group rather than the phosphate groups of nucleic acids (Summerton and Weller, 1997). These changes result in a molecule which is much more stable, less charged and has a high binding affinity for RNA, allowing the use of short, highly specific sequences to target mRNA. A particular advantage of morpholino technology is its ability to bind pre-mRNA before the splicing machinery affects inclusion of the exons in the final transcript. By using two morpholinos targeted to the donor and acceptor splice sites of the xN1-Src micro-exon (Collett and Steele, 1992) it is possible to prevent the

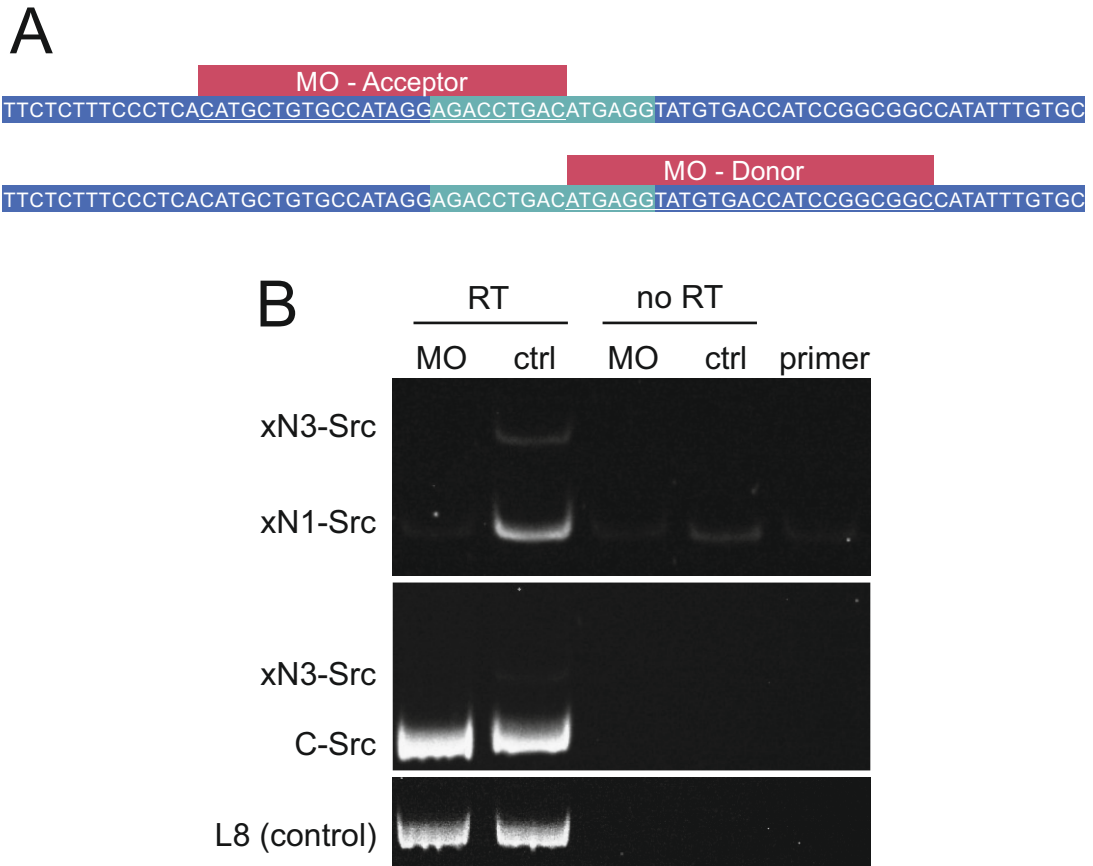


Fig. 5-5. Confirmation of xN1-Src Morpholino function.

A) Exon skipping xN1-Src Morpholino design. Donor and acceptor Morpholinos were designed with the assistance of staff at Gene Tools. The Morpholinos are designed to be used in combination to anneal to and inhibit the donor and acceptor splice sites. The Morpholino is indicated in red, exons 3 (left) and 4 (right) of Src in blue, and the xN1-Src exon in green. B) rtPCR testing the efficiency of Morpholino exon skipping by injection of 625 pM of each XN1-Src Morpholino. The embryos were injected bi-laterally at 2 and 4 cell and flash frozen at stage 15. xN1-Src abundance in cDNA and noRT control samples was identified by PCR using xN1-Src primers (which also identify xN3-Src), Pan-Src primers and L8 primers. Amplified DNA samples were run on 15% TBE polyacrylamide gels.

splicing machinery from including the xN1-Src micro-exon in the final transcript (Fig. 5-5A). For this series of experiments *Xenopus tropicalis* was used rather than *laevis* because the latter has two versions of xN1-Src exon in its tetraploid genome with differing nucleotide sequences (Collett and Steele, 1992) (Fig. 5-1A).

To confirm the effectiveness of the donor and acceptor xN1-Src morpholino combination, 10 ng of each morpholino was co-injected into *Xenopus tropicalis* embryos at the 2 cell stage (Fig. 5-5A). Total mRNA was extracted from these embryos at stage 17 and rtPCR was performed on the samples to confirm the knockdown of xN1-Src and the preservation of xC-Src expression. xN1-Src was knocked down almost entirely and the additional splice variant xN3-Src (expressed concomitantly with xN1-Src) was undetectable (Fig. 5B). The results also showed that xC-Src expression remains unaffected sequencing suggests that the mRNA sequence across the exon 3/exon 4 boundary of xC-Src is unchanged by altered splicing (data not shown).

5.2.6 xN1-Src knockdown causes aberrant tail formation and a severe locomotive phenotype

The combination of xN1-Src donor and acceptor targeted morpholinos (xN1-Src morpholinos) was injected bilaterally at the 2 cell stage at doses of 625 pmol and 1250 pmol (approximately 10 and 20 ng respectively) across the embryo. Whilst a 625 pmol dosage gave no significant phenotype in the embryo, doubling the dose resulted in a dramatic effect upon the tail development of the embryo, in addition to a locomotive defect (Fig. 5-6A, B). Embryos injected with an identical dosage of a standard control morpholino sequence did not develop any phenotype, allowing us to rule out morpholino toxicity as a cause of any phenotypes.

xN1-Src morpholino-induced malformation of the tail is a highly penetrant phenotype, occurring in 95% of n=40 embryos (Fig. 5-6A). In this condition the dorsal portion of the embryo was consistently shortened and the tail was usually angled downwards, as opposed to protruding straight out from the body, as is seen in uninjected and control morpholino conditions (Fig. 5-6A).

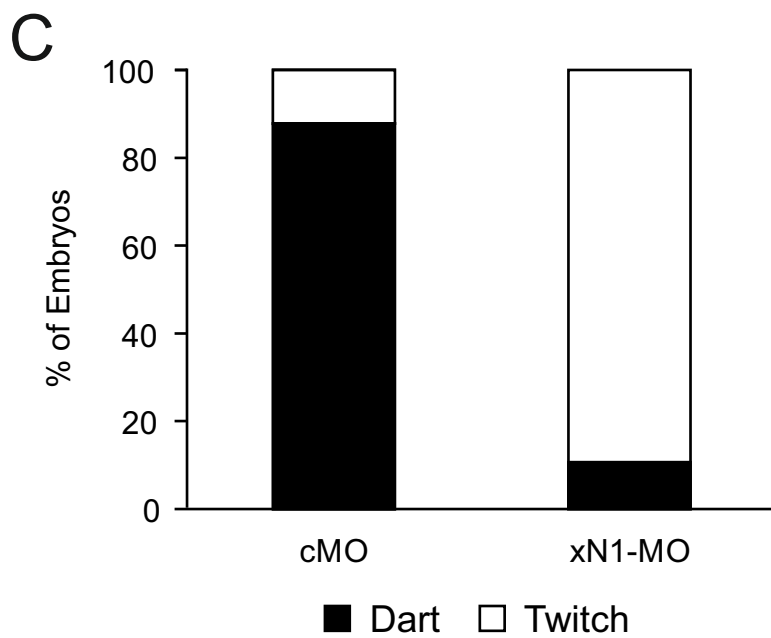
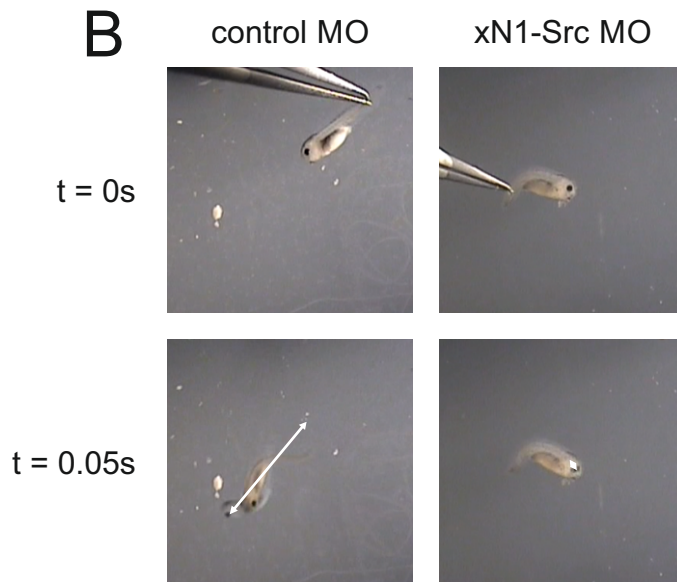
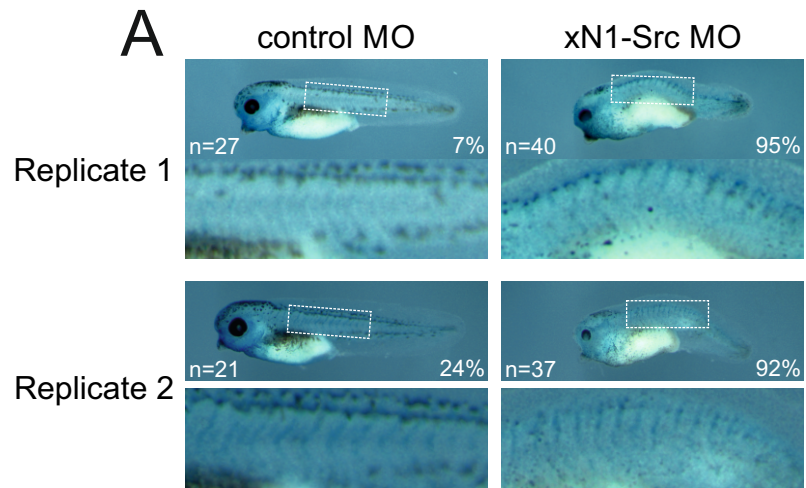


Figure. 5-6 (page 164). Effects of exon-skipping xN1-Src Morpholinos on *Xenopus tropicalis* development.

Embryos were injected with 1250 pmol total of xN1-Src or control Morpholino bilaterally at stages 2 and 4 and allowed to develop to approximately stage 42. A) Fixed phenotypes of xN1-Src Morpholino and control morpholino injections. Embryos are stained with lacz (blue). The experiment was performed twice. The proportion of embryos with significant abnormalities is indicated in white. Replicate 1; cMO n=27, xN1-MO n=40. N replicate 2; cMO n=21, xN1-MO n=37. 3x magnified images of somites are shown, taken from the regions shown by white boxes. B) Locomotive phenotype of control and xN1-Src morpholino injected embryos. This experiment was performed twice, however in the first instance the same phenotype was observed but not recorded. Video of this phenotype is available on an attached CD as Fig. 5-6D. Embryos were filmed at room temperature in 1% agarose coated dishes and filmed at rest then moving in response to physical stimulation. The image shows the movement of the embryos from the point of contact to the next frame of the video. C) Quantification of the movement phenotype observed in (B). Embryos response to physical stimulation was classified as either a 'dart' or a 'twitch'. 'Dart' phenotypes righted themselves and swiftly swam a short distance from the point of contact, 'Twitch' phenotypes remained horizontal and moved slowly from the point of contact by an uncoordinated twitching movement. D) Attached video file of the phenotype shown in (B).

Healthy stage 40 embryos are capable of sensing touch and respond with a fast, co-ordinated movement; first righting themselves from a resting position on their sides, then immediately swimming away from the stimulus, as is seen in embryos injected with control morpholino (Fig. 5-6B). Whilst the ability for xN1-Src knockdown embryos to sense the touch stimulus was not impeded by xN1-Src knockdown, the ability for co-ordinated movement in response to the stimulus was absent in 88% of embryos (Fig. 5-6C). xN1-Src knockdown embryos responded to the stimulus with a characteristic twitching phenotype, which propelled the embryo slowly forwards, maintaining flank downwards position, rather than righting themselves to a normal dorsal-up orientation (Fig, 5-6B; Fig. 5-6, video attached to thesis). This does not appear to be as a result of aberrant somite formation, as somites appear to form in their typical 'chevron' pattern with and without xN1-Src knockdown, as indicated by lacz accumulation shown in figure 5-6A.

5.2.7 xN1-Src knockdown inhibits n-tubulin expression at primary neuritogenesis

In order to confirm whether the cause of the morpholino-induced locomotive defect is derived from altered body patterning, or aberrant neuronal development it

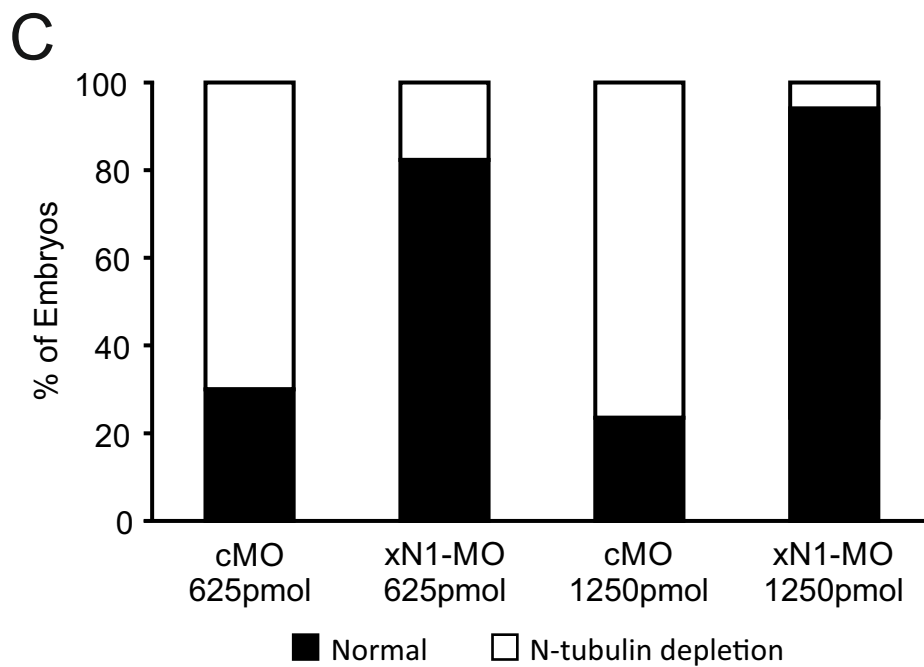
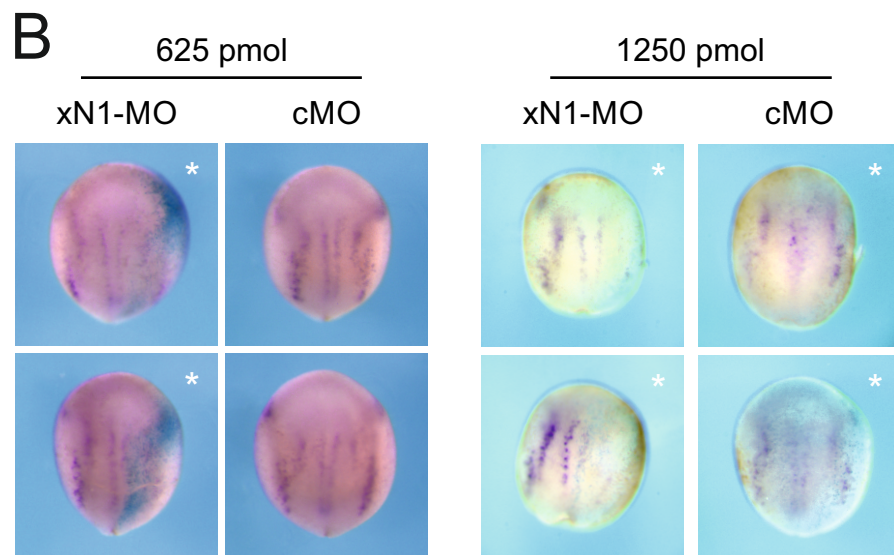
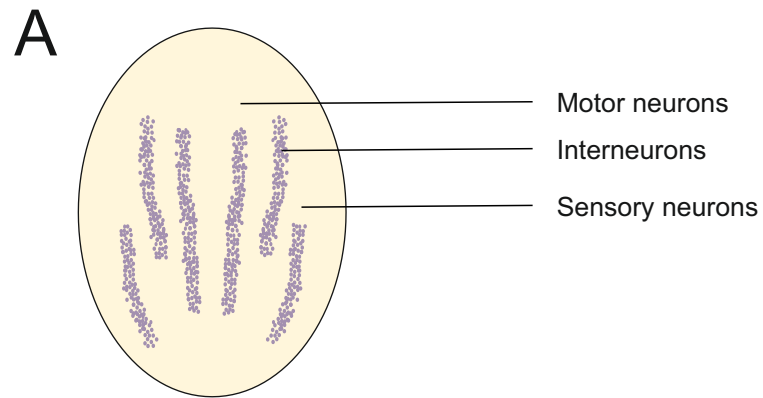


Figure. 5-7 (page 166). Effects of exon-skipping xN1-Src Morpholinos on n-tubulin expression during primary neurogenesis.

A) Diagram depicting stereotypical N-tubulin staining at stage 14 of *Xenopus* development. B) Control and xN1-Src Morpholino injection (625 and 1250 pmol total) effects on N-tubulin expression detected by *in situ* hybridisation. Embryos were injected unilaterally at 2 and 4 cell stage with 625 or 1250 pmol of total Morpholino, in addition to between 50-100pg of lacz mRNA. Embryos are oriented anterior upwards and the hemisphere of injection is indicated by an asterisk. N-tubulin *in situ* staining is in purple and lacz staining is in blue. 625 pmol; xN1-MO n=24, cMO n=22. 1250 pmol; xN1-MO n=20, cMO n=23. C) Quantification of (B) the proportion of embryos showing decreased N-tubulin expression on the side of injection is expressed as a percentage of total embryos. For the control Morpholino samples of the 625 pmol injection the lacz stain failed, so embryos were counted where significant asymmetry of N-tubulin signal between hemispheres of the embryo were counted as N-tubulin depleted.

was necessary to study the differentiation of neurons during neurogenesis. One of the key advantages of gene expression in *Xenopus* species is the ability to target one half of the embryo by injecting material unilaterally at the two cell stage. Unilateral injections are particularly useful for *in situ* hybridisation analysis of mRNA expression, as direct comparison of expression levels and localisation can be made between the experimental and contralateral sides of the embryo.

In separate experiments, 625 pmol and 313 pmol of the xN1-Src morpholinos were unilaterally co-injected with lac-z tracer mRNA, in order to later identify the experimental hemisphere. The embryos were then fixed for *in situ* hybridisation at stage 14. Corresponding bilateral injections of the same dosage were performed alongside unilateral injections, and the embryos incubated to stage 40-42 to identify overall patterning or locomotive phenotypes.

At *Xenopus* stage 14, the neural plate is a flat portion of the dorsal ectoderm, undergoing neural specification as a result of signalling from the underlying mesoderm. Progenitor neurons are beginning to differentiate in the neural plate, and can be identified by *in situ* hybridisation for N-tubulin staining, a well-studied marker of *Xenopus* primary neurogenesis (Min et al., 2011, Blumberg, 1997). N-tubulin staining labels three stereotypic domains of N-tubulin expression, which (from outside to in) label the sensory, inter and motor neurons (Fig. 5-7A).

N-tubulin bands are observed in embryos injected with 313 pmol and 625 pmol of control morpholino, however in 30% and 24% of the respective embryos, the injected hemisphere appears to have decreased n-tubulin expression (Fig. 5-7B, C).

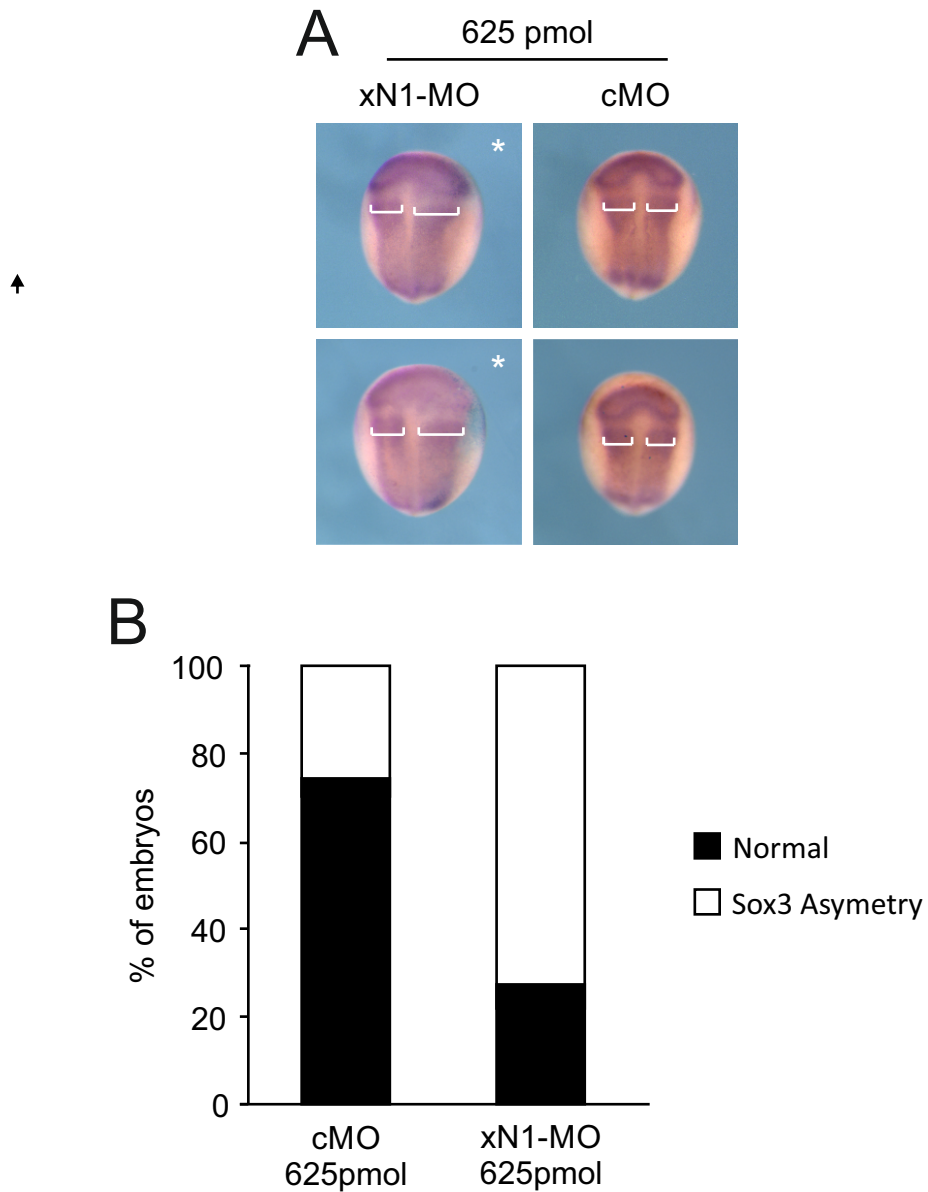


Fig. 5-8. Effects of exon-skipping xN1-Src Morpholinos on Sox3 expression during primary neurogenesis.

A) *In situ* hybridisation staining for Sox3 mRNA expression. Embryos were injected unilaterally at 2 and 4 cell stages with 625 pmol of either control or combined xN1-Src Morpholinos in addition to 50-100 pg of lacz mRNA. Sox3 staining is shown in purple, lacz staining shown in blue. The hemisphere of injection is indicated by astrices, however control Morpholino embryos failed to stain for lacz. B) Quantification of (A). Embryos showing asymmetrical Sox3 expression were expressed as a percentage of total embryos. The widths of the Sox3 bands were measured where indicated in white (A). xN1-MO n=21, cMO n=23.

In both 313 pmol and 625 pmol xN1-Src morpholino injections, a significant decrease was observed in the amount of n-tubulin expressed on the side of injection. With the lower dose this decrease in expression occurs in 80% of the embryos and was limited to the sensory neurons and often the inter-neuron stripe appeared shorter or weaker (Fig. 5-7B). When the larger 625 pmol dose of xN1-Src morpholino was injected, there was an almost complete ablation of n-tubulin expression on the side of injection in approximately 90% of the embryos (Fig. 5-7C). This indicates that xN1-Src is necessary for the normal expression of at least a subset of neuronal marker genes at the start of neuronal differentiation.

5.2.8 xN1-Src knockdown does not decrease Sox3 expression during neurulation

To identify whether xN1-Src has an effect on neuronal, the expression of Sox3 was analysed by *in situ* hybridisation. Sox3 is expressed throughout the entire neural ectoderm starting at late gastrulation stages. During neurulation Sox3 is highly expressed in the neural plate in the undifferentiated neuroectoderm cells covering the area between the motor neuron and inter neuron stripes of N-tubulin expression (Bellefroid et al., 1998, Moody and Je, 2002). *X.tropicalis* embryos were injected unilaterally at two and four cell with a total of 625 pmol of xN1-Src morpholino and incubated to stage 14 when they were fixed and probed by *in situ* hybridisation. Whilst xN1-Src knockdown decreases N-tubulin expression, indicative of an inhibition of primary neurogenesis, Sox3 expression does not appear to be affected in the same way (Fig. 5-8A). No significant change in the amount of Sox3 expression was observed between control and xN1-Src morpholino. That said, 75% of n=21 xN1-Src morpholino injected embryos had asymmetrical expression of Sox3 (Fig. 5-8B). This asymmetry manifested as either a widening of the Sox3 band on the side of injection and/or a blurring of the boundary between cranial and spinal Sox3 expression regions. This contrasts sharply with only 25% asymmetry observed in n=24 controls. This result suggests that, whilst xN1-Src knockdown decreases the primary neurogenesis, as indicated by reduced N-tubulin expression, xN1-Src knockdown does not negatively affect neuronal specification. On the contrary, decreased xN1-Src

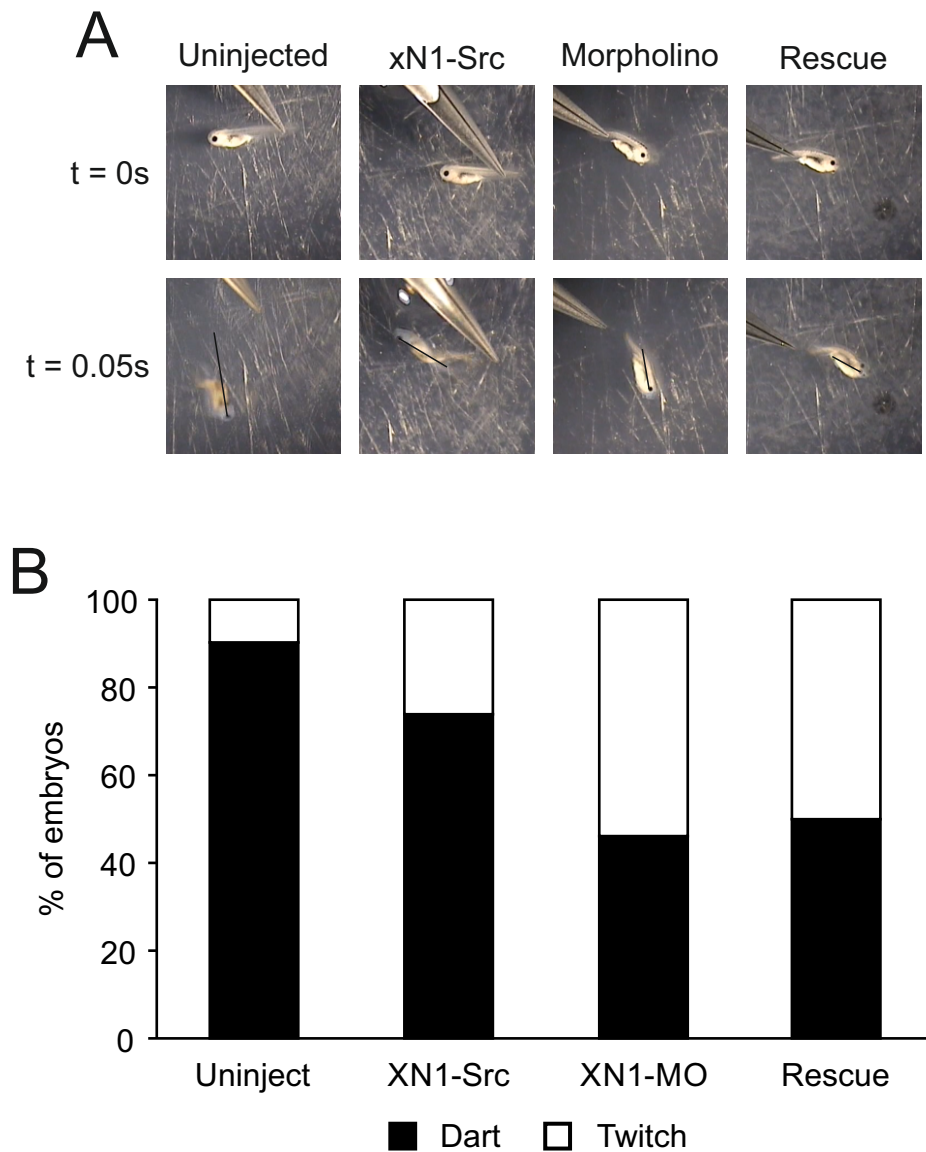


Fig. 5-9. xN1-Src Morpholino rescue.

A) xN1-Src Morpholino rescue experiment. Locomotive phenotype of control and xN1-Src Morpholino injected embryos in addition to a rescue condition where 500 pg of xN1-Src RNA was added to the xN1-Src Morpholino condition. Embryos were filmed at room temperature in 1% agarose coated dishes and filmed at rest then moving in response to physical stimulation. The image shows the movement of the embryos from the point of contact to the next frame of the video. B) Quantification of (A) the response of the embryos to physical stimulation was classified as either a ‘Dart’ or a ‘Twitch’ response. These responses were counted for each condition and expressed as a percentage. Uninjected controls n=31, xN1-Src overexpression n=23, xN1-MO n=26, rescue n=24.

expression may maintain more neuro ectoderm cells in an undifferentiated, proliferative phenotype demonstrated by broader Sox3 expression.

5.2.9 Attempting to rescue xN1-Src knockdown with xN1-Src mRNA expression

In an attempt to discover whether any off-target effects of the xN1-Src morpholinos are responsible for the xN1-Src morpholino phenotypes, a rescue experiment was conducted using the xN1-Src morpholinos co-injected with xN1-Src mRNA. This experiment was possible because xN1-Src morpholinos only target pre-mRNA, before splicing has occurred, so should not bind to mature xN1-Src mRNA. In the rescue condition, 1250 pg of combined xN1-Src morpholino was co-injected with 500 pg of mRNA bilaterally into embryos at 2 cell and 4 cell stages. Controls were also injected for mRNA and morpholino only, and healthy embryos were also selected as uninjected controls. These embryos were allowed to develop to stage 42, at which point the locomotive phenotype was assayed and recorded.

Under these conditions xN1-Src mRNA did not significantly rescue the morpholino induced phenotype, which in this experiment was far less penetrant than has previously been observed (Fig. 5-9A, B). Only 55% of embryos expressed the twitching phenotype, down from 90% in previous experiments. The number of embryos exhibiting this phenotype was not decreased with the addition of xN1-Src mRNA, with only 5% fewer embryos showing a locomotive phenotype (Fig. 5-9B).

5.3 Discussion

In this chapter, the data have revealed a significant up-regulation of endogenous *Xenopus* N1-Src during neurulation and primary neurogenesis. When inclusion of the xN1-Src micro-exon is prevented, there is a significant decrease in locomotion of the embryos in response to touch stimulus, coupled with a decrease in the expression of neuronal markers at primary neurogenesis. Taken together, these data suggest an essential role for N-Src expression for effective neurogenesis during early development.

5.3.1 xN1-Src as a model for N1-Src in development

The endogenous *Xenopus* N1-Src provides an excellent model for the roles of mammalian N1-Src during development. Previous studies have shown that mammalian and *Xenopus* N1-Src share significant sequence homology and are both exclusively expressed in tissues of the neural plate which gives rise to neurons during primary neurogenesis (Martinez et al., 1987, Levy et al., 1987, Raulf et al., 1989). Transient transfection of the fibroblast cell line COS7 with mammalian N-Src constructs has previously been shown to have a profound effect upon cellular morphology (Keenan et al, unpublished). Whilst C-Src overexpression increases cell body area, N1 and N2-Src overexpression induce decreased cell body size and a significant amount of outgrowth of neurite-like processes, as is seen in neuroblastoma cells in Chapter 5. Although N1-Src is highly conserved through evolution, there are differences between the xN1-Src and N1-Src amino acid sequences that might cause these splice variants to have different cellular functions. Since C- and N-Srcs elicit such quantifiably distinct phenotypes upon fibroblast cells, the COS7 experimental system was useful for revealing any differential cellular effects of xN1- and N1-Src. My data show that both mammalian and *Xenopus* derived N1-Src induce significant cytoskeletal rearrangement, encouraging outgrowth of neurite-like processes in a fashion similar both in their morphology and their rate of occurrence (Fig 1B, 1C). The largely comparable phenotypes of N1-Src and xN1-Src splice variants within the cells suggests that the function, and substrates, of these genes have been conserved throughout evolution. This also adds weight to the idea that the functions of xN1-Src during amphibian neuronal development will be conserved in mammals and therefore that *Xenopus* species will make an excellent model to study the roles of neuronal Srcs during development.

These data support published data in several systems, both *in vitro* and *in vivo*, which have shown that N1-Src expression is closely linked to the times of neuronal differentiation or specification (Cartwright et al., 1987). Induction of neuronal differentiation by serum starvation in rat striatum (Cartwright et al., 1987), neural induction in ectoderm by mesoderm derived signals (Collett and Steele, 1993) and retinoic acid in embryonal carcinoma cells (Lynch et al., 1986) all result in greater

than seven-fold increases in N1-Src expression and activity above that of C-Src. In the developing mouse brain N1-Src activity and expression peaks when the number of differentiating neuroblasts is at its highest level (Wiestler and Walter, 1988). The significant effect of neuronal Srcs on the morphology of a heterologous cell line also demonstrates a profound effect upon signalling pathways controlling cytoskeletal rearrangement by all neuronal variants. Taken together, these data demonstrate that N1-Src expression is consistently expressed concurrent with neuronal differentiation, though the specific role played by N1-Src in the organisation of neurite outgrowth and associated differentiation processes or in the specification of neuronal progenitors for differentiation has yet to be elucidated.

5.3.2 Increased xN1-Src expression begins at the very beginning of neurulation

By clarifying the time-course of expression of xN1-Src mRNA in early *Xenopus* development, I have shown that although xN1-Src is not detected in the maternal mRNA pool, xN1-Src is expressed at detectible levels when zygotic transcription begins at the mid-blastula transition (MBT); stage 8. xN1-Src expression increases dramatically immediately prior to the beginning of neurulation, peaking at stage 18, late neurula, and remaining high throughout neurulation before dropping to lower levels at stage 20 once neurulation is complete (Fig. 5-2B, C).

The peak in xN1-Src expression correlates strongly with the decreased mitotic activity and increased differentiation in the neural plate identified at stages 17 and 18 (Hartenstein, 1989). This correlation between increased neuronal differentiation and increased expression of xN1-Src supports a hypothesis that N1-Src is a key regulator of neuronal expression during development. Collett and Steele (1992) proposed that the expression pattern of xN1-Src, as well as previous literature on its intracellular localisation in dendritic processes and axons suggests N-Src regulates growth cone morphology. The specific focus on growth cone formation rather than other cellular events associated with differentiation was due to the authors detecting xN1-Src mRNA expression at stage 15, but not at stage 11. Their suggestion is that early markers of neuronal specification such as N-CAM expression begin between stages 10 and 12 and xN1-Src expression is later than this, so unlikely to take part in early neuronal

differentiation. My data show xN1-Src expression is detectable at stage 8, and expression begins increasing between stages 10½ and 12 (Fig. 5-2C), suggesting that N1-Src is expressed in direct response to the same early differentiation cues as the very earliest markers of neuronal specification. Collett and Steele (1993) themselves later demonstrated that xN1-Src mRNA is expressed in TPA treated ectoderm in a protein synthesis independent fashion by blocking protein synthesis with cyclohexamide. TPA has previously been shown to induce neural differentiation in competent ectoderm via PKC, which suggests that xN1-Src expression is occurring rapidly in response to early signal transduction events that are regulating splice regulators by post-translational modification (Otte et al., 1988). The expression occurs 30-60 minutes after TPA treatment, causing Collett and Steele to suggest that xN1-Src would be well suited as a marker for neural induction. This rapid xN1-Src expression in response to neural induction places its expression at the very earliest point in neuronal differentiation which lends weight to the hypothesis that it is involved in much earlier neural differentiation processes than neurite outgrowth, which begins at stage 20 (Kullberg et al., 1977). Although no work has yet identified the expression levels of N1-Src during neurulation in mice, data from Wiestler and Walter (1988) shows that N1-Src activity later in mouse brain development peaks during the highest period of neuronal precursor differentiation of the brain.

It is noteworthy that xN1-Src expression decreases around stages 20-25, after neurulation is complete and other body patterning is occurring (Fig. 5-2C). This decrease in xN1-Src expression seems to contradict a hypothesis that xN1-Src is associated with growth cone formation and neuronal differentiation. Interestingly, this decrease was also present at stage 26 in the time-course published by Collett and Steele (1992). This sudden decrease in xN1-Src expression levels occurs during a period of increased mitotic activity in the neural plate (Hartenstein, 1989). Whilst almost no divisions are occurring in neural tissues at stages 17 and 18, following stage 20 mitotic activity is resumed (Hartenstein, 1989). Collett and Steele showed that by stage 30, the expression level of xN1-Src had increased once more, suggesting that xN1-Src expression is only transiently suppressed during the period of increased mitotic activity in neural progenitors immediately following neurulation, and expression increases once more during later phases of neurogenesis. This further correlates with a role for xN1-Src in the differentiation of neuronal progenitors.

5.3.3 Expression of the novel Src splice variant xN3

Utilising primers that overlapped the xN1-Src/exon 4 boundary I have also identified a novel splice variant of Src that we termed xN3-Src (Fig. 5-2D). xN3-Src is consistently less abundant than xN1-Src in the cDNA, however changes in mRNA abundance during neurulation are remarkably well conserved between xN1- and xN3-Src (Fig. 5-2C). Introduction of the 70 base pair xN3-Src exon immediately prior to the xN1-Src micro-exon also causes a frame-shift and introduces a stop codon prior to the xN1-Src exon (Fig. 5-2D). Translation of xN3-Src would be terminated before the SH2 and kinase domain, as well as before residues essential for SH3 stability and subsequently the xN3-Src variant would not encode a functioning tyrosine kinase. Whilst the resulting protein would be non-functional as a kinase, the presence of the sequence in the cDNA implies a functional mRNA of the splice variant is being actively expressed, and potentially translated. The xN3-Src cDNA does code for a complete N-terminal unique domain, which is proposed to have roles in regulating the intracellular localisation and activity of C-Src, in response to phosphorylation events (Amata et al., 2014). It is, therefore, not unreasonable to hypothesise that xN3-Src may have roles as a scaffold protein, or a competitive inhibitor of phosphorylation by C-Src or xN1-Src, mediated by the N-terminal unique domain, myristoylation site and incomplete SH3 domain. Discovering whether xN3-Src performs these roles would be interesting, however, the fact that no similar variants have been identified in mammalian development (a BLAST search for highly similar sequences returns only Collett and Steele's (1992) genomic sequence of the xC-Src intron 3), it did not warrant further investigation.

5.3.4 Isoform-specific effects of Src overexpression in *X.laevis*

Overexpression of the mammalian neuronal Src constructs in *Xenopus laevis* provides strong evidence of isoform specific actions of the three Src variants during the developmental process. Interestingly, as previously identified in B104 cells (Fig. 3-1A), the detection of N1- and particularly N2-Src by blotting was significantly lower than that of C-Src. This decreased detection could be due to either decreased

translation of N1- and N2-Src splice variants, increased degradation of the mature protein, or possibly decreased proliferation of cells injected with N2-Src. It seems unlikely that differential translation of these splice variants would occur, as Black and colleagues showed that the N1-Src RNA regulatory sequences occur in genomic DNA immediately up- and down-stream of the exon (Black, 2003). Activated Src is known to be serine phosphorylated in the unique domain by CDK5, resulting in cullin-5-dependent degradation (Pan et al., 2011), since N1- and N2-Src have much higher basal pY416 phosphorylation in *Xenopus* cells than C-Src, it could be that this mechanism is resulting in increased degradation of neuronal splice variants. N1- and N2-Src have been shown to be both associated with times of endogenous neuronal differentiation (Fig. 5-2A) as well as inducing neuronal differentiation when overexpressed (Fig. 5-1 A). As such it would be tempting to suggest that the decreased signal detection of N1- and N2-Src is due to increased neuronal differentiation of the cells in which these splice variants are expressed, resulting in decreased proliferation of these cells.

C-Src is ubiquitously expressed through development, and when overexpressed in dorsal tissues it appears to be highly regulated and inactive, with no detectable phosphorylation of Y416 (Fig. 5-3B). Consequently mammalian C-Src overexpression in *X.laevis* does not induce a change in the phenotype of the embryos at stage 40 (Fig. 5-3A). By contrast N1-Src and, to an even greater extent, N2-Src were shown to be highly active by pY416 immunoblotting (Fig. 5-3B). This differential activity was reflected in the resulting embryo phenotypes, with N1- and N2-Src overexpression showing strikingly different effects (Fig. 5-3A).

The different basal levels of kinase activity of C-, N1- and N2-Src could be hypothesised to be the cause of the differential phenotypes, however, nowhere in the literature has constitutively active (CA) C-Src, or the oncogenic V-Src been associated with similar anterior defects in *Xenopus*. Additionally, studies in *Xenopus* embryonic fibroblasts have shown that overexpression of CA-C-Src and xN1-Src have profoundly different effects on cellular morphology, CA-C-Src causes rounding of the cell, whereas both CA-xN1-Src and xN1-Src expression cause cell elongation and process outgrowth similar to that observed in COS7 cells (Collett and Steele, 1993). The only comparable phenotype caused by overexpression of a Src family kinase is

that of Laloo, which causes a similar failure to develop anterior structures in *Xenopus* due to its role in FGF mediated mesoderm induction (Weinstein et al., 1998).

The distinct phenotypes resulting from N1- and N2-Src expression also oppose the hypothesis that kinase activity alone is causing progressive increases in anterior defects. The lowest N2-Src dose causes significant loss of anterior structures, whereas a four-fold higher expression of N1-Src causes a less severe crano-facial phenotype. This suggests that there is significantly different specificity of N1- and N2-Src SH3 domains for developmental substrates, as these isoforms exhibit similar but divergent embryo phenotypes. Because *Xenopus* species lack endogenous N2-Src it could be postulated that the targets of N2-Src in higher vertebrates simply aren't modified in the same way during *Xenopus* development, which is causing the more potent defects seen with N2-Src overexpression.

Interestingly a similar dose-dependent phenotype is seen in retinoic acid (RA) treatment of *Xenopus* embryos (Sive et al., 1990) and RA is a key driver of neuronal differentiation and neurogenesis, both during neurulation and in adult neurogenesis (Blumberg, 1997, Jacobs et al., 2006). Similarly, activation of the FGF receptor pathway by eFGF, as well as manipulation of Wnt activity have been shown to suppress formation of anterior structures in *Xenopus* (Kuhl, 2003, Isaacs et al., 1994). These signalling pathways have diverse effects on the embryos and regulation of their expression is crucial to healthy neuronal development, with aberrant signalling resulting in significant changes to body patterning, including posteriorisation similar to that seen with N2-Src overexpression (Min et al., 2011, Jacobs et al., 2006). This suggests that N-Srcs might act upon downstream effectors of these key developmental receptors, and could be tested by rescue experiments, co-expressing dominant negative forms of the receptors in these signalling pathways, alongside N1- and N2-Src.

5.3.5 Blocking neuronal splicing of C-Src causes defects in *Xenopus* locomotion

I have demonstrated that simultaneously injecting two morpholinos that target the donor and acceptor sites of the xN1-Src mini-exon results in a significant knockdown of xN1-Src expression at stage 14 of neurulation (Fig. 5-5A, B). Exon skipping xN1-Src morpholinos allowed me to specifically exclude xN1-Src exon

inclusion into Src mRNA without affecting C-Src expression, which is ubiquitously expressed and an essential gene throughout development. xN1-Src exon skipping in *X.tropicalis* causes a significant locomotive phenotype whereby the embryo is less capable of responding to touch stimulus with co-ordinated movement (Fig. 5-6B). This phenotype does not seem to stem from a failure in somitogenesis, as the characteristic formation of somite 'chevrons' at this stage appears unaffected (Fig. 5-6A). It could be suggested that a failure of primary neuritogenesis (Fig. 5-7) could be leading to a decrease in the number of neurons available to elaborate the early nervous system of these embryos, leading to an inability to co-ordinate behaviour (Fig. 5-6).

This locomotive phenotype was accompanied by a morphological phenotype whereby the tail of the embryo was malformed, being slightly shorter than in control conditions, and noticeably slanted either downwards or upwards from the body, as opposed to straight outwards (Fig. 6B). The effect of xN1-Src knockdown on tail formation could be due to the signalling role of the neural tube in tail bud development (Beck and Slack, 1998). There are two important phases of gene expression vital for tail formation, early genes expressed between stage 13 and 25 prior to tail bud formation in the region in which the tail will later form, and late genes expressed after stage 26 during tail bud extension (Beck and Slack, 1998). Beck and Slack provide an excellent model for the interaction between these tissues and how expression from each of these tissues modulates the formation of the tail (Beck and Slack, 1999).

In this model interaction between the main neural plate and the posterior 100 μm of the neural plate, as well as the notochord during neurulation are required for the expression of *Lfng* and *Wnt3a* at stage 26. Expression of *Lfng* in the dorsal portion of the closed neural tube induces activation of Notch/Delta signalling in the posterior portion of the neural tube and at the dorsal/ventral boundary that becomes the leading edge of tail bud outgrowth. Notch/Delta signalling at the leading edge of tail-bud outgrowth results in *Wnt3a*-dependent expression of *Hox3* which then allows extension of the tail bud and neural tube to occur. Notch signalling is central to correct tail formation and inhibition causes results in aberrant tail formation (Beck and Slack, 2002). As such, xN1-Src depletion in the posterior neural plate and neural tube could be impacting the regulation of signalling events associated with tail formation. This

could be causing a signalling imbalance between signals from neural tube and from mesodermal tissues, an asymmetry which could contribute to the characteristic kink in the tail of xN1-Src knockdown embryos.

The effect of neuronal Src expression on body patterning is also evident in embryos injected with mammalian N1- and N2-Src mRNA (Fig. 5-3). Injection of mammalian N-Src constructs induces a dose dependent posteriorisation and failure to form anterior crano-facial structures in injected embryos. Similar phenotypes are observed when RA, FGF or Wnt signalling pathways are manipulated (Kuhl, 2003, Isaacs et al., 1994, Sive et al., 1990). This suggests that the signalling pathways to which neuronal Srcs contribute during development can be driven by neuronal Srcs even in non-neuronal tissues.

5.3.6 xN1-Src knockdown reduces neuronal marker expression during primary neurogenesis

As part of the same experiment in which embryos developed locomotive defects in response to bilateral xN1-Src knockdown, embryos were also injected unilaterally. These embryos were fixed during open neural plate stage and probed for n-tubulin expression, a marker of primary neuronal differentiation, by *in situ* hybridisation. Expression of three domains of n-tubulin across the neural plate during primary neurogenesis has been used extensively in *Xenopus* species as a marker for primary neurogenesis (Chitnis et al., 1995). N-tubulin RNA expression was dramatically decreased as a result of xN1-Src knock-down, indicating that effective primary neurogenesis was not taking place (Fig. 5-7A). This dramatic ablation of n-tubulin expression suggests that xN1-Src, rather than functioning as simply an organiser of the cellular structures associated with neuronal differentiation, as has previously been suggested, may be requisite in primary neuronal differentiation.

Whilst xN1-Src knockdown appears to inhibit primary neurogenesis, it does not decrease neuronal specificity. Cells are specified for a neuronal lineage by the blocking of BMP signalling by neutralising molecules such as Chordin and noggin and it appears that xN1-Src plays no significant part in this process (Penzel et al., 1997). This aligns with observations of the temporal expression of xN1-Src, as Sox3 (a

marker of neuralised ectoderm) expression occurs during gastrulation, whereas xN1-Src is not expressed until the gastrula/neurula transition. It is highly noteworthy that xN1-Src knockdown expands the region of Sox3 expression, as previous data indicates that N-tubulin and Sox3 expression is mutually exclusive (Bourguignon et al., 1998). It is tempting to suggest therefore that the region of expanded Sox3 consists of cells which would, in the presence of xN1-Src be differentiated into N-tubulin expressing neurons.

Inhibition of neuronal differentiation at primary neurogenesis would explain the locomotive defects seen in later embryos as the primary function of neurogenesis is to provide early locomotion to the developing tadpole (Roberts, 2000). It is likely that although xN1-Src morpholino decreases N-tubulin transcription, degradation of the morpholino over time may be allowing neuronal differentiation later in development. To test this possibility, later neurogenesis could be identified by an extended time-course of injected embryos, to identify at which point n-tubulin expression re-establishes. Additionally antigen-tagged morpholinos are available, and could be utilized to observe their degradation over time and identify a correlation between any degradation and the resumption of neurogenesis.

5.4 Conclusion

To date, the consensus in the literature is that xN1-Src only functions in post-mitotic development of growth cones and in the regulation and formation of synapses. However, my data suggest that xN1-Src has a more fundamental role in primary neurogenesis and possibly pathways associated with wider signalling events. xN1-Src expression is increased throughout primary neurogenesis and knockdown of this expression by Morpholino exon-skipping appears to prevent primary neurogenesis from occurring (Fig 5-7). Manipulation of neuronal Src expression in *Xenopus* also has a significant effect on body patterning, with overexpression of mammalian N-Src constructs causing a failure in anterior structure formation and xN1-Src knockdown causing aberrant tail development (Fig 5-6). The pathways through which xN1-Src exhibits its functions, and its specific targets are yet to be elucidated but the effects of

xN1-Src knockdown, and mammalian Src overexpression in *Xenopus*, are reminiscent of experiments in both FGF, RA and Wnt signalling.

eFGF or RA injection into *Xenopus* both cause similar posteriorisation phenotypes to those seen in N1- or N2-Src injected embryos (Sive et al., 1990, Isaacs et al., 1994), whilst the characteristic ‘tail kink’ observed in xN1-Src knockdown embryos is also described in dominant negative FGF and Frzb (a negative regulator of frizzled signalling through Wnt) injections (Itoh and Sokol, 1999, Isaacs et al., 1994). Similarly, expression of a dominant negative Retinoic Acid Receptor (RAR α 1) prevents the expression of n-tubulin at primary neurogenesis (Blumberg, 1997) in an identical fashion to that observed in xN1-Src knockdown. Additionally morpholino knockdown of SuFu, a negative regulator of hedgehog, similarly prevents expression of all three bands of n-tubulin expression in the *Xenopus* neurula (Min et al., 2011). These data point towards xN1-Src as a transducer, or regulator of differentiation signals in neuralised cells downstream of several important signalling molecules, although further work using dominant negative receptors or knockdown approaches could identify exactly which signalling pathways utilize xN1-Src as a signal transducer.

In the mature rat brain, N1-Src has protein been identified by immunocytochemistry throughout many brain regions, however, no obvious commonality was observed between these regions, in terms of either their function or the classification of enriched neurons. (Sugrue et al., 1990). A similar *in situ* hybridisation study did, however, localise N1-Src mRNA expression to regions of the brain associated with extensive plasticity (Walaas et al., 1988, Ross et al., 1988). These brain regions contained clusters of neurons expressed substantially higher levels of N1-Src, however these cell clusters matched no obvious subpopulation of neurons (Sugrue et al., 1990). In these clusters of neurons, N1-Src was localised to dendritic processes, the cell soma as well as nerve terminals and growth cones (Maness et al., 1988, Sugrue et al., 1990). Given what we now know about xN1-Src during differentiation it could be that these clusters of neurons are cells differentiating from the neuronal stem cell population in the adult brain. It is known that RA is a key signalling molecule in adult neuritogenesis and given the comparable effects of retinoic acid signalling and xN1-Src expression/knockdown on *Xenopus* embryos it

could well be hypothesised that N1-Src is involved in retinoic acid-dependent adult neurogenesis of these clusters of neurons (Jacobs et al., 2006).

The work presented in this chapter has progressed the understanding of N1-Src during development, from a casual association between the abundance of post-mitotic neuronal cells and N1-Src expression, to one of a causal role of xN1-Src in primary neurogenesis in response to neuronal induction and wider signalling. Further work is now needed to identify the specific signalling pathways through which splicing of the xN1-Src micro-exon inclusion is driven, and through which xN1-Src is functioning within these cells to drive neuronal differentiation.

General discussion

6.1 Summary of works

The work presented in this thesis represents the first significant contribution towards analysis of the functional roles of N1- and N2-Src during neuronal differentiation, both during development and neuroblastoma differentiation. The identification of the importance of xN1-Src expression during primary neurogenesis indicates a central role for N1-Src during the neuronal development. This observation reflects data in the neuroblastoma cell lines KELLY and SK-N-AS where neuronal Src expression induced neuritogenesis and quiescence respectively. Whilst it is now clear that neuronal Srcs have a fundamental role in the differentiation of neuronal progenitors, the mechanism of this action is unclear. The primary difference between C-Src and its neuronal splice variants is in sequence of the n-src loop of the SH3 domain which I have shown increases the constitutive activation of N1- and N2-Src in neuroblastoma cells. N1- and N2-Src exon insertion will also have a significant impact upon substrate specificity and, although no specific substrates have been confirmed by this study, mass spectrometry of phosphotyrosine immunoprecipitations from C- and N2-Src HeLa lysates has demonstrated extensive differences in the abundance of phosphotyrosine within these cells, and provided many N2-Src substrate candidates.

6.2 Differential regulation of C-, N1- and N2-Src

Characterisation of FLAG tagged C-, N1- and N2-Src constructs by Western blotting demonstrated differential post-translational Src regulation, both when overexpressed in B104 and HeLa cells, and when expressed in *Xenopus laevis* embryos (Fig. 3-1; Fig. 4-13; Fig. 5-3). My data show that in all cases where the activating Y416 phosphorylation of C-, N1- and N2-Src are compared by Western blotting, activity is always highest in N2-Src, and lowest in C-Src (Fig. 3-1; Fig. 4-13; Fig. 5-3). Similarly, in N2-Src expressing B104 cells, Y527 phosphorylation, indicative of auto-inhibition and inactivity, is constitutively lower than in C- and N1-Src expressing cells (Fig. 3-1).

Observations of C-, N1- and N2-Src expression in a variety of systems has demonstrated that the effects of the neuronal Src splice variants upon cells differ only by the degree of the effect (with N2-Src eliciting the strongest response) rather than the nature of the effect. This is the case for cytoskeletal rearrangements in cell lines such as COS7 (Fig. 5-1), KELLY (Fig. 3-7) and SK-N-AS (Fig. 3.6), where N2-Src causes the highest amount of neuritogenesis, and N1-Src causes an intermediate effect. This is in stark comparison to the effects of C-Src overexpression in these cells which has minimal effects on cell morphology, if anything increasing the size of the cell soma. Similarly, in stable, inducible HeLa cells, N1-Src demonstrates a similar, but weaker effect on elongation (Fig. 4-3) and motility (Fig. 4-4) when compared with N2-Src. In *Xenopus*, N1- and N2-Src injected embryos develop anterior defects, however the effect is much more potent in N2-Src injected embryos (Fig. 5-3).

With these data in mind I would propose a hypothesis that the magnitude of the effects of N1- and N2-Src relate to the increasing disruption of substrate binding by the n-src loop. Whilst N1- and N2-Src exon insertion may contribute to the interaction interface of the SH3 domain for a small subset of substrates, providing additional specificity for SH3 domain binding, I would propose that the principal difference is the degree to which n-src loop-mediated substrate binding is disrupted.

Auto-inhibition of Src depends on SH3 binding of the SH2-kinase linker and association with the n-terminal lobe of the kinase domain (Xu et al., 1999). Mutation of the n-src loop of C-Src has been shown to decrease the affinity of the SH3 domain for the n-terminal lobe of the kinase domain, resulting in increased activity (Brábek et al., 2002). As such, it is likely that introduction of 6 and 17 amino acid residues into this interaction interface would have significant effects on the inhibition of Src. Further, the differential substrate specificity of N1- and N2-Src when compared to C- may largely be the result of an increased reliance upon the PxxP binding motifs, and decreased binding at the R/K binding specificity pocket. As such, rather than changing the SH3 binding preference, N1- and N2-Src exon inclusion may be principally acting to restrict binding to a smaller subset of proteins. This is reflected in the results of the mass spectrometry of C- and N2-Src HeLa IP samples, in which only eight proteins were detected exclusively in N2-Src HeLa cells, and not C-Src (Table 4-1). Whilst neuronal insertion will certainly cause specific, novel binding to new substrates, as

demonstrated by N1-Src binding to HCN1 (Santoro et al., 1997), I would propose that the majority of the differential effects of N1- and N2-Src is the result of binding site disruption, rather than creation.

In this model, N2-Src would largely share N1-Src substrates, and, phosphorylate them at a higher rate due to the constitutively increased activity. This model would explain why N1-Src consistently has an intermediate effect upon cells relative to N2-Src, why N2-Src is always expressed endogenously at lower levels and how lower vertebrates such as *Xenopus* species do not require N2-Src for complex neuronal developmental processes. This hypothesis could be tested by identification of the specific N1- and N2-Src SH3 binding motifs by testing the SH3 domains against a phage display library, or by yeast 2-hybrid screening.

6.3 Neuronal Srcs in development

6.3.1 Neuronal Srcs contribute to differentiation of neuronal progenitors

Primary neurogenesis enables non-amniotic vertebrates such as amphibians to develop the neuronal circuit necessary to control early larval behaviour (Hartenstein, 1989). During this process a small portion of the progenitor neurons of the neural plate differentiate into post-mitotic neurons, whilst the majority of progenitors remain proliferating to form the adult central nervous system (Hartenstein, 1989). These two populations of neurons, (the mitotic progenitors and the terminally differentiated primary neurons) can be identified by the expression of two marker genes, Sox3 and N-tubulin (Kishi et al., 2000, Moody et al., 1996). Sox3 expression is limited to the proliferative, neuronal progenitors of the neural plate, and expression decreases when the cells differentiate (Kishi et al., 2000). By contrast, N-tubulin is exclusively expressed in differentiating neurons, resulting in the three bands of expression on the open neural plate which indicate the site of differentiating motor, inter and sensory neurons (Moody et al., 1996).

Knockdown of xN1-Src expression in *Xenopus tropicalis* embryos inhibited expression of N-tubulin expression during primary neurogenesis, and increased the width of the Sox3 band (Fig. 5-7 and 8). These two observations reveal a great deal

about the potential role of xN1-Src in *Xenopus* neurogenesis. Sox3 staining of embryos injected with xN1-Src morpholinos demonstrates that the process of neuronal specification does not require xN1-Src expression (Fig. 5-8). In fact, since Sox3 and N-tubulin expression tend to be mutually exclusive (Bourguignon et al., 1998), expanded Sox3 expression may correlate with the location of precursor neurons that are no longer expressing N-tubulin as a result of xN1-Src knockdown (Kishi et al., 2000). Morpholino knockdown of xN1-Src expression also results in a locomotive phenotype indicative of a poorly developed primary nervous system (Fig. 5-6). Taken together, these data suggest that xN1-Src is a crucial component of one or more of the signal transduction pathways that are responsible for the differentiation of neural progenitors, but not their specification. This role is supported by other data, such as the observation in SK-N-AS cells that overexpression of N2-Src causes a 20% decrease in the number of proliferating cells (Fig. 3-8).

6.3.2 Development: Patterning effects of neuronal Src expression

In addition to disrupting regulated movement of the embryo, knockdown of xN1-Src expression also contributed to a patterning defect in the tail of the embryos (Fig. 5-6). This suggests that xN1-Src depletion in the posterior neural plate and neural tube could be impacting on the regulation of signalling events associated with tail formation as discussed in (5.3.5). Patterning defects are also seen in embryos injected with mammalian N1- and N2-Src mRNA (Fig 5-3). In these embryos there is a dose dependent failure to form anterior structures, similar to phenotypes observed when RA, FGF or Wnt signalling pathways are manipulated (Kuhl, 2003, Isaacs et al., 1994, Sive et al., 1990). These effects of Src overexpression and knockdown on *Xenopus* body patterning suggests that the Src splice variants are regulating signalling pathways with roles not just involving neuronal differentiation. Identification of the specific proteins that are phosphorylated by neuronal Srcs that are transducing or driving these signalling events is the next crucial step in understanding the roles of neuronal Srcs in development.

6.3.3 Potential substrates of Neuronal Srcs during development

Based on the conclusions of an earlier section (6.2), it could tentatively be suggested, N1- and N2-Src share a considerable amount of their substrate proteins, differing only in the activity-dependent phosphorylation of these proteins. The mass spectrometry of N2-Src expressing HeLa cells may therefore provide some insight into which specific pathways xN1-Src is contributing to in *Xenopus* embryos. Of particular note are Notch2 and β -catenin, both of which are over two-fold enriched in the phosphotyrosine IP eluate from N2-Src overexpressing HeLa cells when compared to C-Src expressing cells (Appendix 1). As discussed in (5.3.6), Notch and Wnt signalling (for which β -catenin is a central component) each have important roles in neurogenesis, anterior-posterior axis regulation and tail formation. Dysregulation of either of these pathways could result in the observed phenotypes caused by xN1-Src knockdown and N1-Src overexpression.

β -catenin is a downstream transducer of Wnt activation through the canonical Wnt pathway. Typically accumulation of β -catenin in the cytosol is prevented by ubiquitin mediated degradation, targeted by a destruction complex including Axin, APC, PP2A and GSK3. Wnt binding to Frizzled and LRP-5/6 induces translocation of members of the destruction complex to the cell membrane where their stability and activity are decreased. This allows cytosolic accumulation of β -catenin resulting in nuclear localisation and gene transcription in association with transcription factors such as LEF. Early neuronal development requires the suppression of Wnt signalling (Heeg-Truesdell and LaBonne, 2006) suggesting it is unlikely that this pathway is being positively regulated by neuronal Srcs during neurogenesis. Additionally tyrosine phosphorylation of β -catenin, particularly by C-Src is strongly associated with proliferation and carcinogenesis rather than differentiation of neuronal progenitors (Zeng et al., 2006). It is, however, known that Src can also inhibit Wnt/ β -catenin signalling by phosphorylation of LRP6 (Chen et al., 2014), which is also detected in the phosphoproteomic screen, however at levels too low to pass through the stringent filtering process. As such, it seems that more likely, due to the enrichment of N-Cadherin and other adherens alongside β -catenin, that β -catenin is enriched in association with its roles in cell adhesion at the cell membrane rather than as a part of the canonical Wnt signalling pathway.

Notch is not known to be directly regulated by tyrosine phosphorylation, however tyrosine phosphorylation sites have been identified by Phosphosite in the Notch Intracellular Domain, suggesting that tyrosine phosphorylation of the Notch C-terminus can occur *in vivo* (Hornbeck et al., 2012). Notch activation is typically associated with an inhibitory effect on neuronal differentiation, with Notch intracellular domain inhibiting primary neurogenesis, and encouraging a tumorigenic phenotype in neuronal stem cells (Chitnis et al., 1995, Tchorz et al., 2012). Notch is activated by the binding of membrane proteins such as Delta or Jagged on neighbouring cells, which stimulates several proteolysis steps, culminating in cleavage by γ -secretase at V1695. γ -secretase cleavage releases the C-terminal intracellular domain of Notch into the cytosol and nucleus, where it can act upon gene transcription. During neurogenesis, the boundary of the neural plate is established by Notch-mediated lateral inhibition, whereby binding of Delta from one cell, to Notch on another cell membrane inhibits expression of Delta. This causes a feedback loop whereby cells in which Notch signalling is activated, express more Notch and less Delta, which suppresses a neuronal fate in cells outside of the neural plate boundary. Interestingly all eight of the unique Notch2 sequences identified by mass spectrometry of N2-Src expressing HeLa cells, occur C-terminally and seven occur after this activating cleavage site suggesting that the Notch2 intracellular domain is released in N2-Src expressing cells. Although activated Notch suppresses neuronal differentiation (Chitnis et al., 1995), no data currently exist on the effects of tyrosine phosphorylation on this. It is tempting to suggest that neuronal Src variants are negatively regulating Notch2 intracellular domain by phosphorylation of either the Notch intracellular protein, or a binding protein. Notch makes a compelling candidate gene for xN1-Src activity, as Notch has a significant role in neuronal differentiation and tail bud formation (Chitnis et al., 1995, Beck and Slack, 1998, Beck and Slack, 2002).

Whilst Notch2 signalling is an excellent candidate for further experimentation on the role of xN1-Src during development, there are several other candidate pathways such as FGF and RA. Rescue experiments utilizing an xN1-Src morpholino in combination with inhibitors or activators of these pathways may contribute to the identification of the specific pathways that are transduced by xN1-Src.

6.3.4 Localisation of xN1-Src during development

Additionally, whilst xN1-Src expression has been temporally localised to primary neurogenesis (Fig. 5-2), identification of the spatial expression of xN1-Src during development could provide further insight into the induction of xN1-Src expression. Steps were made towards the development of an xN3-Src *in situ* hybridisation probe, in an attempt to identify xN1-Src expression (which appears to be co-regulated and is longer, making it a more appropriate probe target), however, to adequately identify xN1-Src expression by *in situ* hybridisation would require a specific xN1-Src probe. Due to the short length of the xN1-Src insert (15 nucleotides), standard antisense RNA technology is likely to result in cross-contamination with C-Src. Use of an LNA probe, a modified RNA nucleotide probe with higher affinity and specificity, would be the optimal method to identify xN1-Src expression in embryos. Through this method it would be possible to identify the temporal and spatial expression of xN1-Src, and by use of inhibitors and activators of various signalling pathways, identify the specific pathways that stimulate xN1-Src exon inclusion.

6.4 Neuroblastoma

6.4.1 The effects of neuronal Srcs on neuroblastoma proliferation and differentiation

Overexpression of N1- and N2-Src induce fold-changes in neuritogenesis in the neuroblastoma cell lines SK-N-AS (Fig. 3-6) and KELLY (Fig. 3-7) and a 20% decrease in the expression of the proliferation marker Ki67 in SK-N-AS cells (Fig. 3-8). Interestingly, in LAN-5 cells that are known to express N-Srcs and differentiate readily, knockdown of N2-Src had no significant effect on the number and length of neurites (Fig. 3-5).

It is likely that the differential gene expression in these cells is responsible for enabling or inhibiting the effect of neuronal Src over-expression upon these cells. The differentially expressed genes are likely to be ubiquitous, rather than neuronal genes, as we observe a significant N-Src induced extension of neurite-like protrusions from

COS7 fibroblasts, and a decrease in migration and proliferation and increase in elongation of N2-Src expressing HeLa cells (Fig. 4-3; Fig 4-4).

The induction of such a remarkable change in the phenotypes in heterologous cell lines suggests that the substrates of neuronal Srcs are not restricted to neurons. Since these kinases elicit their cellular response by phosphorylation, we can safely assume that the effects of N2-Src phosphorylation on neuroblastoma cells are due to differential phosphorylation of signalling elements in the cells. Identification of possible pathways for N2-Src induced neuroblastoma differentiation can therefore be determined by the other experiments performed, including those in *Xenopus*, and the data retrieved from the mass spectrometry experiment in HeLa cells. These data suggest that N1- and N2-Src may have a complex signalling role in the differentiation of neuroblastoma cells.

N1-Src and N2-Src both consistently induce some degree of increased neuritogenesis in neuroblastoma cells (Fig. 3-6, 7). This effect was particularly pronounced in the N2-Src expressing cells of the retinoic acid resistant cell lines KELLY and SK-N-AS (Fig. 3-7). Since neuroblastoma cells are derived from stem cells of the sympathetic nervous system, and xN1-Src deletion decreases neuronal differentiation in *Xenopus* (Fig. 5-7), it can be assumed that the mechanisms of differentiation and neuritogenesis in neuroblastoma cells are largely similar to developmental mechanisms of neuritogenesis.

6.4.2 FAK and Paxillin as potential N-Src substrates

Whilst no specific N2-Src substrates have been identified, the well characterised Src substrate FAK was 1.7-fold enriched in phosphotyrosine immunoprecipitations from N2-Src expressing HeLa cells compared to C-Src cells (Appendix 1). FAK is a cytosolic protein tyrosine kinase that accumulates at focal adhesions to, facilitate turnover of adhesions required for cell migration as well as the proliferation of signalling events associated with cell-cell or cell-substrate contact. Src binding to FAK requires an initial step of FAK activation via phosphorylation at Y397. This phosphorylation provides an SH2 domain to which Src can bind, both targeting

and activating Src (Cobb et al., 1994), however this step can be skipped by v-Src (Guan and Shalloway, 1992), so it is possible that constitutively active N-Srcs may not require this initial step. FAK is then multiply phosphorylated by SH2-bound Src which substantially increases its activity, leading to the activation of a variety of signalling events within the cell (Calalb et al., 1995). Activation of FAK by Src has been shown to be necessary for a variety of FAK substrate phosphorylation events, including that of Paxillin (Shen and Schaller, 1999), which is also 1.8-fold enriched in the N2-Src HeLa mass spec data (Appendix 1). Paxillin phosphorylation at Y88 was identified in N2-Src cells, and only the corresponding dephosphorylated peptide identified in C-Src HeLa cells.

The role of FAK in neuroblastoma differentiation was first characterised by Bozzo and colleagues who demonstrated that blocking FAK phosphorylation in SH-SY5Y neuroblastoma cells prevented neuritogenesis (Bozzo et al., 1994). Whilst FAK appears to be necessary for neuroblastoma differentiation, it is also specifically up-regulated in metastatic, stage 4 neuroblastoma cases, likely due to its roles in migration and proliferation (Beierle et al., 2008).

6.4.3 Potential downstream effectors of FAK/N-Src

The actions and pathways regulated by Src-activated FAK are many and varied. Phosphorylation of FAK by Src is necessary for the assembly of components of the Ras/MAPK pathway at focal adhesions (Miyamoto et al., 1995), as well as recruitment of Grb2, which in turn activates Erk/MAPK signalling (Schlaepfer et al., 1994). Src-activated FAK is also an adaptor which enables the p130Cas (BCAR1), in complex with BCAR1 to be phosphorylated on by Src on multiple sites (Cheng et al., 2014). This leads to a cascade of recruitment and interaction which ends in activation of the JNK/MAPK signalling cascade, associated with control of cell proliferation by gene transcription (Giancotti and Ruoslahti, 1999, Schlaepfer et al., 1994). In the phosphotyrosine IP from N2-Src expressing HeLa cells, several members of the Src/FAK signalling cascade are enriched (log₂ ratios of N2-Src/C-Src shown in brackets), including Paxillin (0.8) (Schaller, 2004), N-Cadherin (1.3) (Schaller, 2004), p130Cas/BRCA1 (0.13) and BCAR3 (1.1) (Cheng et al., 2014). Similarly, there are

proteins associated with FAK signalling that are enriched in C-Src and absent, or less abundant in N2-Src HeLa IPs such as Cdc42, which is associated with both cellular proliferation and formation of filopodia, and is detected in both replicates of the C-Src MS data, however not in any N2-Src samples (Appendix 1).

The increased abundance of so many proteins modulated by Src/FAK activity suggests that in N2-Src overexpressing HeLa cells, these proteins are either increased in tyrosine phosphorylation, or in their interactions. Modulation of this pathway by N2-Src provides a viable pathway for N2-Src modulation of neuritogenesis and proliferation. FAK activation of the Ras/MAPK pathway is known to be a crucial component in the onset of N-CAM induced neurite outgrowth (Kolkova et al., 2000). Similarly, during adhesion signal-induced differentiation, Src/FAK activation can result in ERK1/2 activation resulting in activation of transcription factors such as Myc (Huang et al., 2012). Though activation of this pathway usually requires an extracellular signal to activate the initial activating phosphorylation of FAK, the constitutive activity of N2-Src may bypass this mechanism in a manner similar to that displayed by v-Src activation of FAK (Guan and Shalloway, 1992).

In addition to the possibility of FAK activation instigating neuronal differentiation, FAK is also enriched in neuronal growth cones, in and correct function of FAK is required for neurite extension (Kim and Feldman, 1998). Although the specific phosphorylation events that triggered the enrichment of Src/FAK associated proteins is not known, it seems highly likely that one or more of these proteins is tyrosine phosphorylated as a result of N2-Src expression. Interestingly a neuronal isoform of Src (assumed to be N1-Src although not specified in the paper) has been demonstrated to bind poorly to both FAK and neuronal FAK+ (Messina et al., 2003). This suggests that FAK is unlikely to be a direct substrate of N2-Src, however the presence of so many FAK associated downstream proteins suggests that one or more of these is likely to be differentially phosphorylated. Paxillin makes a particularly strong candidate for this due to the identification of a phosphopeptide in N2- but not C-Src samples. Future experiments to confirm this could include blotting for FAK phosphorylation in C- and N2-Src expressing HeLa cells, or immunoprecipitation for Paxillin followed by Western blotting for phosphotyrosine. In addition, to identify whether this pathway was having an effect on neuroblastoma neuritogenesis and

quiescence, the N2-Src induced neuritogenesis could be tested in the presence and absence of inhibitors of these processes.

6.4.4 Notch as an N-Src substrate

As discussed in **6.3.3** the Notch signalling pathway has multiple roles in neuronal differentiation during development, and Notch2 is up-regulated in the phosphotyrosine IP from N2-Src expressing HeLa cells (Chitnis et al., 1995) (Table 4-4). The role of Notch signalling in neuroblastoma, however, remains unclear. Notch1 expression is associated with both repression of RA induced differentiation (Hooper et al., 2006), and an unfavourable prognosis in neuroblastoma (Chang et al., 2010). More recently Zage and colleagues demonstrated that neuroblastoma cell lines express multiple variants of the Notch receptor that are inactive under basal conditions (Zage et al., 2012). Activation of Notch2 was demonstrated to cause inhibition of differentiation of medulloblastoma cell lines and high Notch2 expression correlated with a poor prognosis in medulloblastoma (Fan et al., 2004). This matches data observed in neuronal precursors where activation of Notch2 signalling inhibits differentiation by maintaining the cells in a proliferative state (Solecki et al., 2001).

As discussed in **6.3.3** there are no Notch2 tyrosine phosphorylation sites confirmed in the literature, however 7 of the 8 unique sequences identified in the HeLa MS screen are from the Notch2 intracellular domain. This suggests that Notch2 is being immunoprecipitated either due to a tyrosine phosphorylation site on its C-terminal tail (several candidates have been identified by Phosphosite (Hornbeck et al., 2012)), or by Notch intracellular domain association with another tyrosine phosphoprotein. The 1.2 log₂ enrichment in N2-Src expressing HeLa cells strongly suggests that the increase in Notch2 abundance in N2-Src samples is due to differential regulation of Notch, or associated proteins. As demonstrated in the literature, activation of Notch2 signalling is strongly associated with proliferation and resistance to differentiation.

An N2-Src mediated inhibition of Notch2 intracellular domain signalling could be causative in the increase differentiation and decreased proliferation observed in

neuroblastoma cells (Fig. 3-7, 8). Regulation of the cleaved Notch intracellular domain by phosphorylation has been studied extensively, CDK8 has previously been shown to hyperphosphorylate the Notch intracellular domain, targeting it for ubiquitin mediated degradation (Fryer et al., 2004). This process of degradation is regulated in a complex fashion, with ubiquitin mediated degradation inhibited by acetylation of the Notch intracellular domain by MAML-1 (Popko-Scibor et al., 2011). It seems likely from the observed effects of N2-Src expression in both *Xenopus* species and human neuroblastoma cells and the occurrence of only the intracellular domain portion of Notch in the N2-Src mass spectrometry samples that N2-Src is having some role in Notch signalling. Given the complex nature of Notch intracellular domain regulation and its importance in both development and neuroblastoma differentiation this is certainly an area worthy of further study.

A simple way to test this hypothesis would be the co-expression of a Notch2 intracellular domain plasmid with N2-Src to identify whether N2-Src abrogates Notch2 activated gene expression.

6.4.5 N-Cadherin, Plakoglobin and β -catenin

In addition to FAK and its associated proteins, several adheren-associated proteins were identified as specifically enriched in the N2-Src MS samples including N-Cadherin (1.3 log₂), Plakoglobin (1.6 log₂) and β -catenin (1.1 log₂). As discussed above, I do not expect that the enrichment of β -catenin is related to its role in Wnt signalling, due to the co-enrichment of several proteins with which is associates as part of its role in adhesion mediated signalling.

Decreased expression of Plakoglobin has been associated with increased metastatic potential in several cancer systems including breast cancer (Bailey et al., 2012), skin cancer (Tada et al., 2000), and sarcoma (Kanazawa et al., 2008), and has been associated with a poor prognosis in neuroblastoma (Amitay et al., 2001). Similarly N-Cadherin expression has been noted to be significantly lower in metastatic tumours with a worse prognosis (Lammens et al., 2012). By contrast, expression of β -catenin has been observed to be relatively similar to in normal ganglion cells, and

increased or decreased expression of these proteins was not correlated to prognosis (Amitay et al., 2001). Deregulated Wnt signalling, and associated β -catenin accumulation has associated with high-risk neuroblastoma cases (Liu et al., 2008) and a knockdown of β -catenin has been reported to inhibit neuroblastoma cell growth, although this is to be expected from such an important molecule for normal cell function and signalling (Yao et al., 2013).

6.5 The role of the COPII transport vesicle system in N2-Src function

Of all of the results gained from the HeLa cell line mass spectrometry, the increase in abundance of proteins of the COPII vesicle pathway was the most exciting evidence of N2-Src specific enrichment of a functionally interacting group of proteins. Increases of protein abundance of over $1\log(2)$ were observed in Sec 16A, 23A, 23B, 24B and 24C. These data indicate that N2-Src expression might be promoting the phosphorylation of one or more of these proteins. It is difficult to suggest which of these proteins is more likely to be differentially phosphorylated although the presence of only a single Sec16 isoform makes it the best candidate protein. Interestingly, whilst Sec23A/B and Sec24B/C form portions of the COPII coat, Sec16A does not, instead acting as a scaffold for COPII coat assembly on the ER. That Sec16A was pulled down as part of this complex, perhaps suggests that the COPII coat is being pulled down whilst in association with the ER, which further points towards Sec16A as the differentially phosphorylated protein, or perhaps phosphorylation of Sec23/24 which prevents detachment of the coat from the ER.

The role of differential regulation of the COPII coat in neuronal differentiation is difficult to interpret. Sec16A is known to interact and be regulated by LRRK2, which is known to have roles in neurological disorders such as Parkinson's disease (Cho et al., 2014). Different Sec23/24 have roles in specific recruitment of COPII cargo and perhaps phosphorylation of one or more of these variants might be influencing cargo selection. Truncation of Sec24b is known to increase the occurrence of spina bifida in mice by decreasing the proper trafficking of Vangl2 (Merte et al., 2010). Sec23 and Sec24 are known to be essential during epithelial differentiation

during *Drosophila* embryogenesis, establishing polarity of epithelial cells and enabling secretion of extracellular matrix proteins in this system (Norum et al., 2010). Regulation of the COPII vesicle transport is also important for dendritic arborisation in *drosophila*. RNAi against Sec23 and Src24 indicates that the COPII coat is transcriptionally regulated during dendritic elaboration to induce dendritic complexity, likely by influencing the rate of vesicle formation in addition to providing dynamic control of cargo selection and recruitment (Iyer et al., 2013). These studies suggest that effective regulation of the COPII vesicle pathway could have crucial roles in several facets of neuronal differentiation and function.

The phosphorylation of these particular members of the COPII vesicle transport pathway may be contributing to neuronal differentiation in several ways. Firstly phosphorylation of Sec23/24 could be influencing the cargo recruitment or rate of formation of the COPII vesicles as has previously been demonstrated by transcriptional regulation of Sec23 (Iyer et al., 2013) and kinase-mediated regulation of COPII coat polymerisation (Aridor and Balch, 2000). Secondly phosphorylation of Sec16A could be modulating COPII vesicle recruitment by increasing the formation of ER exit sites as has been previously demonstrated by Erk2 phosphorylation of Sec16 (Farhan et al., 2010). The role of COPII regulation in neuritogenesis would likely be to provide increased membrane and/or recruitment of specific membrane-bound proteins during differentiation, in addition to possible roles in secretion of developmentally important proteins.

To test these hypotheses, first the specific phosphorylation event associated with N2-Src expression should be identified. This could be accomplished using a mass spectrometry method more focussed on specific phosphorylation events rather than on identification of protein complexes, as described in (4.3.3). Upon identification of the specific phosphorylation event, placing tyrosine to phenylalanine mutants of the phosphorylation site into the COS7 N2-Src induced neuritogenesis assay could determine whether the phosphorylation event is central to neurite outgrowth.

6.6 Neuronal Srcs as a therapeutic target in neuroblastoma

Decreasing proliferation and increasing neuritogenesis in response to N-Src overexpression (Fig. 3-7, 8), in addition to the strong correlation between N-Src expression and patient prognosis (Matsunaga et al., 1994b, Matsunaga et al., 1998), suggests that neuronal Srcs could be a potential novel target for neuroblastoma therapy. Whilst overexpression of N1- and N2-Src in neuroblastoma tumours is not a viable treatment method, these results do provide several other potential options.

Matsunaga and colleagues identified that a ratio of N2-Src mRNA expression to total Src mRNA expression above 0.15 was indicative of a positive prognosis in neuroblastoma, suggesting that a relative increase in N2-Src activity over C-Src would improve prognosis. Extensive work has been performed to study the potential of C-Src inhibition as a cancer therapy. The potent tyrosine kinase inhibitor dasatinib is already approved for clinical treatment of solid tumours (Demetri et al., 2009) and additionally has been shown to decrease the proliferation and anchorage independence growth of some neuroblastoma cells *in vitro*, although this did not consistently translate to *in vivo* results in mouse models (Vitali et al., 2009). Tyrosine kinase inhibitors such as dasatinib are not specific C-Src inhibitors as they elicit their effects by acting upon tyrosine kinase domains and as such would inhibit C-Src, N1- and N2-Src equally. To specifically target C-Src activity, without inhibiting N2-Src, would require specific targeting of the SH3 domain of C-Src in a way that excluded N2-Src. Though SH3 targeted C-Src inhibitors have been attempted previously, only modest success is reported (Tiwari et al., 2010) and the effect of SH3 targeted inhibition on cellular function is not known. As such specifically targeting Src activities does not currently seem like a viable option for therapy.

Whilst directly targeting Src with drugs is not a viable option for possible neuroblastoma therapies, regulating the effectors of N1- and N2-Src induced neuronal differentiation may provide some therapeutic advantage. It is known that N2-Src increases the overall level of tyrosine phosphorylation in neuroblastoma cells (Fig. 3-1) and that vanadate treatment increases RA induced neuroblastoma differentiation (Clark et al., 2013). Whilst the specific substrates of N2-Src have yet to be identified, several notable candidates have been listed for further study in the course of this thesis.

Targeting the phosphorylation of these proteins, or inhibiting their dephosphorylation, may provide a viable target for neuroblastoma therapies in the future.

Finally, whilst expression of neuronal Srcs seems to correlate extensively with neuronal differentiation, both during normal development (Wiestler and Walter, 1988) and in induced differentiation of neuroblastoma (Matsunaga et al., 1993a). The regulation of neuronal Src expression in these instances may also be a therapeutic target. The N1-Src exon is included by the complex interaction of proteins including PTB, hnRNP F, hnRNP H and KSRP (Chou et al., 1999, Hall et al., 2004). We know from the literature that xN1-Src inclusion occurs in a protein synthesis independent fashion in *Xenopus* ectoderm undergoing neuronal differentiation (Collett and Steele, 1993). As such, whilst the intracellular signals which induce the activity of the N1-Src splicing machinery are not currently known, the mechanism the activation of N-Src inclusion could provide a novel therapeutic target. Interestingly the expression of N2-Src could well be contributing to the expression of further neuronal proteins. Whilst the splicing factor hnRNP H is expressed ubiquitously, its association with the N-Src exon contributes to its alternative splicing. This protein is specifically enriched in the MS of N2-Src expressing cells, suggesting that N2-Src splicing may contribute to auto-regulatory feedback. It is tempting also to suggest that the same factors responsible for neuronal splicing of Src may also be contributing to neuronal splicing of other genes. N2-Src regulation of hnRNP H may be part of a wider transcriptional role for the protein.

6.7 Final words

Utilizing a variety of biological techniques I have demonstrated that neuronal Srcs have essential roles to play during neuronal differentiation, both *in vivo* and *in vitro*, and have provided a road-map for future experiments to identify the specific molecular mechanisms through which N-Srcs mediate their effects upon cells. The understanding of the role of N1-Srcs during development has progressed from the correlative implications identified in the late 1980's, to identification of the importance of N1-Src in neuritogenesis of neuronal precursors. This study has also identified several pathways and substrates which may be specifically targeted by N1-

and N2-Src and provides a considerable base of knowledge from which more in depth studies can progress in the coming years.

Appendix 1 – Table showing relative protein abundance in C- & N2-Src LC/MS/MS experiments

Gene name	Accession	Log change %emPAI	C-Src %emPAI AVG	N2-Src %emPAI AVG	C-Src Sig mat AVG	N2 Sig mat AVG	C-Src Sig Seq AVG	N2-Sig Seq AVG
CAPRIN1	E9PLA9	n/a	0.000	0.501	0.0	4.0	0.0	4.0
RPS14	P62263	n/a	0.000	0.412	0.0	3.0	0.0	3.0
DDX5	B4DLW8	n/a	0.000	0.329	0.0	10.5	0.0	9.0
HNRNPA0	Q13151	n/a	0.000	0.126	0.0	2.0	0.0	2.0
KIRREL	B4DN67	n/a	0.000	0.119	0.0	4.5	0.0	4.0
RPL4	P36578	n/a	0.000	0.115	0.0	3.5	0.0	3.0
CRBN	J3QT87	n/a	0.000	0.101	0.0	3.0	0.0	2.5
PKP2	Q99959	n/a	0.000	0.038	0.0	2.0	0.0	2.0
LRRC59	Q96AG4	-3.106	0.043	0.373	1.0	6.0	1.0	5.5
RPS20	P60866	-3.031	0.123	1.008	1.0	4.5	1.0	3.5
LIMD1	C9JRJ5	-2.768	0.014	0.097	0.5	3.5	0.5	3.5
GTF2I	P78347	-2.473	0.009	0.047	0.5	3.0	0.5	3.0
HNRNPAB	D6R9P3	-2.443	0.031	0.170	0.5	3.0	0.5	2.5
EIF2S1	P05198	-2.296	0.041	0.202	1.0	3.5	1.0	3.5
RPS2	H0YEN5	-2.287	0.074	0.359	1.5	4.0	1.0	3.5
VPS29	F8VXU5	-2.246	0.065	0.308	1.0	3.5	1.0	2.5
CKAP5	Q14008	-2.134	0.005	0.022	1.0	3.0	1.0	3.0
CCAR1	Q8IX12	-1.990	0.011	0.043	1.0	3.5	1.0	3.0
QARS	B4DWJ2	-1.952	0.011	0.044	0.5	2.0	0.5	2.0
SEC24C	G5EA31	-1.904	0.073	0.275	4.5	18.0	4.5	13.0
SEC23B	Q15437	-1.835	0.071	0.255	3.5	12.5	3.5	9.0
TIA1	F8W8I6	-1.737	0.128	0.426	3.5	8.0	2.0	7.0
LDHA	P00338	-1.640	0.041	0.128	1.0	2.5	1.0	2.5

Appendix 1 – Table showing relative protein abundance in C- & N2-Src LC/MS/MS experiments

Gene name	Accession	Log change %emPAI	C-Src %emPAI AVG	N2-Src %emPAI AVG	C-Src Sig mat AVG	N2 Sig mat AVG	C-Src Sig Seq AVG	N2-Sig Seq AVG
JUP	P14923	-1.619	0.203	0.625	9.5	21.5	8.5	17.0
EIF4G1	E7EUU4	-1.599	0.011	0.034	1.0	3.0	1.0	3.0
PDCD6IP	Q8WUM4	-1.570	0.113	0.335	6.0	16.5	6.0	14.5
PCBP1	Q15365	-1.563	0.063	0.185	1.5	3.5	1.5	3.5
TIAL1	Q01085	-1.545	0.099	0.290	2.0	5.5	2.0	5.5
HGS	O14964	-1.543	0.037	0.109	2.0	5.0	2.0	4.5
GN=RPS19	P39019	-1.534	0.235	0.681	2.5	4.0	2.0	4.0
CCT7	F5GZK5	-1.503	0.040	0.113	1.0	3.0	1.0	3.0
SLC25A13	F5GX33	-1.467	0.025	0.069	1.0	2.5	1.0	2.5
PHGDH	Q5SZU1	-1.463	0.077	0.211	3.0	8.5	2.0	5.5
SRP14	P37108	-1.418	0.148	0.394	1.5	3.0	1.0	2.5
SEC24B	B7ZKM8	-1.378	0.141	0.366	12.0	40.5	8.0	17.0
YTHDF3	R4GN55	-1.373	0.045	0.118	2.0	4.0	1.5	3.5
TCP1	F5H282	-1.361	0.054	0.138	1.0	2.5	1.0	2.0
CARM1	Q86X55	-1.343	0.058	0.148	2.5	5.5	2.5	5.0
HNRNPDL	O14979	-1.333	0.043	0.107	1.0	2.5	1.0	2.5
HNRNP3	P31942	-1.323	0.153	0.383	3.5	10.0	2.0	4.5
CLTC	Q00610	-1.319	0.009	0.021	1.0	2.5	1.0	2.5
RPL30	E5RI99	-1.310	0.135	0.335	1.0	2.0	1.0	2.0
CPSF7	F5H669	-1.301	0.056	0.139	1.5	3.0	1.5	3.0
RPS5	M0R0F0	-1.288	0.369	0.900	5.5	11.5	2.5	6.0
CDH2	A8MWK3	-1.267	0.046	0.111	2.5	6.5	2.0	4.5
SEC23A	F5H365	-1.259	0.191	0.457	8.5	25.0	7.5	13.0

Appendix 1 – Table showing relative protein abundance in C- & N2-Src LC/MS/MS experiments

Gene name	Accession	Log change %emPAI	C-Src %emPAI AVG	N2-Src %emPAI AVG	C-Src Sig mat AVG	N2 Sig mat AVG	C-Src Sig Seq AVG	N2-Sig Seq AVG
RPS10	P46783	-1.211	0.182	0.421	3.0	7.5	1.5	3.5
RPL7	A8MUD9	-1.198	0.414	0.951	3.5	9.0	3.5	6.0
PHB	P35232	-1.184	0.146	0.332	2.5	4.5	2.5	4.5
CLASP2	E3W994	-1.183	0.014	0.032	1.0	2.5	1.0	2.5
NOTCH2	Q04721	-1.162	0.019	0.042	3.5	7.0	3.5	6.5
CTNNB1	B4DGU4	-1.143	0.139	0.307	7.5	13.0	6.5	11.5
FUBP1	E9PEB5	-1.134	0.113	0.247	5.5	9.0	4.5	7.5
SEC16A	J3KNL6	-1.120	0.096	0.209	14.0	26.5	13.5	22.5
FUS	H3BPE7	-1.114	0.058	0.127	2.0	3.5	1.5	3.0
BCAR3	O75815	-1.111	0.089	0.193	5.0	9.5	5.0	8.0
TANC2	Q9HCD6	-1.107	0.049	0.105	6.5	13.0	6.5	11.5
HNRNPA2B1	P22626	-1.080	0.138	0.291	4.0	6.0	3.0	5.0
SLC25A5	P05141	-1.079	0.353	0.747	6.5	11.0	5.0	8.0
VPS35	Q96QK1	-1.078	0.092	0.195	5.0	11.5	5.0	8.0
ATP5B	H0YH81	-1.062	0.086	0.180	2.0	3.5	2.0	3.5
RPS8	Q5JR95	-1.001	0.223	0.446	3.0	5.0	2.5	4.0
PHB2	J3KPX7	-0.981	0.128	0.253	2.5	4.0	2.5	4.0
RPS13	P62277	-0.980	0.355	0.701	3.5	5.5	3.0	4.5
RPL27A	E9PJD9	-0.960	0.298	0.579	1.5	2.5	1.5	2.5
PCMT1	J3KP72	-0.957	0.081	0.157	1.5	2.5	1.5	2.5
SEC23IP	F5H0L8	-0.942	0.020	0.038	1.0	2.0	1.0	2.0
ANXA11	B4DVE7	-0.930	0.078	0.148	2.5	4.5	2.5	4.0
NCKAP1	Q9Y2A7	-0.929	0.101	0.193	7.5	13.5	6.0	12.0

Appendix 1 – Table showing relative protein abundance in C- & N2-Src LC/MS/MS experiments

Gene name	Accession	Log change %emPAI	C-Src %emPAI AVG	N2-Src %emPAI AVG	C-Src Sig mat AVG	N2 Sig mat AVG	C-Src Sig Seq AVG	N2-Sig Seq AVG
TJP1	G3V1L9	-0.914	0.034	0.063	4.5	8.0	4.0	7.0
HSP90AB1	P08238	-0.909	0.080	0.149	4.5	7.0	4.0	6.5
CYFIP1	Q7L576	-0.907	0.103	0.192	8.5	15.0	8.0	13.0
PTK2	H0YBP1	-0.857	0.045	0.082	3.5	7.5	3.5	5.0
PICALM	Q13492	-0.830	0.043	0.076	1.5	3.0	1.5	3.0
PXN	F5GZ78	-0.806	0.075	0.131	3.0	5.0	3.0	3.0
KRT9	P35527	-0.785	0.102	0.176	3.5	5.5	3.5	5.5
PARD3	Q5VWV2	-0.772	0.056	0.095	5.0	8.0	4.5	7.0
EIF3A	F5H335	-0.770	0.016	0.027	1.5	2.5	1.5	2.5
RPLP0	P05388	-0.710	0.255	0.418	4.5	7.5	3.5	5.5
HNRNPU	Q00839	-0.676	0.075	0.120	4.0	5.5	4.0	4.5
PIK3R2	E9PFP1	-0.672	0.058	0.093	2.5	3.0	2.0	2.5
MRPS34	C9JJ19	-0.637	0.095	0.148	1.5	2.0	1.5	2.0
VDAC2	B4DKM5	-0.629	0.089	0.137	1.5	2.0	1.5	2.0
RPS18	P62269	-0.620	0.587	0.903	5.0	7.5	4.5	5.5
AGFG1	B8ZZY2	-0.616	0.043	0.066	2.0	2.0	1.5	2.0
KRT18	F8VZY9	-0.616	0.057	0.088	1.5	2.0	1.5	2.0
ACTB	P60709	-0.586	0.251	0.377	6.5	7.0	5.0	6.5
KHSRP	Q92945	-0.573	0.238	0.354	11.0	13.5	9.0	11.5
ATAD3B	Q5T9A4	-0.530	0.095	0.137	5.5	6.0	4.0	5.0
HIST1H2AG	P0C0S8	-0.515	0.452	0.646	4.0	7.5	2.5	2.5
SRC	P12931	-0.489	0.174	0.244	5.0	7.0	5.0	6.5
ARAP1	Q96P48	-0.486	0.031	0.044	3.0	4.5	3.0	4.0

Appendix 1 – Table showing relative protein abundance in C- & N2-Src LC/MS/MS experiments

Gene name	Accession	Log change %emPAI	C-Src %emPAI AVG	N2-Src %emPAI AVG	C-Src Sig mat AVG	N2 Sig mat AVG	C-Src Sig Seq AVG	N2-Sig Seq AVG
PKP3	Q9Y446	-0.468	0.111	0.153	5.5	7.0	5.5	6.5
EIF3C	H3BRV0	-0.454	0.045	0.062	3.0	3.5	3.0	3.5
KPNA2	P52292	-0.437	0.073	0.099	2.5	3.0	2.5	3.0
IGF2BP3	O00425	-0.412	0.045	0.060	1.5	2.0	1.5	2.0
FUBP3	Q96I24	-0.408	0.217	0.288	7.0	8.5	6.0	7.5
KPNB1	Q14974	-0.399	0.056	0.074	3.5	4.0	3.0	3.5
ANKS1A	Q92625	-0.399	0.042	0.055	3.0	3.5	3.0	3.5
DDX3X	O00571	-0.396	0.556	0.732	22.0	27.5	16.0	17.5
EIF3L	B0QY89	-0.378	0.045	0.059	2.0	2.0	2.0	2.0
SNX18	Q96RF0	-0.375	0.085	0.110	3.5	4.0	3.5	3.5
MCM3	J3KQ69	-0.372	0.049	0.063	2.5	3.0	2.5	3.0
KRT1	P04264	-0.343	0.183	0.232	8.5	9.0	6.5	7.5
CTNND1	C9JZR2	-0.334	1.135	1.432	67.0	96.5	30.5	30.0
BCR	P11274	-0.334	0.029	0.037	2.5	3.0	2.5	3.0
NCL	P19338	-0.330	0.056	0.071	3.0	3.0	2.5	3.0
HSPA9	P38646	-0.307	0.223	0.276	12.5	14.5	8.0	8.0
CAND1	Q86VP6	-0.290	0.067	0.082	6.0	6.0	5.5	6.0
ALB	H0YA55	-0.288	0.058	0.071	2.5	2.0	1.5	2.0
EMD	P50402	-0.279	0.278	0.337	4.5	4.5	4.0	4.0
PKP4	Q99569	-0.259	0.224	0.268	17.0	17.5	14.0	16.0
EEF1A1P5	Q5VTE0	-0.247	0.297	0.353	9.5	9.5	5.5	6.5
GIT1	Q9Y2X7	-0.226	0.162	0.189	6.0	8.5	5.5	8.0
ARHGEF7	B1ALK7	-0.181	0.204	0.232	9.5	9.5	8.0	8.5

Appendix 1 – Table showing relative protein abundance in C- & N2-Src LC/MS/MS experiments

Gene name	Accession	Log change %emPAI	C-Src %emPAI AVG	N2-Src %emPAI AVG	C-Src Sig mat AVG	N2 Sig mat AVG	C-Src Sig Seq AVG	N2-Sig Seq AVG
TUFM	P49411	-0.179	0.083	0.094	2.5	2.5	2.5	2.5
HSPD1	P10809	-0.166	0.336	0.377	12.5	11.0	9.0	9.0
SLC3A2	J3KPF3	-0.148	0.127	0.141	6.0	5.5	5.0	5.0
PABPC1	P11940	-0.146	0.358	0.396	13.5	18.0	8.0	9.5
PRKDC	E7EUY0	-0.136	0.031	0.034	9.0	9.0	9.0	9.0
RPS7	B5MCP9	-0.136	0.532	0.585	7.0	8.0	4.5	4.5
BCAR1	P56945	-0.132	0.324	0.355	16.5	18.5	13.5	14.0
DSG2	Q14126	-0.110	0.115	0.124	8.0	9.0	7.5	8.0
RPL12	P30050	-0.107	0.673	0.724	5.5	4.5	4.5	4.5
CTTN	Q14247	-0.085	2.154	2.286	45.0	42.0	27.0	26.5
ILF2	Q12905	-0.066	0.131	0.137	3.5	3.5	2.5	3.0
KRT2	P35908	-0.054	0.093	0.097	3.5	4.0	3.5	3.5
NUP88	J3KMX1	-0.043	0.054	0.056	2.5	2.5	2.5	2.5
HSPA5	P11021	-0.035	0.291	0.298	13.5	12.5	10.5	9.0
HSPA1A	P08107	-0.031	0.365	0.373	15.0	15.0	11.0	9.5
CBL	P22681	-0.017	0.059	0.059	3.5	3.5	3.5	3.5
ILF3	Q12906	0.017	0.083	0.082	4.0	4.0	4.0	4.0
VANGL1	Q8TAA9	0.020	0.112	0.110	4.5	3.5	3.5	3.5
RPL31	B7Z4C8	0.045	0.283	0.275	2.0	2.0	2.0	2.0
PTBP1	P26599	0.046	0.288	0.279	12.0	12.0	7.0	6.0
CPS1	P31327	0.061	0.215	0.206	20.0	21.5	17.0	16.0
INPPL1	O15357	0.068	0.090	0.086	7.0	7.0	7.0	6.0
RPS12	P25398	0.099	0.413	0.386	2.5	2.5	2.0	2.0

Appendix 1 – Table showing relative protein abundance in C- & N2-Src LC/MS/MS experiments

Gene name	Accession	Log change %emPAI	C-Src %emPAI AVG	N2-Src %emPAI AVG	C-Src Sig mat AVG	N2 Sig mat AVG	C-Src Sig Seq AVG	N2-Sig Seq AVG
RPS16	M0R210	0.100	1.266	1.181	9.0	8.5	5.0	5.0
DAB2	P98082	0.125	0.119	0.109	6.0	4.5	5.5	4.5
VDAC3	F5H740	0.128	0.250	0.229	4.0	5.0	4.0	3.5
EFTUD2	K7EJ81	0.148	0.037	0.033	2.5	2.0	2.5	2.0
RELA	Q2TAM5	0.180	0.100	0.088	2.5	2.0	2.5	2.0
PARP1	P09874	0.195	0.075	0.066	5.0	4.5	4.5	4.0
C14orf166	Q9Y224	0.210	0.200	0.173	3.0	2.5	3.0	2.5
COPA	P53621	0.215	0.042	0.036	3.5	3.0	3.5	3.0
RPN1	P04843	0.228	0.184	0.157	7.5	6.0	6.5	5.0
IPO5	H0Y8C6	0.235	0.077	0.065	6.0	4.5	6.0	4.5
HNRNPR	O43390	0.243	0.122	0.103	5.0	5.0	4.0	4.0
ARHGEF10	H0YAN8	0.246	0.037	0.031	3.0	2.0	2.5	2.0
RPL23	J3KT29	0.258	0.379	0.317	3.0	2.0	2.0	1.5
VCP	P55072	0.261	3.623	3.025	114.5	92.0	41.0	37.0
UBAP2L	F8W726	0.270	0.088	0.073	5.5	6.0	5.5	4.0
DRG1	Q9Y295	0.277	0.173	0.143	3.5	3.0	3.5	3.0
CANX	B4DGP8	0.283	0.045	0.037	3.0	3.0	2.0	1.5
TRIM25	Q14258	0.283	0.045	0.037	2.0	1.5	2.0	1.5
CCT4	B7Z2F4	0.292	0.192	0.157	4.5	4.0	4.0	3.0
PA2G4	Q9UQ80	0.315	0.170	0.137	4.5	2.5	4.0	2.5
RPL18A	M0R0P7	0.320	0.315	0.253	2.5	2.0	2.5	2.0
DHX15	O43143	0.320	0.084	0.067	4.5	3.5	3.5	3.0
U2AF2	K7ENG2	0.345	0.100	0.079	2.0	1.5	2.0	1.5

Appendix 1 – Table showing relative protein abundance in C- & N2-Src LC/MS/MS experiments

Gene name	Accession	Log change %emPAI	C-Src %emPAI AVG	N2-Src %emPAI AVG	C-Src Sig mat AVG	N2 Sig mat AVG	C-Src Sig Seq AVG	N2-Sig Seq AVG
CTNNA1	G3XAM7	0.346	0.075	0.059	5.0	4.0	3.5	2.0
TUBA1A	Q71U36	0.350	1.321	1.036	51.0	39.5	14.5	12.5
GNL3	Q9BVP2	0.362	0.072	0.056	3.0	2.0	2.0	2.0
RPL14	E7EPB3	0.366	0.359	0.279	3.0	2.5	2.5	2.0
SLC25A3	F8VVM2	0.376	0.095	0.073	2.0	1.5	2.0	1.5
DDX1	Q92499	0.388	0.086	0.065	4.0	3.0	4.0	3.0
RPS4X	P62701	0.414	0.642	0.482	9.0	6.5	7.5	6.0
EZR	E7EQR4	0.415	0.298	0.223	10.5	7.0	8.5	6.0
CCT3	B4DUR8	0.426	0.163	0.121	6.5	3.5	5.0	3.5
RPL13	P26373	0.426	0.196	0.146	2.5	2.0	2.5	1.5
DHX9	Q08211	0.438	0.105	0.078	8.5	6.0	7.5	6.0
DDX6	P26196	0.444	0.119	0.088	3.5	3.0	2.5	2.5
KRT10	P13645	0.474	0.127	0.091	4.0	3.0	4.0	3.0
PLEC	Q15149	0.483	0.014	0.010	5.0	3.5	4.5	3.5
ATAD3A	H0Y2W2	0.484	0.140	0.100	6.0	4.0	5.0	3.5
CCT5	B4DYD8	0.484	0.070	0.050	2.0	2.0	2.0	1.5
KHDRBS1	Q07666	0.487	0.169	0.121	4.0	4.0	3.5	2.5
RBM14	Q96PK6	0.514	0.078	0.055	3.0	2.0	3.0	2.0
HNRNPH1	G8JLB6	0.545	0.288	0.198	10.0	13.0	5.5	4.0
HNRNPD	H0Y8G5	0.546	0.129	0.088	2.0	1.5	2.0	1.5
HSPA8	P11142	0.548	0.810	0.554	25.0	21.5	17.0	13.0
DDB1	Q16531	0.588	0.079	0.052	6.5	5.0	6.0	4.0
DYNC1H1	Q14204	0.588	0.007	0.005	3.0	2.0	3.0	2.0

Appendix 1 – Table showing relative protein abundance in C- & N2-Src LC/MS/MS experiments

Gene name	Accession	Log change %emPAI	C-Src %emPAI AVG	N2-Src %emPAI AVG	C-Src Sig mat AVG	N2 Sig mat AVG	C-Src Sig Seq AVG	N2-Sig Seq AVG
MYBBP1A	I3L1L3	0.596	0.031	0.020	2.5	1.5	2.5	1.5
HNRNPM	P52272	0.600	0.085	0.056	3.5	2.5	3.5	2.0
HIST1H4A	P62805	0.604	1.959	1.289	6.0	3.5	5.5	3.0
HNRNPA1	F8W6I7	0.636	0.570	0.367	9.5	5.5	7.0	5.0
MOV10	Q5JR04	0.643	0.037	0.024	2.0	1.5	2.0	1.5
TUBA4A	A8MUB1	0.652	1.135	0.722	50.0	36.0	12.5	9.5
DNAJC10	Q8IXB1	0.671	0.046	0.029	2.5	1.5	2.5	1.5
TUBB4B	P68371	0.680	2.450	1.529	55.5	36.5	20.5	16.5
RPL9	D6RAN4	0.687	0.280	0.174	3.0	1.5	2.5	1.5
SYNCRIP	O60506	0.748	0.283	0.168	11.0	8.0	9.0	5.5
SERBP1	Q8NC51	0.761	0.140	0.082	3.5	2.0	3.0	2.0
DHX36	F5GZS0	0.799	0.054	0.031	3.5	2.0	3.5	2.0
NUDT21	O43809	0.844	0.266	0.148	3.5	2.5	3.5	2.0
DDX17	C9JMU5	0.847	0.180	0.100	7.0	4.0	7.0	4.0
NONO	Q15233	0.849	0.285	0.158	8.0	4.5	5.0	2.5
G3BP1	Q13283	0.864	0.305	0.168	12.0	5.0	6.0	3.0
IARS	J3KR24	0.887	0.034	0.018	2.5	1.5	2.5	1.5
DDX21	Q9NR30	0.913	0.083	0.044	4.0	2.5	4.0	2.0
NUPL1	Q5JRG1	0.925	0.105	0.055	3.0	1.5	3.0	1.5
SFPQ	P23246	0.934	0.213	0.112	10.0	4.5	7.0	3.5
TMPO	P42167	0.956	0.223	0.115	6.5	3.0	6.0	2.5
HNRNPK	Q5T6W5	1.010	0.288	0.143	8.0	4.5	6.5	3.5
SNRNP200	O75643	1.020	0.019	0.010	3.0	1.5	3.0	1.5

Appendix 1 – Table showing relative protein abundance in C- & N2-Src LC/MS/MS experiments

Gene name	Accession	Log change %emPAI	C-Src %emPAI AVG	N2-Src %emPAI AVG	C-Src Sig mat AVG	N2 Sig mat AVG	C-Src Sig Seq AVG	N2-Sig Seq AVG
DBNL	Q9UJU6	1.020	0.189	0.093	5.0	2.0	5.0	2.0
PABPC4	B1ANR0	1.020	0.420	0.207	13.5	11.5	10.5	5.5
REL	Q17RU2	1.024	0.179	0.088	7.0	4.0	6.0	3.0
TUBB	P07437	1.039	3.282	1.597	63.0	25.5	21.5	10.5
RPS3	P23396	1.069	0.510	0.243	6.5	3.0	6.0	3.0
VDAC1	P21796	1.069	0.115	0.055	2.0	2.0	2.0	1.0
MCM7	P33993	1.069	0.040	0.019	2.0	1.0	2.0	1.0
G3BP2	Q9UN86	1.099	0.193	0.090	5.5	2.5	4.5	2.0
SLITRK5	O94991	1.102	0.087	0.040	7.0	3.0	5.0	2.5
BUB3	J3QT28	1.105	0.118	0.055	2.0	1.0	2.0	1.0
XRCC5	P13010	1.107	0.265	0.123	11.0	6.0	10.5	5.5
ANKRD17	H0YM23	1.139	0.034	0.016	5.0	2.0	5.0	1.5
TUBA8	V9GZ17	1.178	0.510	0.226	10.5	5.5	5.0	3.5
ROBO1	Q9Y6N7	1.184	0.095	0.042	9.5	5.5	9.0	4.5
ATP5O	P48047	1.201	0.269	0.117	3.5	1.5	2.5	1.0
ATP5A1	P25705	1.242	0.299	0.126	9.5	5.0	8.5	4.0
ASS1	P00966	1.323	0.426	0.170	9.5	4.5	8.5	4.0
UPF1	Q92900	1.332	0.081	0.032	6.0	2.0	5.5	2.0
LARP1	Q6PKG0	1.347	0.049	0.019	3.5	1.5	3.5	1.5
EIF2S3L	Q2VIR3	1.414	0.108	0.040	4.0	1.0	3.0	1.0
HNRNPF	P52597	1.490	0.154	0.055	6.0	3.0	2.5	1.0
AFAP1	Q8N556	1.524	0.091	0.031	4.0	1.5	4.0	1.5
EEF1G	B4DTG2	1.529	0.095	0.033	3.0	1.0	3.0	1.0

Appendix 1 – Table showing relative protein abundance in C- & N2-Src LC/MS/MS experiments

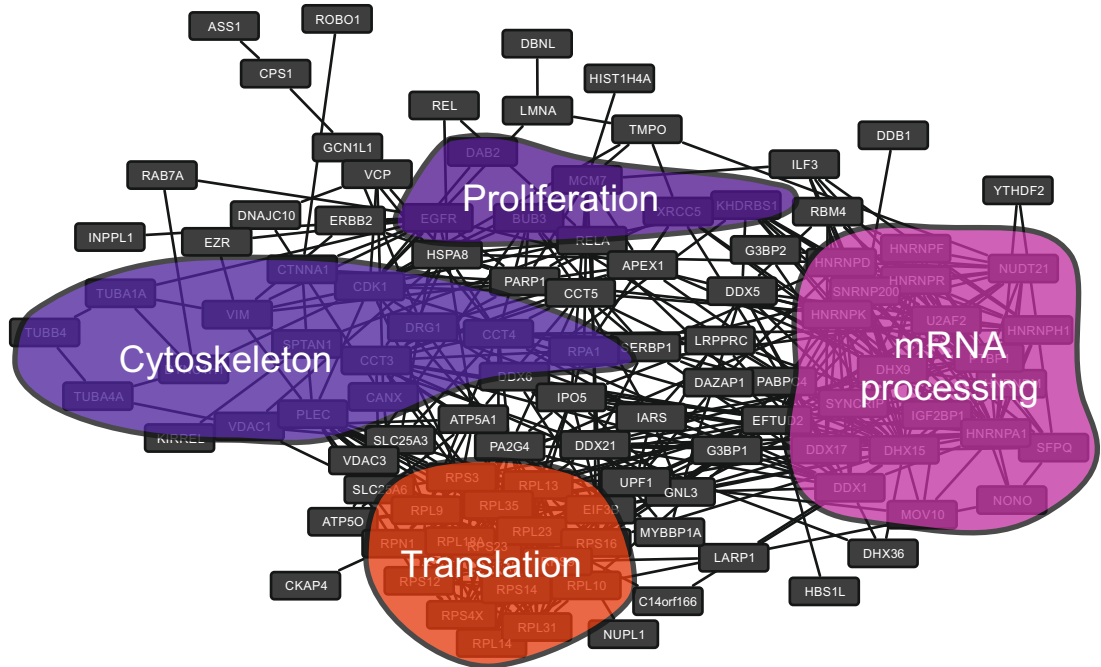
Gene name	Accession	Log change %emPAI	C-Src %emPAI AVG	N2-Src %emPAI AVG	C-Src Sig mat AVG	N2 Sig mat AVG	C-Src Sig Seq AVG	N2-Sig Seq AVG
ERBB2	J3QLU9	1.583	0.079	0.026	6.0	2.0	5.5	2.0
RPA1	P27694	1.587	0.140	0.047	6.0	2.0	5.5	1.5
EGFR	P00533	1.851	0.291	0.081	23.0	6.0	16.5	4.0
RPS23	P62266	2.076	0.472	0.112	3.5	1.0	3.5	1.0
APEX1	P27695	2.147	0.095	0.021	2.0	0.5	2.0	0.5
SPTAN1	A6NG51	2.173	0.022	0.005	4.0	1.0	4.0	1.0
CKAP4	Q07065	2.402	0.063	0.012	2.5	0.5	2.0	0.5
IGF2BP1	Q9NZI8	2.473	0.086	0.016	3.0	0.5	2.5	0.5
HBS1L	H0YDX7	2.596	0.072	0.012	2.5	0.5	2.5	0.5
GIT2	F8VXI9	2.898	0.142	0.019	5.5	1.0	5.0	1.0
LMNA	P02545	3.281	0.725	0.075	23.5	2.5	16.5	2.5
LRPPRC	P42704	3.690	0.080	0.006	7.5	0.5	7.5	0.5
VIM	B0YJC4	n/a	0.171	0.000	4.5	0.0	4.5	0.0
RPS9	B5MCT8	n/a	0.539	0.000	4.5	0.0	4.0	0.0
RPS14	H0YB22	n/a	0.554	0.000	3.0	0.0	3.0	0.0
RPL10	H7C123	n/a	0.534	0.000	2.5	0.0	2.0	0.0
DDX5	J3KTA4	n/a	0.394	0.000	13.0	0.0	11.5	0.0
CDK1	P06493	n/a	0.225	0.000	4.0	0.0	4.0	0.0
SLC25A6	P12236	n/a	0.305	0.000	6.0	0.0	4.5	0.0
RPL35	P42766	n/a	0.260	0.000	2.0	0.0	2.0	0.0
RAB7A	P51149	n/a	0.150	0.000	2.0	0.0	2.0	0.0
EIF3B	P55884	n/a	0.044	0.000	2.5	0.0	2.5	0.0
TRIP10	Q15642	n/a	0.205	0.000	7.5	0.0	7.0	0.0

Appendix 1 – Table showing relative protein abundance in C- & N2-Src LC/MS/MS experiments

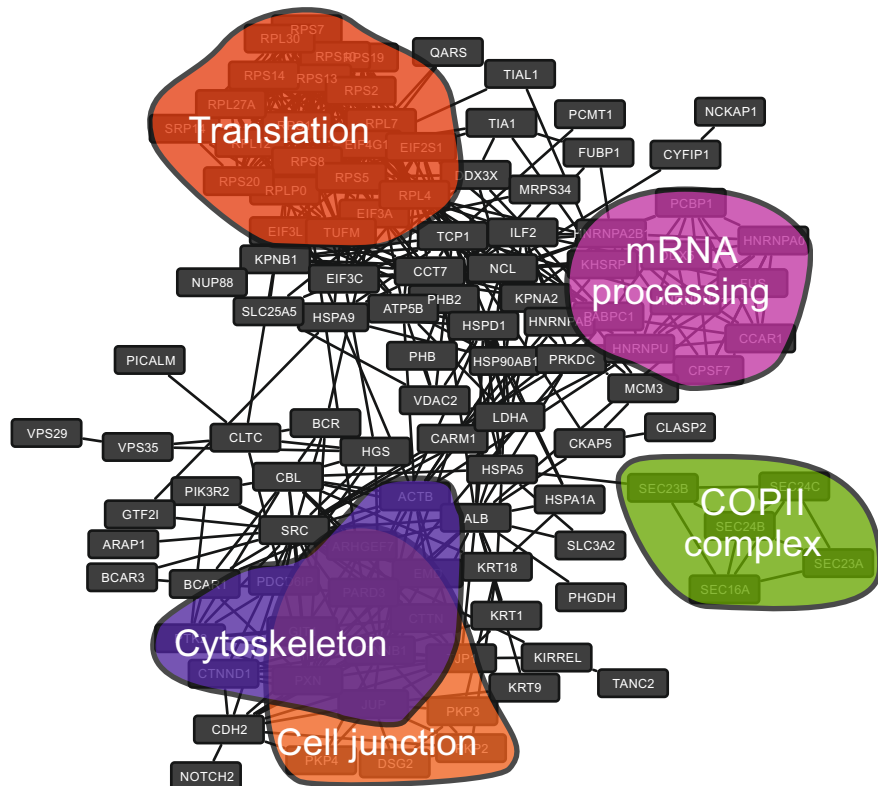
Gene name	Accession	Log change %emPAI	C-Src %emPAI AVG	N2-Src %emPAI AVG	C-Src Sig mat AVG	N2 Sig mat AVG	C-Src Sig Seq AVG	N2-Sig Seq AVG
GCN1L1	Q92616	n/a	0.019	0.000	4.5	0.0	3.5	0.0
DAZAP1	Q96EP5	n/a	0.114	0.000	2.5	0.0	2.5	0.0
KIRREL	Q96J84	n/a	0.169	0.000	8.5	0.0	7.0	0.0
YTHDF2	Q9Y5A9	n/a	0.055	0.000	2.0	0.0	2.0	0.0

Appendix 2 - STRING interaction network including gene names

A



B



Appendix 3 – Table showing C-Src STRING interaction network

Node 1	Node 2	Neighborhood	Fusion	Cooccurrence	Homology	Coexpression	Experimental	Knowledge	Textmining	Combined score
RPS9	RPS23	0.255	0	0	0	0.803	0.669	0.9	0.349	0.995
RELA	DDX21	0	0	0	0	0	0.139	0	0.563	0.598
HNRNPK	HNRNPD	0	0	0	0	0.292	0.974	0.9	0.54	0.998
DHX9	EFTUD2	0	0	0	0	0	0	0.9	0.087	0.902
DHX15	U2AF2	0	0	0	0	0.118	0.231	0	0.378	0.52
UPF1	DDX5	0	0	0	0	0	0.388	0	0.092	0.406
CPS1	ASS1	0.539	0.326	0	0	0.524	0	0	0.675	0.941
HNRNPR	HNRNPA1	0	0	0	0.7	0.134	0.736	0	0.271	0.772
RPL23	IPO5	0	0	0	0	0	0.62	0	0.168	0.662
RPS9	RPN1	0	0	0	0	0.072	0	0.9	0.065	0.901
HNRNPM	SNRNP200	0	0	0	0	0.071	0	0.9	0.258	0.921
GNL3	CCT3	0	0	0	0	0.514	0	0	0	0.514
RPL31	RPN1	0	0	0	0	0	0	0.9	0	0.899
CCT3	RPL35	0	0	0	0	0.337	0.238	0	0	0.461
DHX15	LRPPRC	0	0	0	0	0.459	0	0	0	0.46
RPL31	EIF3B	0	0	0	0	0.124	0	0.9	0	0.906
SFPQ	U2AF2	0	0	0	0	0	0.62	0	0.284	0.709
RPL9	RPS14	0.41	0	0	0	0.937	0.58	0.9	0.379	0.998
DNAJC10	CANX	0	0	0	0	0.187	0	0	0.604	0.656
RPS14	RPS3	0.41	0	0	0	0.959	0.744	0.9	0.524	0.999
DHX9	DDX21	0	0	0	0	0.257	0.62	0	0.261	0.762
RELA	DDX1	0	0	0	0	0	0.621	0	0.8	0.919
DHX9	XRCC5	0	0	0	0	0.216	0.937	0	0.17	0.953

Appendix 3 – Table showing C-Src STRING interaction network

Node 1	Node 2	Neighborhood	Fusion	Cooccurrence	Homology	Coexpression	Experimental	Knowledge	Textmining	Combined score
DHX9	U2AF2	0	0	0	0	0	0	0.9	0.215	0.916
HNRNPM	RBM4	0	0	0	0	0.092	0.997	0	0	0.997
CDK1	EGFR	0	0	0	0.717	0	0.394	0	0.44	0.462
EIF3B	RPS9	0	0	0	0	0.226	0	0.9	0	0.917
RPL31	RPS9	0	0	0	0	0.589	0	0.9	0.341	0.969
RPS9	RPL18A	0	0	0	0	0.894	0.58	0.9	0.161	0.995
RPS23	RPS16	0.243	0	0	0	0.915	0.735	0.9	0.239	0.998
EFTUD2	RPL35	0.265	0	0	0	0.16	0.29	0	0	0.501
DHX9	RBM4	0	0	0	0	0	0.974	0	0	0.974
PARP1	MCM7	0	0	0	0	0.442	0	0	0.168	0.505
CDK1	PA2G4	0	0	0	0	0.165	0.62	0	0.071	0.664
HNRNPA1	LRPPRC	0	0	0	0	0.189	0.425	0	0.817	0.903
ILF3	PTBP1	0	0	0	0	0.238	0	0	0.379	0.495
RPL10	RPL18A	0	0	0	0	0.607	0.352	0	0.239	0.779
DDX21	DDX1	0	0	0.5	0.629	0.354	0	0	0.241	0.503
SFPQ	HNRNPA1	0	0	0	0.535	0.205	0.425	0	0.308	0.571
RPL23	RPS23	0.41	0	0	0	0.906	0	0.9	0.241	0.994
DHX9	HNRNPH1	0	0	0	0	0.39	0	0	0.106	0.418
HNRNPM	U2AF2	0	0	0	0	0	0	0.9	0.269	0.921
SLC25A6	SLC25A3	0	0	0	0.672	0.499	0.141	0	0.23	0.568
RPL10	RPL35	0.341	0	0	0	0.568	0.387	0	0.379	0.868
PTBP1	PA2G4	0	0	0	0	0.08	0.357	0	0.144	0.424
HNRNPD	EFTUD2	0	0	0	0	0.067	0.136	0.9	0.108	0.912

Appendix 3 – Table showing C-Src STRING interaction network

Node 1	Node 2	Neighborhood	Fusion	Cooccurrence	Homology	Coexpression	Experimental	Knowledge	Textmining	Combined score
U2AF2	NUDT21	0	0	0	0	0	0	0.9	0.202	0.914
BUB3	MCM7	0	0	0	0	0.664	0	0	0.204	0.714
RPS4X	RPL18A	0	0	0	0	0.762	0.35	0	0.305	0.877
SFPQ	HNRNPH1	0	0	0	0	0.585	0	0	0.309	0.694
SYNCRIP	HNRNPH1	0	0	0	0.544	0.24	0.658	0	0.27	0.75
EIF3B	RPL18A	0	0	0	0	0.224	0	0.9	0	0.917
EIF3B	PA2G4	0	0	0	0	0.625	0	0	0	0.625
HNRNPM	HNRNPD	0	0	0	0.613	0.252	0	0.9	0.343	0.929
PARP1	EGFR	0	0	0	0	0	0	0	0.528	0.528
IPO5	DDX1	0	0	0	0	0.439	0	0	0	0.439
DDX17	HNRNPH1	0	0	0	0	0.174	0.68	0	0.309	0.792
HNRNPK	DDX1	0	0	0	0	0.214	0.621	0	0.275	0.754
HNRNPR	SNRNP200	0	0	0	0	0.068	0	0.9	0	0.9
DHX9	IGF2BP1	0	0	0	0	0	0	0.9	0.236	0.918
ATP5A1	VDAC1	0	0	0	0	0.321	0.16	0	0.22	0.493
RPL35	RPS12	0.068	0	0	0	0.775	0.385	0	0.38	0.903
EGFR	RAB7A	0	0	0	0	0	0.621	0	0.079	0.627
PA2G4	IPO5	0	0	0	0	0.169	0.358	0	0.081	0.442
UPF1	DAZAP1	0	0	0	0	0.103	0.58	0	0.071	0.602
CCT3	APEX1	0	0	0	0	0.58	0	0	0	0.581
RPL23	PA2G4	0.357	0	0	0	0.308	0	0	0.1	0.545
RPL31	RPL18A	0.378	0	0	0	0.666	0.384	0.9	0.306	0.988
RPL31	RPS3	0	0	0	0	0.804	0	0.9	0.318	0.984

Appendix 3 – Table showing C-Src STRING interaction network

Node 1	Node 2	Neighborhood	Fusion	Cooccurrence	Homology	Coexpression	Experimental	Knowledge	Textmining	Combined score
RPS23	UPF1	0	0	0	0	0	0	0.9	0	0.899
PLEC	RPL18A	0	0	0	0	0.551	0	0	0	0.551
RPS4X	RPS9	0	0	0	0	0.715	0.386	0	0.224	0.845
ATP50	ATP5A1	0.472	0	0.268	0	0.637	0.8	0.9	0.721	0.998
ATP50	RPL35	0	0	0	0	0.404	0	0	0.1	0.428
DHX36	DDX1	0	0	0	0	0.256	0	0	0.413	0.534
NUDT21	EFTUD2	0	0	0	0	0.077	0	0.9	0.087	0.904
RPS4X	RPL10	0	0	0	0	0.702	0.226	0	0.112	0.767
HNRNPK	HNRNPR	0	0	0	0	0.35	0	0.9	0.29	0.947
HNRNPH1	DDX5	0	0	0	0	0.569	0.996	0	0.258	0.998
HNRNPK	DHX15	0	0	0	0	0.541	0	0	0.065	0.542
RPL14	RPS3	0.186	0	0	0	0.865	0.384	0	0.499	0.959
DRG1	APEX1	0	0	0	0	0.416	0	0	0	0.416
ILF3	HNRNPA1	0	0	0	0	0	0.571	0	0.379	0.715
GNL3	IARS	0	0	0	0	0.45	0	0	0	0.45
HNRNPM	EFTUD2	0	0	0	0	0.112	0	0.9	0.183	0.917
DHX15	CCT5	0	0	0	0	0.494	0	0	0	0.494
CCT4	IARS	0.1	0	0	0	0.49	0	0	0.182	0.572
YTHDF2	HNRNPH1	0	0	0	0	0.087	0.721	0	0	0.728
EZR	EGFR	0	0	0	0	0	0.621	0	0.877	0.95
UPF1	RPL18A	0	0	0	0	0	0	0.9	0	0.899
ILF3	DHX9	0	0	0	0	0.329	0.621	0	0.537	0.866
RPL23	RPL18A	0	0	0	0	0.779	0.387	0.9	0.264	0.987

Appendix 3 – Table showing C-Src STRING interaction network

Node 1	Node 2	Neighborhood	Fusion	Cooccurrence	Homology	Coexpression	Experimental	Knowledge	Textmining	Combined score
HNRNPH1	HNRNPF	0	0	0	0.965	0.128	0.621	0	0.675	0.655
MOV10	HNRNPA1	0	0	0	0	0	0.571	0	0	0.571
RPS3	RPS12	0.071	0	0	0	0.855	0.58	0	0.331	0.954
RPL23	C14orf166	0	0	0	0	0.449	0	0	0	0.449
RELA	SPTAN1	0	0	0	0	0	0	0	0.504	0.504
CCT3	PARP1	0	0	0	0	0.691	0	0	0.086	0.699
HNRNPK	PARP1	0	0	0	0	0.066	0	0	0.824	0.825
PTBP1	HNRNPM	0	0	0	0	0	0	0.9	0.42	0.938
MCM7	APEX1	0	0	0	0	0.444	0	0	0.08	0.455
HNRNPK	NUDT21	0	0	0	0	0.188	0	0.9	0.107	0.917
VDAC1	TUBA4A	0	0	0	0	0	0.621	0	0	0.621
RPS14	RPS9	0.357	0	0	0	0.862	0.671	0.9	0.371	0.997
MCM7	RPA1	0	0	0	0	0.723	0.923	0	0.187	0.98
DDX17	U2AF2	0	0	0	0	0	0.974	0	0.201	0.977
LARP1	RPS9	0	0	0	0	0.097	0.388	0	0	0.41
RPL13	RPL18A	0	0	0	0	0.82	0.735	0	0.273	0.96
DHX9	KHDRBS1	0	0	0	0	0.11	0.993	0	0.156	0.994
RPS14	RPS12	0.082	0	0	0	0.878	0.58	0	0.374	0.964
LARP1	DHX15	0	0	0	0	0.091	0.388	0	0	0.406
DYNC1H1	TUBA1A	0	0	0	0	0	0.116	0.8	0.332	0.865
RPL23	RPS14	0.41	0	0.259	0	0.896	0	0.9	0.271	0.995
G3BP1	IGF2BP1	0	0	0	0	0	0	0	0.411	0.411
RPS9	EFTUD2	0.181	0	0	0	0.266	0.295	0	0	0.518

Appendix 3 – Table showing C-Src STRING interaction network

Node 1	Node 2	Neighborhood	Fusion	Cooccurrence	Homology	Coexpression	Experimental	Knowledge	Textmining	Combined score
G3BP1	HNRNPA1	0	0	0	0.635	0.07	0.425	0	0.274	0.476
EIF3B	RPS3	0	0	0	0	0.175	0	0.9	0.092	0.914
DHX9	PTBP1	0	0	0	0	0.183	0	0.9	0.203	0.925
DDX17	UPF1	0	0	0	0	0	0.388	0	0.092	0.406
LMNA	TMPO	0	0	0	0	0.085	0.846	0	0.585	0.933
HNRNPK	KHDRBS1	0	0	0	0	0.159	0.993	0	0.66	0.997
HNRNPR	HNRNPF	0	0	0	0	0.077	0	0.9	0.238	0.919
RPS14	RPL18A	0	0	0	0	0.828	0.58	0.9	0.122	0.992
SYNCRIP	DHX15	0	0	0	0	0.574	0	0	0	0.574
SERBP1	DDX21	0	0	0	0	0.435	0	0	0.073	0.442
RPL14	RPL10	0.079	0	0	0	0.425	0.231	0	0.342	0.674
HNRNPF	U2AF2	0	0	0	0	0	0	0.9	0.513	0.948
RELA	PARP1	0	0	0	0	0	0.939	0	0.87	0.991
RPL13	IPO5	0	0	0	0	0.071	0.62	0	0	0.623
HNRNPF	EFTUD2	0	0	0	0	0	0	0.9	0.065	0.9
CCT4	GCN1L1	0	0	0	0	0	0.667	0	0	0.667
RPS14	EFTUD2	0.194	0	0	0	0.309	0.295	0	0	0.553
RPL23	RPL13	0	0	0	0	0.852	0.387	0	0.33	0.931
RPL31	RPS12	0	0	0	0	0.793	0.238	0	0.307	0.876
HNRNPR	PTBP1	0	0	0	0	0	0	0.9	0.201	0.914
RPL23	EFTUD2	0.329	0	0	0	0.308	0.29	0	0.104	0.641
DHX15	EFTUD2	0	0	0	0	0.093	0.492	0	0.272	0.618
KHDRBS1	HNRNPD	0	0	0	0	0.29	0	0	0.3	0.47

Appendix 3 – Table showing C-Src STRING interaction network

Node 1	Node 2	Neighborhood	Fusion	Cooccurrence	Homology	Coexpression	Experimental	Knowledge	Textmining	Combined score
SLC25A6	RPL35	0	0	0	0	0.401	0	0	0.076	0.41
RPS23	RPN1	0	0	0	0	0.076	0	0.9	0	0.901
RPL23	RPN1	0	0	0	0	0.078	0	0.9	0	0.901
PARP1	CTNNA1	0	0	0	0	0.4	0	0	0	0.4
EGFR	HSPA8	0	0	0	0	0	0.472	0	0.148	0.52
RPS3	EFTUD2	0.329	0	0	0	0.431	0.388	0	0	0.734
EZR	VIM	0	0	0	0	0	0	0	0.43	0.43
HNRNPF	RBM4	0	0	0	0	0	0.974	0	0.086	0.974
RPL9	RPL13	0	0	0	0	0.801	0.58	0	0.219	0.926
G3BP1	DDX6	0	0	0	0	0.071	0.621	0	0.425	0.769
HNRNPK	G3BP1	0	0	0	0	0.174	0	0	0.319	0.4
IARS	IPO5	0	0	0	0	0.494	0	0	0	0.494
RPS23	RPS12	0.212	0	0	0	0.866	0.58	0	0.371	0.966
CCT4	SLC25A3	0	0	0	0	0.404	0.292	0	0	0.55
RPL23	RPL14	0.188	0	0	0	0.826	0.266	0	0.306	0.913
ILF3	HNRNPD	0	0	0	0	0.208	0	0	0.341	0.443
RPS3	RPS16	0.253	0	0	0	0.922	0.744	0.9	0.498	0.999
GNL3	SYNCRIP	0	0	0	0	0.436	0	0	0	0.436
CCT4	LRPPRC	0	0	0	0	0.426	0	0	0	0.426
RPS12	RPL18A	0	0	0	0	0.7	0.231	0	0.243	0.801
PTBP1	NUDT21	0	0	0	0	0	0	0.9	0.094	0.903
CCT3	RPS3	0	0	0	0	0.39	0	0	0.122	0.428
UPF1	RPS16	0	0	0	0	0	0	0.9	0.078	0.901

Appendix 3 – Table showing C-Src STRING interaction network

Node 1	Node 2	Neighborhood	Fusion	Cooccurrence	Homology	Coexpression	Experimental	Knowledge	Textmining	Combined score
TUBA1A	VIM	0	0	0	0	0.066	0	0	0.434	0.436
BUB3	DHX15	0	0	0	0	0.45	0	0	0	0.45
SERBP1	DDX1	0	0	0	0	0.487	0	0	0	0.487
HNRNPA1	XRCC5	0	0	0	0	0.186	0.425	0	0	0.5
CDK1	CCT5	0	0	0	0	0.373	0	0	0.128	0.417
SLC25A6	RPL18A	0	0	0	0	0.593	0	0	0.078	0.6
PLEC	RPS23	0	0	0	0	0.55	0.488	0	0	0.754
EGFR	VIM	0	0	0	0	0	0	0	0.693	0.693
RPL9	RPS3	0.472	0	0	0	0.936	0.653	0.9	0.429	0.999
DHX9	HNRNPF	0	0	0	0	0	0	0.9	0.179	0.912
RPL14	RPL13	0	0	0	0	0.748	0.489	0	0.273	0.893
SYNCRIP	SFPQ	0	0	0	0.524	0.383	0	0	0.201	0.427
CCT3	EIF3B	0	0	0	0	0.482	0	0	0	0.482
LMNA	CDK1	0	0	0	0	0.114	0.621	0	0.447	0.788
RPL23	RPS3	0.472	0	0	0	0.89	0	0.9	0.424	0.995
CCT5	HSPA8	0.08	0	0	0	0.443	0	0	0.211	0.54
U2AF2	NONO	0	0	0	0.518	0	0.62	0	0.275	0.661
SYNCRIP	HNRNPD	0	0	0	0.673	0.311	0.846	0	0.341	0.898
HNRNPF	NUDT21	0	0	0	0	0.087	0	0.9	0	0.902
CCT4	BUB3	0	0	0	0	0.533	0	0	0	0.533
SERBP1	SYNCRIP	0	0	0	0	0.58	0	0	0.128	0.609
RPS14	RPS16	0.357	0	0	0	0.905	0.74	0.9	0.379	0.998
KHDRBS1	DDX5	0	0	0	0	0.107	0.974	0	0.2	0.978

Appendix 3 – Table showing C-Src STRING interaction network

Node 1	Node 2	Neighborhood	Fusion	Cooccurrence	Homology	Coexpression	Experimental	Knowledge	Textmining	Combined score
EIF3B	DHX15	0	0	0	0	0.4	0	0	0	0.4
DHX15	HNRNPD	0	0	0	0	0.463	0	0	0.13	0.502
RPS4X	PLEC	0	0	0	0	0.365	0.235	0	0	0.482
HNRNPD	HSPA8	0	0	0	0	0	0.845	0	0.404	0.901
SERBP1	LRPPRC	0	0	0	0	0.485	0	0	0	0.486
RPN1	CANX	0	0	0	0	0.265	0	0	0.47	0.584
MYBBP1A	PA2G4	0	0	0	0	0.567	0.141	0	0	0.604
TUBB4	TUBA4A	0	0	0	0.921	0.104	0	0.8	0	0.808
BUB3	PARP1	0	0	0	0	0.242	0.621	0	0.842	0.948
RPS14	RPL35	0.41	0	0	0	0.91	0.58	0.9	0.379	0.998
SFPQ	KHDRBS1	0	0	0	0	0.347	0	0	0.163	0.417
SPTAN1	PLEC	0	0	0	0.485	0.076	0.845	0	0.104	0.851
SYNCRIP	HNRNPA1	0	0	0	0.704	0.151	0.736	0	0.331	0.781
VCP	CDK1	0	0	0	0	0	0	0	0.806	0.806
RPL14	RPS9	0.16	0	0	0	0.755	0.113	0	0.318	0.849
PLEC	RPS12	0	0	0	0	0.397	0.292	0	0	0.544
RPL13	RPS16	0	0	0	0	0.85	0.58	0	0.34	0.952
HNRNPR	DHX15	0	0	0	0	0.571	0	0	0	0.571
PTBP1	EFTUD2	0	0	0	0	0.077	0	0.9	0.089	0.904
RPL9	UPF1	0	0	0	0	0	0	0.9	0	0.899
PA2G4	RPL35	0.357	0	0	0	0.229	0.228	0	0.078	0.572
HNRNPR	SYNCRIP	0	0	0	0.968	0.575	0	0	0.426	0.58
MYBBP1A	EIF3B	0	0	0	0	0.548	0	0	0	0.548

Appendix 3 – Table showing C-Src STRING interaction network

Node 1	Node 2	Neighborhood	Fusion	Cooccurrence	Homology	Coexpression	Experimental	Knowledge	Textmining	Combined score
RPL23	EIF3B	0	0	0	0	0.136	0	0.9	0	0.907
RPS4X	RPS16	0	0	0	0	0.763	0.386	0	0.227	0.872
PABPC4	HNRNPA1	0	0	0	0.655	0.103	0.45	0	0.16	0.492
ATP5A1	RPS3	0	0	0	0	0.39	0	0	0.12	0.428
MCM7	IPO5	0	0	0	0	0.358	0	0	0.141	0.412
VCP	HSPA8	0	0	0	0	0.113	0.62	0	0.306	0.733
DDX1	DDX5	0	0	0.51	0.682	0.26	0	0	0.255	0.413
ATP5O	SLC25A3	0	0	0	0	0.382	0	0	0.22	0.486
RPL14	RPL18A	0	0	0	0	0.768	0.489	0	0.198	0.892
RPN1	RPS3	0	0	0	0	0.159	0	0.9	0.22	0.925
DHX15	RPS16	0	0	0	0	0	0.58	0	0	0.58
CCT4	HNRNPH1	0	0	0	0	0.157	0.68	0	0	0.712
DHX9	HNRNPA1	0	0	0	0	0.196	0.425	0	0.309	0.636
SYNCRIP	DHX9	0	0	0	0	0.35	0	0.9	0.197	0.94
CCT3	DHX15	0	0	0	0	0.436	0	0	0	0.437
DHX15	DDX1	0	0	0	0	0.613	0	0	0.136	0.644
HNRNPK	U2AF2	0	0	0	0	0	0.974	0.9	0.41	0.998
RPL14	RPL35	0.184	0	0	0	0.868	0.384	0	0.37	0.949
DHX9	SNRNP200	0	0	0	0	0	0	0.9	0	0.899
SPTAN1	KIRREL	0	0	0	0	0	0	0.9	0	0.899
HNRNPK	SYNCRIP	0	0	0	0	0.29	0.986	0	0.308	0.992
HNRNPA1	DDX5	0	0	0	0	0.088	0.736	0	0.349	0.821
RPS23	RPS3	0.41	0	0	0	0.907	0.732	0.9	0.433	0.998

Appendix 3 – Table showing C-Src STRING interaction network

Node 1	Node 2	Neighborhood	Fusion	Cooccurrence	Homology	Coexpression	Experimental	Knowledge	Textmining	Combined score
RPS9	UPF1	0	0	0	0	0	0	0.9	0.076	0.901
RPL14	RPS23	0	0	0	0	0.829	0.113	0	0.272	0.874
DHX36	DDX21	0	0	0	0	0.329	0	0	0.265	0.474
PLEC	RPL35	0	0	0	0	0.568	0	0	0.11	0.589
RPL13	EFTUD2	0	0	0	0	0.4	0	0	0	0.4
RPL9	RPL18A	0	0	0	0	0.841	0.58	0.9	0.163	0.993
SLC25A6	CCT3	0	0	0	0	0.249	0.14	0	0.374	0.54
EIF3B	UPF1	0	0	0	0	0.121	0.62	0	0.064	0.643
RPN1	RPL18A	0	0	0	0	0	0	0.9	0	0.899
DDX17	XRCC5	0	0	0	0	0	0.62	0	0.13	0.647
HNRNPD	NUDT21	0	0	0	0	0.119	0	0.9	0	0.905
RELA	HSPA8	0	0	0	0	0	0.132	0	0.845	0.856
PLEC	RPS3	0	0	0	0	0.551	0.491	0	0.092	0.764
HNRNPH1	CCT5	0	0	0	0	0.155	0.571	0	0.146	0.647
G3BP2	NUDT21	0	0	0	0	0.434	0	0	0	0.434
RPS4X	RPS23	0	0	0	0	0.772	0.297	0	0.237	0.861
ROBO1	CTNNA1	0	0	0	0	0	0	0.9	0.124	0.906
CCT4	DHX15	0	0	0	0	0.656	0	0	0	0.656
RPS4X	RPS14	0	0	0	0	0.732	0.386	0	0.222	0.855
U2AF2	DDX6	0	0	0	0	0.074	0.62	0	0.07	0.627
VDAC3	ATP5A1	0	0	0	0	0.392	0.16	0	0	0.456
DRG1	DDX1	0	0	0	0	0.325	0.323	0	0	0.513
DHX9	NUDT21	0	0	0	0	0.241	0	0.9	0	0.918

Appendix 3 – Table showing C-Src STRING interaction network

Node 1	Node 2	Neighborhood	Fusion	Cooccurrence	Homology	Coexpression	Experimental	Knowledge	Textmining	Combined score
CANX	HSPA8	0	0	0	0	0.145	0.188	0	0.374	0.505
CCT3	DDX1	0	0	0	0	0.571	0	0	0	0.571
HNRNPA1	IGF2BP1	0	0	0	0	0	0.571	0	0.18	0.624
GNL3	PA2G4	0	0	0	0	0.623	0.577	0	0.22	0.858
DHX15	DDX5	0	0	0	0	0.653	0.188	0	0.272	0.767
PLEC	RPL13	0	0	0	0	0.551	0	0	0.065	0.552
VDAC3	BUB3	0	0	0	0	0.464	0	0	0	0.464
EIF3B	EFTUD2	0	0	0	0	0.606	0.112	0	0.086	0.636
SERBP1	CCT5	0	0	0	0	0.772	0	0	0	0.772
CTNNA1	EGFR	0	0	0	0	0	0.394	0.9	0.202	0.944
RPL13	RPS3	0	0	0	0	0.822	0.6	0	0.308	0.944
VDAC3	SLC25A6	0	0	0	0	0.076	0.113	0.8	0.235	0.847
HNRNPK	HNRNPA1	0	0	0	0	0.181	0.736	0	0.752	0.939
CCT4	SERBP1	0	0	0	0	0.798	0	0	0.067	0.799
RPS14	RPN1	0	0	0	0	0	0	0.9	0.069	0.9
GNL3	DHX15	0	0	0	0	0.648	0.16	0	0	0.685
SNRNP200	DDB1	0	0	0	0	0.116	0.352	0	0.09	0.407
DDX21	RPL18A	0	0	0	0	0	0.658	0	0	0.657
PABPC4	DHX15	0	0	0	0	0.136	0.35	0	0.125	0.441
CCT4	HSPA8	0.08	0	0	0	0.477	0	0	0.102	0.508
ILF3	MCM7	0	0	0	0	0.469	0	0	0	0.469
GNL3	MYBBP1A	0	0	0	0	0.568	0	0	0	0.568
PTBP1	HNRNPA1	0	0	0	0	0	0.425	0	0.752	0.847

Appendix 3 – Table showing C-Src STRING interaction network

Node 1	Node 2	Neighborhood	Fusion	Cooccurrence	Homology	Coexpression	Experimental	Knowledge	Textmining	Combined score
DHX15	IPO5	0	0	0	0	0.684	0	0	0.091	0.694
HNRNPA1	HNRNPF	0	0	0	0	0.154	0.425	0	0.647	0.804
HNRNPD	U2AF2	0	0	0	0	0.071	0.974	0.9	0.196	0.997
RPS23	RPL35	0.367	0	0	0	0.898	0.58	0.9	0.308	0.997
RPL9	PA2G4	0.357	0	0	0	0.271	0.141	0	0.071	0.546
RBM4	U2AF2	0	0	0	0	0.064	0.974	0	0.18	0.977
DHX9	HNRNPD	0	0	0	0	0.176	0	0.9	0.149	0.92
HNRNPD	IGF2BP1	0	0	0	0	0	0	0	0.43	0.43
VCP	CANX	0	0	0	0	0.067	0.929	0	0.725	0.979
RPL13	RPL35	0	0	0	0	0.883	0.58	0	0.412	0.967
RPS23	EFTUD2	0.287	0	0	0	0.23	0.577	0	0	0.736
RPL14	RPS12	0	0	0.247	0	0.685	0.078	0	0.229	0.795
RPL9	RPL10	0.341	0	0	0	0.568	0.387	0	0.377	0.868
IARS	DDX21	0	0	0	0	0.48	0	0	0.171	0.54
RPS9	RPS12	0.072	0	0	0	0.758	0.58	0	0.184	0.906
HNRNPF	HNRNPM	0	0	0	0	0.164	0	0.9	0.379	0.94
HNRNPR	EFTUD2	0	0	0	0	0	0	0.9	0	0.899
RPL10	NONO	0	0	0	0	0.538	0	0	0	0.538
HIST1H4A	MCM7	0	0	0	0	0	0.583	0	0.308	0.692
SERBP1	CCT3	0	0	0	0	0.478	0	0	0	0.478
EIF3B	RPL9	0	0	0	0	0.24	0	0.9	0	0.918
RPL9	RPS23	0.41	0	0	0	0.943	0	0.9	0.426	0.997
HNRNPR	HNRNPM	0	0	0	0	0.222	0	0.9	0.27	0.935

Appendix 3 – Table showing C-Src STRING interaction network

Node 1	Node 2	Neighborhood	Fusion	Cooccurrence	Homology	Coexpression	Experimental	Knowledge	Textmining	Combined score
DDX21	DHX15	0	0	0	0.466	0.598	0.077	0	0	0.604
GNL3	EIF3B	0	0	0	0	0.466	0	0	0	0.466
IARS	CCT5	0.1	0	0	0	0.618	0	0	0	0.633
RPL31	UPF1	0	0	0	0	0	0	0.9	0	0.899
VCP	DNAJC10	0	0	0	0	0	0.115	0	0.386	0.42
INPPL1	EGFR	0	0	0	0	0	0.846	0	0.248	0.876
SLC25A6	RPS3	0	0	0	0	0.554	0	0	0.07	0.558
RPS3	RPL18A	0	0	0	0	0.9	0.6	0.9	0.236	0.996
HNRNPR	NUDT21	0	0	0	0	0.294	0	0.9	0	0.924
HNRNPR	HNRNPD	0	0	0	0.653	0.356	0	0.9	0.306	0.937
GNL3	DDX17	0	0	0	0	0.499	0	0	0.108	0.523
U2AF2	EFTUD2	0	0	0	0	0.067	0	0.9	0.229	0.918
RPL31	RPL14	0	0	0	0	0.614	0.236	0	0.27	0.755
REL	HSPA8	0	0	0	0	0	0.731	0	0.298	0.799
CCT4	PA2G4	0.068	0	0	0	0.401	0	0	0	0.405
VDAC1	SLC25A3	0	0	0	0	0.293	0	0	0.331	0.496
PLEC	RPS14	0	0	0	0	0.545	0.488	0	0	0.752
GNL3	DDX1	0	0	0	0	0.445	0	0	0	0.445
RPL31	RPL13	0	0	0	0	0.64	0.384	0	0.227	0.805
SFPQ	PTBP1	0	0	0	0	0.07	0.974	0	0.318	0.981
HNRNPK	RBM4	0	0	0	0	0.148	0.974	0	0.07	0.976
DDX17	DHX15	0	0	0	0	0.5	0.188	0	0.2	0.631
XRCC5	APEX1	0	0	0	0	0.297	0.621	0	0.319	0.793

Appendix 3 – Table showing C-Src STRING interaction network

Node 1	Node 2	Neighborhood	Fusion	Cooccurrence	Homology	Coexpression	Experimental	Knowledge	Textmining	Combined score
HNRNPK	RPS3	0	0	0	0	0.247	0	0	0.305	0.441
RPL9	ATP50	0.074	0	0	0	0.564	0	0	0.067	0.571
RPL9	SLC25A3	0	0	0	0	0.442	0	0	0	0.442
HNRNPA1	NONO	0	0.002	0	0	0.124	0.425	0	0.318	0.608
IPO5	RPA1	0	0	0	0	0.237	0.358	0	0	0.477
HNRNPH1	HNRNPA1	0	0	0	0.583	0.325	0.736	0	0.656	0.86
RPL23	RPS12	0.064	0	0	0	0.849	0.384	0	0.34	0.93
RPL23	RPL10	0.341	0	0	0	0.568	0.387	0	0.341	0.86
CCT3	EFTUD2	0	0	0	0	0.389	0.115	0	0	0.424
SLC25A6	VDAC1	0	0	0	0	0.076	0.113	0.8	0.514	0.903
RPL23	UPF1	0	0	0	0	0	0	0.9	0.069	0.9
HNRNPA1	SNRNP200	0	0	0	0	0	0.425	0	0.128	0.465
CCT3	HSPA8	0.08	0	0	0	0.36	0.621	0	0.22	0.788
KHDRBS1	CDK1	0	0	0	0	0.108	0.621	0	0.148	0.671
HNRNPF	HNRNPD	0	0	0	0.572	0.075	0.974	0.9	0.378	0.997
RPL35	RPS16	0.231	0	0	0	0.918	0.58	0.9	0.365	0.997
RPS14	RPS23	0.267	0	0	0	0.929	0.716	0.9	0.427	0.998
NUPL1	PA2G4	0	0	0	0	0.066	0.357	0	0.3	0.522
SNRNP200	U2AF2	0	0	0	0	0	0	0.9	0.309	0.926
IARS	UPF1	0	0	0	0	0	0	0	0.552	0.552
RPL31	RPL9	0	0	0	0	0.93	0.495	0.9	0.412	0.997
RPL23	RPL35	0.472	0	0	0	0.896	0.76	0.9	0.331	0.998
CPS1	GCN1L1	0	0	0	0	0.436	0	0	0	0.436

Appendix 3 – Table showing C-Src STRING interaction network

Node 1	Node 2	Neighborhood	Fusion	Cooccurrence	Homology	Coexpression	Experimental	Knowledge	Textmining	Combined score
RPS16	RPS12	0.084	0	0	0	0.848	0.58	0	0.319	0.951
DHX9	DDX5	0	0	0	0	0.114	0.987	0	0.317	0.991
RPL10	RPS16	0.172	0	0	0	0.606	0.352	0	0.43	0.853
DDX17	RBM4	0	0	0	0	0	0.974	0	0.082	0.974
HNRNPH1	HNRNPD	0	0	0	0.613	0.341	0.658	0	0.341	0.787
RPL35	RPL18A	0	0	0	0	0.907	0.58	0.9	0.32	0.996
RPS23	RPL18A	0	0	0	0	0.813	0	0.9	0.227	0.983
SFPQ	DHX15	0	0	0	0	0.463	0	0	0.123	0.497
GNL3	IPO5	0	0	0	0	0.334	0.139	0	0.131	0.434
HNRNPA1	IPO5	0	0	0	0	0.14	0.166	0	0.425	0.53
SPTAN1	CTNNA1	0	0	0	0.438	0	0.621	0	0	0.621
PTBP1	HNRNPD	0	0	0	0	0	0.998	0.9	0.43	0.999
RPL10	RPS23	0.297	0	0	0	0.568	0.114	0	0.341	0.785
MOV10	UPF1	0	0	0	0.631	0	0.384	0	0.569	0.506
RPS4X	RPL35	0.357	0	0	0	0.774	0.35	0	0.26	0.915
PARP1	CDK1	0	0	0	0	0.362	0	0	0.464	0.635
IPO5	LRPPRC	0	0	0	0	0.498	0	0	0.141	0.541
RPS3	RPL35	0.472	0	0	0	0.935	0	0.9	0.331	0.997
DAB2	CDK1	0	0	0	0	0	0.621	0	0	0.621
RPL10	RPS3	0.341	0	0	0	0.568	0.386	0	0.373	0.867
HNRNPR	U2AF2	0	0	0	0	0	0	0.9	0	0.9
DYNC1H1	TUBA4A	0	0	0	0	0	0.116	0.8	0	0.811
SPTAN1	VIM	0	0	0	0	0	0.62	0	0.092	0.631

Appendix 3 – Table showing C-Src STRING interaction network

Node 1	Node 2	Neighborhood	Fusion	Cooccurrence	Homology	Coexpression	Experimental	Knowledge	Textmining	Combined score
HNRNPR	DHX9	0	0	0	0	0.328	0	0.9	0.115	0.932
RPL13	RPS12	0	0	0	0	0.744	0.231	0	0.424	0.871
MOV10	DHX15	0	0	0	0	0	0.384	0	0.237	0.499
XRCC5	RPA1	0	0	0	0	0.12	0.64	0	0.097	0.674
PLEC	VIM	0	0	0	0.608	0	0.845	0	0.669	0.884
KHDRBS1	DDX6	0	0	0	0	0.502	0	0	0.094	0.519
RPS3	SLC25A3	0	0	0	0	0.416	0	0	0	0.416
ILF3	HNRNPH1	0	0	0	0	0.31	0	0	0.275	0.466
RPL31	RPL35	0	0	0	0	0.817	0.495	0.9	0.394	0.993
RPL9	EFTUD2	0.268	0	0	0	0.312	0.29	0	0	0.593
RPL9	ATP5A1	0.074	0	0	0	0.454	0	0	0	0.461
HNRNPK	PTBP1	0	0	0	0	0	0.62	0.9	0.61	0.983
DHX9	DHX15	0	0	0.525	0.769	0.508	0	0	0.23	0.582
HNRNPF	SNRNP200	0	0	0	0	0	0	0.9	0	0.899
HNRNPK	EFTUD2	0	0	0	0	0	0	0.9	0	0.899
CDK1	DDX6	0	0	0	0	0.159	0.384	0	0	0.447
GNL3	DDX5	0	0	0	0	0.528	0	0	0.108	0.552
YTHDF2	HNRNPA1	0	0	0	0	0	0.571	0	0	0.571
EFTUD2	RPS16	0.112	0	0	0	0.398	0.295	0	0	0.571
VDAC1	HSPA8	0	0	0	0	0.3	0	0	0.275	0.458
SERBP1	DHX15	0	0	0	0	0.695	0	0	0	0.695
SPTAN1	DDX21	0	0	0	0	0	0	0	0.515	0.515
TUBA1A	EGFR	0	0	0	0	0	0.584	0	0.216	0.652

Appendix 3 – Table showing C-Src STRING interaction network

Node 1	Node 2	Neighborhood	Fusion	Cooccurrence	Homology	Coexpression	Experimental	Knowledge	Textmining	Combined score
XRCC5	TMPO	0	0	0	0	0.102	0.62	0	0	0.635
DHX15	PA2G4	0	0	0	0	0.429	0.117	0	0	0.462
C14orf166	DDX1	0	0	0	0	0.374	0.64	0.9	0.2	0.978
HNRNPH1	DHX15	0	0	0	0	0.681	0	0	0.09	0.69
SYNCRIP	DDX21	0	0	0	0	0.58	0	0	0	0.58
RPL9	RPL35	0.472	0	0	0	0.935	0.792	0.9	0.235	0.999
DYNC1H1	CDK1	0	0	0	0	0	0.184	0.9	0.159	0.921
CCT4	RPL9	0	0	0	0	0.393	0.078	0	0	0.404
G3BP1	RPS9	0	0	0	0	0	0.388	0	0.092	0.406
HNRNPK	EGFR	0	0	0	0	0	0.394	0	0.147	0.448
MCM7	TMPO	0	0	0	0	0.432	0	0	0	0.433
RPL31	RPS14	0	0	0	0	0.865	0.384	0.9	0.341	0.993
RPL23	RPS4X	0.357	0	0	0	0.725	0	0	0.171	0.834
EGFR	SLC25A3	0	0	0	0	0	0.394	0	0.077	0.403
HNRNPA1	NUDT21	0	0	0	0	0.115	0.425	0	0	0.457
RPL9	RPN1	0	0	0	0	0	0	0.9	0	0.899
HNRNPR	HNRNPH1	0	0	0	0.55	0.49	0	0	0.263	0.539
RPL31	RPL10	0	0	0	0	0.224	0.268	0	0.167	0.462
SLC25A6	RPS9	0	0	0	0	0.405	0	0	0	0.405
SYNCRIP	DDX1	0	0	0	0	0.462	0	0	0.34	0.621
DDX17	DDX5	0	0	0.525	0.956	0	0.998	0	0.658	0.998
SERBP1	HNRNPD	0	0	0	0	0.297	0	0	0.202	0.401
GNL3	DDX21	0	0	0	0	0.702	0	0	0.203	0.747

Appendix 3 – Table showing C-Src STRING interaction network

Node 1	Node 2	Neighborhood	Fusion	Cooccurrence	Homology	Coexpression	Experimental	Knowledge	Textmining	Combined score
RPL9	RPL14	0.21	0	0	0	0.86	0.384	0	0.374	0.948
RPS14	UPF1	0	0	0	0	0	0	0.9	0.08	0.901
CDK1	VIM	0	0	0	0	0.092	0.621	0	0.892	0.957
RPL14	RPS14	0.177	0	0	0	0.843	0.384	0	0.348	0.937
RPL9	RPS16	0.255	0	0	0	0.909	0.58	0.9	0.318	0.997
RPL10	RPS12	0	0	0	0	0.504	0.228	0	0.341	0.712
RPL9	PLEC	0	0	0	0	0.568	0	0	0	0.567
HNRNPA1	HNRNPD	0	0	0.498	0.867	0.359	0.425	0	0.648	0.662
DYNC1H1	RAB7A	0	0	0	0	0	0	0.9	0.065	0.9
DHX15	HNRNPM	0	0	0	0	0.224	0.388	0	0	0.493
TUBA1A	TUBB4	0	0	0	0.922	0.147	0	0.8	0.163	0.819
BUB3	CDK1	0	0	0	0	0.706	0.143	0.9	0.43	0.982
RELA	REL	0	0	0	0.899	0	0.982	0	0.861	0.984
HNRNPR	SERBP1	0	0	0	0	0.555	0	0	0.078	0.563
CDK1	RPS3	0	0	0	0	0	0	0	0.8	0.8
IARS	LRPPRC	0	0	0	0	0.551	0	0	0	0.551
HBS1L	EFTUD2	0.176	0	0.401	0.456	0.154	0.077	0	0	0.411
DDX17	HNRNPK	0	0	0	0	0.096	0.974	0	0.239	0.979
DHX15	APEX1	0	0	0	0	0.445	0	0	0	0.445
RPL31	RPL23	0	0	0	0	0.894	0.492	0.9	0.332	0.995
PARP1	ERBB2	0	0	0	0	0	0	0	0.499	0.499
RPL23	RPL9	0.472	0	0	0	0.92	0.792	0.9	0.317	0.999
PA2G4	RPS3	0.357	0	0	0	0.229	0	0	0.07	0.475

Appendix 3 – Table showing C-Src STRING interaction network

Node 1	Node 2	Neighborhood	Fusion	Cooccurrence	Homology	Coexpression	Experimental	Knowledge	Textmining	Combined score
ERBB2	VIM	0	0	0	0	0	0	0	0.638	0.639
EIF3B	RPL35	0	0	0	0	0.071	0	0.9	0	0.9
RPL31	RPS16	0	0	0	0	0.792	0.384	0.9	0.263	0.988
RELA	DHX9	0	0	0	0	0	0.653	0	0.095	0.665
DHX15	SNRNP200	0	0	0	0	0.123	0.489	0	0.394	0.691
EIF3B	RPS16	0	0	0	0	0.115	0	0.9	0	0.905
RPL23	RPS16	0.253	0	0	0	0.892	0	0.9	0.203	0.992
PTBP1	U2AF2	0	0	0	0	0.152	0	0.9	0.751	0.975
PTBP1	KHDRBS1	0	0	0	0	0	0	0	0.43	0.43
DHX9	HNRNPM	0	0	0	0	0.119	0	0.9	0.158	0.915
RPS9	RPL35	0.305	0	0	0	0.866	0	0.9	0.26	0.991
RPS4X	RPS3	0.357	0	0	0	0.756	0.387	0	0.318	0.92
PARP1	XRCC5	0	0	0	0	0.13	0.995	0	0.29	0.997
RPL23	RPS9	0.41	0	0	0	0.793	0	0.9	0.37	0.99
RPS14	RPL13	0	0	0	0	0.82	0.58	0	0.201	0.931
EIF3B	DDX6	0	0	0	0	0	0.387	0	0.115	0.421
DRG1	PA2G4	0.223	0	0	0	0.546	0	0	0.086	0.633
PLEC	CDK1	0	0	0	0	0	0.621	0	0	0.621
RPL13	RPS23	0	0	0	0	0.84	0	0	0.19	0.862
ATP5A1	CCT5	0	0	0	0	0.479	0	0	0.121	0.512
DDX21	HNRNPA1	0	0	0	0	0.212	0.425	0	0.176	0.574
PARP1	APEX1	0	0	0	0	0.289	0	0	0.319	0.483
PTBP1	SNRNP200	0	0	0	0	0	0	0.9	0	0.899

Appendix 3 – Table showing C-Src STRING interaction network

Node 1	Node 2	Neighborhood	Fusion	Cooccurrence	Homology	Coexpression	Experimental	Knowledge	Textmining	Combined score
RPL10	RPS9	0.297	0	0	0	0.591	0.352	0	0.261	0.833
DDX6	UPF1	0	0	0	0	0	0.62	0	0.659	0.861
DDX6	EFTUD2	0	0	0	0	0	0.744	0	0	0.744
RPS9	RPS3	0.41	0	0	0	0.91	0.671	0.9	0.465	0.998
HNRNPM	NUDT21	0	0	0	0	0.071	0	0.9	0.106	0.905
EGFR	ERBB2	0	0	0	0.936	0	0.999	0.9	0.982	0.999
RPS9	PA2G4	0.311	0	0	0	0.268	0	0	0.065	0.463
PA2G4	RPL18A	0	0	0	0	0.154	0.576	0	0.065	0.618
CCT4	DDX1	0	0	0	0	0.482	0	0	0	0.483
ATP5A1	SLC25A3	0	0	0	0	0.769	0	0	0.107	0.781
HNRNPA1	KHDRBS1	0	0	0	0	0.25	0.621	0	0.926	0.976
RPL10	RPS14	0.297	0	0	0	0.568	0.352	0	0.274	0.826
HNRNPA1	DDX1	0	0	0	0	0.133	0.425	0	0.182	0.535
RPL9	RPS12	0	0	0	0	0.88	0.385	0	0.273	0.939
RPS9	RPS16	0.357	0	0	0	0.866	0.671	0.9	0.379	0.997
PLEC	RPS9	0	0	0	0	0.503	0.488	0	0.102	0.74
EIF3B	IPO5	0	0	0	0	0.424	0.235	0	0	0.529
MOV10	IGF2BP1	0	0	0	0	0	0.62	0	0.166	0.661
RPL23	PLEC	0	0	0	0	0.568	0	0	0	0.567
LRPPRC	DDX1	0	0	0	0	0.581	0	0	0	0.581
DDX21	RPS16	0	0	0	0	0	0.636	0	0.155	0.672
SFPQ	NONO	0	0	0	0.944	0.207	0.978	0	0.691	0.982
G3BP2	DHX15	0	0	0	0	0.421	0.115	0	0.088	0.469

Appendix 3 – Table showing C-Src STRING interaction network

Node 1	Node 2	Neighborhood	Fusion	Cooccurrence	Homology	Coexpression	Experimental	Knowledge	Textmining	Combined score
PA2G4	CCT5	0.068	0	0	0	0.572	0	0	0	0.575
HNRNPK	HNRNPH1	0	0	0	0	0.445	0.721	0	0.43	0.899
HNRNPK	HNRNPM	0	0	0	0	0.202	0.238	0.9	0.426	0.957
HNRNPH1	HNRNPM	0	0	0	0	0.365	0.571	0	0.425	0.821
MYBBP1A	DDX21	0	0	0	0	0.399	0	0	0.242	0.513
CCT4	RPL35	0	0	0	0	0.436	0.238	0	0	0.541
RPL31	RPS23	0	0	0	0	0.888	0	0.9	0.462	0.993
HNRNPK	DHX9	0	0	0	0	0.371	0.974	0.9	0.261	0.998
CCT3	PA2G4	0.068	0	0	0	0.676	0	0	0.08	0.684
CDK1	TMPO	0	0	0	0	0.742	0	0	0.144	0.764
UPF1	RPL35	0	0	0	0	0	0	0.9	0	0.899
SYNCRIP	IGF2BP1	0	0	0	0.48	0	0	0.9	0.317	0.914
RBM4	DDX5	0	0	0	0	0	0.974	0	0.161	0.976
EIF3B	RPS23	0	0	0	0	0.122	0	0.9	0	0.906
CCT3	CCT5	0	0	0.525	0.88	0.874	0.648	0.9	0.624	0.995
HNRNPA1	HNRNPM	0	0	0	0.589	0.189	0.736	0	0.507	0.816
RPN1	RPS16	0	0	0	0	0.064	0	0.9	0	0.9
PLEC	RPS16	0	0	0	0	0.545	0.489	0	0	0.752
DHX36	DHX15	0	0	0.525	0.815	0.429	0	0	0.092	0.484
RPS3	UPF1	0	0	0	0	0	0.585	0.9	0.085	0.956
HNRNPK	DDX5	0	0	0	0	0.357	0.974	0	0.19	0.984
DRG1	GCN1L1	0	0	0	0	0.065	0.416	0	0.076	0.426
EIF3B	RPS14	0	0	0	0	0.112	0	0.9	0	0.905

Appendix 3 – Table showing C-Src STRING interaction network

Node 1	Node 2	Neighborhood	Fusion	Cooccurrence	Homology	Coexpression	Experimental	Knowledge	Textmining	Combined score
RPL13	RPS9	0	0	0	0	0.796	0	0	0.378	0.865
CCT4	CCT3	0	0	0.525	0.884	0.906	0.745	0.9	0.379	0.997
CDK1	RPA1	0	0	0	0	0.162	0.845	0	0.17	0.877
HNRNPK	SNRNP200	0	0	0	0	0.076	0	0.9	0	0.901
PARP1	VIM	0	0	0	0	0	0	0	0.864	0.864
RPL9	RPS9	0.41	0	0	0	0.879	0.58	0.9	0.245	0.997
RPL10	RPL13	0	0	0	0	0.607	0.352	0	0.425	0.833
SERBP1	BUB3	0	0	0	0	0.425	0	0	0	0.425
CKAP4	RPN1	0	0	0	0	0.068	0	0.8	0.108	0.81
EIF3B	MCM7	0	0	0	0	0.436	0	0	0.093	0.454
RPS4X	RPL9	0.357	0	0	0	0.823	0	0	0.34	0.914
PTBP1	HNRNPF	0	0	0	0	0	0	0.9	0.563	0.953
SNRNP200	EFTUD2	0	0	0	0	0.092	0.792	0.9	0.318	0.984
RPS16	RPL18A	0	0	0	0	0.869	0.58	0.9	0.366	0.995
SNRNP200	NUDT21	0	0	0	0	0.068	0	0.9	0	0.9
DBNL	LMNA	0	0	0	0	0	0.62	0	0	0.619
MCM7	CDK1	0	0	0	0	0.833	0	0	0.412	0.895
VDAC1	CANX	0	0	0	0	0.331	0	0	0.274	0.481
RPN1	RPL35	0	0	0	0	0.069	0	0.9	0	0.9
DDX17	HNRNPA1	0	0	0	0	0.073	0.736	0	0.317	0.81
RPL31	RPS4X	0	0	0	0	0.542	0	0	0.244	0.631
SNRNP200	HNRNPD	0	0	0	0	0	0	0.9	0	0.899
ATP5A1	HSPA8	0	0	0	0	0.257	0	0	0.272	0.422

Appendix 3 – Table showing C-Src STRING interaction network

Node 1	Node 2	Neighborhood	Fusion	Cooccurrence	Homology	Coexpression	Experimental	Knowledge	Textmining	Combined score
HNRNPK	HNRNPF	0	0	0	0	0.115	0	0.9	0.884	0.988
CCT4	CCT5	0	0	0.525	0.9	0.907	0.644	0.9	0.507	0.996
HNRNPD	DAZAP1	0	0	0	0.825	0.363	0.388	0	0.435	0.613
KHDRBS1	U2AF2	0	0	0	0	0	0.974	0	0.412	0.983
RPS4X	RPS12	0	0	0	0	0.675	0.35	0	0.244	0.819
RPS4X	RPL13	0	0	0.208	0	0.701	0.35	0	0.133	0.838
RPL10	EFTUD2	0.239	0	0.254	0	0.227	0.16	0	0	0.553
HNRNPA1	DHX15	0	0	0	0	0.231	0.425	0	0	0.528
BUB3	CCT5	0	0	0	0	0.523	0	0	0.133	0.559
RPS4X	RPL14	0.118	0	0	0	0.619	0.231	0	0.261	0.768
NUDT21	TMPO	0	0	0	0	0.423	0	0	0	0.423
RPL14	RPS16	0.094	0	0	0	0.76	0.384	0	0.34	0.892

Appendix 4 – Table showing N2-Src STRING interaction network

Node 1	Node 2	Neighborhood	Fusion	Cooccurrence	Homology	Coexpression	Experimental	Knowledge	Textmining	Combined score
DDX3X	EIF2S1	0	0	0	0	0.069	0.83	0	0.14	0.846
HNRNPA0	HNRNPH3	0	0	0.363	0	0.135	0.974	0	0	0.983
ILF2	RPS5	0	0	0	0	0.417	0	0	0	0.417
HSPD1	NCL	0	0	0	0	0.746	0	0	0.165	0.774
HSPD1	TCP1	0	0	0.38	0.56	0.867	0	0	0.612	0.916
HNRNPA0	DDX5	0	0	0	0	0.16	0.974	0	0.078	0.977
RPS10	RPL4	0	0	0	0	0.78	0	0.9	0.424	0.985
RPL12	RPL27A	0.222	0	0	0	0.757	0.582	0.9	0.307	0.992
RPL4	RPS13	0	0	0	0	0.914	0	0.9	0.461	0.994
ILF2	EIF2S1	0	0	0	0	0.166	0	0	0.462	0.521
TIA1	DDX3X	0	0	0	0	0	0.583	0	0.084	0.592
FUBP1	HNRNPA2B1	0	0	0	0	0.362	0	0	0.146	0.419
RPL12	RPL7	0.168	0	0	0	0.68	0.293	0	0.533	0.893
RPS13	RPS5	0	0	0	0	0.937	0.582	0.9	0.379	0.998
RPS10	RPS13	0	0	0	0	0.848	0.489	0.9	0.51	0.995
CPSF7	HNRNPU	0	0	0	0	0	0	0.9	0	0.899
TCP1	HNRNPH3	0	0	0	0	0.504	0	0	0	0.504
EIF3A	PABPC1	0	0	0	0	0.152	0.35	0	0.168	0.478
RPL27A	EIF4G1	0	0	0	0	0	0	0.9	0	0.899
RPS2	RPS13	0	0	0	0	0.64	0.384	0	0.465	0.865
DDX3X	EIF3C	0	0	0	0	0.071	0.837	0	0.064	0.839
SRP14	RPS13	0	0	0	0	0.421	0	0.9	0.219	0.948
TUFM	RPL4	0.41	0	0	0	0.292	0.416	0	0.113	0.737

Appendix 4 – Table showing N2-Src STRING interaction network

Node 1	Node 2	Neighborhood	Fusion	Cooccurrence	Homology	Coexpression	Experimental	Knowledge	Textmining	Combined score
RPLP0	RPL30	0	0	0	0	0.863	0.388	0.9	0.341	0.993
RPL27A	RPS13	0	0	0	0	0.88	0.582	0.9	0.173	0.995
RPS13	RPS19	0	0	0	0	0.857	0.671	0.9	0.46	0.996
RPLP0	ATP5B	0	0	0	0	0.442	0	0	0.118	0.476
SRC	CTTN	0	0	0	0	0	0.621	0.9	0.962	0.998
PTK2	CBL	0	0	0	0	0	0.846	0	0.242	0.875
RPS8	RPS19	0	0	0.246	0	0.875	0.62	0.9	0.515	0.997
HSPA9	ATP5B	0	0	0	0	0.322	0	0	0.229	0.442
RPL12	RPS20	0.261	0	0	0	0.908	0	0.9	0.342	0.994
PICALM	CLTC	0	0	0	0	0.078	0.621	0.36	0.136	0.765
PTK2	PDCD6IP	0	0	0	0	0	0.621	0	0	0.621
RPLP0	RPS14	0.19	0	0	0	0.903	0.388	0.9	0.27	0.995
RPS14	RPS20	0.41	0	0	0	0.894	0.74	0.9	0.465	0.998
ALB	KRT9	0	0	0	0	0	0.302	0	0.202	0.405
PRKDC	ALB	0	0	0	0	0	0	0	0.426	0.425
RPL12	RPS10	0	0	0	0	0.857	0.188	0.9	0.464	0.992
CTTN	TJP1	0	0	0	0	0	0.621	0.8	0.926	0.993
ARHGEF7	SRC	0	0	0	0.483	0	0	0.9	0.926	0.947
TCP1	EIF2S1	0	0	0	0	0.602	0	0	0	0.602
EIF3A	EIF2S1	0	0	0	0	0.331	0.792	0.8	0.098	0.969
PRKDC	RPL4	0	0	0	0	0	0	0	0.583	0.583
CTNNB1	KRT1	0	0	0	0	0	0	0.9	0.182	0.912
SRC	CTNNB1	0	0	0	0	0	0.621	0.9	0.515	0.979

Appendix 4 – Table showing N2-Src STRING interaction network

Node 1	Node 2	Neighborhood	Fusion	Cooccurrence	Homology	Coexpression	Experimental	Knowledge	Textmining	Combined score
RPS7	EIF4G1	0	0	0	0	0.076	0	0.9	0	0.901
EIF3C	CCT7	0	0	0	0	0.492	0	0	0	0.492
GIT1	SRC	0	0	0	0	0	0.621	0	0.878	0.95
RPL4	DDX5	0	0	0	0	0.119	0.388	0	0.068	0.427
RPLP0	RPS5	0.268	0	0.212	0	0.876	0.505	0.9	0.317	0.996
RPS2	TUFM	0.258	0	0	0	0.217	0.345	0	0	0.567
SLC25A5	TCP1	0	0	0	0	0.301	0.14	0	0.158	0.425
HSPD1	HSPA9	0.08	0	0	0	0.857	0.232	0	0.401	0.926
RPL7	RPL4	0.297	0	0	0	0.829	0.294	0	0.341	0.932
ARHGEF7	ALB	0	0	0	0	0	0	0	0.426	0.425
SEC23A	SEC24B	0	0	0	0.571	0.332	0.621	0.9	0.923	0.982
DDX3X	PABPC1	0	0	0	0	0	0.831	0	0.169	0.85
TCP1	CCT7	0	0	0.525	0.875	0.878	0.83	0.9	0.773	0.998
RPL27A	RPS2	0.278	0	0	0	0.48	0.384	0	0.244	0.788
CDH2	NOTCH2	0	0	0	0	0	0	0	0.411	0.412
RPL4	SRP14	0	0	0	0	0.333	0	0.9	0.148	0.935
RPS7	RPS19	0	0	0	0	0.813	0.667	0.9	0.725	0.997
SRC	TJP1	0	0	0	0	0	0	0	0.923	0.923
HGS	CBL	0	0	0	0.445	0	0	0.9	0.371	0.918
HNRNPA2B1	TCP1	0	0	0	0	0.534	0	0	0.159	0.582
TIA1	EIF4G1	0	0	0	0	0	0.352	0	0.508	0.66
HNRNPA2B1	KPNB1	0	0	0	0	0.383	0.077	0	0.157	0.454
LDHA	HSPD1	0	0	0	0	0.53	0.117	0	0.21	0.627

Appendix 4 – Table showing N2-Src STRING interaction network

Node 1	Node 2	Neighborhood	Fusion	Cooccurrence	Homology	Coexpression	Experimental	Knowledge	Textmining	Combined score
RPS13	RPS20	0	0	0	0	0.909	0.756	0.9	0.514	0.998
EIF3C	RPL4	0	0	0	0	0.547	0	0	0	0.547
PARD3	HSPD1	0	0	0	0	0	0.62	0	0	0.619
CPSF7	PCBP1	0	0	0	0	0	0	0.9	0	0.899
EIF3L	QARS	0	0	0	0	0.468	0	0	0	0.468
CCT7	RPS5	0	0	0	0	0.46	0	0	0	0.46
ACTB	CBL	0	0	0	0	0	0.62	0	0.086	0.629
HNRNPA2B1	CCAR1	0	0	0	0	0.218	0	0.9	0.135	0.923
PHB2	RPS5	0	0	0	0	0.556	0	0	0	0.556
ILF2	CCT7	0	0	0	0	0.605	0	0	0.117	0.628
RPS2	RPS20	0.32	0	0	0	0.581	0.384	0	0.514	0.896
GIT1	ARHGEF7	0	0	0	0	0	0.995	0.9	0.504	0.999
RPS18	RPL4	0.287	0	0	0	0.504	0	0	0.342	0.735
HNRNPA2B1	DDX5	0	0	0	0	0.516	0	0	0.283	0.63
HSPD1	HSPA5	0.08	0	0	0	0.4	0.619	0	0.429	0.854
SEC16A	SEC23B	0	0	0	0	0	0	0	0.406	0.407
RPLP0	RPL4	0.208	0	0	0	0.895	0.576	0.9	0.412	0.997
TCP1	HSPA9	0.08	0	0	0	0.544	0	0	0.113	0.577
RPS8	RPS14	0	0	0	0	0.896	0.576	0.9	0.461	0.997
JUP	CDH2	0	0	0	0	0	0.937	0.9	0.947	0.999
KPNA2	TCP1	0	0	0	0	0.723	0	0	0	0.723
RPL30	RPS20	0.268	0	0	0	0.898	0	0.9	0.498	0.995
SRP14	RPS20	0	0	0	0	0.326	0	0.9	0.202	0.938

Appendix 4 – Table showing N2-Src STRING interaction network

Node 1	Node 2	Neighborhood	Fusion	Cooccurrence	Homology	Coexpression	Experimental	Knowledge	Textmining	Combined score
EIF3L	EIF3A	0	0	0	0	0.271	0.86	0.9	0.317	0.991
RPS7	RPL4	0	0	0	0	0.911	0.388	0.9	0.317	0.995
NCL	HNRNPU	0	0	0	0	0.378	0	0	0.521	0.682
TUFM	RPS5	0.41	0	0	0	0.268	0.576	0	0.135	0.808
RPS7	SRP14	0	0	0	0	0.465	0	0.9	0	0.942
HNRNPA2B1	HNRNPH3	0	0	0	0.63	0.624	0	0	0.369	0.669
CTNND1	TJP1	0	0	0	0	0	0	0.9	0.611	0.958
CBL	PXN	0	0	0	0	0	0.845	0	0.535	0.923
CTTN	ALB	0	0	0	0	0	0	0	0.423	0.423
CTNND1	JUP	0	0	0	0.473	0	0.621	0.9	0.752	0.975
CTNND1	CDH2	0	0	0	0	0	0.974	0.9	0.947	0.999
RPL27A	RPS20	0.41	0	0	0	0.846	0.667	0.9	0.22	0.996
RPLP0	TUFM	0.307	0	0	0	0.176	0	0	0.17	0.46
EIF4G1	RPS19	0	0	0	0	0	0	0.9	0.127	0.906
RPS2	ATP5B	0	0	0	0	0.48	0	0	0	0.48
GIT1	PXN	0	0	0	0	0	0.937	0.8	0.925	0.998
VPS35	CLTC	0	0	0	0	0.164	0.359	0	0.105	0.454
LDHA	TCP1	0	0	0	0	0.544	0.117	0	0	0.571
RPS10	SRP14	0	0	0	0	0.198	0	0.9	0	0.914
CTNNB1	CTTN	0	0	0	0	0.076	0	0.9	0.3	0.926
RPL4	RPS14	0.357	0	0	0	0.924	0.58	0.9	0.37	0.998
EIF4G1	RPS5	0	0	0	0	0	0	0.9	0.124	0.906
RPS8	RPS13	0	0	0	0	0.941	0.62	0.9	0.43	0.998

Appendix 4 – Table showing N2-Src STRING interaction network

Node 1	Node 2	Neighborhood	Fusion	Cooccurrence	Homology	Coexpression	Experimental	Knowledge	Textmining	Combined score
KRT18	PKP3	0	0	0	0	0	0.62	0	0.112	0.639
TIA1	EIF2S1	0	0	0	0	0.075	0	0	0.43	0.437
RPS8	RPS5	0	0	0	0	0.87	0.388	0.9	0.43	0.994
KRT18	CBL	0	0	0	0	0	0.62	0	0.07	0.622
HSPA5	SEC23B	0	0	0	0	0.45	0	0	0.186	0.523
CTNNB1	HGS	0	0	0	0	0	0.115	0.9	0.079	0.907
CPSF7	CCAR1	0	0	0	0	0.12	0	0.9	0	0.906
PHGDH	ALB	0	0	0	0	0	0	0	0.43	0.43
RPS10	RPS7	0	0	0	0	0.79	0.488	0.9	0.651	0.995
CTNND1	CTNNB1	0	0	0	0.482	0	0.845	0.9	0.659	0.988
KHSRP	NCL	0	0	0	0	0.074	0	0	0.411	0.418
RPS8	EIF3A	0	0	0	0	0.096	0.388	0	0.102	0.435
NCL	DDX5	0	0	0	0	0.576	0.508	0	0.318	0.838
RPL7	RPL30	0	0	0	0	0.813	0.347	0	0.428	0.92
TCP1	KPNB1	0	0	0	0	0.516	0	0	0	0.516
RPL12	TUFM	0.41	0	0	0	0.225	0.388	0	0.146	0.71
EIF3L	CCT7	0	0	0	0	0.432	0	0	0	0.432
CTTN	CBL	0	0	0	0	0	0	0	0.428	0.428
PABPC1	PXN	0	0	0	0	0	0.621	0	0.355	0.739
RPL12	RPS14	0.221	0	0	0	0.866	0.58	0.9	0.424	0.996
SRC	CDH2	0	0	0	0	0	0	0	0.949	0.949
HNRNPU	HNRNPH3	0	0	0	0	0.164	0.98	0	0.08	0.982
ALB	FUS	0	0	0	0	0	0	0	0.43	0.43

Appendix 4 – Table showing N2-Src STRING interaction network

Node 1	Node 2	Neighborhood	Fusion	Cooccurrence	Homology	Coexpression	Experimental	Knowledge	Textmining	Combined score
HGS	CLTC	0	0	0	0	0	0.845	0	0.124	0.855
ALB	KRT1	0	0	0	0	0	0.302	0	0.34	0.508
RPS18	RPS19	0	0	0	0	0.504	0.356	0	0.498	0.817
HGS	PDCD6IP	0	0	0	0	0.089	0.24	0	0.241	0.401
RPL7	RPS13	0	0	0.332	0	0.68	0.292	0	0.412	0.892
RPS10	RPS5	0	0	0	0	0.829	0.388	0.9	0.891	0.998
HNRNPA2B1	PCBP1	0	0	0	0	0.163	0	0.9	0.919	0.992
PHB2	TUFM	0	0	0	0	0.5	0	0	0.07	0.504
VDAC2	ATP5B	0	0	0	0	0.593	0.141	0	0.203	0.683
RPS2	RPS19	0	0	0	0	0.688	0.384	0	0.507	0.892
RPS18	RPS8	0	0	0	0	0.427	0.229	0	0.426	0.711
RPS7	RPS14	0	0	0	0	0.856	0.576	0.9	0.42	0.995
DDX3X	RPS5	0	0	0	0	0	0.388	0	0.126	0.43
EIF4G1	RPL30	0	0	0	0	0	0	0.9	0.164	0.91
RPS18	RPS2	0.223	0	0	0	0.292	0.224	0	0.466	0.723
HNRNPA2B1	HSPD1	0	0	0	0	0.444	0	0	0.23	0.543
RPS10	RPLP0	0	0	0	0	0.84	0.077	0.9	0.242	0.986
CDH2	PKP2	0	0	0	0	0	0	0	0.463	0.462
DDX3X	EIF3A	0	0	0	0	0.113	0.599	0	0.072	0.624
RPLP0	RPS19	0.189	0	0	0	0.867	0	0.9	0.184	0.989
RPS8	RPLP0	0	0	0	0	0.915	0.352	0.9	0.374	0.995
TIA1	KHSRP	0	0	0	0	0.079	0	0	0.54	0.547
RPL7	RPLP0	0.156	0	0	0	0.754	0.24	0	0.341	0.873

Appendix 4 – Table showing N2-Src STRING interaction network

Node 1	Node 2	Neighborhood	Fusion	Cooccurrence	Homology	Coexpression	Experimental	Knowledge	Textmining	Combined score
CARM1	PABPC1	0	0	0	0	0	0.62	0	0.842	0.936
RPL4	CCT7	0	0	0	0	0.407	0	0	0	0.407
RPL7	RPS14	0.297	0	0	0	0.827	0.231	0	0.374	0.929
RPS8	RPL27A	0	0	0	0	0.746	0.388	0.9	0.318	0.987
SRC	PDCD6IP	0	0	0	0	0	0.845	0	0.242	0.875
RPS2	RPS7	0	0	0	0	0.54	0.29	0	0.429	0.787
VDAC2	TCP1	0	0	0	0	0.402	0.077	0	0.077	0.421
EIF4G1	PABPC1	0	0	0	0.472	0.069	0.846	0	0.963	0.925
RPS18	TUFM	0.224	0	0	0	0.154	0.355	0	0	0.518
RPL12	RPLP0	0.329	0	0	0	0.855	0.505	0.9	0.342	0.995
TANC2	KIRREL	0	0	0	0	0	0.238	0	0.394	0.508
EIF3C	EIF2S1	0	0	0	0	0.271	0.578	0.8	0.22	0.941
HSPD1	RPL7	0	0	0	0	0.247	0	0	0.305	0.441
CTNND1	SRC	0	0	0	0	0	0.846	0.9	0.949	0.999
PRKDC	MCM3	0	0	0	0	0.302	0.8	0	0.214	0.875
HSPD1	ATP5B	0	0	0	0	0.303	0	0	0.273	0.459
CCAR1	HNRNPH3	0	0	0	0	0.606	0	0	0.123	0.632
ILF2	FUS	0	0	0	0	0.127	0	0	0.463	0.499
CTNNB1	JUP	0	0	0	0.956	0	0.845	0.9	0.751	0.984
PTK2	CTTN	0	0	0	0	0	0.621	0	0.561	0.822
PXN	BCAR1	0	0	0	0	0	0.937	0.8	0.946	0.999
RPL12	RPS19	0.228	0	0	0	0.846	0	0.9	0.22	0.988
RPS14	SRP14	0	0	0	0	0.217	0	0.9	0	0.916

Appendix 4 – Table showing N2-Src STRING interaction network

Node 1	Node 2	Neighborhood	Fusion	Cooccurrence	Homology	Coexpression	Experimental	Knowledge	Textmining	Combined score
LDHA	KPNA2	0	0	0	0	0.591	0	0	0	0.591
EIF3C	HGS	0	0	0	0	0	0	0	0.528	0.528
HSPD1	KPNA2	0	0	0	0	0.631	0	0	0	0.631
RPS10	RPS2	0	0	0	0	0.675	0.237	0	0.5	0.858
SEC24C	SEC24B	0	0	0	0.824	0.087	0.352	0.9	0.88	0.943
SEC16A	SEC23A	0	0	0	0	0	0.621	0	0.801	0.919
RPL27A	RPL30	0	0	0	0	0.8	0.671	0.9	0.272	0.994
ACTB	TJP1	0	0	0	0	0	0.592	0.8	0.221	0.927
TIA1	FUBP1	0	0	0	0	0.401	0	0	0.111	0.431
RPS18	RPLP0	0.152	0	0	0	0.396	0.236	0	0.33	0.681
GIT1	PTK2	0	0	0	0	0	0.937	0	0.448	0.963
JUP	PKP2	0	0	0	0	0	0.62	0	0.947	0.978
RPS8	SRP14	0	0	0	0	0.323	0	0.9	0	0.927
RPL4	RPS19	0	0	0	0	0.859	0	0.9	0.341	0.989
EIF4G1	EIF2S1	0	0	0	0	0	0.388	0.9	0.47	0.963
RPS18	RPS5	0.23	0	0	0	0.544	0.348	0	0.341	0.817
HSPD1	CCT7	0	0	0.491	0.618	0.579	0	0	0.285	0.683
RPL12	RPL30	0	0	0	0	0.895	0.582	0.9	0.393	0.996
PKP3	JUP	0	0	0	0.457	0.077	0.62	0	0.611	0.744
TJP1	KRT1	0	0	0	0	0	0.592	0	0.171	0.639
KPNA2	KPNB1	0	0	0	0	0.366	0.992	0	0.885	0.999
HSP90AB1	HSPA5	0	0	0	0	0.224	0	0	0.38	0.487
RPL7	RPS20	0.341	0	0	0	0.701	0	0	0.658	0.923

Appendix 4 – Table showing N2-Src STRING interaction network

Node 1	Node 2	Neighborhood	Fusion	Cooccurrence	Homology	Coexpression	Experimental	Knowledge	Textmining	Combined score
CBL	PIK3R2	0	0	0	0	0	0.977	0.8	0.193	0.995
RPL27A	RPS14	0.357	0	0	0	0.78	0.58	0.9	0.283	0.994
TUFM	ATP5B	0	0	0	0	0.419	0	0	0.207	0.509
PCBP1	HNRNPU	0	0	0	0	0	0	0.9	0.18	0.912
CBL	BCAR1	0	0	0	0.448	0	0	0.9	0.317	0.914
SRC	BCR	0	0	0	0	0	0.62	0	0.653	0.859
PARD3	CTNNB1	0	0	0	0	0	0.923	0	0.144	0.929
NCL	TCP1	0	0	0	0	0.443	0	0	0	0.443
RPS8	EIF3C	0	0	0	0	0.321	0.352	0	0.2	0.6
RPL27A	RPS19	0	0	0	0	0.891	0.58	0.9	0.371	0.996
SLC3A2	ALB	0	0	0	0	0	0	0	0.461	0.461
RPL27A	RPL4	0.357	0	0	0	0.552	0.735	0.9	0.285	0.992
RPLP0	RPS20	0.242	0	0	0	0.901	0.576	0.9	0.22	0.996
CTNNB1	CDH2	0	0	0	0	0	0.999	0.9	0.929	0.999
RPL12	RPS5	0.291	0	0	0	0.874	0.58	0.9	0.373	0.996
RPL7	RPS19	0	0	0	0	0.667	0	0	0.622	0.866
SRC	ACTB	0	0	0	0	0	0.621	0	0.346	0.735
EIF4G1	RPL4	0	0	0	0	0	0	0.9	0.12	0.906
HSPA9	CCT7	0.08	0	0	0	0.4	0	0	0.167	0.477
RPS10	RPL30	0	0	0	0	0.857	0	0.9	0.374	0.989
CTNND1	PXN	0	0	0	0	0	0	0	0.429	0.429
RPS14	EIF2S1	0	0	0	0	0.121	0	0.9	0	0.906
ACTB	RPLP0	0	0	0	0	0.093	0.143	0	0.515	0.57

Appendix 4 – Table showing N2-Src STRING interaction network

Node 1	Node 2	Neighborhood	Fusion	Cooccurrence	Homology	Coexpression	Experimental	Knowledge	Textmining	Combined score
HNRNPA2B1	CPSF7	0	0	0	0	0.077	0	0.9	0	0.901
ACTB	BCAR1	0	0	0	0	0	0.621	0	0	0.621
RPS8	RPS2	0	0	0	0	0.613	0.239	0	0.484	0.827
KPNA2	CCT7	0	0	0	0	0.434	0.141	0	0	0.482
EIF3A	RPS7	0	0	0	0	0.093	0.6	0	0.103	0.629
PKP4	CDH2	0	0	0	0	0	0.619	0	0.167	0.661
HNRNPA0	FUS	0	0	0	0	0.112	0	0.9	0.107	0.909
PCBP1	ATP5B	0	0	0	0	0.444	0	0	0	0.444
VDAC2	PHB	0	0	0	0	0	0.289	0	0.341	0.5
RPS10	RPL7	0	0	0	0	0.719	0	0	0.318	0.796
RPL12	RPL4	0.24	0	0	0	0.815	0.582	0.9	0.371	0.995
CTNNB1	CARM1	0	0	0	0	0	0.621	0	0.085	0.629
HNRNPA0	PCBP1	0	0	0	0	0.165	0	0.9	0	0.91
SRC	BCAR3	0	0	0	0	0	0	0	0.543	0.544
CKAP5	ALB	0	0	0	0	0	0	0	0.41	0.409
SRP14	RPS5	0	0	0	0	0.289	0	0.9	0	0.924
HSPA5	CBL	0	0	0	0	0	0.62	0	0	0.619
RPS10	EIF2S1	0	0	0	0	0.097	0	0.9	0	0.903
SEC16A	SEC24B	0	0	0	0	0.067	0.352	0	0.629	0.745
RPS14	RPS13	0	0	0.261	0	0.913	0.671	0.9	0.424	0.998
RPS14	RPS5	0.268	0	0	0	0.88	0.633	0.9	0.468	0.997
NCL	PABPC1	0	0	0	0.636	0.163	0.62	0	0.379	0.702
ACTB	ATP5B	0	0	0	0	0.243	0	0	0.34	0.467

Appendix 4 – Table showing N2-Src STRING interaction network

Node 1	Node 2	Neighborhood	Fusion	Cooccurrence	Homology	Coexpression	Experimental	Knowledge	Textmining	Combined score
KRT18	HSPA1A	0	0	0	0	0	0.621	0	0.095	0.633
RPS18	RPL30	0	0	0	0	0.544	0	0	0.29	0.655
ACTB	HSP90AB1	0	0	0	0	0.291	0.143	0	0.38	0.571
RPS18	PARD3	0	0	0	0	0	0.62	0	0	0.619
LDHA	VDAC2	0	0	0	0	0.381	0	0	0.128	0.424
DDX3X	NCL	0	0	0	0	0.16	0.388	0	0.151	0.503
FUBP1	ILF2	0	0	0	0	0.436	0	0	0	0.436
VDAC2	HSPD1	0	0	0	0	0.286	0.384	0	0.18	0.589
TUFM	RPS20	0.472	0	0	0	0.367	0.647	0	0.12	0.873
SRC	PTK2	0	0	0	0.801	0	0.999	0.8	0.954	0.999
SRC	HNRNPU	0	0	0	0	0	0	0	0.852	0.852
GTF2I	HSPA9	0	0	0	0	0.12	0.357	0	0.393	0.61
RPLP0	SRP14	0	0	0	0	0.302	0	0.9	0	0.925
RPS8	RPS7	0	0	0	0	0.871	0.386	0.9	0.542	0.995
PKP3	DSG2	0	0	0	0	0.087	0.62	0	0.563	0.827
TIAL1	EIF4G1	0	0	0	0	0	0.352	0	0.234	0.47
EIF2S1	RPS5	0	0	0	0	0.088	0	0.9	0.09	0.905
HNRNPA2B1	NCL	0	0	0	0.74	0.407	0	0	0.425	0.467
JUP	DSG2	0	0	0	0	0	0.974	0	0.947	0.998
RPS18	RPL12	0.177	0	0	0	0.568	0	0	0.289	0.712
PKP4	CTNNB1	0	0	0	0.475	0	0.619	0	0.127	0.632
CPSF7	HNRNPA0	0	0	0	0	0	0	0.9	0.079	0.901
RPL30	RPS13	0	0	0	0	0.936	0.6	0.9	0.431	0.998

Appendix 4 – Table showing N2-Src STRING interaction network

Node 1	Node 2	Neighborhood	Fusion	Cooccurrence	Homology	Coexpression	Experimental	Knowledge	Textmining	Combined score
ARHGEF7	PXN	0	0	0	0	0	0.62	0	0.54	0.813
SRC	ALB	0	0	0	0	0	0	0	0.752	0.752
RPS10	EIF4G1	0	0	0	0	0	0	0.9	0.078	0.901
RPS18	RPS13	0	0	0	0	0.544	0.384	0	0.375	0.8
SRC	PRKDC	0	0	0	0	0	0	0	0.851	0.851
SRC	CARM1	0	0	0	0	0	0.62	0	0.861	0.943
RPS14	RPS19	0	0	0	0	0.865	0.671	0.9	0.61	0.997
CDH2	PXN	0	0	0	0	0	0	0	0.465	0.465
RPS10	RPS14	0	0	0	0	0.87	0.488	0.9	0.467	0.995
RPS8	RPL7	0	0	0	0	0.674	0.187	0	0.366	0.809
HSPD1	PHB	0	0	0	0	0.154	0	0	0.374	0.435
RPS2	RPS5	0.278	0	0	0	0.702	0.356	0	0.515	0.918
HSP90AB1	RPS5	0	0	0	0	0.435	0	0	0.148	0.486
RPL27A	RPL7	0.297	0	0	0	0.434	0.294	0	0.229	0.737
HSP90AB1	ATP5B	0	0	0	0	0.379	0.239	0	0.196	0.567
BCR	CBL	0	0	0	0	0	0.846	0.8	0.43	0.98
HNRNPH3	DDX5	0	0	0	0	0.34	0.974	0	0.148	0.983
RPL30	SRP14	0	0	0	0	0.368	0	0.9	0.161	0.939
EIF3L	EIF3C	0	0	0	0	0.568	0.387	0.9	0.425	0.981
ILF2	HNRNPAB	0	0	0	0	0.562	0	0	0	0.562
HSPA1A	ALB	0	0	0	0	0	0	0	0.42	0.421
SRC	CBL	0	0	0	0	0	0.999	0.9	0.752	0.999
SEC24C	SEC23B	0	0	0	0.552	0.124	0.517	0.36	0.522	0.759

Appendix 4 – Table showing N2-Src STRING interaction network

Node 1	Node 2	Neighborhood	Fusion	Cooccurrence	Homology	Coexpression	Experimental	Knowledge	Textmining	Combined score
CTNNB1	PKP2	0	0	0	0	0	0.62	0	0.374	0.746
RPS10	RPS19	0	0	0	0	0.883	0.488	0.9	0.571	0.996
RPS7	RPS5	0	0	0	0	0.933	0.577	0.9	0.427	0.998
CLASP2	CKAP5	0	0	0	0.437	0.104	0	0.9	0.486	0.928
HNRNPAB	ACTB	0	0	0	0	0.093	0.621	0	0.107	0.65
RPL30	EIF2S1	0	0	0	0	0.119	0	0.9	0	0.905
HSP90AB1	HSPA9	0	0	0	0	0.388	0.118	0	0.235	0.531
LDHA	ATP5B	0	0	0	0	0.501	0	0	0.228	0.589
RPS18	RPS20	0.329	0	0	0	0.55	0.384	0	0.429	0.871
HSP90AB1	CCT7	0	0	0	0	0.485	0	0	0.201	0.561
BCR	PXN	0	0	0	0	0	0.846	0	0.33	0.89
KPNB1	CCT7	0	0	0	0	0.632	0	0	0.133	0.66
VPS29	VPS35	0	0	0	0	0.134	0.959	0	0.983	0.999
RPS2	RPL7	0.231	0	0	0	0.528	0	0	0.429	0.764
RPS18	RPL27A	0.287	0	0	0	0.425	0	0	0.304	0.675
CYFIP1	NCL	0	0	0	0	0	0.62	0	0.196	0.673
QARS	RPS5	0	0	0	0	0.402	0.104	0	0.14	0.476
EIF3A	EIF4G1	0	0	0	0	0.144	0.62	0	0.262	0.726
ALB	CDH2	0	0	0	0	0	0	0	0.46	0.46
HSP90AB1	NCL	0	0	0	0	0.402	0	0	0.163	0.465
LDHA	HSP90AB1	0	0	0	0	0.243	0	0	0.26	0.402
CTNNB1	TJP1	0	0	0	0	0	0	0.9	0.517	0.948
EMD	ACTB	0	0	0	0	0	0.852	0	0.079	0.855

Appendix 4 – Table showing N2-Src STRING interaction network

Node 1	Node 2	Neighborhood	Fusion	Cooccurrence	Homology	Coexpression	Experimental	Knowledge	Textmining	Combined score
RPL12	SRP14	0	0	0	0	0.16	0	0.9	0	0.91
PABPC1	PCBP1	0	0	0	0	0.144	0.619	0	0.29	0.736
SRC	PXN	0	0	0	0	0	0.937	0	0.968	0.997
RPL12	EIF2S1	0	0	0	0	0.1	0	0.9	0	0.904
RPS10	RPS20	0	0	0	0	0.843	0.491	0.9	0.465	0.994
SRC	HGS	0	0	0	0	0	0	0.9	0.305	0.925
RPS14	RPL30	0	0	0	0	0.907	0.58	0.9	0.653	0.998
PRKDC	HNRNPU	0	0	0	0	0	0	0	0.845	0.845
HSPD1	HSP90AB1	0	0	0	0	0.737	0	0	0.379	0.825
RPS8	RPS20	0	0	0	0	0.918	0.576	0.9	0.463	0.997
SEC24C	SEC23A	0	0	0	0.558	0.124	0.845	0.9	0.844	0.99
HSPA1A	HSP90AB1	0	0	0	0	0.154	0.079	0	0.345	0.419
RPS2	RPL30	0	0	0	0	0.608	0	0	0.38	0.741
HNRNPU	CCAR1	0	0	0	0	0	0	0.9	0.159	0.91
CKAP5	MCM3	0	0	0	0	0.451	0.115	0	0	0.482
RPS8	RPS10	0	0	0	0	0.839	0.271	0.9	0.428	0.991
EIF3A	BCR	0	0	0	0	0	0	0	0.488	0.488
PHB2	ALB	0	0	0	0	0	0	0	0.412	0.412
RPL30	RPS5	0.41	0	0	0	0.886	0.615	0.9	0.341	0.997
RPS5	RPS20	0.41	0	0	0	0.791	0.64	0.9	0.412	0.996
KRT18	PKP2	0	0	0	0	0	0.62	0	0.149	0.654
RPL12	RPS13	0	0	0	0	0.909	0.58	0.9	0.379	0.997
ARHGEF7	CBL	0	0	0	0	0	0.974	0.9	0.513	0.998

Appendix 4 – Table showing N2-Src STRING interaction network

Node 1	Node 2	Neighborhood	Fusion	Cooccurrence	Homology	Coexpression	Experimental	Knowledge	Textmining	Combined score
PARD3	BCAR1	0	0	0	0	0	0	0	0.47	0.469
ALB	TJP1	0	0	0	0	0	0	0	0.563	0.563
RPL27A	EIF2S1	0	0	0	0	0.16	0	0.9	0	0.91
PHB2	CCT7	0	0	0	0	0.729	0	0	0	0.729
MRPS34	TUFM	0	0	0	0	0.483	0	0	0.12	0.515
RPS18	RPS7	0	0	0	0	0.426	0.356	0	0.371	0.735
RPL12	RPS7	0	0	0	0	0.884	0.388	0.9	0.32	0.994
ILF2	PRKDC	0	0	0	0	0.163	0.967	0	0.809	0.994
EIF3C	NCL	0	0	0	0	0.429	0.079	0	0.068	0.442
ILF2	KPNA2	0	0	0	0	0.459	0	0	0.138	0.502
HNRNPA0	CCAR1	0	0	0	0	0	0	0.9	0	0.899
RPS7	RPL30	0	0	0	0	0.905	0.6	0.9	0.236	0.996
PHB2	HSPA9	0	0	0	0	0.244	0.079	0	0.34	0.476
HSPD1	TUFM	0	0	0.252	0	0.544	0.228	0	0.145	0.727
KHSRP	CARM1	0	0	0	0	0.191	0	0	0.464	0.537
SLC25A5	RPL4	0	0	0	0	0.439	0	0	0.116	0.471
ILF2	MCM3	0	0	0	0	0.415	0.8	0	0	0.875
PCMT1	TCP1	0	0	0	0	0.64	0	0	0	0.64
HNRNPA2B1	HNRNPA0	0	0	0.525	0.934	0.108	0	0.9	0.379	0.909
LDHA	ALB	0	0	0	0	0	0	0	0.51	0.51
RPL4	ATP5B	0	0	0	0	0.489	0	0	0.125	0.523
DSG2	PKP2	0	0	0	0	0.066	0.62	0	0.783	0.912
NCKAP1	CYFIP1	0	0	0	0	0.071	0.993	0	0.757	0.998

Appendix 4 – Table showing N2-Src STRING interaction network

Node 1	Node 2	Neighborhood	Fusion	Cooccurrence	Homology	Coexpression	Experimental	Knowledge	Textmining	Combined score
RPL4	RPL30	0	0	0	0	0.904	0.67	0.9	0.341	0.997
RPS2	RPL4	0.278	0	0	0	0.763	0	0	0.412	0.885
EIF2S1	RPS19	0.156	0	0	0	0.117	0	0.9	0	0.915
EIF4G1	RPS13	0	0	0	0	0	0	0.9	0.551	0.952
NCL	RPL4	0	0	0	0	0.309	0	0	0.236	0.436
TCP1	RPS19	0	0	0.38	0	0.132	0	0	0	0.426
EIF3A	NCL	0	0	0	0	0.408	0.233	0	0.08	0.524
CTNND1	CTTN	0	0	0	0	0	0.62	0.9	0.896	0.995
NCL	ALB	0	0	0	0	0	0	0	0.425	0.424
PTK2	PIK3R2	0	0	0	0	0	0.62	0.8	0.201	0.93
EIF3L	PHB2	0	0	0	0	0.403	0	0	0	0.404
PHB2	PHB	0	0	0.372	0.935	0.536	0.619	0	0.919	0.826
SLC3A2	HSPA5	0	0	0	0	0.121	0	0	0.38	0.418
KIRREL	TJP1	0	0	0	0	0	0.846	0.9	0.909	0.998
SRC	GTF2I	0	0	0	0	0	0.619	0	0.266	0.701
SRC	PIK3R2	0	0	0	0.508	0	0.62	0.8	0.239	0.926
EIF2S1	RPS20	0	0	0	0	0.126	0	0.9	0	0.906
SEC16A	SEC24C	0	0	0	0.435	0.159	0.236	0	0.726	0.589
RPS7	RPLP0	0	0	0	0	0.87	0	0.9	0.305	0.989
SLC25A5	ATP5B	0	0	0	0	0.565	0	0	0.182	0.62
VDAC2	SLC25A5	0	0	0	0	0.325	0.113	0.8	0.2	0.883
EIF3A	EIF3C	0	0	0	0	0.585	0.846	0.9	0.427	0.995
TUFM	CCT7	0	0	0	0	0.442	0.228	0	0.154	0.586

Appendix 4 – Table showing N2-Src STRING interaction network

Node 1	Node 2	Neighborhood	Fusion	Cooccurrence	Homology	Coexpression	Experimental	Knowledge	Textmining	Combined score
HNRNPAB	TCP1	0	0	0	0	0.406	0	0	0.07	0.411
TUFM	RPS13	0.132	0	0	0	0.154	0.647	0	0.086	0.712
CCAR1	FUS	0	0	0	0	0.064	0	0.9	0	0.9
RPL27A	RPS5	0.32	0	0	0	0.768	0.615	0.9	0.893	0.999
ILF2	HSP90AB1	0	0	0	0	0.534	0	0	0.102	0.553
KRT18	ALB	0	0	0	0	0.107	0	0	0.43	0.456
KHSRP	TIAL1	0	0	0	0	0.079	0	0	0.425	0.434
HSPA5	EIF2S1	0	0	0	0	0.13	0	0	0.379	0.424
RPS19	RPS5	0	0	0	0	0.882	0.58	0.9	0.429	0.996
PTK2	TJP1	0	0	0	0	0	0	0	0.415	0.416
PCBP1	CCAR1	0	0	0	0	0	0	0.9	0	0.899
RPS8	EIF2S1	0.064	0	0	0	0.122	0	0.9	0	0.906
HSPD1	ALB	0	0	0	0	0	0	0	0.563	0.563
HSP90AB1	RPL4	0	0	0	0	0.375	0	0	0.133	0.422
SLC25A5	RPLP0	0	0	0	0	0.308	0	0	0.201	0.41
CTTN	PXN	0	0	0	0	0.075	0	0	0.946	0.947
PHB2	MRPS34	0	0	0	0	0.408	0	0	0	0.408
RPLP0	EIF4G1	0	0	0	0	0.068	0	0.9	0	0.9
NCL	HSPA9	0	0	0	0	0.373	0	0	0.144	0.428
RPL4	RPS20	0.41	0	0	0	0.805	0	0.9	0.371	0.991
ACTB	CTNNB1	0	0	0	0	0	0.143	0	0.476	0.522
ALB	PXN	0	0	0	0	0	0	0	0.541	0.54
TJP1	CDH2	0	0	0	0	0	0	0	0.67	0.669

Appendix 4 – Table showing N2-Src STRING interaction network

Node 1	Node 2	Neighborhood	Fusion	Cooccurrence	Homology	Coexpression	Experimental	Knowledge	Textmining	Combined score
NCL	EIF4G1	0	0	0	0	0.227	0	0	0.475	0.567
RPS8	EIF4G1	0	0	0	0	0.096	0	0.9	0.188	0.916
ACTB	PXN	0	0	0	0	0	0	0.8	0.19	0.827
EIF3L	RPLP0	0	0	0	0	0.432	0	0	0	0.432
CTTN	CDH2	0	0	0	0	0	0	0	0.901	0.902
EIF3L	RPL4	0	0	0	0	0.725	0	0	0.071	0.727
HNRNPA2B1	HNRNPU	0	0	0	0	0.285	0	0.9	0.433	0.953
RPL4	RPS5	0.357	0	0	0	0.941	0.58	0.9	0.317	0.998
HSP90AB1	TCP1	0	0	0	0	0.455	0	0	0.161	0.513
PTK2	BCAR1	0	0	0	0	0	0.999	0.9	0.6	0.999
RPL12	EIF4G1	0	0	0	0	0	0	0.9	0	0.899
JUP	KRT9	0	0	0	0	0	0	0	0.426	0.425
HGS	VPS35	0	0	0	0	0	0.077	0	0.466	0.474
RPS10	RPL27A	0	0	0	0	0.768	0	0.9	0.891	0.997
RPS19	RPS20	0	0	0	0	0.877	0.671	0.9	0.726	0.998
ACTB	HNRNPU	0	0	0	0	0	0.62	0	0.121	0.643
ILF2	ATP5B	0	0	0	0	0.447	0	0	0	0.448
EIF3L	RPS13	0	0	0	0	0.54	0	0	0	0.54
CLTC	PXN	0	0	0	0	0	0.62	0	0	0.619
RPL27A	SRP14	0	0	0	0	0.14	0	0.9	0	0.908
RPL7	RPS5	0.22	0	0	0	0.653	0.292	0	0.331	0.844
HSPA1A	HSPD1	0.08	0	0	0	0.103	0	0	0.585	0.61
EIF2S1	RPS13	0	0	0	0	0.155	0	0.9	0	0.909

Appendix 4 – Table showing N2-Src STRING interaction network

Node 1	Node 2	Neighborhood	Fusion	Cooccurrence	Homology	Coexpression	Experimental	Knowledge	Textmining	Combined score
RPS18	RPL7	0.239	0	0	0	0.365	0	0	0.341	0.637
BCAR3	BCAR1	0	0	0	0	0	0.846	0	0.516	0.92
KPNB1	NUP88	0	0	0	0	0.096	0	0.9	0.25	0.922
RPL4	EIF2S1	0.07	0	0	0	0.24	0	0.9	0	0.919
ILF2	TCP1	0	0	0	0	0.407	0	0	0.124	0.446
KPNB1	CLTC	0	0	0	0	0.107	0.62	0	0.117	0.658
KPNA2	MCM3	0	0	0	0	0.475	0	0	0.193	0.549
EIF4G1	RPS14	0	0	0	0	0	0	0.9	0.112	0.905
PABPC1	CCAR1	0	0	0	0	0	0	0	0.675	0.675
HNRNPU	FUS	0	0	0	0	0	0	0.9	0.191	0.913
TUFM	RPS14	0.277	0	0	0	0.175	0.576	0	0.086	0.719
SRC	BCAR1	0	0	0	0	0	0.999	0.9	0.939	0.999
HNRNPAB	NCL	0	0	0	0.739	0.507	0	0	0.078	0.509
EIF3A	RPS13	0	0	0	0	0	0.6	0	0.087	0.61
JUP	TJP1	0	0	0	0	0	0	0	0.61	0.609
RPS2	RPLP0	0.148	0	0	0	0.789	0.232	0	0.373	0.895
PCBP1	FUS	0	0	0	0	0	0	0.9	0.082	0.902
ARAP1	SRC	0	0	0	0	0	0	0	0.833	0.833
SRC	JUP	0	0	0	0	0	0.621	0.9	0.899	0.995
RPS18	RPS14	0.287	0	0	0	0.544	0.357	0	0.41	0.85
EIF3C	EIF4G1	0	0	0	0	0.172	0	0	0.526	0.581
SRP14	RPS19	0	0	0	0	0.143	0	0.9	0	0.908
RPLP0	RPS13	0	0	0	0	0.892	0.495	0.9	0.215	0.994

Appendix 4 – Table showing N2-Src STRING interaction network

Node 1	Node 2	Neighborhood	Fusion	Cooccurrence	Homology	Coexpression	Experimental	Knowledge	Textmining	Combined score
ILF2	NCL	0	0	0	0	0.363	0	0	0.201	0.457
KIRREL	PIK3R2	0	0	0	0	0	0	0.9	0	0.899
RPLP0	EIF2S1	0	0	0	0	0.155	0	0.9	0.072	0.91
EMD	SRC	0	0	0	0	0	0	0	0.802	0.802
RPS7	RPS20	0	0	0	0	0.842	0.671	0.9	0.481	0.996
PKP4	JUP	0	0	0	0	0	0	0	0.462	0.462
PHB2	ATP5B	0	0	0	0	0.672	0	0	0	0.672
HNRNPA0	HNRNPU	0	0	0	0	0.068	0	0.9	0.757	0.974
RPL7	RPS7	0	0	0	0	0.772	0.236	0	0.319	0.865
RPS8	RPL12	0	0	0	0	0.902	0.388	0.9	0.378	0.995
PABPC1	RPL4	0	0	0	0	0.341	0	0	0.16	0.41
SEC24B	SEC23B	0	0	0	0.579	0.127	0	0.36	0.775	0.594
RPS2	RPS14	0.278	0	0	0	0.778	0.384	0	0.467	0.936
RPS8	RPL4	0	0	0	0	0.865	0.388	0.9	0.424	0.994
RPL12	RPS2	0.179	0	0	0	0.604	0.293	0	0.271	0.796
KRT18	HSPA5	0	0	0	0	0	0.621	0	0.121	0.644
RPL27A	RPLP0	0.191	0	0	0	0.692	0.576	0.9	0.107	0.987
RPS18	RPS10	0	0	0	0	0.424	0.232	0	0.379	0.687
ATP5B	CCT7	0	0	0	0	0.56	0	0	0	0.561
BCR	CLTC	0	0	0	0	0	0.62	0	0.065	0.62
CPSF7	FUS	0	0	0	0	0.068	0	0.9	0	0.9
EMD	CTNNB1	0	0	0	0	0	0.621	0	0.139	0.651
HNRNPA2B1	FUS	0	0	0	0.718	0.226	0	0.9	0.305	0.923

Appendix 4 – Table showing N2-Src STRING interaction network

Node 1	Node 2	Neighborhood	Fusion	Cooccurrence	Homology	Coexpression	Experimental	Knowledge	Textmining	Combined score
ALB	CBL	0	0	0	0	0	0	0	0.462	0.462
RPS7	EIF2S1	0	0	0	0	0.126	0	0.9	0	0.906
TJP1	PXN	0	0	0	0	0	0	0	0.433	0.433
TUFM	HSPA9	0	0	0.291	0	0.166	0	0	0.109	0.401
EIF4G1	RPS20	0	0	0	0	0	0	0.9	0.073	0.901
NCL	KPNB1	0	0	0	0	0.335	0	0	0.269	0.481
EIF3L	RPS5	0	0	0	0	0.685	0	0	0	0.685
PTK2	PXN	0	0	0	0	0	0.999	0.8	0.962	0.999
RPS8	RPL30	0	0	0	0	0.879	0.388	0.9	0.369	0.994
ACTB	ALB	0	0	0	0	0	0	0	0.514	0.514
RPS7	RPS13	0	0	0	0	0.931	0.667	0.9	0.43	0.998
RPL27A	RPS7	0	0	0	0	0.606	0.388	0.9	0.216	0.977
ACTB	CARM1	0	0	0	0	0	0.62	0	0.144	0.652
RPL30	RPS19	0	0	0	0	0.84	0	0.9	0.378	0.988
CKAP5	TCP1	0	0	0	0	0.269	0.231	0	0	0.4

List of Abbreviations

ALK	Anaplastic lymphoma kinase
ATP	Adenosine Triphosphate
BCAR1	Breast cancer associated receptor 1
BDNF	Brain-derived neurotrophic factor
BMB	Boehringer Mannheim Blocking
CAM	Cell-adhesion molecule
cAMP	Cyclic adenosine monophosphate
CDK	Cyclin dependent kinase
CFP	Cyan fluorescent protein
Chk	Csk-homology kinase
CMV	Cytomegalovirus
CNS	Central nervous system
CSK	C-terminal Src Kinase
DAVID	Database for annotation, visualization and Integrated discovery
DIG	Digoxygenin
ECM	Extracellular matrix
eFGF	Embryonic Fibroblast Growth Factor
emPAI	Exponentially modified Protein Abundance Index
ER	Endoplasmic reticulum
ERK	Extracellular-Signal-Regulated kinase
ESCRT	Endosomal sorting complexes required for transport
FAK	Focal Adhesion Kinase
FBS	Foetal bovine serum
FGF	Fibroblast Growth Factor
Fig	Figure
GABA	Gamma aminobutyric acid
GAP	GTPase activating protein
GEF	Guanine nucleotide exchange factor
GFP	Green fluorescent protein
GO term	Gene Ontology term
GPS	Group-based prediction system
GRID2	Glutamate Receptor Ionotropic Delta 2
GTP	Guanosine tri-phosphate
HCN	Hyperpolarization-activated cyclic nucleotide-gated
HEK	Human Embryonic Kidney
HRP	Horse radish peroxidase
IDP	Intrinsically disordered protein
IDR	Intrinsically disordered region
LC	Liquid Chromatography
LTP	Long-term potentiation
MAP	Mitogen activated protein
MCM7	Minichromosome maintenance complex component 7
MS	Mass spectrometry

NMDA	N-methyl-D-aspartic acid
nRTK	Non-receptor tyrosine kinase
PBS	Phosphate buffered saline
PCR	Polymerase Chain Reaction
PDGF	Platelet-derived growth factor
PHOX2B	Paired-like homeobox 2b
PI3K	Phosphoinositide-3 kinase
PKA	Protein Kinase A
PKC	Protein kinase C
PPII	Poly-proline type- II
PTK	Protein tyrosine kinase
PTM	Post-translational modification
PTP	Protein tyrosine phosphatase
PVDF	Polyvinylidene fluoride
RA	Retinoic acid
RPMI	Roswell Park Memorial Institute
RTK	Receptor tyrosine kinase
rtPCR	Reverse transcriptase polymerase chain reaction
SDS PAGE	Sodium dodecyl sulfate polyagarose gel electrophoresis
SFK	Src family kinase
SH2	Src Homology 2
SH3	Src Homology 3
SH3BP1	Src Homology 3 binding protein
SH4	Src Homology 4
shRNA	Short hairpin RNA
siRNA	Short interfering RNA
TGN	Trans-golgi network
TPA	12-O-tetradecanoylphorbol-13-O-acetate
WASp	Wiskott–Aldrich Syndrome protein
WebGestalt	WEB-based GENE SeT Analysis Toolkit

References

- AMATA, I., MAFFEI, M., IGEA, A., GAY, M., VILASECA, M., NEBREDA, A. R. & PONS, M. 2013. Multi-phosphorylation of the intrinsically disordered unique domain of c-Src studied by in-cell and real-time NMR spectroscopy. *Chembiochem*, 14, 1820-7.
- AMATA, I., MAFFEI, M. & PONS, M. 2014. Phosphorylation of Unique domains of Src family kinases. *Frontiers in Genetics*, 5.
- AMITAY, R., NASS, D., MEITAR, D., GOLDBERG, I., DAVIDSON, B., TRAKHTENBROT, L., BROK-SIMONI, F., BEN-ZE'EV, A., RECHAVI, G. & KAUFMANN, Y. 2001. Reduced expression of plakoglobin correlates with adverse outcome in patients with neuroblastoma. *Am J Pathol*, 159, 43-9.
- ARIDOR, M. & BALCH, W. E. 2000. Kinase signaling initiates coat complex II (COPII) recruitment and export from the mammalian endoplasmic reticulum. *J Biol Chem*, 275, 35673-6.
- ARIKI, M., TANABE, O., USUI, H., HAYASHI, H., INOUE, R., NISHITO, Y., KAGAMIYAMA, H. & TAKEDA, M. 1997. Identification of autophosphorylation sites in c-Yes purified from rat liver plasma membranes. *J Biochem*, 121, 104-11.
- ARINSBURG, S. S., COHEN, I. S. & YU, H. G. 2006. Constitutively active Src tyrosine kinase changes gating of HCN4 channels through direct binding to the channel proteins. *J Cardiovasc Pharmacol*, 47, 578-86.
- ATSUMI, S., WAKABAYASHI, K., TITANI, K., FUJII, Y. & KAWATE, T. 1993. Neuronal pp60c-src(+) in the developing chick spinal cord as revealed with anti-hexapeptide antibody. *J Neurocytol*, 22, 244-58.
- BAILEY, C. K., MITTAL, M. K., MISRA, S. & CHAUDHURI, G. 2012. High motility of triple-negative breast cancer cells is due to repression of plakoglobin gene by metastasis modulator protein SLUG. *J Biol Chem*, 287, 19472-86.
- BECK, C. W. & SLACK, J. M. 1998. Analysis of the developing *Xenopus* tail bud reveals separate phases of gene expression during determination and outgrowth. *Mech Dev*, 72, 41-52.
- BECK, C. W. & SLACK, J. M. 1999. A developmental pathway controlling outgrowth of the *Xenopus* tail bud. *Development*, 126, 1611-20.
- BECK, C. W. & SLACK, J. M. 2002. Notch is required for outgrowth of the *Xenopus* tail bud. *Int J Dev Biol*, 46, 255-8.
- BEIERLE, E. A., MASSOLL, N. A., HARTWICH, J., KURENOVA, E. V., GOLUBOVSKAYA, V. M., CANCE, W. G., MCGRADY, P. & LONDON, W. B. 2008. Focal adhesion kinase expression in human neuroblastoma: immunohistochemical and real-time PCR analyses. *Clin Cancer Res*, 14, 3299-305.
- BELLEFROID, E. J., KOBBE, A., GRUSS, P., PIELER, T., GURDON, J. B. & PAPANALOPULU, N. 1998. Xiro3 encodes a *Xenopus* homolog of the

- Drosophila Iroquois genes and functions in neural specification. *EMBO J*, 17, 191-203.
- BEN-TAL, N., HONIG, B., PEITZSCH, R. M., DENISOV, G. & MCLAUGHLIN, S. 1996. Binding of small basic peptides to membranes containing acidic lipids: theoretical models and experimental results. *Biophys J*, 71, 561-75.
- BERGMAN, M., MUSTELIN, T., OETKEN, C., PARTANEN, J., FLINT, N. A., AMREIN, K. E., AUTERO, M., BURN, P. & ALITALO, K. 1992. The human p50csk tyrosine kinase phosphorylates p56lck at Tyr-505 and down regulates its catalytic activity. *EMBO J*, 11, 2919-24.
- BESSHO, F. 1998. Colloquy on Neuroblastoma Screening: Is there a future for neuroblastoma mass screening? *Medical and Pediatric Oncology*, 31, 106-110.
- BJORGE, J. D., JAKYMIW, A. & FUJITA, D. J. 2000. Selected glimpses into the activation and function of Src kinase. *Oncogene*, 19, 5620-35.
- BLACK, D. L. 1991. Does steric interference between splice sites block the splicing of a short c-src neuron-specific exon in non-neuronal cells? *Genes Dev*, 5, 389-402.
- BLACK, D. L. 1992. Activation of c-src neuron-specific splicing by an unusual RNA element in vivo and in vitro. *Cell*, 69, 795-807.
- BLACK, D. L. 2003. Mechanisms of alternative pre-messenger RNA splicing. *Annual review of biochemistry*, 72, 291-336.
- BLUMBERG, B. 1997. An essential role for retinoid signaling in anteroposterior neural specification and neuronal differentiation. *Semin Cell Dev Biol*, 8, 417-28.
- BLUME-JENSEN, P. & HUNTER, T. 2001. Oncogenic kinase signalling. *Nature*, 411, 355-65.
- BOERNER, R. J., KASSEL, D. B., BARKER, S. C., ELLIS, B., DELACY, P. & KNIGHT, W. B. 1996. Correlation of the phosphorylation states of pp60c-src with tyrosine kinase activity: the intramolecular pY530-SH2 complex retains significant activity if Y419 is phosphorylated. *Biochemistry*, 35, 9519-25.
- BOGGON, T. J. & ECK, M. J. 2004. Structure and regulation of Src family kinases. *Oncogene*, 23, 7918-27.
- BORRIELLO, A., PIETRA, V. D., CRISCUOLO, M., OLIVA, A., TONINI, G. P., IOLASCON, A., ZAPPIA, V. & RAGIONE, F. D. 2000. p27Kip1 accumulation is associated with retinoic-induced neuroblastoma differentiation: evidence of a decreased proteasome-dependent degradation. *Oncogene*, 19, 51-60.
- BOULVEN, I., ROBIN, P., DESMYTER, C., HARBON, S. & LEIBER, D. 2002. Differential involvement of Src family kinases in pervanadate-mediated responses in rat myometrial cells. *Cell Signal*, 14, 341-9.
- BOURGUIGNON, C., LI, J. & PAPALOPULU, N. 1998. XBF-1, a winged helix transcription factor with dual activity, has a role in positioning neurogenesis in *Xenopus* competent ectoderm. *Development*, 125, 4889-900.

- BOZZO, C., DEFILIPPI, P., SILENGO, L. & TARONE, G. 1994. Role of tyrosine phosphorylation in matrix-induced neurite outgrowth in human neuroblastoma cells. *Exp Cell Res*, 214, 313-22.
- BRANNETTI, B., VIA, A., CESTRA, G., CESARENI, G. & HELMER-CITTERICH, M. 2000. SH3-SPOT: an algorithm to predict preferred ligands to different members of the SH3 gene family. *J Mol Biol*, 298, 313-28.
- BREITKOPF, S. B., YUAN, M., PIHAN, G. A. & ASARA, J. M. 2012. Detection of a rare BCR-ABL tyrosine kinase fusion protein in H929 multiple myeloma cells using immunoprecipitation (IP)-tandem mass spectrometry (MS/MS). *Proc Natl Acad Sci U S A*, 109, 16190-5.
- BRESLER, S. C., WOOD, A. C., HAGLUND, E. A., COURTRIGHT, J., BELCASTRO, L. T., PLEGARIA, J. S., COLE, K., TOPOROVSKAYA, Y., ZHAO, H., CARPENTER, E. L., CHRISTENSEN, J. G., MARIS, J. M., LEMMON, M. A. & MOSSÉ, Y. P. 2011. Differential inhibitor sensitivity of anaplastic lymphoma kinase variants found in neuroblastoma. *Sci Transl Med*, 3, 108ra114.
- BRIGNATZ, C., PARONETTO, M. P., OPI, S., CAPPELLARI, M., AUDEBERT, S., FEUILLET, V., BISMUTH, G., ROCHE, S., AROLD, S. T., SETTE, C. & COLLETTE, Y. 2009. Alternative splicing modulates autoinhibition and SH3 accessibility in the Src kinase Fyn. *Mol Cell Biol*, 29, 6438-48.
- BRODEUR, G. M. 2003. Neuroblastoma: biological insights into a clinical enigma. *Nat Rev Cancer*, 3, 203-16.
- BROWN, D. J. & GORDON, J. A. 1984. The stimulation of pp60v-src kinase activity by vanadate in intact cells accompanies a new phosphorylation state of the enzyme. *J Biol Chem*, 259, 9580-6.
- BROWN, M. T. & COOPER, J. A. 1996. Regulation, substrates and functions of src. *Biochim Biophys Acta*, 1287, 121-49.
- BRUGGE, J., COTTON, P., LUSTIG, A., YONEMOTO, W., LIPSICH, L., COUSSENS, P., BARRETT, J. N., NONNER, D. & KEANE, R. W. 1987. Characterization of the altered form of the c-src gene product in neuronal cells. *Genes Dev*, 1, 287-96.
- BRUGGE, J. S., COTTON, P. C., QUERAL, A. E., BARRETT, J. N., NONNER, D. & KEANE, R. W. 1985. Neurones express high levels of a structurally modified, activated form of pp60c-src. *Nature*, 316, 554-7.
- BRUGGE, J. S. & ERIKSON, R. L. 1977. Identification of a transformation-specific antigen induced by an avian sarcoma virus. *Nature*, 269, 346-8.
- BRUMMELKAMP, T. R., BERNARDS, R. & AGAMI, R. 2002. A system for stable expression of short interfering RNAs in mammalian cells. *Science*, 296, 550-3.
- BRÁBEK, J., MOJZITA, D., NOVOTNÝ, M., PŮTA, F. & FOLK, P. 2002. The SH3 domain of Src can downregulate its kinase activity in the absence of the SH2 domain-pY527 interaction. *Biochem Biophys Res Commun*, 296, 664-70.

- BUSINARO, R., LEONE, S., FABRIZI, C., SORCI, G., DONATO, R., LAURO, G. M. & FUMAGALLI, L. 2006. S100B protects LAN-5 neuroblastoma cells against Abeta amyloid-induced neurotoxicity via RAGE engagement at low doses but increases Abeta amyloid neurotoxicity at high doses. *J Neurosci Res*, 83, 897-906.
- BUSS, J. E., KAMPS, M. P. & SEFTON, B. M. 1984. Myristic acid is attached to the transforming protein of Rous sarcoma virus during or immediately after synthesis and is present in both soluble and membrane-bound forms of the protein. *Mol Cell Biol*, 4, 2697-704.
- CALALB, M. B., POLTE, T. R. & HANKS, S. K. 1995. Tyrosine phosphorylation of focal adhesion kinase at sites in the catalytic domain regulates kinase activity: a role for Src family kinases. *Mol Cell Biol*, 15, 954-63.
- CAPUTI, M. & ZAHLER, A. M. 2001. Determination of the RNA binding specificity of the heterogeneous nuclear ribonucleoprotein (hnRNP) H/H'/F/2H9 family. *J Biol Chem*, 276, 43850-9.
- CARLIN, S., MAIRS, R. J., MCCLUSKEY, A. G., TWEDDLE, D. A., SPRIGG, A., ESTLIN, C., BOARD, J., GEORGE, R. E., ELLERSHAW, C., PEARSON, A. D., LUNEC, J., MONTALDO, P. G., PONZONI, M., VAN ECK-SMIT, B. L., HOEFNAGEL, C. A., VAN DEN BRUG, M. D., TYTGAT, G. A. & CARON, H. N. 2003. Development of a real-time polymerase chain reaction assay for prediction of the uptake of meta-[(131)I]iodobenzylguanidine by neuroblastoma tumors. *Clin Cancer Res*, 9, 3338-44.
- CARTWRIGHT, C. A., SIMANTOV, R., KAPLAN, P. L., HUNTER, T. & ECKHART, W. 1987. Alterations in pp60c-src accompany differentiation of neurons from rat embryo striatum. *Mol Cell Biol*, 7, 1830-40.
- CATALDI, M., TAGLIALATELA, M., GUERRIERO, S., AMOROSO, S., LOMBARDI, G., DI RENZO, G. & ANNUNZIATO, L. 1996. Protein-tyrosine kinases activate while protein-tyrosine phosphatases inhibit L-type calcium channel activity in pituitary GH3 cells. *J Biol Chem*, 271, 9441-6.
- CERNAIANU, G., BRANDMAIER, P., SCHOLZ, G., ACKERMANN, O. P., ALT, R., ROTHE, K., CROSS, M., WITZIGMANN, H. & TRÖBS, R. B. 2008. All-trans retinoic acid arrests neuroblastoma cells in a dormant state. Subsequent nerve growth factor/brain-derived neurotrophic factor treatment adds modest benefit. *J Pediatr Surg*, 43, 1284-94.
- CHACKALAPARAMPIL, I. & SHALLOWAY, D. 1988. Altered phosphorylation and activation of pp60c-src during fibroblast mitosis. *Cell*, 52, 801-10.
- CHANG, C. M., SHU, H. K. & KUNG, H. J. 1995. Disease specificity of kinase domains: the src-encoded catalytic domain converts erbB into a sarcoma oncogene. *Proc Natl Acad Sci U S A*, 92, 3928-32.
- CHANG, H. H., LEE, H., HU, M. K., TSAO, P. N., JUAN, H. F., HUANG, M. C., SHIH, Y. Y., WANG, B. J., JENG, Y. M., CHANG, C. L., HUANG, S. F., TSAY, Y. G., HSIEH, F. J., LIN, K. H., HSU, W. M. & LIAO, Y. F. 2010. Notch1 expression predicts an unfavorable prognosis and serves as a

- therapeutic target of patients with neuroblastoma. *Clin Cancer Res*, 16, 4411-20.
- CHANTHERY, Y. H., GUSTAFSON, W. C., ITSARA, M., PERSSON, A., HACKETT, C. S., GRIMMER, M., CHARRON, E., YAKOVENKO, S., KIM, G., MATTHAY, K. K. & WEISS, W. A. 2012. Paracrine signaling through MYCN enhances tumor-vascular interactions in neuroblastoma. *Sci Transl Med*, 4, 115ra3.
- CHEN, C. & LEONARD, J. P. 1996. Protein tyrosine kinase-mediated potentiation of currents from cloned NMDA receptors. *J Neurochem*, 67, 194-200.
- CHEN, Q., SU, Y., WESSLOWSKI, J., HAGEMANN, A. I., RAMIALISON, M., WITTBRODT, J., SCHOLPP, S. & DAVIDSON, G. 2014. Tyrosine phosphorylation of LRP6 by Src and Fer inhibits Wnt/ β -catenin signalling. *EMBO Rep*, 15, 1254-67.
- CHEN, X., BONNE, S., HATZFELD, M., VAN ROY, F. & GREEN, K. J. 2002. Protein binding and functional characterization of plakophilin 2. Evidence for its diverse roles in desmosomes and beta -catenin signaling. *J Biol Chem*, 277, 10512-22.
- CHENG, S. Y., SUN, G., SCHLAEPFER, D. D. & PALLEN, C. J. 2014. Grb2 promotes integrin-induced focal adhesion kinase (FAK) autophosphorylation and directs the phosphorylation of protein tyrosine phosphatase α by the Src-FAK kinase complex. *Mol Cell Biol*, 34, 348-61.
- CHEUNG, H. H. & GURD, J. W. 2001. Tyrosine phosphorylation of the N-methyl-D-aspartate receptor by exogenous and postsynaptic density-associated Src-family kinases. *J Neurochem*, 78, 524-34.
- CHEUNG, N. K., ZHANG, J., LU, C., PARKER, M., BAHRAMI, A., TICKOO, S. K., HEGUY, A., PAPPO, A. S., FEDERICO, S., DALTON, J., CHEUNG, I. Y., DING, L., FULTON, R., WANG, J., CHEN, X., BECKSFORT, J., WU, J., BILLUPS, C. A., ELLISON, D., MARDIS, E. R., WILSON, R. K., DOWNING, J. R., DYER, M. A. & PROJECT, S. J. C. S. R. H. W. U. P. C. G. 2012. Association of age at diagnosis and genetic mutations in patients with neuroblastoma. *JAMA*, 307, 1062-71.
- CHITNIS, A., HENRIQUE, D., LEWIS, J., ISH-HOROWICZ, D. & KINTNER, C. 1995. Primary neurogenesis in *Xenopus* embryos regulated by a homologue of the *Drosophila* neurogenic gene Delta. *Nature*, 375, 761-6.
- CHO, H. J., YU, J., XIE, C., RUDRABHATLA, P., CHEN, X., WU, J., PARISIADOU, L., LIU, G., SUN, L., MA, B., DING, J., LIU, Z. & CAI, H. 2014. Leucine-rich repeat kinase 2 regulates Sec16A at ER exit sites to allow ER-Golgi export. *EMBO J*.
- CHONG, Y. P., IA, K. K., MULHERN, T. D. & CHENG, H. C. 2005. Endogenous and synthetic inhibitors of the Src-family protein tyrosine kinases. *Biochim Biophys Acta*, 1754, 210-20.
- CHOU, M. Y., ROOKE, N., TURCK, C. W. & BLACK, D. L. 1999. hnRNP H is a component of a splicing enhancer complex that activates a c-src alternative exon in neuronal cells. *Mol Cell Biol*, 19, 69-77.

- CLARK, E. A., SHATTIL, S. J. & BRUGGE, J. S. 1994a. Regulation of protein tyrosine kinases in platelets. *Trends Biochem Sci*, 19, 464-9.
- CLARK, M. R., JOHNSON, S. A. & CAMBIER, J. C. 1994b. Analysis of Ig-alpha-tyrosine kinase interaction reveals two levels of binding specificity and tyrosine phosphorylated Ig-alpha stimulation of Fyn activity. *EMBO J*, 13, 1911-9.
- CLARK, O., DAGA, S. & STOKER, A. W. 2013. Tyrosine phosphatase inhibitors combined with retinoic acid can enhance differentiation of neuroblastoma cells and trigger ERK- and AKT-dependent, p53-independent senescence. *Cancer Lett*, 328, 44-54.
- CLINE, H. 2005. Synaptogenesis: a balancing act between excitation and inhibition. *Curr Biol*, 15, R203-5.
- COBB, B. S., SCHALLER, M. D., LEU, T. H. & PARSONS, J. T. 1994. Stable association of pp60src and pp59fyn with the focal adhesion-associated protein tyrosine kinase, pp125FAK. *Mol Cell Biol*, 14, 147-55.
- COHEN, P. 2000. The regulation of protein function by multisite phosphorylation--a 25 year update. *Trends Biochem Sci*, 25, 596-601.
- COHEN, P. 2001. The role of protein phosphorylation in human health and disease. The Sir Hans Krebs Medal Lecture. *Eur J Biochem*, 268, 5001-10.
- COLLETT, J. W. & STEELE, R. E. 1992. Identification and developmental expression of Src+ mRNAs in *Xenopus laevis*. *Dev Biol*, 152, 194-8.
- COLLETT, J. W. & STEELE, R. E. 1993. Alternative splicing of a neural-specific Src mRNA (Src+) is a rapid and protein synthesis-independent response to neural induction in *Xenopus laevis*. *Dev Biol*, 158, 487-95.
- COLLINS, M. O., YU, L. & CHOUDHARY, J. S. 2007. Analysis of protein phosphorylation on a proteome-scale. *Proteomics*, 7, 2751-68.
- COLUCCIA, A. M., BENATI, D., DEKIL, H., DE FILIPPO, A., LAN, C. & GAMBACORTI-PASSERINI, C. 2006. SKI-606 decreases growth and motility of colorectal cancer cells by preventing pp60(c-Src)-dependent tyrosine phosphorylation of beta-catenin and its nuclear signaling. *Cancer Res*, 66, 2279-86.
- CONSORTIUM, U. 2014. Activities at the Universal Protein Resource (UniProt). *Nucleic Acids Res*, 42, D191-8.
- COOPER, J. A., GOULD, K. L., CARTWRIGHT, C. A. & HUNTER, T. 1986. Tyr527 is phosphorylated in pp60c-src: implications for regulation. *Science*, 231, 1431-4.
- COOPER, J. A. & MACAULEY, A. 1988. Potential positive and negative autoregulation of p60c-src by intermolecular autophosphorylation. *Proc Natl Acad Sci U S A*, 85, 4232-6.
- COTTERMAN, R., JIN, V. X., KRIG, S. R., LEMEN, J. M., WEY, A., FARNHAM, P. J. & KNOEPFLER, P. S. 2008. N-Myc regulates a widespread euchromatic

- program in the human genome partially independent of its role as a classical transcription factor. *Cancer research*, 68, 9654-62.
- COTTON, P. C. & BRUGGE, J. S. 1983. Neural tissues express high levels of the cellular src gene product pp60c-src. *Mol Cell Biol*, 3, 1157-62.
- COULTER, D. W., BLATT, J., D'ERCOLE, A. J. & MOATS-STAAATS, B. M. 2008. IGF-I receptor inhibition combined with rapamycin or temsirolimus inhibits neuroblastoma cell growth. *Anticancer Res*, 28, 1509-16.
- COURTNEIDGE, S. A., LEVINSON, A. D. & BISHOP, J. M. 1980. The protein encoded by the transforming gene of avian sarcoma virus (pp60src) and a homologous protein in normal cells (pp60proto-src) are associated with the plasma membrane. *Proc Natl Acad Sci U S A*, 77, 3783-7.
- CROSS, F. R., GARBER, E. A. & HANAFUSA, H. 1985. N-terminal deletions in Rous sarcoma virus p60src: effects on tyrosine kinase and biological activities and on recombination in tissue culture with the cellular src gene. *Mol Cell Biol*, 5, 2789-95.
- CROSS, F. R., GARBER, E. A., PELLMAN, D. & HANAFUSA, H. 1984. A short sequence in the p60src N terminus is required for p60src myristylation and membrane association and for cell transformation. *Mol Cell Biol*, 4, 1834-42.
- CUADRADO, A. & NEBREDA, A. R. 2010. Mechanisms and functions of p38 MAPK signalling. *Biochem J*, 429, 403-17.
- CUNNINGHAM, D. L., SWEET, S. M., COOPER, H. J. & HEATH, J. K. 2010. Differential phosphoproteomics of fibroblast growth factor signaling: identification of Src family kinase-mediated phosphorylation events. *J Proteome Res*, 9, 2317-28.
- DAVIDOFF, A. M. 2012. Neuroblastoma. *Semin Pediatr Surg*, 21, 2-14.
- DEFILIPPI, P., RETTA, S. F., OLIVO, C., PALMIERI, M., VENTURINO, M., SILENGO, L. & TARONE, G. 1995. p125FAK tyrosine phosphorylation and focal adhesion assembly: studies with phosphotyrosine phosphatase inhibitors. *Exp Cell Res*, 221, 141-52.
- DELAUNE, E., LEMAIRE, P. & KODJABACHIAN, L. 2005. Neural induction in *Xenopus* requires early FGF signalling in addition to BMP inhibition. *Development*, 132, 299-310.
- DEMETRI, G. D., LO RUSSO, P., MACPHERSON, I. R., WANG, D., MORGAN, J. A., BRUNTON, V. G., PALIWAL, P., AGRAWAL, S., VOI, M. & EVANS, T. R. 2009. Phase I dose-escalation and pharmacokinetic study of dasatinib in patients with advanced solid tumors. *Clin Cancer Res*, 15, 6232-40.
- DERGAI, M., TSYBA, L., DERGAI, O., ZLATSKII, I., SKRYPKINA, I., KOVALENKO, V. & RYNDITCH, A. 2010. Microexon-based regulation of ITSN1 and Src SH3 domains specificity relies on introduction of charged amino acids into the interaction interface. *Biochem Biophys Res Commun*, 399, 307-12.
- DINGLELINE, R., BORGES, K., BOWIE, D. & TRAYNELIS, S. F. 1999. The glutamate receptor ion channels. *Pharmacol Rev*, 51, 7-61.

- ECK, M. J., SHOELSON, S. E. & HARRISON, S. C. 1993. Recognition of a high-affinity phosphotyrosyl peptide by the Src homology-2 domain of p56lck. *Nature*, 362, 87-91.
- ECKHART, W., HUTCHINSON, M. A. & HUNTER, T. 1979. An activity phosphorylating tyrosine in polyoma T antigen immunoprecipitates. *Cell*, 18, 925-33.
- EGEA, J. & KLEIN, R. 2007. Bidirectional Eph-ephrin signaling during axon guidance. *Trends Cell Biol*, 17, 230-8.
- EVANS, A. E., GERSON, J. & SCHNAUFER, L. 1976. Spontaneous regression of neuroblastoma. *Natl Cancer Inst Monogr*, 44, 49-54.
- EVANS, G. J. & COUSIN, M. A. 2005. Tyrosine phosphorylation of synaptophysin in synaptic vesicle recycling. *Biochem Soc Trans*, 33, 1350-3.
- FADOOL, D. A., HOLMES, T. C., BERMAN, K., DAGAN, D. & LEVITAN, I. B. 1997. Tyrosine phosphorylation modulates current amplitude and kinetics of a neuronal voltage-gated potassium channel. *J Neurophysiol*, 78, 1563-73.
- FAN, X., MIKOLAENKO, I., ELHASSAN, I., NI, X., WANG, Y., BALL, D., BRAT, D. J., PERRY, A. & EBERHART, C. G. 2004. Notch1 and notch2 have opposite effects on embryonal brain tumor growth. *Cancer Res*, 64, 7787-93.
- FARHAN, H., WENDELER, M. W., MITROVIC, S., FAVA, E., SILBERBERG, Y., SHARAN, R., ZERIAL, M. & HAURI, H. P. 2010. MAPK signaling to the early secretory pathway revealed by kinase/phosphatase functional screening. *J Cell Biol*, 189, 997-1011.
- FAURE, R., VINCENT, M., DUFOUR, M., SHAVER, A. & POSNER, B. I. 1995. Arrest at the G2/M transition of the cell cycle by protein-tyrosine phosphatase inhibition: studies on a neuronal and a glial cell line. *J Cell Biochem*, 59, 389-401.
- FENG, S., CHEN, J. K., YU, H., SIMON, J. A. & SCHREIBER, S. L. 1994. Two binding orientations for peptides to the Src SH3 domain: development of a general model for SH3-ligand interactions. *Science*, 266, 1241-7.
- FENG, S., KASAHARA, C., RICKLES, R. J. & SCHREIBER, S. L. 1995. Specific interactions outside the proline-rich core of two classes of Src homology 3 ligands. *Proc Natl Acad Sci U S A*, 92, 12408-15.
- FILIPPAKOPOULOS, P., MÜLLER, S. & KNAPP, S. 2009. SH2 domains: modulators of nonreceptor tyrosine kinase activity. *Curr Opin Struct Biol*, 19, 643-9.
- FINAN, P. M., HALL, A. & KELLIE, S. 1996. Sam68 from an immortalised B-cell line associates with a subset of SH3 domains. *FEBS Lett*, 389, 141-4.
- FOSTER-BARBER, A. & BISHOP, J. M. 1998. Src interacts with dynamin and synapsin in neuronal cells. *Proc Natl Acad Sci U S A*, 95, 4673-7.
- FRANCESCHINI, A., SZKLARCZYK, D., FRANKILD, S., KUHN, M., SIMONOVIC, M., ROTH, A., LIN, J., MINGUEZ, P., BORK, P., VON MERING, C. & JENSEN, L. J. 2013. STRING v9.1: protein-protein

- interaction networks, with increased coverage and integration. *Nucleic Acids Res*, 41, D808-15.
- FRYER, C. J., WHITE, J. B. & JONES, K. A. 2004. Mastermind recruits CycC:CDK8 to phosphorylate the Notch ICD and coordinate activation with turnover. *Mol Cell*, 16, 509-20.
- FULDA, S. 2009. The PI3K/Akt/mTOR pathway as therapeutic target in neuroblastoma. *Curr Cancer Drug Targets*, 9, 729-37.
- FULTS, D. W., TOWLE, A. C., LAUDER, J. M. & MANESS, P. F. 1985. pp60c-src in the developing cerebellum. *Mol Cell Biol*, 5, 27-32.
- GERDES, J., SCHWAB, U., LEMKE, H. & STEIN, H. 1983. Production of a mouse monoclonal antibody reactive with a human nuclear antigen associated with cell proliferation. *Int J Cancer*, 31, 13-20.
- GIANCOTTI, F. G. & RUOSLAHTI, E. 1999. Integrin signaling. *Science*, 285, 1028-32.
- GILLON, A. D., LATHAM, C. F. & MILLER, E. A. 2012. Vesicle-mediated ER export of proteins and lipids. *Biochim Biophys Acta*, 1821, 1040-9.
- GMEINER, W. H. & HORITA, D. A. 2001. Implications of SH3 domain structure and dynamics for protein regulation and drug design. *Cell Biochem Biophys*, 35, 127-40.
- GOLDBERG, G. S., ALEXANDER, D. B., PELLICENA, P., ZHANG, Z. Y., TSUDA, H. & MILLER, W. T. 2003. Src phosphorylates Cas on tyrosine 253 to promote migration of transformed cells. *J Biol Chem*, 278, 46533-40.
- GRANTCHAROVA, V. P., RIDDLE, D. S. & BAKER, D. 2000. Long-range order in the src SH3 folding transition state. *Proc Natl Acad Sci U S A*, 97, 7084-9.
- GROVEMAN, B. R., FENG, S., FANG, X. Q., PFLUEGER, M., LIN, S. X., BIENKIEWICZ, E. A. & YU, X. 2012. The regulation of N-methyl-D-aspartate receptors by Src kinase. *FEBS J*, 279, 20-8.
- GUAN, J. L. & SHALLOWAY, D. 1992. Regulation of focal adhesion-associated protein tyrosine kinase by both cellular adhesion and oncogenic transformation. *Nature*, 358, 690-2.
- GUGLIELMI, L., CINNELLA, C., NARDELLA, M., MARESCA, G., VALENTINI, A., MERCANTI, D., FELSANI, A. & D'AGNANO, I. 2014. MYCN gene expression is required for the onset of the differentiation programme in neuroblastoma cells. *Cell Death Dis*, 5, e1081.
- GURNEY, J. G., SEVERSON, R. K., DAVIS, S. & ROBISON, L. L. 1995. Incidence of cancer in children in the United States. Sex-, race-, and 1-year age-specific rates by histologic type. *Cancer*, 75, 2186-95.
- GÄRTNER, A., FORNASIERO, E. F., MUNCK, S., VENNEKENS, K., SEUNTJENS, E., HUTTNER, W. B., VALTORTA, F. & DOTTI, C. G. 2012. N-cadherin specifies first asymmetry in developing neurons. *EMBO J*, 31, 1893-903.

- HALL, M. P., HUANG, S. & BLACK, D. L. 2004. Differentiation-induced colocalization of the KH-type splicing regulatory protein with polypyrimidine tract binding protein and the c-src pre-mRNA. *Mol Biol Cell*, 15, 774-86.
- HAMMOND, D. E., HYDE, R., KRATCHMAROVA, I., BEYNON, R. J., BLAGOEV, B. & CLAGUE, M. J. 2010. Quantitative analysis of HGF and EGF-dependent phosphotyrosine signaling networks. *J Proteome Res*, 9, 2734-42.
- HANKS, S. K. & POLTE, T. R. 1997. Signaling through focal adhesion kinase. *Bioessays*, 19, 137-45.
- HANSEN, K., ALONSO, G., COURTNEIDGE, S. A., RÖNNSTRAND, L. & HELDIN, C. H. 1997. PDGF-induced phosphorylation of Tyr28 in the N-terminus of Fyn affects Fyn activation. *Biochem Biophys Res Commun*, 241, 355-62.
- HARTENSTEIN, V. 1989. Early neurogenesis in *Xenopus*: the spatio-temporal pattern of proliferation and cell lineages in the embryonic spinal cord. *Neuron*, 3, 399-411.
- HAUPT, R., GARAVENTA, A., GAMBINI, C., PARODI, S., CANGEMI, G., CASALE, F., VISCARDI, E., BIANCHI, M., PRETE, A., JENKNER, A., LUKSCH, R., DI CATALDO, A., FAVRE, C., D'ANGELO, P., ZANAZZO, G. A., ARCAMONE, G., IZZI, G. C., GIGLIOTTI, A. R., PASTORE, G. & DE BERNARDI, B. 2010. Improved survival of children with neuroblastoma between 1979 and 2005: a report of the Italian Neuroblastoma Registry. *J Clin Oncol*, 28, 2331-8.
- HEEG-TRUESDELL, E. & LABONNE, C. 2006. Neural induction in *Xenopus* requires inhibition of Wnt-beta-catenin signaling. *Dev Biol*, 298, 71-86.
- HILLEN, W. & BERENS, C. 1994. Mechanisms underlying expression of Tn10 encoded tetracycline resistance. *Annu Rev Microbiol*, 48, 345-69.
- HINSBY, A. M., OLSEN, J. V., BENNETT, K. L. & MANN, M. 2003. Signaling initiated by overexpression of the fibroblast growth factor receptor-1 investigated by mass spectrometry. *Mol Cell Proteomics*, 2, 29-36.
- HOCHBERG, Y. & BENJAMINI, Y. 1990. More powerful procedures for multiple significance testing. *Stat Med*, 9, 811-8.
- HOOPER, C., TAVASSOLI, M., CHAPPLE, J. P., UWANOGHO, D., GOODYEAR, R., MELINO, G., LOVESTONE, S. & KILLICK, R. 2006. TAp73 isoforms antagonize Notch signalling in SH-SY5Y neuroblastomas and in primary neurones. *J Neurochem*, 99, 989-99.
- HORNBECK, P. V., KORNHAUSER, J. M., TKACHEV, S., ZHANG, B., SKRZYPEK, E., MURRAY, B., LATHAM, V. & SULLIVAN, M. 2012. PhosphoSitePlus: a comprehensive resource for investigating the structure and function of experimentally determined post-translational modifications in man and mouse. *Nucleic Acids Res*, 40, D261-70.
- HOWLADER, NOONE, KRAPCHO, NEYMAN, AMINOU, WALDRON, ALTEKRUSE, KOSARY, RUHL, TATALOVICH, CHO, MARIOTT,

- EISNER, LEWIS, CHEN, FEUER & CRONIN 2011. SEER Cancer Statistics Review, 1975-2009 (Vintage 2009 Populations). National Cancer Institute. Bethesda, MD.
- HUANG, D. W., SHERMAN, B. T. & LEMPICKI, R. A. 2009a. Bioinformatics enrichment tools: paths toward the comprehensive functional analysis of large gene lists. *Nucleic Acids Res*, 37, 1-13.
- HUANG, D. W., SHERMAN, B. T. & LEMPICKI, R. A. 2009b. Systematic and integrative analysis of large gene lists using DAVID bioinformatics resources. *Nat Protoc*, 4, 44-57.
- HUANG, T. H., HUO, L., WANG, Y. N., XIA, W., WEI, Y., CHANG, S. S., CHANG, W. C., FANG, Y. F., CHEN, C. T., LANG, J. Y., TU, C., WANG, Y., HSU, M. C., KUO, H. P., KO, H. W., SHEN, J., LEE, H. H., LEE, P. C., WU, Y., CHEN, C. H. & HUNG, M. C. 2013. Epidermal growth factor receptor potentiates MCM7-mediated DNA replication through tyrosine phosphorylation of Lyn kinase in human cancers. *Cancer Cell*, 23, 796-810.
- HUANG, Y. S., CHENG, C. Y., CHUEH, S. H., HUENG, D. Y., HUANG, Y. F., CHU, C. M., WU, S. T., TAI, M. C., LIANG, C. M., LIAO, M. H., CHEN, C. C., SHEN, L. H. & MA, K. H. 2012. Involvement of SHP2 in focal adhesion, migration and differentiation of neural stem cells. *Brain Dev*, 34, 674-84.
- HUBBARD, S. R. & TILL, J. H. 2000. Protein tyrosine kinase structure and function. *Annu Rev Biochem*, 69, 373-98.
- HUBBARD, S. R., WEI, L., ELLIS, L. & HENDRICKSON, W. A. 1994. Crystal structure of the tyrosine kinase domain of the human insulin receptor. *Nature*, 372, 746-54.
- HUNTER, T. & ECKHART, W. 2004. The discovery of tyrosine phosphorylation: it's all in the buffer! *Cell*, 116, S35-9, 1 p following S48.
- HUSE, M. & KURIYAN, J. 2002. The conformational plasticity of protein kinases. *Cell*, 109, 275-82.
- HUSI, H., WARD, M. A., CHOUDHARY, J. S., BLACKSTOCK, W. P. & GRANT, S. G. 2000. Proteomic analysis of NMDA receptor-adhesion protein signaling complexes. *Nat Neurosci*, 3, 661-9.
- IMAMOTO, A. & SORIANO, P. 1993. Disruption of the csk gene, encoding a negative regulator of Src family tyrosine kinases, leads to neural tube defects and embryonic lethality in mice. *Cell*, 73, 1117-24.
- ISAACS, H. V., POWNALL, M. E. & SLACK, J. M. 1994. eFGF regulates Xbra expression during Xenopus gastrulation. *EMBO J*, 13, 4469-81.
- ISHIHAMA, Y., ODA, Y., TABATA, T., SATO, T., NAGASU, T., RAPPSILBER, J. & MANN, M. 2005. Exponentially modified protein abundance index (emPAI) for estimation of absolute protein amount in proteomics by the number of sequenced peptides per protein. *Mol Cell Proteomics*, 4, 1265-72.
- ISHOLA, T. A. & CHUNG, D. H. 2007. Neuroblastoma. *Surg Oncol*, 16, 149-56.

- ITOH, K. & SOKOL, S. Y. 1999. Axis determination by inhibition of Wnt signaling in *Xenopus*. *Genes Dev*, 13, 2328-36.
- IWAHARA, T., FUJIMOTO, J., WEN, D., CUPPLES, R., BUCAY, N., ARAKAWA, T., MORI, S., RATZKIN, B. & YAMAMOTO, T. 1997. Molecular characterization of ALK, a receptor tyrosine kinase expressed specifically in the nervous system. *Oncogene*, 14, 439-49.
- IYER, S. C., RAMACHANDRAN IYER, E. P., MEDURI, R., RUBAHARAN, M., KUNTIMADDI, A., KARAMSETTY, M. & COX, D. N. 2013. Cut, via CrebA, transcriptionally regulates the COPII secretory pathway to direct dendrite development in *Drosophila*. *J Cell Sci*, 126, 4732-45.
- JACOBS, S., LIE, D. C., DECICCO, K. L., SHI, Y., DELUCA, L. M., GAGE, F. H. & EVANS, R. M. 2006. Retinoic acid is required early during adult neurogenesis in the dentate gyrus. *Proc Natl Acad Sci U S A*, 103, 3902-7.
- JOHNSON, T. M., WILLIAMSON, N. A., SCHOLZ, G., JAWOROWSKI, A., WETTENHALL, R. E., DUNN, A. R. & CHENG, H. C. 2000. Modulation of the catalytic activity of the Src family tyrosine kinase Hck by autophosphorylation at a novel site in the unique domain. *J Biol Chem*, 275, 33353-64.
- JOUNG, I., KIM, T., STOLZ, L. A., PAYNE, G., WINKLER, D. G., WALSH, C. T., STROMINGER, J. L. & SHIN, J. 1995. Modification of Ser59 in the unique N-terminal region of tyrosine kinase p56lck regulates specificity of its Src homology 2 domain. *Proc Natl Acad Sci U S A*, 92, 5778-82.
- JØRGENSEN, C., SHERMAN, A., CHEN, G. I., PASCULESCU, A., POLIAKOV, A., HSIUNG, M., LARSEN, B., WILKINSON, D. G., LINDING, R. & PAWSON, T. 2009. Cell-specific information processing in segregating populations of Eph receptor ephrin-expressing cells. *Science*, 326, 1502-9.
- KALIA, L. V., GINGRICH, J. R. & SALTER, M. W. 2004. Src in synaptic transmission and plasticity. *Oncogene*, 23, 8007-16.
- KANAZAWA, Y., UEDA, Y., SHIMASAKI, M., KATSUDA, S., YAMAMOTO, N., TOMITA, K. & TSUCHIYA, H. 2008. Down-regulation of plakoglobin in soft tissue sarcoma is associated with a higher risk of pulmonary metastasis. *Anticancer Res*, 28, 655-64.
- KANEHISA, M. & GOTO, S. 2000. KEGG: kyoto encyclopedia of genes and genomes. *Nucleic Acids Res*, 28, 27-30.
- KANEKO, T., LI, L. & LI, S. S. 2008. The SH3 domain--a family of versatile peptide- and protein-recognition module. *Front Biosci*, 13, 4938-52.
- KATO, G. & MAEDA, S. 1999. Neuron-specific Cdk5 kinase is responsible for mitosis-independent phosphorylation of c-Src at Ser75 in human Y79 retinoblastoma cells. *J Biochem*, 126, 957-61.
- KAY, B. K., WILLIAMSON, M. P. & SUDOL, M. 2000. The importance of being proline: the interaction of proline-rich motifs in signaling proteins with their cognate domains. *FASEB J*, 14, 231-41.

- KEHASSE, A., RICH, C. B., LEE, A., MCCOMB, M. E., COSTELLO, C. E. & TRINKAUS-RANDALL, V. 2013. Epithelial wounds induce differential phosphorylation changes in response to purinergic and EGF receptor activation. *Am J Pathol*, 183, 1841-52.
- KELDER, T., VAN IERSEL, M. P., HANSPERS, K., KUTMON, M., CONKLIN, B. R., EVELO, C. T. & PICO, A. R. 2012. WikiPathways: building research communities on biological pathways. *Nucleic Acids Res*, 40, D1301-7.
- KESAVAN, K. P., ISAACSON, C. C., ASHENDEL, C. L., GEAHLEN, R. L. & HARRISON, M. L. 2002. Characterization of the in vivo sites of serine phosphorylation on Lck identifying serine 59 as a site of mitotic phosphorylation. *J Biol Chem*, 277, 14666-73.
- KIM, B. & FELDMAN, E. L. 1998. Differential regulation of focal adhesion kinase and mitogen-activated protein kinase tyrosine phosphorylation during insulin-like growth factor-I-mediated cytoskeletal reorganization. *J Neurochem*, 71, 1333-6.
- KIM, J., MOSIOR, M., CHUNG, L. A., WU, H. & MCLAUGHLIN, S. 1991. Binding of peptides with basic residues to membranes containing acidic phospholipids. *Biophys J*, 60, 135-48.
- KING, H., ALEKSIC, T., HALUSKA, P. & MACAULAY, V. M. 2014. Can we unlock the potential of IGF-1R inhibition in cancer therapy? *Cancer Treat Rev*.
- KISHI, M., MIZUSEKI, K., SASAI, N., YAMAZAKI, H., SHIOTA, K., NAKANISHI, S. & SASAI, Y. 2000. Requirement of Sox2-mediated signaling for differentiation of early *Xenopus* neuroectoderm. *Development*, 127, 791-800.
- KMIECIK, T. E. & SHALLOWAY, D. 1987. Activation and suppression of pp60c-src transforming ability by mutation of its primary sites of tyrosine phosphorylation. *Cell*, 49, 65-73.
- KNIGHTON, D. R., ZHENG, J. H., TEN EYCK, L. F., ASHFORD, V. A., XUONG, N. H., TAYLOR, S. S. & SOWADSKI, J. M. 1991. Crystal structure of the catalytic subunit of cyclic adenosine monophosphate-dependent protein kinase. *Science*, 253, 407-14.
- KNOEPFLER, P. S., ZHANG, X.-Y., CHENG, P. F., GAFKEN, P. R., MCMAHON, S. B. & EISENMAN, R. N. 2006. Myc influences global chromatin structure. *The EMBO journal*, 25, 2723-34.
- KOEGL, M., ZLATKINE, P., LEY, S. C., COURTNEIDGE, S. A. & MAGEE, A. I. 1994. Palmitoylation of multiple Src-family kinases at a homologous N-terminal motif. *Biochem J*, 303 (Pt 3), 749-53.
- KOLKOVA, K., NOVITSKAYA, V., PEDERSEN, N., BEREZIN, V. & BOCK, E. 2000. Neural cell adhesion molecule-stimulated neurite outgrowth depends on activation of protein kinase C and the Ras-mitogen-activated protein kinase pathway. *J Neurosci*, 20, 2238-46.

- KOTANI, T., MORONE, N., YUASA, S., NADA, S. & OKADA, M. 2007. Constitutive activation of neuronal Src causes aberrant dendritic morphogenesis in mouse cerebellar Purkinje cells. *Neurosci Res*, 57, 210-9.
- KUHL, M. 2003. *Wnt signaling in development*, Georgetown, Tex. ; [Great Britain], Landes Bioscience ; Austin, Tex. : Eureka.com.
- KULLBERG, R. W., LENTZ, T. L. & COHEN, M. W. 1977. Development of the myotomal neuromuscular junction in *Xenopus laevis*: an electrophysiological and fine-structural study. *Dev Biol*, 60, 101-29.
- KURIYAN, J. & EISENBERG, D. 2007. The origin of protein interactions and allostery in colocalization. *Nature*, 450, 983-90.
- KÄRKKÄINEN, S., HIIPAKKA, M., WANG, J. H., KLEINO, I., VÄHÄ-JAAKKOLA, M., RENKEMA, G. H., LISS, M., WAGNER, R. & SAKSELA, K. 2006. Identification of preferred protein interactions by phage-display of the human Src homology-3 proteome. *EMBO Rep*, 7, 186-91.
- KÖHR, G. & SEEBURG, P. H. 1996. Subtype-specific regulation of recombinant NMDA receptor-channels by protein tyrosine kinases of the src family. *J Physiol*, 492 (Pt 2), 445-52.
- LAMMENS, T., SWERTS, K., DERYCKE, L., DE CRAEMER, A., DE BROUWER, S., DE PRETER, K., VAN ROY, N., VANDESOMPELE, J., SPELEMAN, F., PHILIPPÉ, J., BENOIT, Y., BEISKE, K., BRACKE, M. & LAUREYS, G. 2012. N-cadherin in neuroblastoma disease: expression and clinical significance. *PLoS One*, 7, e31206.
- LAVERDIÈRE, C., CHEUNG, N. K., KUSHNER, B. H., KRAMER, K., MODAK, S., LAQUAGLIA, M. P., WOLDEN, S., NESS, K. K., GURNEY, J. G. & SKLAR, C. A. 2005. Long-term complications in survivors of advanced stage neuroblastoma. *Pediatr Blood Cancer*, 45, 324-32.
- LEMMON, M. A. & SCHLESSINGER, J. 2010. Cell signaling by receptor tyrosine kinases. *Cell*, 141, 1117-34.
- LENNON, G., AUFRAY, C., POLYMEROPOULOS, M. & SOARES, M. B. 1996. The I.M.A.G.E. Consortium: an integrated molecular analysis of genomes and their expression. *Genomics*, 33, 151-2.
- LEVY, J. B., DORAI, T., WANG, L. H. & BRUGGE, J. S. 1987. The structurally distinct form of pp60c-src detected in neuronal cells is encoded by a unique c-src mRNA. *Mol Cell Biol*, 7, 4142-5.
- LEWIS, L. A., CHUNG, C. D., CHEN, J., PARNES, J. R., MORAN, M., PATEL, V. P. & MICELI, M. C. 1997. The Lck SH2 phosphotyrosine binding site is critical for efficient TCR-induced processive tyrosine phosphorylation of the zeta-chain and IL-2 production. *J Immunol*, 159, 2292-300.
- LI, S., IAKOUCHEVA, L. M., MOONEY, S. D. & RADIVOJAC, P. 2010. Loss of post-translational modification sites in disease. *Pac Symp Biocomput*, 337-47.
- LI, W., YOUNG, S. L., KING, N. & MILLER, W. T. 2008. Signaling properties of a non-metazoan Src kinase and the evolutionary history of Src negative regulation. *J Biol Chem*, 283, 15491-501.

- LIM, H. J., CROWE, P. & YANG, J. L. 2014. Current clinical regulation of PI3K/PTEN/Akt/mTOR signalling in treatment of human cancer. *J Cancer Res Clin Oncol*.
- LIM, W. A. & RICHARDS, F. M. 1994. Critical residues in an SH3 domain from Sem-5 suggest a mechanism for proline-rich peptide recognition. *Nat Struct Biol*, 1, 221-5.
- LIM, W. A., RICHARDS, F. M. & FOX, R. O. 1994. Structural determinants of peptide-binding orientation and of sequence specificity in SH3 domains. *Nature*, 372, 375-9.
- LINSTEDT, A. D., VETTER, M. L., BISHOP, J. M. & KELLY, R. B. 1992. Specific association of the proto-oncogene product pp60c-src with an intracellular organelle, the PC12 synaptic vesicle. *J Cell Biol*, 117, 1077-84.
- LIU, B. A., JABLONOWSKI, K., RAINA, M., ARCÉ, M., PAWSON, T. & NASH, P. D. 2006. The human and mouse complement of SH2 domain proteins-establishing the boundaries of phosphotyrosine signaling. *Mol Cell*, 22, 851-68.
- LIU, X., MAZANEK, P., DAM, V., WANG, Q., ZHAO, H., GUO, R., JAGANNATHAN, J., CNAAN, A., MARIS, J. M. & HOGARTY, M. D. 2008. Deregulated Wnt/beta-catenin program in high-risk neuroblastomas without MYCN amplification. *Oncogene*, 27, 1478-88.
- LOWELL, C. A. & SORIANO, P. 1996. Knockouts of Src-family kinases: stiff bones, wimpy T cells, and bad memories. *Genes Dev*, 10, 1845-57.
- LU, Y. M., RODER, J. C., DAVIDOW, J. & SALTER, M. W. 1998. Src activation in the induction of long-term potentiation in CA1 hippocampal neurons. *Science*, 279, 1363-7.
- LUTTRELL, D. K., LUTTRELL, L. M. & PARSONS, S. J. 1988. Augmented mitogenic responsiveness to epidermal growth factor in murine fibroblasts that overexpress pp60c-src. *Mol Cell Biol*, 8, 497-501.
- LYNCH, S. A., BRUGGE, J. S. & LEVINE, J. M. 1986. Induction of altered c-src product during neural differentiation of embryonal carcinoma cells. *Science*, 234, 873-6.
- MAA, M. C. & LEU, T. H. 1998. Vanadate-dependent FAK activation is accomplished by the sustained FAK Tyr-576/577 phosphorylation. *Biochem Biophys Res Commun*, 251, 344-9.
- MANESS, P. F., AUBRY, M., SHORES, C. G., FRAME, L. & PFENNINGER, K. H. 1988. c-src gene product in developing rat brain is enriched in nerve growth cone membranes. *Proc Natl Acad Sci U S A*, 85, 5001-5.
- MANESS, P. F. & MATTEN, W. T. 1990. Tyrosine phosphorylation of membrane-associated tubulin in nerve growth cones enriched in pp60c-src. *Ciba Found Symp*, 150, 57-69; discussion 69-78.
- MANESS, P. F., SORGE, L. K. & FULTS, D. W. 1986. An early developmental phase of pp60c-src expression in the neural ectoderm. *Dev Biol*, 117, 83-9.

- MANNING, G., WHYTE, D. B., MARTINEZ, R., HUNTER, T. & SUDARSANAM, S. 2002. The protein kinase complement of the human genome. *Science*, 298, 1912-34.
- MARINER, D. J., ANASTASIADIS, P., KEILHACK, H., BÖHMER, F. D., WANG, J. & REYNOLDS, A. B. 2001. Identification of Src phosphorylation sites in the catenin p120ctn. *J Biol Chem*, 276, 28006-13.
- MARTINEZ, R., MATHEY-PREVOT, B., BERNARDS, A. & BALTIMORE, D. 1987. Neuronal pp60c-src contains a six-amino acid insertion relative to its non-neuronal counterpart. *Science*, 237, 411-5.
- MATSUDA, M., MAYER, B. J., FUKUI, Y. & HANAFUSA, H. 1990. Binding of transforming protein, P47gag-crk, to a broad range of phosphotyrosine-containing proteins. *Science*, 248, 1537-9.
- MATSUNAGA, T., SHIRASAWA, H., ENOMOTO, H., YOSHIDA, H., IWAI, J., TANABE, M., KAWAMURA, K., ETOH, T. & OHNUMA, N. 1998. Neuronal src and trk a protooncogene expression in neuroblastomas and patient prognosis. *International journal of cancer. Journal international du cancer*, 79, 226-31.
- MATSUNAGA, T., SHIRASAWA, H., HISHIKI, T., YOSHIDA, H., KOUCHI, K., OHTSUKA, Y., KAWAMURA, K., ETOH, T. & OHNUMA, N. 2000. Enhanced expression of N-myc messenger RNA in neuroblastomas found by mass screening. *Clinical Cancer Research*, 6, 3199-3204.
- MATSUNAGA, T., SHIRASAWA, H., TANABE, M., OHNUMA, N., KAWAMURA, K., ETOH, T., TAKAHASHI, H. & SIMIZU, B. 1994a. Expression of Neuronal Src Messenger-Rna as a Favorable Marker and Inverse Correlation to N-Myc Gene Amplification in Human Neuroblastomas. *International Journal of Cancer*, 58, 793-798.
- MATSUNAGA, T., SHIRASAWA, H., TANABE, M., OHNUMA, N., KAWAMURA, K., ETOH, T., TAKAHASHI, H. & SIMIZU, B. 1994b. Expression of neuronal src mRNA as a favorable marker and inverse correlation to N-myc gene amplification in human neuroblastomas. *Int J Cancer*, 58, 793-8.
- MATSUNAGA, T., SHIRASAWA, H., TANABE, M., OHNUMA, N., TAKAHASHI, H. & SIMIZU, B. 1993a. Expression of alternatively spliced src messenger RNAs related to neuronal differentiation in human neuroblastomas. *Cancer Res*, 53, 3179-85.
- MATSUNAGA, T., SHIRASAWA, H., TANABE, M., OHNUMA, N., TAKAHASHI, H. & SIMIZU, B. 1993b. Expression of Alternatively Spliced Src Messenger-Rnas Related to Neuronal Differentiation in Human Neuroblastomas. *Cancer Research*, 53, 3179-3185.
- MATTHAY, K. K., GEORGE, R. E. & YU, A. L. 2012. Promising therapeutic targets in neuroblastoma. *Clin Cancer Res*, 18, 2740-53.
- MATTHAY, K. K., VILLABLANCA, J. G., SEEGER, R. C., STRAM, D. O., HARRIS, R. E., RAMSAY, N. K., SWIFT, P., SHIMADA, H., BLACK, C. T., BRODEUR, G. M., GERBING, R. B. & REYNOLDS, C. P. 1999.

- Treatment of high-risk neuroblastoma with intensive chemotherapy, radiotherapy, autologous bone marrow transplantation, and 13-cis-retinoic acid. Children's Cancer Group. *N Engl J Med*, 341, 1165-73.
- MAYER, B. J., HAMAGUCHI, M. & HANAFUSA, H. 1988. A novel viral oncogene with structural similarity to phospholipase C. *Nature*, 332, 272-5.
- MAYER, B. J., HIRAI, H. & SAKAI, R. 1995. Evidence that SH2 domains promote processive phosphorylation by protein-tyrosine kinases. *Curr Biol*, 5, 296-305.
- MEIJERING, E., JACOB, M., SARRIA, J. C., STEINER, P., HIRLING, H. & UNSER, M. 2004. Design and validation of a tool for neurite tracing and analysis in fluorescence microscopy images. *Cytometry A*, 58, 167-76.
- MELLSTRÖM, K., BJELFMAN, C., HAMMERLING, U. & PÅHLMAN, S. 1987. Expression of c-src in cultured human neuroblastoma and small-cell lung carcinoma cell lines correlates with neurocrine differentiation. *Mol Cell Biol*, 7, 4178-84.
- MERTE, J., JENSEN, D., WRIGHT, K., SARFIELD, S., WANG, Y., SCHEKMAN, R. & GINTY, D. D. 2010. Sec24b selectively sorts Vangl2 to regulate planar cell polarity during neural tube closure. *Nat Cell Biol*, 12, 41-6; sup pp 1-8.
- MESSINA, S., ONOFRI, F., BONGIORNO-BORBONE, L., GIOVEDÌ, S., VALTORTA, F., GIRAULT, J. A. & BENFENATI, F. 2003. Specific interactions of neuronal focal adhesion kinase isoforms with Src kinases and amphiphysin. *J Neurochem*, 84, 253-65.
- MIN, H., CHAN, R. C. & BLACK, D. L. 1995. The generally expressed hnRNP F is involved in a neural-specific pre-mRNA splicing event. *Genes Dev*, 9, 2659-71.
- MIN, T. H., KRIEBEL, M., HOU, S. & PERA, E. M. 2011. The dual regulator Sufu integrates Hedgehog and Wnt signals in the early *Xenopus* embryo. *Dev Biol*, 358, 262-76.
- MIRAVET, S., PIEDRA, J., CASTAÑO, J., RAURELL, I., FRANCÍ, C., DUÑACH, M. & GARCÍA DE HERREROS, A. 2003. Tyrosine phosphorylation of plakoglobin causes contrary effects on its association with desmosomes and adherens junction components and modulates beta-catenin-mediated transcription. *Mol Cell Biol*, 23, 7391-402.
- MIYAGI, Y., YAMASHITA, T., FUKAYA, M., SONODA, T., OKUNO, T., YAMADA, K., WATANABE, M., NAGASHIMA, Y., AOKI, I., OKUDA, K., MISHINA, M. & KAWAMOTO, S. 2002. Delphilin: a novel PDZ and formin homology domain-containing protein that synaptically colocalizes and interacts with glutamate receptor delta 2 subunit. *J Neurosci*, 22, 803-14.
- MIYAMOTO, S., TERAMOTO, H., COSO, O. A., GUTKIND, J. S., BURBELO, P. D., AKIYAMA, S. K. & YAMADA, K. M. 1995. Integrin function: molecular hierarchies of cytoskeletal and signaling molecules. *J Cell Biol*, 131, 791-805.
- MIYAZAKI, T., TANAKA, S., SANJAY, A. & BARON, R. 2006. The role of c-Src kinase in the regulation of osteoclast function. *Mod Rheumatol*, 16, 68-74.

- MODAFFERI, E. F. & BLACK, D. L. 1997. A complex intronic splicing enhancer from the c-src pre-mRNA activates inclusion of a heterologous exon. *Mol Cell Biol*, 17, 6537-45.
- MOODY, S. A. & JE, H. S. 2002. Neural induction, neural fate stabilization, and neural stem cells. *ScientificWorldJournal*, 2, 1147-66.
- MOODY, S. A., MILLER, V., SPANOS, A. & FRANKFURTER, A. 1996. Developmental expression of a neuron-specific beta-tubulin in frog (*Xenopus laevis*): a marker for growing axons during the embryonic period. *J Comp Neurol*, 364, 219-30.
- MORAN, M. F., KOCH, C. A., ANDERSON, D., ELLIS, C., ENGLAND, L., MARTIN, G. S. & PAWSON, T. 1990. Src homology region 2 domains direct protein-protein interactions in signal transduction. *Proc Natl Acad Sci U S A*, 87, 8622-6.
- MORRIS, S. W., KIRSTEIN, M. N., VALENTINE, M. B., DITTMER, K. G., SHAPIRO, D. N., SALTMAN, D. L. & LOOK, A. T. 1994. Fusion of a kinase gene, ALK, to a nucleolar protein gene, NPM, in non-Hodgkin's lymphoma. *Science*, 263, 1281-4.
- MOSS, S. J., GORRIE, G. H., AMATO, A. & SMART, T. G. 1995. Modulation of GABAA receptors by tyrosine phosphorylation. *Nature*, 377, 344-8.
- MOSSÉ, Y. P., LAUDENSLAGER, M., LONGO, L., COLE, K. A., WOOD, A., ATTIYEH, E. F., LAQUAGLIA, M. J., SENNETT, R., LYNCH, J. E., PERRI, P., LAUREYS, G., SPELEMAN, F., KIM, C., HOU, C., HAKONARSON, H., TORKAMANI, A., SCHORK, N. J., BRODEUR, G. M., TONINI, G. P., RAPPAPORT, E., DEVOTO, M. & MARIS, J. M. 2008. Identification of ALK as a major familial neuroblastoma predisposition gene. *Nature*, 455, 930-5.
- MUKHERJEE, A., ARNAUD, L. & COOPER, J. A. 2003. Lipid-dependent recruitment of neuronal Src to lipid rafts in the brain. *J Biol Chem*, 278, 40806-14.
- MUSACCHIO, A., NOBLE, M., PAUPTIT, R., WIERENGA, R. & SARASTE, M. 1992. Crystal structure of a Src-homology 3 (SH3) domain. *Nature*, 359, 851-5.
- NADA, S., YAGI, T., TAKEDA, H., TOKUNAGA, T., NAKAGAWA, H., IKAWA, Y., OKADA, M. & AIZAWA, S. 1993. Constitutive activation of Src family kinases in mouse embryos that lack Csk. *Cell*, 73, 1125-35.
- NAKAZAWA, T., KOMAI, S., WATABE, A. M., KIYAMA, Y., FUKAYA, M., ARIMA-YOSHIDA, F., HORAI, R., SUDO, K., EBINE, K., DELAWARY, M., GOTO, J., UMEMORI, H., TEZUKA, T., IWAKURA, Y., WATANABE, M., YAMAMOTO, T. & MANABE, T. 2006. NR2B tyrosine phosphorylation modulates fear learning as well as amygdaloid synaptic plasticity. *EMBO J*, 25, 2867-77.
- NEET, K. & HUNTER, T. 1996. Vertebrate non-receptor protein-tyrosine kinase families. *Genes Cells*, 1, 147-69.

- NIEBER, F., HEDDERICH, M., JAHN, O., PIELER, T. & HENNINGFELD, K. A. 2013. NumbL is essential for *Xenopus* primary neurogenesis. *BMC Dev Biol*, 13, 36.
- NOBLE, M. E., MUSACCHIO, A., SARASTE, M., COURTNEIDGE, S. A. & WIERENGA, R. K. 1993. Crystal structure of the SH3 domain in human Fyn; comparison of the three-dimensional structures of SH3 domains in tyrosine kinases and spectrin. *EMBO J*, 12, 2617-24.
- NORUM, M., TANG, E., CHAVOSHI, T., SCHWARZ, H., LINKE, D., UV, A. & MOUSSIAN, B. 2010. Trafficking through COPII stabilises cell polarity and drives secretion during *Drosophila* epidermal differentiation. *PLoS One*, 5, e10802.
- OBARA, Y., LABUDDA, K., DILLON, T. J. & STORK, P. J. 2004. PKA phosphorylation of Src mediates Rap1 activation in NGF and cAMP signaling in PC12 cells. *J Cell Sci*, 117, 6085-94.
- OBENAUER, J. C., CANTLEY, L. C. & YAFFE, M. B. 2003. Scansite 2.0: Proteome-wide prediction of cell signaling interactions using short sequence motifs. *Nucleic Acids Res*, 31, 3635-41.
- OLSEN, J. V., BLAGOEV, B., GNAD, F., MACEK, B., KUMAR, C., MORTENSEN, P. & MANN, M. 2006. Global, in vivo, and site-specific phosphorylation dynamics in signaling networks. *Cell*, 127, 635-48.
- ONEYAMA, C., HIKITA, T., NADA, S. & OKADA, M. 2008. Functional dissection of transformation by c-Src and v-Src. *Genes Cells*, 13, 1-12.
- OPPERMANN, F. S., GNAD, F., OLSEN, J. V., HORNBERGER, R., GREFF, Z., KÉRI, G., MANN, M. & DAUB, H. 2009. Large-scale proteomics analysis of the human kinome. *Mol Cell Proteomics*, 8, 1751-64.
- OTTE, A. P., KOSTER, C. H., SNOEK, G. T. & DURSTON, A. J. 1988. Protein kinase C mediates neural induction in *Xenopus laevis*. *Nature*, 334, 618-20.
- OTTLIE, S., RAULF, F., BARNEKOW, A., HANNIG, G. & SCHARTL, M. 1992. Multiple src-related kinase genes, srk1-4, in the fresh water sponge *Spongilla lacustris*. *Oncogene*, 7, 1625-30.
- OU, C. Y., LABONTE, M. J., MANEGOLD, P. C., SO, A. Y., IANCULESCU, I., GERKE, D. S., YAMAMOTO, K. R., LADNER, R. D., KAHN, M., KIM, J. H. & STALLCUP, M. R. 2011. A coactivator role of CARM1 in the dysregulation of β -catenin activity in colorectal cancer cell growth and gene expression. *Mol Cancer Res*, 9, 660-70.
- OZKIRIMLI, E. & POST, C. B. 2006. Src kinase activation: A switched electrostatic network. *Protein Sci*, 15, 1051-62.
- PAIGE, L. A., NADLER, M. J., HARRISON, M. L., CASSADY, J. M. & GEAHLEN, R. L. 1993. Reversible palmitoylation of the protein-tyrosine kinase p56lck. *J Biol Chem*, 268, 8669-74.
- PALMER, R. H., VERNERSSON, E., GRABBE, C. & HALLBERG, B. 2009. Anaplastic lymphoma kinase: signalling in development and disease. *Biochem J*, 420, 345-61.

- PAN, Q., QIAO, F., GAO, C., NORMAN, B., OPTICAN, L. & ZELENKA, P. S. 2011. Cdk5 targets active Src for ubiquitin-dependent degradation by phosphorylating Src(S75). *Cell Mol Life Sci*, 68, 3425-36.
- PAN, Z. Q., KENTSIS, A., DIAS, D. C., YAMOA, K. & WU, K. 2004. Nedd8 on cullin: building an expressway to protein destruction. *Oncogene*, 23, 1985-97.
- PARSONS, J. T. & PARSONS, S. J. 1997. Src family protein tyrosine kinases: cooperating with growth factor and adhesion signaling pathways. *Curr Opin Cell Biol*, 9, 187-92.
- PATWARDHAN, P. & MILLER, W. T. 2007. Processive phosphorylation: mechanism and biological importance. *Cell Signal*, 19, 2218-26.
- PELKEY, K. A., ASKALAN, R., PAUL, S., KALIA, L. V., NGUYEN, T. H., PITCHER, G. M., SALTER, M. W. & LOMBROSO, P. J. 2002. Tyrosine phosphatase STEP is a tonic brake on induction of long-term potentiation. *Neuron*, 34, 127-38.
- PELLICENA, P. & MILLER, W. T. 2001. Processive phosphorylation of p130Cas by Src depends on SH3-polyproline interactions. *J Biol Chem*, 276, 28190-6.
- PENZEL, R., OSCHWALD, R., CHEN, Y., TACKE, L. & GRUNZ, H. 1997. Characterization and early embryonic expression of a neural specific transcription factor xSOX3 in *Xenopus laevis*. *Int J Dev Biol*, 41, 667-77.
- PEUKERT, K., STALLER, P., SCHNEIDER, A., CARMICHAEL, G., HÄNEL, F. & EILERS, M. 1997. An alternative pathway for gene regulation by Myc. *The EMBO journal*, 16, 5672-86.
- PFEFFER, S. R. 2001. Membrane transport: retromer to the rescue. *Curr Biol*, 11, R109-11.
- POPKO, J., FERNANDES, A., BRITES, D. & LANIER, L. M. 2009. Automated analysis of NeuronJ tracing data. *Cytometry A*, 75, 371-6.
- POPKO-SCIBOR, A. E., LINDBERG, M. J., HANSSON, M. L., HOLMLUND, T. & WALLBERG, A. E. 2011. Ubiquitination of Notch1 is regulated by MAML1-mediated p300 acetylation of Notch1. *Biochem Biophys Res Commun*, 416, 300-6.
- POTTS, W. M., REYNOLDS, A. B., LANSING, T. J. & PARSONS, J. T. 1988. Activation of pp60c-src transforming potential by mutations altering the structure of an amino terminal domain containing residues 90-95. *Oncogene Res*, 3, 343-55.
- PYPER, J. M. & BOLEN, J. B. 1989. Neuron-specific splicing of C-SRC RNA in human brain. *J Neurosci Res*, 24, 89-96.
- PYPER, J. M. & BOLEN, J. B. 1990. Identification of a novel neuronal C-SRC exon expressed in human brain. *Mol Cell Biol*, 10, 2035-40.
- PÉREZ, Y., GAIRÍ, M., PONS, M. & BERNADÓ, P. 2009. Structural characterization of the natively unfolded N-terminal domain of human c-Src kinase: insights into the role of phosphorylation of the unique domain. *J Mol Biol*, 391, 136-48.

- PÉREZ, Y., MAFFEI, M., IGEA, A., AMATA, I., GAIRÍ, M., NEBREDA, A. R., BERNADÓ, P. & PONS, M. 2013. Lipid binding by the Unique and SH3 domains of c-Src suggests a new regulatory mechanism. *Sci Rep*, 3, 1295.
- QI, J., WANG, J., ROMANYUK, O. & SIU, C. H. 2006. Involvement of Src family kinases in N-cadherin phosphorylation and beta-catenin dissociation during transendothelial migration of melanoma cells. *Mol Biol Cell*, 17, 1261-72.
- RAULF, F., ROBERTSON, S. M. & SCHARTL, M. 1989. Evolution of the neuron-specific alternative splicing product of the c-src proto-oncogene. *J Neurosci Res*, 24, 81-8.
- REN, R., MAYER, B. J., CICCETTI, P. & BALTIMORE, D. 1993. Identification of a ten-amino acid proline-rich SH3 binding site. *Science*, 259, 1157-61.
- RESH, M. D. 1993. Interaction of tyrosine kinase oncoproteins with cellular membranes. *Biochim Biophys Acta*, 1155, 307-22.
- RESH, M. D. 1994. Myristylation and palmitoylation of Src family members: the fats of the matter. *Cell*, 76, 411-3.
- REYNOLDS, C. H., GARWOOD, C. J., WRAY, S., PRICE, C., KELLIE, S., PERERA, T., ZVELEBIL, M., YANG, A., SHEPPARD, P. W., VARNDELL, I. M., HANGER, D. P. & ANDERTON, B. H. 2008. Phosphorylation regulates tau interactions with Src homology 3 domains of phosphatidylinositol 3-kinase, phospholipase Cgamma1, Grb2, and Src family kinases. *J Biol Chem*, 283, 18177-86.
- RICKLES, R. J., BOTFIELD, M. C., WENG, Z., TAYLOR, J. A., GREEN, O. M., BRUGGE, J. S. & ZOLLER, M. J. 1994. Identification of Src, Fyn, Lyn, PI3K and Abl SH3 domain ligands using phage display libraries. *EMBO J*, 13, 5598-604.
- RICKLES, R. J., BOTFIELD, M. C., ZHOU, X. M., HENRY, P. A., BRUGGE, J. S. & ZOLLER, M. J. 1995. Phage display selection of ligand residues important for Src homology 3 domain binding specificity. *Proc Natl Acad Sci U S A*, 92, 10909-13.
- RILEY, R. D., HENEY, D., JONES, D. R., SUTTON, A. J., LAMBERT, P. C., ABRAMS, K. R., YOUNG, B., WAILOO, A. J. & BURCHILL, S. A. 2004. A systematic review of molecular and biological tumor markers in neuroblastoma. *Clin Cancer Res*, 10, 4-12.
- ROBBINS, S. M., QUINTRELL, N. A. & BISHOP, J. M. 1995. Myristoylation and differential palmitoylation of the HCK protein-tyrosine kinases govern their attachment to membranes and association with caveolae. *Mol Cell Biol*, 15, 3507-15.
- ROBERTS, A. 2000. Early functional organization of spinal neurons in developing lower vertebrates. *Brain Res Bull*, 53, 585-93.
- ROCHE, S., FUMAGALLI, S. & COURTNEIDGE, S. A. 1995a. Requirement for Src family protein tyrosine kinases in G2 for fibroblast cell division. *Science*, 269, 1567-9.

- ROCHE, S., KOEGL, M., BARONE, M. V., ROUSSEL, M. F. & COURTNEIDGE, S. A. 1995b. DNA synthesis induced by some but not all growth factors requires Src family protein tyrosine kinases. *Mol Cell Biol*, 15, 1102-9.
- RODRÍGUEZ-FERNÁNDEZ, J. L. & ROZENGURT, E. 1998. Bombesin, vasopressin, lysophosphatidic acid, and sphingosylphosphorylcholine induce focal adhesion kinase activation in intact Swiss 3T3 cells. *J Biol Chem*, 273, 19321-8.
- ROSKOSKI, R. 2004. Src protein-tyrosine kinase structure and regulation. *Biochem Biophys Res Commun*, 324, 1155-64.
- ROSKOSKI, R. 2005. Src kinase regulation by phosphorylation and dephosphorylation. *Biochem Biophys Res Commun*, 331, 1-14.
- ROSS, C. A., WRIGHT, G. E., RESH, M. D., PEARSON, R. C. & SNYDER, S. H. 1988. Brain-specific src oncogene mRNA mapped in rat brain by in situ hybridization. *Proc Natl Acad Sci U S A*, 85, 9831-5.
- SACCO, F., PERFETTO, L., CASTAGNOLI, L. & CESARENI, G. 2012. The human phosphatase interactome: An intricate family portrait. *FEBS Lett*, 586, 2732-9.
- SAKSELA, K. & PERMI, P. 2012. SH3 domain ligand binding: What's the consensus and where's the specificity? *FEBS Lett*, 586, 2609-14.
- SAMKARI, A., COOPER, Z. A., HOLLOWAY, M. P., LIU, J. & ALTURA, R. A. 2012. Rapamycin induces the anti-apoptotic protein survivin in neuroblastoma. *Int J Biochem Mol Biol*, 3, 28-35.
- SANDILANDS, E., CANS, C., FINCHAM, V. J., BRUNTON, V. G., MELLOR, H., PRENDERGAST, G. C., NORMAN, J. C., SUPERTI-FURGA, G. & FRAME, M. C. 2004. RhoB and actin polymerization coordinate Src activation with endosome-mediated delivery to the membrane. *Dev Cell*, 7, 855-69.
- SANTORO, B., GRANT, S. G., BARTSCH, D. & KANDEL, E. R. 1997. Interactive cloning with the SH3 domain of N-src identifies a new brain specific ion channel protein, with homology to eag and cyclic nucleotide-gated channels. *Proc Natl Acad Sci U S A*, 94, 14815-20.
- SCHALLER, M. D. 2004. FAK and paxillin: regulators of N-cadherin adhesion and inhibitors of cell migration? *J Cell Biol*, 166, 157-9.
- SCHALLER, M. D. & SCHAEFER, E. M. 2001. Multiple stimuli induce tyrosine phosphorylation of the Crk-binding sites of paxillin. *Biochem J*, 360, 57-66.
- SCHILLING, F. H., SPIX, C., BERTHOLD, F., ERTTMANN, R., FEHSE, N., HERO, B., KLEIN, G., SANDER, J., SCHWARZ, K., TREUNER, J., ZORN, U. & MICHAELIS, J. 2002. Neuroblastoma screening at one year of age. *N Engl J Med*, 346, 1047-53.
- SCHLAEPFER, D. D., HANKS, S. K., HUNTER, T. & VAN DER GEER, P. 1994. Integrin-mediated signal transduction linked to Ras pathway by GRB2 binding to focal adhesion kinase. *Nature*, 372, 786-91.

- SCHMIDT, M. H., DIKIC, I. & BÖGLER, O. 2005. Src phosphorylation of Alix/AIP1 modulates its interaction with binding partners and antagonizes its activities. *J Biol Chem*, 280, 3414-25.
- SCHMIDT, M. R. & HAUCKE, V. 2007. Recycling endosomes in neuronal membrane traffic. *Biol Cell*, 99, 333-42.
- SCHNEIDER, C. A., RASBAND, W. S. & ELICEIRI, K. W. 2012. NIH Image to ImageJ: 25 years of image analysis. *Nat Methods*, 9, 671-5.
- SCHWARTZ, M. A., SCHALLER, M. D. & GINSBERG, M. H. 1995. Integrins: emerging paradigms of signal transduction. *Annu Rev Cell Dev Biol*, 11, 549-99.
- SEGERSTRÖM, L., BARYAWNO, N., SVEINBJÖRNSSON, B., WICKSTRÖM, M., ELFMAN, L., KOGNER, P. & JOHNSEN, J. I. 2011. Effects of small molecule inhibitors of PI3K/Akt/mTOR signaling on neuroblastoma growth in vitro and in vivo. *Int J Cancer*, 129, 2958-65.
- SENIS, Y. A., MAZHARIAN, A. & MORI, J. 2014. Src family kinases: at the forefront of platelet activation. *Blood*.
- SHAW, A. S., AMREIN, K. E., HAMMOND, C., STERN, D. F., SEFTON, B. M. & ROSE, J. K. 1989. The lck tyrosine protein kinase interacts with the cytoplasmic tail of the CD4 glycoprotein through its unique amino-terminal domain. *Cell*, 59, 627-36.
- SHEN, Y. & SCHALLER, M. D. 1999. Focal adhesion targeting: the critical determinant of FAK regulation and substrate phosphorylation. *Mol Biol Cell*, 10, 2507-18.
- SHENOY, S., CHACKALAPARAMPIL, I., BAGRODIA, S., LIN, P. H. & SHALLOWAY, D. 1992. Role of p34cdc2-mediated phosphorylations in two-step activation of pp60c-src during mitosis. *Proc Natl Acad Sci U S A*, 89, 7237-41.
- SHI, X., OPI, S., LUGARI, A., RESTOUIN, A., COURSEINDEL, T., PARROT, I., PEREZ, J., MADORE, E., ZIMMERMANN, P., CORBEIL, J., HUANG, M., AROLD, S. T., COLLETTE, Y. & MORELLI, X. 2010. Identification and biophysical assessment of the molecular recognition mechanisms between the human haemopoietic cell kinase Src homology domain 3 and ALG-2-interacting protein X. *Biochem J*, 431, 93-102.
- SIDELL, N. 1982. Retinoic acid-induced growth inhibition and morphologic differentiation of human neuroblastoma cells in vitro. *J Natl Cancer Inst*, 68, 589-96.
- SINDELKA, R., FERJENTSIK, Z. & JONÁK, J. 2006. Developmental expression profiles of *Xenopus laevis* reference genes. *Dev Dyn*, 235, 754-8.
- SIVE, H. L., DRAPER, B. W., HARLAND, R. M. & WEINTRAUB, H. 1990. Identification of a retinoic acid-sensitive period during primary axis formation in *Xenopus laevis*. *Genes Dev*, 4, 932-42.
- SMART, J. E., OPPERMAN, H., CZERNILOFSKY, A. P., PURCHIO, A. F., ERIKSON, R. L. & BISHOP, J. M. 1981. Characterization of sites for tyrosine

phosphorylation in the transforming protein of Rous sarcoma virus (pp60v-src) and its normal cellular homologue (pp60c-src). *Proc Natl Acad Sci U S A*, 78, 6013-7.

- SMOOT, M. E., ONO, K., RUSCHEINSKI, J., WANG, P. L. & IDEKER, T. 2011. Cytoscape 2.8: new features for data integration and network visualization. *Bioinformatics*, 27, 431-2.
- SODA, M., CHOI, Y. L., ENOMOTO, M., TAKADA, S., YAMASHITA, Y., ISHIKAWA, S., FUJIWARA, S., WATANABE, H., KURASHINA, K., HATANAKA, H., BANDO, M., OHNO, S., ISHIKAWA, Y., ABURATANI, H., NIKI, T., SOHARA, Y., SUGIYAMA, Y. & MANO, H. 2007. Identification of the transforming EML4-ALK fusion gene in non-small-cell lung cancer. *Nature*, 448, 561-6.
- SOLECKI, D. J., LIU, X. L., TOMODA, T., FANG, Y. & HATTEN, M. E. 2001. Activated Notch2 signaling inhibits differentiation of cerebellar granule neuron precursors by maintaining proliferation. *Neuron*, 31, 557-68.
- SONGYANG, Z., CARRAWAY, K. L., ECK, M. J., HARRISON, S. C., FELDMAN, R. A., MOHAMMADI, M., SCHLESSINGER, J., HUBBARD, S. R., SMITH, D. P. & ENG, C. 1995. Catalytic specificity of protein-tyrosine kinases is critical for selective signalling. *Nature*, 373, 536-9.
- SONGYANG, Z., SHOELSON, S. E., CHAUDHURI, M., GISH, G., PAWSON, T., HASER, W. G., KING, F., ROBERTS, T., RATNOFSKY, S. & LECHLEIDER, R. J. 1993. SH2 domains recognize specific phosphopeptide sequences. *Cell*, 72, 767-78.
- SPITZENBERG, V., KÖNIG, C., ULM, S., MARONE, R., RÖPKE, L., MÜLLER, J. P., GRÜN, M., BAUER, R., RUBIO, I., WYMANN, M. P., VOIGT, A. & WETZKER, R. 2010. Targeting PI3K in neuroblastoma. *J Cancer Res Clin Oncol*, 136, 1881-90.
- SRIRAM, G., REICHMAN, C., TUNCEROGLU, A., KAUSHAL, N., SALEH, T., MACHIDA, K., MAYER, B., GE, Q., LI, J., HORNBECK, P., KALODIMOS, C. G. & BIRGE, R. B. 2011. Phosphorylation of Crk on tyrosine 251 in the RT loop of the SH3C domain promotes Abl kinase transactivation. *Oncogene*, 30, 4645-55.
- STEHELIN, D., VARMUS, H. E., BISHOP, J. M. & VOGT, P. K. 1976. DNA related to the transforming gene(s) of avian sarcoma viruses is present in normal avian DNA. *Nature*, 260, 170-3.
- STEIN, P. L., VOGEL, H. & SORIANO, P. 1994. Combined deficiencies of Src, Fyn, and Yes tyrosine kinases in mutant mice. *Genes Dev*, 8, 1999-2007.
- STERN, K. A., VISSER SMIT, G. D., PLACE, T. L., WINISTORFER, S., PIPER, R. C. & LILL, N. L. 2007. Epidermal growth factor receptor fate is controlled by Hrs tyrosine phosphorylation sites that regulate Hrs degradation. *Mol Cell Biol*, 27, 888-98.
- STOVER, D. R., LIEBETANZ, J. & LYDON, N. B. 1994. Cdc2-mediated modulation of pp60c-src activity. *J Biol Chem*, 269, 26885-9.

- SUGIMOTO, Y., ERIKSON, E., GRAZIANI, Y. & ERIKSON, R. L. 1985. Inter- and intramolecular interactions of highly purified Rous sarcoma virus-transforming protein, pp60v-src. *J Biol Chem*, 260, 13838-43.
- SUGRUE, M. M., BRUGGE, J. S., MARSHAK, D. R., GREENGARD, P. & GUSTAFSON, E. L. 1990. Immunocytochemical localization of the neuron-specific form of the c-src gene product, pp60c-src(+), in rat brain. *J Neurosci*, 10, 2513-27.
- SUMMERTON, J. & WELLER, D. 1997. Morpholino antisense oligomers: design, preparation, and properties. *Antisense Nucleic Acid Drug Dev*, 7, 187-95.
- SUPERTI-FURGA, G., FUMAGALLI, S., KOEGL, M., COURTNEIDGE, S. A. & DRAETTA, G. 1993. Csk inhibition of c-Src activity requires both the SH2 and SH3 domains of Src. *EMBO J*, 12, 2625-34.
- TADA, H., HATOKO, M., TANAKA, A., KUWAHARA, M. & MURAMATSU, T. 2000. Expression of desmoglein I and plakoglobin in skin carcinomas. *J Cutan Pathol*, 27, 24-9.
- TCHORZ, J. S., TOME, M., CLOËTTA, D., SIVASANKARAN, B., GRZMIL, M., HUBER, R. M., RUTZ-SCHATZMANN, F., KIRCHHOFF, F., SCHAEEREN-WIEMERS, N., GASSMANN, M., HEMMINGS, B. A., MERLO, A. & BETTLER, B. 2012. Constitutive Notch2 signaling in neural stem cells promotes tumorigenic features and astroglial lineage entry. *Cell Death Dis*, 3, e325.
- TERUI, E., MATSUNAGA, T., YOSHIDA, H., KOUCHI, K., KURODA, H., HISHIKI, T., SAITO, T., YAMADA, S., SHIRASAWA, H. & OHNUMA, N. 2005. Shc family expression in neuroblastoma: high expression of shcC is associated with a poor prognosis in advanced neuroblastoma. *Clin Cancer Res*, 11, 3280-7.
- THOMAS, J. W., ELLIS, B., BOERNER, R. J., KNIGHT, W. B., WHITE, G. C. & SCHALLER, M. D. 1998. SH2- and SH3-mediated interactions between focal adhesion kinase and Src. *J Biol Chem*, 273, 577-83.
- TIWARI, R., BROWN, A., NARRAMANENI, S., SUN, G. & PARANG, K. 2010. Synthesis and evaluation of conformationally constrained peptide analogues as the Src SH3 domain binding ligands. *Biochimie*, 92, 1153-63.
- TOJIMA, T., KOBAYASHI, S. & ITO, E. 2003. Dual role of cyclic AMP-dependent protein kinase in neuritogenesis and synaptogenesis during neuronal differentiation. *J Neurosci Res*, 74, 829-37.
- TSUBONO, Y. & HISAMICHI, S. 2004. A halt to neuroblastoma screening in Japan. *N Engl J Med*, 350, 2010-1.
- UVERSKY, V. N., OLDFIELD, C. J. & DUNKER, A. K. 2008. Intrinsically disordered proteins in human diseases: introducing the D2 concept. *Annu Rev Biophys*, 37, 215-46.
- VAZQUEZ, M. L. 2007. *Biological consequences of Phosphorylation of Serine 59 on Tyrosine kinase Lck*. Purdue University.

- VITALI, R., MANCINI, C., CESI, V., TANNO, B., PISCITELLI, M., MANCUSO, M., SESTI, F., PASQUALI, E., CALABRETTA, B., DOMINICI, C. & RASCHELLÀ, G. 2009. Activity of tyrosine kinase inhibitor Dasatinib in neuroblastoma cells in vitro and in orthotopic mouse model. *Int J Cancer*, 125, 2547-55.
- WAHL-SCHOTT, C. & BIEL, M. 2009. HCN channels: structure, cellular regulation and physiological function. *Cell Mol Life Sci*, 66, 470-94.
- WAKSMAN, G., KOMINOS, D., ROBERTSON, S. C., PANT, N., BALTIMORE, D., BIRGE, R. B., COWBURN, D., HANAFUSA, H., MAYER, B. J., OVERDUIN, M., RESH, M. D., RIOS, C. B., SILVERMAN, L. & KURIYAN, J. 1992. Crystal structure of the phosphotyrosine recognition domain SH2 of v-src complexed with tyrosine-phosphorylated peptides. *Nature*, 358, 646-53.
- WAKSMAN, G., SHOELSON, S. E., PANT, N., COWBURN, D. & KURIYAN, J. 1993. Binding of a high affinity phosphotyrosyl peptide to the Src SH2 domain: crystal structures of the complexed and peptide-free forms. *Cell*, 72, 779-90.
- WALAAS, S. I., LUSTIG, A., GREENGARD, P. & BRUGGE, J. S. 1988. Widespread distribution of the c-src gene product in nerve cells and axon terminals in the adult rat brain. *Brain Res*, 427, 215-22.
- WANG, M., ZHOU, C., SUN, Q., CAI, R., LI, Y., WANG, D. & GONG, L. 2013. ALK amplification and protein expression predict inferior prognosis in neuroblastomas. *Exp Mol Pathol*, 95, 124-30.
- WANG, S. & BASSON, M. D. 2011. Protein kinase B/AKT and focal adhesion kinase: two close signaling partners in cancer. *Anticancer Agents Med Chem*, 11, 993-1002.
- WANG, Y. T. & SALTER, M. W. 1994. Regulation of NMDA receptors by tyrosine kinases and phosphatases. *Nature*, 369, 233-5.
- WANG, Y. T., YU, X. M. & SALTER, M. W. 1996. Ca²⁺-independent reduction of N-methyl-D-aspartate channel activity by protein tyrosine phosphatase. *Proc Natl Acad Sci U S A*, 93, 1721-5.
- WEBB, D. J., DONAIS, K., WHITMORE, L. A., THOMAS, S. M., TURNER, C. E., PARSONS, J. T. & HORWITZ, A. F. 2004. FAK-Src signalling through paxillin, ERK and MLCK regulates adhesion disassembly. *Nat Cell Biol*, 6, 154-61.
- WEINSTEIN, D. C., MARDEN, J., CARNEVALI, F. & HEMMATI-BRIVANLOU, A. 1998. FGF-mediated mesoderm induction involves the Src-family kinase Lalloo. *Nature*, 394, 904-8.
- WENG, Z., TAYLOR, J. A., TURNER, C. E., BRUGGE, J. S. & SEIDEL-DUGAN, C. 1993. Detection of Src homology 3-binding proteins, including paxillin, in normal and v-Src-transformed Balb/c 3T3 cells. *J Biol Chem*, 268, 14956-63.
- WHISSTOCK, J. C. & LESK, A. M. 1999. SH3 domains in prokaryotes. *Trends Biochem Sci*, 24, 132-3.

- WIESTLER, O. D. & WALTER, G. 1988. Developmental expression of two forms of pp60c-src in mouse brain. *Mol Cell Biol*, 8, 502-4.
- WILDE, A., BEATTIE, E. C., LEM, L., RIETHOF, D. A., LIU, S. H., MOBLEY, W. C., SORIANO, P. & BRODSKY, F. M. 1999. EGF receptor signaling stimulates SRC kinase phosphorylation of clathrin, influencing clathrin redistribution and EGF uptake. *Cell*, 96, 677-87.
- WILLIAMS, J. C., WEIJLAND, A., GONFLONI, S., THOMPSON, A., COURTNEIDGE, S. A., SUPERTI-FURGA, G. & WIERENGA, R. K. 1997. The 2.35 Å crystal structure of the inactivated form of chicken Src: a dynamic molecule with multiple regulatory interactions. *J Mol Biol*, 274, 757-75.
- WILLINGHAM, M. C., JAY, G. & PASTAN, I. 1979. Localization of the ASV src gene product to the plasma membrane of transformed cells by electron microscopic immunocytochemistry. *Cell*, 18, 125-34.
- WILSON, L. K., LUTTRELL, D. K., PARSONS, J. T. & PARSONS, S. J. 1989. pp60c-src tyrosine kinase, myristylation, and modulatory domains are required for enhanced mitogenic responsiveness to epidermal growth factor seen in cells overexpressing c-src. *Mol Cell Biol*, 9, 1536-44.
- WINKLER, D. G., PARK, I., KIM, T., PAYNE, N. S., WALSH, C. T., STROMINGER, J. L. & SHIN, J. 1993. Phosphorylation of Ser-42 and Ser-59 in the N-terminal region of the tyrosine kinase p56lck. *Proc Natl Acad Sci U S A*, 90, 5176-80.
- WOODS, W. G., GAO, R. N., SHUSTER, J. J., ROBISON, L. L., BERNSTEIN, M., WEITZMAN, S., BUNIN, G., LEVY, I., BROSSARD, J., DOUGHERTY, G., TUCHMAN, M. & LEMIEUX, B. 2002. Screening of infants and mortality due to neuroblastoma. *N Engl J Med*, 346, 1041-6.
- WORLEY, T. L., CORNEL, E. & HOLT, C. E. 1997. Overexpression of c-src and n-src in the developing *Xenopus* retina differentially impairs axonogenesis. *Mol Cell Neurosci*, 9, 276-92.
- WU, H. & PARSONS, J. T. 1993. Cortactin, an 80/85-kilodalton pp60src substrate, is a filamentous actin-binding protein enriched in the cell cortex. *J Cell Biol*, 120, 1417-26.
- XIONG, Z. G., PELKEY, K. A., LU, W. Y., LU, Y. M., RODER, J. C., MACDONALD, J. F. & SALTER, M. W. 1999. Src potentiation of NMDA receptors in hippocampal and spinal neurons is not mediated by reducing zinc inhibition. *J Neurosci*, 19, RC37.
- XU, W., DOSHI, A., LEI, M., ECK, M. J. & HARRISON, S. C. 1999. Crystal structures of c-Src reveal features of its autoinhibitory mechanism. *Mol Cell*, 3, 629-38.
- XU, W., HARRISON, S. C. & ECK, M. J. 1997. Three-dimensional structure of the tyrosine kinase c-Src. *Nature*, 385, 595-602.
- XUE, Y., REN, J., GAO, X., JIN, C., WEN, L. & YAO, X. 2008. GPS 2.0, a tool to predict kinase-specific phosphorylation sites in hierarchy. *Mol Cell Proteomics*, 7, 1598-608.

- YACIUK, P., CHOI, J. K. & SHALLOWAY, D. 1989. Mutation of amino acids in pp60c-src that are phosphorylated by protein kinases C and A. *Mol Cell Biol*, 9, 2453-63.
- YAMAGUCHI, H. & HENDRICKSON, W. A. 1996. Structural basis for activation of human lymphocyte kinase Lck upon tyrosine phosphorylation. *Nature*, 384, 484-9.
- YANG, M. & LEONARD, J. P. 2001. Identification of mouse NMDA receptor subunit NR2A C-terminal tyrosine sites phosphorylated by coexpression with v-Src. *J Neurochem*, 77, 580-8.
- YANG, W., XIA, Y., JI, H., ZHENG, Y., LIANG, J., HUANG, W., GAO, X., ALDAPE, K. & LU, Z. 2011. Nuclear PKM2 regulates β -catenin transactivation upon EGFR activation. *Nature*, 480, 118-22.
- YAO, W., LI, K., ZHENG, S., XIAO, X., MA, Y. & ZHAI, X. 2013. Knockdown of β -catenin expression inhibits neuroblastoma cell growth in vitro and in vivo. *J Pediatr Surg*, 48, 2466-73.
- YEO, M. G., OH, H. J., CHO, H. S., CHUN, J. S., MARCANTONIO, E. E. & SONG, W. K. 2011. Phosphorylation of Ser 21 in Fyn regulates its kinase activity, focal adhesion targeting, and is required for cell migration. *J Cell Physiol*, 226, 236-47.
- YU, A. L., GILMAN, A. L., OZKAYNAK, M. F., LONDON, W. B., KREISSMAN, S. G., CHEN, H. X., SMITH, M., ANDERSON, B., VILLABLANCA, J. G., MATTHAY, K. K., SHIMADA, H., GRUPP, S. A., SEEGER, R., REYNOLDS, C. P., BUXTON, A., REISFELD, R. A., GILLIES, S. D., COHN, S. L., MARIS, J. M., SONDEL, P. M. & GROUP, C. S. O. 2010. Anti-GD2 antibody with GM-CSF, interleukin-2, and isotretinoin for neuroblastoma. *N Engl J Med*, 363, 1324-34.
- YU, H., CHEN, J. K., FENG, S., DALGARNO, D. C., BRAUER, A. W. & SCHREIBER, S. L. 1994. Structural basis for the binding of proline-rich peptides to SH3 domains. *Cell*, 76, 933-45.
- YU, H., ROSEN, M. K., SHIN, T. B., SEIDEL-DUGAN, C., BRUGGE, J. S. & SCHREIBER, S. L. 1992. Solution structure of the SH3 domain of Src and identification of its ligand-binding site. *Science*, 258, 1665-8.
- YU, X. M., ASKALAN, R., KEIL, G. J. & SALTER, M. W. 1997. NMDA channel regulation by channel-associated protein tyrosine kinase Src. *Science*, 275, 674-8.
- ZAGE, P. E., NOLO, R., FANG, W., STEWART, J., GARCIA-MANERO, G. & ZWEIDLER-MCKAY, P. A. 2012. Notch pathway activation induces neuroblastoma tumor cell growth arrest. *Pediatr Blood Cancer*, 58, 682-9.
- ZARRINPAR, A., BHATTACHARYYA, R. P. & LIM, W. A. 2003. The structure and function of proline recognition domains. *Sci STKE*, 2003, RE8.
- ZENG, G., APTE, U., MICSENYI, A., BELL, A. & MONGA, S. P. 2006. Tyrosine residues 654 and 670 in beta-catenin are crucial in regulation of Met-beta-catenin interactions. *Exp Cell Res*, 312, 3620-30.

- ZHANG, B., KIROV, S. & SNODDY, J. 2005. WebGestalt: an integrated system for exploring gene sets in various biological contexts. *Nucleic Acids Res*, 33, W741-8.
- ZHANG, P., GUO, A., POSSEMATO, A., WANG, C., BEARD, L., CARLIN, C., MARKOWITZ, S. D., POLAKIEWICZ, R. D. & WANG, Z. 2013. Identification and functional characterization of p130Cas as a substrate of protein tyrosine phosphatase nonreceptor 14. *Oncogene*, 32, 2087-95.
- ZHANG, X., HØJLUND, K., LUO, M., MEYER, C., GEETHA, T. & YI, Z. 2012. Novel tyrosine phosphorylation sites in rat skeletal muscle revealed by phosphopeptide enrichment and HPLC-ESI-MS/MS. *J Proteomics*, 75, 4017-26.
- ZHAO, Y., ZHANG, X., GUDA, K., LAWRENCE, E., SUN, Q., WATANABE, T., IWAKURA, Y., ASANO, M., WEI, L., YANG, Z., ZHENG, W., DAWSON, D., WILLIS, J., MARKOWITZ, S. D., SATAKE, M. & WANG, Z. 2010. Identification and functional characterization of paxillin as a target of protein tyrosine phosphatase receptor T. *Proc Natl Acad Sci U S A*, 107, 2592-7.
- ZHENG, F., GINGRICH, M. B., TRAYNELIS, S. F. & CONN, P. J. 1998. Tyrosine kinase potentiates NMDA receptor currents by reducing tonic zinc inhibition. *Nat Neurosci*, 1, 185-91.
- ZHENG, X. M., RESNICK, R. J. & SHALLOWAY, D. 2000. A phosphotyrosine displacement mechanism for activation of Src by PTPalpha. *EMBO J*, 19, 964-78.
- ZONG, X., ECKERT, C., YUAN, H., WAHL-SCHOTT, C., ABICHT, H., FANG, L., LI, R., MISTRİK, P., GERSTNER, A., MUCH, B., BAUMANN, L., MICHALAKIS, S., ZENG, R., CHEN, Z. & BIEL, M. 2005. A novel mechanism of modulation of hyperpolarization-activated cyclic nucleotide-gated channels by Src kinase. *J Biol Chem*, 280, 34224-32.